

# Development of novel supramolecular framework materials based on organic salts

by

Helene Wahl

*Dissertation presented in partial fulfilment of the requirements for the degree of*

*Doctor of Philosophy*



Stellenbosch University

Supervisor: Dr Tanya le Roex

Co-supervisor: Prof. Delia A. Haynes

Department of Chemistry and Polymer Science

Faculty of Science

December 2014

## **Declaration**

By submitting this thesis electronically, I declare that the entirety of the work contained therein is my own, original work, that I am the authorship owner thereof (unless to the extent explicitly otherwise stated) and that I have not previously in its entirety or in part submitted it for obtaining any qualification.

Date: December 2014

Copyright © 2014 Stellenbosch University

All rights reserved



## Abstract

The aim of the work presented in this thesis was to design ionic organic framework materials based on carboxylate salts with the intention of engineering interesting properties, such as porosity, into these framework materials.

The first section focuses on the characterisation and porosity studies of an ionic framework material, 3,4-lutidinium pamoate hemihydrate, with THF-filled channels in the solid state. It was shown that this framework is able to exchange the THF in the channels for a wide variety of compounds, with many of these exchanges occurring in a single-crystal to single-crystal fashion. Competition experiments conducted with the framework, both by immersing crystals of the framework in solvent mixtures, as well as by exposing crystals of the framework to mixtures of solvent vapours, indicated that it is able to selectively exchange for one guest over another. The kinetics of exchange of this framework were studied, and it was possible to identify a kinetic model describing this process.

A second novel framework-type material, 4-phenylpyridinium pamoate, was identified during the course of this study, as well as five isostructural frameworks containing different guest molecules. In this case the framework consists of discrete units that close-pack in such a way that guest molecules are included in constricted cavities in the solid state. Although this framework-type material is not porous, it is thermally quite stable and also highly selective. It is able to selectively encapsulate 1,4-dioxane when crystallised from various solvent combinations including 1,4-dioxane. In addition, eight novel structures with pamoic acid in combination with various pyridyl derivatives were obtained.

A third novel framework material was obtained with N,N'-bis(glyciny)pyromellitic diimide in which, due to the extended hydrogen-bonded network formed between the constituents of the framework, DMF molecules are aligned in channels. It was found that this framework material can also be formed by mechanochemical synthesis, and investigation of the thermal behaviour of this framework showed that it has the potential to be porous, since the framework appears to remain intact after desolvation. Furthermore, six novel structures with N,N'-bis(glyciny)pyromellitic diimide in combination with various N-heterocycles were obtained.

All structures obtained in this study were also further analysed to determine whether there are particular structural features that are required for framework formation. Insights gained from

these investigations, in terms of degree of ionisation of the anion, packing arrangements and hydrogen bonding patterns as well as the molecular shape of the components are discussed.

## Opsomming

Die doel van die werk wat in hierdie tesis voorgelê word is om ioniese organiese raamwerkmateriale gebaseer op karboksilaatone te ontwerp, met die voorneme om interessante eienskappe in hierdie materiale te bewerkstellig.

Die eerste afdeling fokus op die karakterisering en porositeit van 'n ioniese organiese raamwerkmateriaal, 3,4-lutidiniumpamoathemihdraat, wat kanale gevul met tetrahydrofuraan (THF) besit. Dit is aangetoon dat dit moontlik is vir hierdie raamwerkmateriaal om die THF in die kanale te verruil vir 'n wye verskeidenheid stowwe, waarvan baie van hierdie uitruilings geskied as 'n enkelkristal tot enkelkristal transformasie. Kompetisie-eksperimente is met hierdie raamwerkmateriaal uitgevoer deur die kristalle in mengsels van oplosmiddels te onderdompel, sowel as deur die kristalle aan mengsels van die oplosmiddeldampe bloot te stel. Die resultate het aangedui dat dit moontlik is vir hierdie raamwerkmateriaal om een gasstof selektief teenoor 'n ander te verruil vir die THF in die kanale. Die kinetika van die uitruilingsproses van hierdie materiaal is ook bestudeer en dit was moontlik om 'n kinetiese model te identifiseer wat die uitruilingsproses beskryf.

'n Tweede nuwe raamwerk-tipe materiaal, 4-fenielpiridiniumpamoaat, is deur die loop van hierdie studie geïdentifiseer, sowel as vyf isostrukturele raamwerkmateriale waarvan net die gasstof verskil. In hierdie geval bestaan die raamwerk uit diskrete eenhede wat op so 'n wyse saampak dat die gasstowwe in vernoude porieë ingesluit word. Alhoewel hierdie raamwerk-tipe materiaal nie poreus is nie, is dit termies stabiel en ook hoogs selektief. Die raamwerkmateriaal kan selektief 1,4-dioksaan enkapsuleer wanneer dit gekristalliseer word vanuit 'n verskeidenheid oplosmiddel kombinasies met 1,4-dioksaan. Verder is agt nuwe strukture verkry met die pamoaat ioon in kombinasie met 'n verskeidenheid piridien-derivate.

'n Derde nuwe raamwerkmateriaal is verkry met N,N'-bis(glisiniel)piromellitiese diïmied waarin, danksy die uitgebreide waterstofgebinde netwerk tussen die komponente van die raamwerk, die DMF molekules in kanale aangetref word. Hierdie raamwerkmateriaal kan deur meganochemiese sintese berei word en verdere ondersoek na die termiese gedrag van hierdie

raamwerk materiaal dui aan dat dit die potensiaal het om porositeit te toon, aangesien die raamwerk behoue bly nadat die DMF molekules verwyder is. Ses nuwe strukture is ook met N,N'-bis(glisiniel)piromellitiese diïmied in kombinasie met 'n wye verskeidenheid stikstof-bevattende heterosikliese verbindings verkry.

Alle strukture wat tydens hierdie studie verkry is, is verder ondersoek om te bepaal of daar spesifieke strukturele kenmerke is wat nodig word vir die vorming van raamwerk materiale. Insigte wat verkry is vanuit hierdie ondersoek, in terme van die graad van ionisasie van die anioon, die rangskikking van molekules in die struktuur en waterstofbindingspatrone, sowel as die molekulêre vorm van die komponente, word bespreek.

## Acknowledgements

First and foremost I would like to thank my mentors, Dr Tanya le Roex and Prof. Delia Haynes, for without their guidance this thesis would not have been possible. You have been an inspiration to me and created a wonderful working environment in which I felt I was constantly learning something new. The past year has been full of difficulties and I thank you for always having time for me and always having a kind word to make me feel like I am accomplishing something great.

I would like to thank the Supramolecular Materials group for their support and office shenanigans that made for an interesting and laughter-filled office. I would also like to thank them for all the help with instruments and experiments. The experience I have gained with the group has been absolutely invaluable. A special word of thanks has to be directed to the members of the musketeers, Laura, Leigh and Varia, who have been wonderful friends throughout my postgraduate studies and have been incredibly supportive. The “thesis survival kit” was much appreciated.

Nothing would of course have been possible without the technical staff that keep the well-oiled machine that is research running. Therefore, thank you to Debbie, Mary, Moebarrick, Raymond and Elsa for all your assistance whenever I needed it.

And, of course, thank you to my family for all their support, as I would have been a lot less calm (and well-fed) throughout the writing process. A special thank you should also be reserved for Haydn, who kept me well supplied in waffles, wine and beer whenever it all became too much!

Lastly, I would like to thank Stellenbosch University and the Wilhelm Frank Trust for funding.

## Publications

### *Part of this work*

1. H. Wahl, D. A. Haynes and T. le Roex, *Chem. Commun.*, 2012, **48**, 1775 – 1777

### *Not part of this work*

2. H. Wahl, D. A. Haynes and T. le Roex, *CrystEngComm*, 2013, **15**, 13, 2450 – 245
3. L. Loots, H. Wahl, L. van der Westhuizen, D.A. Haynes and T. le Roex, *Chem. Commun.*, 2012, **48**, 11507-11509
4. H. Wahl, D. A. Haynes and T. le Roex, *Cryst. Growth Des.*, 2012, **12**, 4031-4038
5. H. Wahl, D. A. Haynes and T. le Roex, *Crystengcomm*, 2011, **13**, 2227-2236

## Conferences

1. **Indaba 7 – Insights from structure**

Skukuza, Kruger National Park, South Africa, 2 – 7 September 2012

Poster presentation: *Development of novel supramolecular framework materials based on organic salts* – awarded second prize for poster presentations

2. **21st International Conference on the Chemistry of the Organic Solid State (ICCOSSXXI)**

St. Catherine's College, Oxford, United Kingdom, 4 – 9 August 2013

Poster presentation: *Development of novel supramolecular framework materials based on organic salts*

3. **Pan African Conference and Summit, IYCR 2014 Africa**

University of the Free State, Bloemfontein, South Africa, 12 – 17 October 2014

Poster presentation: *Development of novel supramolecular framework materials based on organic salts* – poster prize

## Abbreviations

1-D	One dimensional
2-D	Two dimensional
3-D	Three dimensional
bp	Boiling point
CIF	Crystallographic information file
COF	Covalent organic framework
CSD	Cambridge Structural Database
DSC	Differential scanning calorimetry
FTIR	Fourier-transform infrared microscopy
HOF	Hydrogen-bonded organic framework
MOF	Metal-organic framework
NMC	Nanoporous molecular crystals
NMR	Nuclear magnetic resonance spectroscopy
SCD	Single crystal X-ray diffraction
TGA	Thermogravimetric analysis
PXRD	Powder X-ray diffraction
VT-PXRD	Variable temperature powder X-ray diffraction
Z	Number of formula units in the cell
Z'	Number of formula units in the asymmetric unit

## Atomic colour key



Carbon



Oxygen



Nitrogen



Hydrogen



Chlorine



Sulfur



Iodine

## Table of contents

Declaration .....	i
Abstract .....	ii
Opsomming .....	iii
Acknowledgements .....	v
Publications .....	vi
Conferences .....	vi
Abbreviations .....	vii
Atomic colour key .....	viii
Table of contents .....	ix

### **Chapter 1 - General introduction .....** **1**

1.1. Supramolecular chemistry .....	1
1.2. Crystal engineering .....	2
1.2.1. Supramolecular synthons .....	2
1.2.2. Intermolecular interactions .....	4
1.2.2.1. van der Waals interactions .....	5
1.2.2.2. $\pi$ - $\pi$ interactions .....	5
1.2.2.3. The hydrogen bond .....	7
1.2.3. Multicomponent systems .....	11
1.2.4. Self-assembly and shape complementarity .....	12
1.3. Host-guest chemistry .....	13
1.4. Porosity .....	18
1.5. Framework materials .....	19
1.5.1. Metal-organic frameworks (MOFs) .....	20
1.5.2. Covalent organic frameworks (COFs) .....	23
1.5.3. Organic cages and nanoporous molecular crystals (NMCs) .....	25
1.5.4. Hydrogen-bonded organic frameworks (HOFs) .....	27
1.6. Aim and scope of this study .....	30
1.6.1. Brief overview of this thesis .....	31



1.7. References.....	33
<b><u>Chapter 2 – A porous ionic framework based on the pamoate ion .....</u></b>	<b>42</b>
2.1. Synthesis and structure of framework <b>1·THF</b> .....	44
2.1.1. The initial study of <b>1·THF</b> .....	49
2.2. Thermal behaviour.....	52
2.3. Exchange studies with framework <b>1</b> .....	57
2.3.1. Successful exchanges with <b>1·THF</b> and supporting SCD data.....	59
2.3.1.1. Discussion of crystal structures .....	62
2.3.2. Successful exchanges with <b>1·THF</b> where no SCD data could be obtained .....	73
2.3.3. Unsuccessful exchanges with <b>1·THF</b> .....	77
2.3.4. Step-wise exchanges with <b>1·THF</b> .....	79
2.3.5. Exchange by immersion of crystals in various solvents.....	80
2.4. Competition experiments.....	82
2.4.1. Competition experiments with mixed solvent vapours .....	82
2.4.2. Competition experiments with vapour mixtures of varying benzene/toluene fractions .....	85
2.4.3. Competition experiments with crystals immersed in varying fractions of benzene/toluene .....	89
2.4.4. Competition experiments with crystals immersed in 1:1 solvent mixtures.....	90
2.5. The effect of immersion in certain solvents on framework <b>1</b> .....	93
2.6. Conclusions and future work .....	101
2.7. References.....	105
<b><u>Chapter 3 – Kinetic studies on framework <b>1</b> .....</u></b>	<b>108</b>
3.1. Attempted studies of the desolvation kinetics of <b>1·THF</b> .....	112
3.2. Studies on the kinetics of exchange with <b>1·THF</b> .....	117
3.2.1. First experimental setup for the kinetic study of <b>1·THF</b> .....	118
3.2.2. Successful study of kinetics of exchange with <b>1·THF</b> .....	120
3.3. Discussion and interpretation of the kinetic data of <b>1·THF</b> .....	126
3.4. Supporting studies for the kinetic model of <b>1·THF</b> .....	128
3.5. Conclusions and future work .....	133

3.6. References.....	136
----------------------	-----

## **Chapter 4 – A highly selective framework-type structure based on the pamoate ion 139**

4.1 Synthesis and description of the 4-phenylpyridine framework-type structure, <b>2·THF</b> .....	140
4.1.1 Solvent exchange studies with <b>2·THF</b> .....	143
4.1.2 Thermal studies of <b>2·THF</b> .....	145
4.2 Isostructural frameworks .....	151
4.3 Competition experiments .....	160
4.4 Novel crystal structures obtained with pamoic acid .....	171
4.4.1 Salt formation with pamoic acid and 4-phenylpyridine .....	171
4.4.2 1,2-(2-(4-pyridyl)ethyl)pyridinium pamoate salt, PA1 .....	179
4.4.3 1,10-phenanthroline pamoate THF solvate, PA2.....	181
4.4.4 2-aminopyrimidinium pamoate THF solvate, PA3 .....	183
4.4.5 2,4-lutidinium pamoate dihydrate, PA4 .....	185
4.4.6 2,5-lutidinium pamoate dihydrate, PA5 .....	187
4.4.7 4-picolinium pamoate hydrate DMF solvate, PA6.....	189
4.5 Important structural requirements for framework formation.....	192
4.6 Summary and conclusion.....	197
4.7 References.....	200

## **Chapter 5 – A host framework based on N,N'-bis(glycinyl)pyromellitic diimide..... 202**

5.1. Synthesis of N,N'-bis(glycinyl)pyromellitic diimide.....	208
5.2. Cocrystallisations with N,N'-bis(glycinyl)pyromellitic diimide.....	211
5.2.1. Hydrate formation in PD001 and PD002 .....	212
5.2.2. Salt vs. cocrystal formation in PD003 and PD004.....	217
5.2.3. Cocrystals with aromatic molecules and pyromellitic diimide .....	222
5.3. The pyromellitic diimide framework.....	227
5.3.1. Thermal behaviour of the framework.....	232
5.3.2. Mechanochemical synthesis of framework 3 .....	236
5.4. Structural features needed for framework formation.....	238
5.5. Conclusions and future work .....	242

5.6. References.....245

**Chapter 6 – Summary and concluding remarks .....246**

**Appendix A – Instruments and experimental procedures .....254**

**Attached CD**

Appendix B

Appendix C

CIF files

# CHAPTER 1

## GENERAL INTRODUCTION

---

In the field of supramolecular chemistry various different streams of chemistry are incorporated in order to design materials, analyse these materials and eventually test the properties of these materials. In the past few decades supramolecular chemistry has advanced in leaps and bounds, therefore this introductory chapter will discuss the basic concepts used in supramolecular chemistry and highlight the research and discoveries made in this field that are related to this project. This project focuses on using purely organic molecules to design and synthesise ionic organic framework materials based on carboxylate salts through noncovalent interactions, with the aim of engineering interesting properties such as porosity, selectivity and non-linear optics into these materials. By examining the history, core concepts and current state of supramolecular chemistry it is possible to understand how supramolecular chemists are able to design some of the most interesting materials known to date, yet *it is still magic even if you know how it is done*.\*

### 1.1. Supramolecular chemistry

Since Donald J. Cram, Jean-Marie Lehn and Charles J. Pedersen were awarded the Nobel prize for chemistry in 1987 for their work in supramolecular chemistry,<sup>1</sup> the field has greatly expanded and is responsible for highly innovative research that has produced many interesting and valuable materials.<sup>2</sup> Supramolecular chemistry as we know it today was first defined by Jean-Marie Lehn in 1978 as “*chemistry of molecular assemblies and of the intermolecular bond*.”<sup>3</sup> It has also been described as “*chemistry beyond the molecule*”, “*the chemistry of the noncovalent bond*,” and, a personal favourite, “*Lego chemistry*”.<sup>4</sup> Generally supramolecular chemistry refers to the association of multicomponent systems through noncovalent interactions between the building blocks.<sup>5</sup> In other words, where synthetic chemistry attempts to covalently link atoms to each other, supramolecular chemistry attempts to connect vast systems of molecules through noncovalent weak intermolecular contacts, prompting Lehn to aptly describe it as the “*designed chemistry of the intermolecular bond*.”<sup>6</sup> He also placed special emphasis on the word “designed” thereby implying that it is not just a random

---

\* Terry Pratchett, *A Hat Full of Sky*

collection of molecules in random arrays. Molecules are specifically chosen for their ability to form a stable contact with a neighbouring molecule. This gives a supramolecular assembly order and directionality which can lead to interesting properties in solution and, specifically related to this project, the bulk solid state. Purposely engineering molecules that can easily interact with each other to form a specific structure in the solid state is known as crystal engineering.

## 1.2. Crystal engineering

Ray Pepinsky was the first to introduce the term crystal engineering at a meeting of the American Physical Society in 1955.<sup>7, 8</sup> Pepinsky also emphasised how it was possible to control how molecules crystallised together and therefore “*crystals with advantageous properties can be engineered*”.<sup>7, 8</sup> In simple terms, crystal engineering is “*making crystals by design*”<sup>9</sup> where the focus is on the collective properties of assemblies of molecules rather than the individual molecules themselves.<sup>9</sup> It is also important to understand how and why molecules arrange themselves in the solid state, since the molecular arrangement in a crystal controls the properties of the material.<sup>10</sup> Therefore in the field of crystal engineering there are a few design strategies that are employed in order to create these functional materials and to afford a degree of predictability to the process.<sup>11</sup> Depending on the type of structure one wishes to create, one would aim to construct patterns such as ribbons, sheets, layers, channels or cavities which could then lead to interesting properties such as porosity.<sup>12, 13</sup> The pattern itself could also encode a specific property,<sup>12</sup> as in the case of polar structures where the alignment of the molecules introduces polar order to the structure. In order to design these particular patterns one has to identify a basic unit of interaction between two molecules that will reliably lead to the formation of the desired structure. This basic unit is known as a supramolecular synthon.<sup>14, 15</sup>

### 1.2.1. Supramolecular synthons

A supramolecular synthon is defined as a repeating structural unit that directs how molecules interact with each other in the solid state.<sup>12</sup> In organic chemistry synthons allow molecules to be covalently linked to each other, while in crystal engineering synthons allow molecules to

form strong directional interactions with each other.<sup>12</sup> The concept is illustrated in Figure 1.1 with terephthalic acid (CSD-TEPHTH<sup>16, 17</sup>).<sup>†</sup>

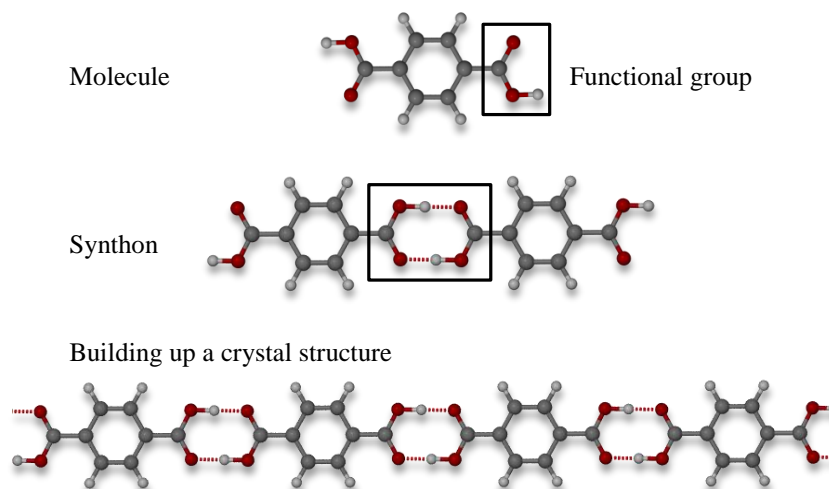


**Figure 1.1** The relationship between a molecule, a functional group and a synthon and how a synthon is used to build a crystal structure. The image has been adapted from reference 13.

Synthons are not only restricted to the interactions between carboxylic acids. There is a vast array of synthons<sup>12, 18</sup> which can be used when attempting to design a crystal structure. A few examples are shown in Figure 1.2.

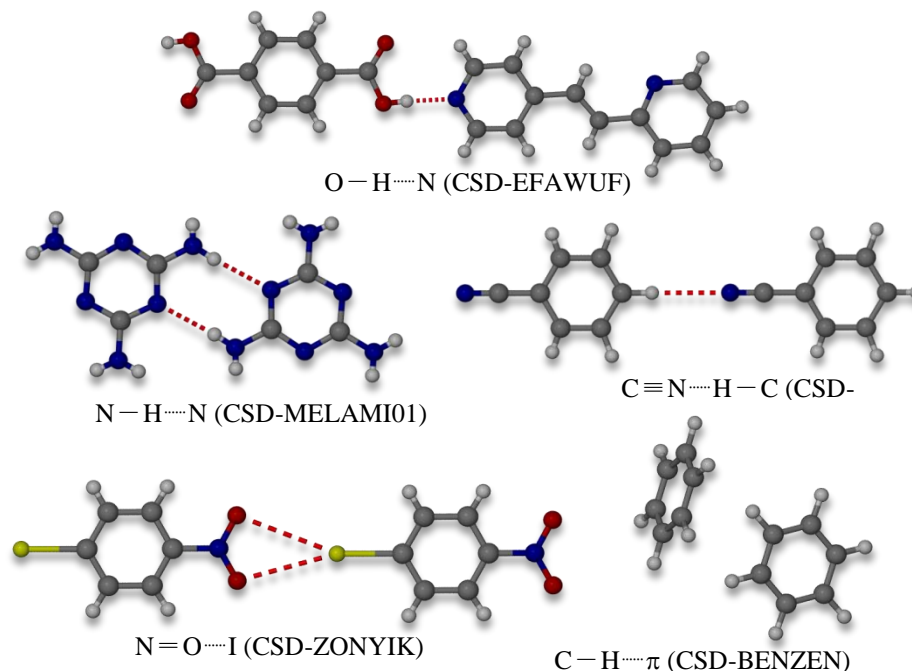


**Figure 1.2** A few examples of synthons often used in crystal engineering.

<sup>†</sup> All published structures in this thesis will be referred to by their CSD refcode. The CSD is the Cambridge Structural Database, an international repository for small-molecule organic and metal-organic crystal structures.<sup>16</sup> The refcode, e.g. TEPHTH, is a unique reference code assigned to each crystal structure submitted to the database.

Supramolecular synthons can be classified as either homosynthons, when the interaction is between identical functional groups such as the carboxylic dimer in Figure 1.1, or as heterosynthons, when the interaction is between different but complementary functional groups such as the carboxylic acid-pyridine synthon shown in Figure 1.2 (EFAWUF).<sup>7, 19</sup>

The distinction between intermolecular interactions and synthons is that synthons are derived from the deliberate combination of functional groups and therefore incorporate chemical and geometrical recognition features of molecular fragments.

### 1.2.2. Intermolecular interactions

Intermolecular interactions are the glue that holds crystal structures together and are the driving force behind the formation of a crystal.<sup>20</sup> It is therefore important to understand these interactions and how they direct structure formation. Some interactions are weaker than others, but this by no means diminishes their role within the crystal structure. Almost all interactions in crystals are electrostatic in nature and the strength of the interaction depends on the degree of polarisation of the molecules involved.<sup>20</sup> Intermolecular interactions can also be directional or nondirectional. Directional forces determine the geometry and spatial alignment of molecules, whereas nondirectional forces exert a long-range influence over the orientation of molecules with respect to each other.<sup>21</sup> Table 1.1 contains the most common intermolecular interactions and information on the directionality and relative strength of each interaction. In general, intermolecular interactions, or non-covalent interactions, are considered to be weak when compared to much stronger covalent interactions. How is it then possible that these weak interactions govern the aggregation of large complex systems into stable crystal structures? During the aggregation of molecules a vast number of weak interactions, such as dispersion interactions, can have a much more pronounced effect than a few strong interactions, such as hydrogen bonds, on the packing of molecules in the solid state. This is known as the Gulliver effect, where something small can have a surprisingly large effect.<sup>7</sup>

Crystal engineers use intermolecular interactions to help direct the assembly of molecules into a desired structure with (hopefully) interesting properties. The intermolecular interactions specifically applicable in this study will be discussed in more detail below.

**Table 1.1** Common intermolecular interactions and their relative strengths. This information has been taken from reference 21.

Intermolecular interaction	Directionality	Interaction energies (kJ/mol)
Ion-ion	Nondirectional	100 – 350
van der Waals	Nondirectional	<5
Closed-shell metal-metal	Nondirectional	5 – 60
Ion-dipole	Slightly directional	50 – 200
Dipole-dipole	Slightly directional	5 – 50
Coordination bonds	Directional	100 – 300
Hydrogen bonds	Directional	4 – 120
Halogen bonds	Directional	10 – 50
$\pi$ - $\pi$ interactions	Directional	2 – 50
Cation- $\pi$ and anion- $\pi$ interactions	Directional	5 – 80

### 1.2.2.1. van der Waals interactions

In crystal engineering van der Waals interactions include long-range inductive and dispersive intermolecular forces in a crystal,<sup>5</sup> but exclude interactions such as hydrogen bonding, ion-dipole and dipole-dipole.<sup>7</sup> Induced dipole to induced dipole interactions (London forces) and interactions between permanent dipoles or a permanent dipole and an induced dipole also form part of van der Waals interactions.<sup>7</sup> van der Waals interactions are generally weak interactions, less than 5 kJ/mol,<sup>21</sup> but due to the large number in which they are normally found within a crystal structure, they often largely determine how molecules pack in the solid state.<sup>7</sup> van der Waals interactions also determine solubility, density and melting points of organic materials.<sup>7</sup> These interactions also tend to increase when there are more non-polar components present in a crystal structure.<sup>7</sup>

### 1.2.2.2. $\pi$ - $\pi$ interactions

These interactions generally occur between aromatic regions of molecules and can be classified as a type of electrostatic interaction due to the arrangement of the electrons of the aromatic system. The electrostatics of the aromatic molecule can be described as a positively charged  $\sigma$ -framework between two regions of  $\pi$ -electron density.<sup>5</sup> The aromatic molecules



will orientate in such a way that there are favourable  $\sigma-\pi$  interactions between the molecules. This explains why there are three different geometries of  $\pi-\pi$  interactions, namely face-to-face, offset parallel and T-shaped or edge-to-face of which the edge-to-face and offset parallel orientations are most often found between aromatic rings (Figure 1.3).<sup>21-23</sup> In the case of the offset parallel (b) and the edge-to-face (c) geometries there is a favourable alignment of the  $\pi$ -electron cloud around the periphery of the ring and the positive  $\sigma$ -framework in the centre. This is observed to a lesser extent in the face-to-face geometry which is why it is the less favoured orientation.<sup>5</sup>

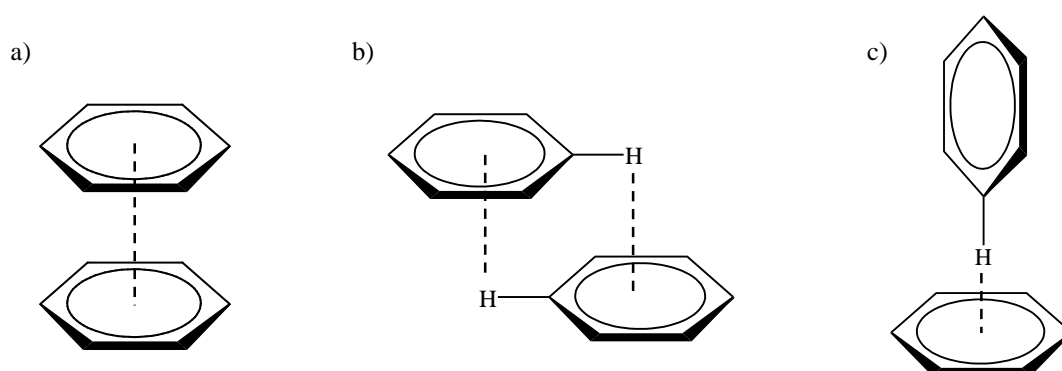


**Figure 1.3** The three orientations of the benzene dimer: a) face-to-face or stacked, b) off-set parallel or off-set stacked and c) edge-to-face or T-shaped. The images have been adapted from references 21 and 23.

Aromatic compounds tend to self-assemble into stacked or herringbone motifs in order to optimise the interactions between the  $\pi$ -electron clouds of molecules.<sup>21, 24, 25</sup> The herringbone motif consists of edge-to-face stacking interactions, while the sandwich herringbone motif consists of molecules stacking in pairs with a combination of offset stacking and edge-to-face interactions. The  $\gamma$ -motif contains molecules that arrange in a face-to-face and/or offset manner along one axis, and then in an edge-to-face herringbone along another axis. The  $\beta$ -type motif is observed when infinite stacks of aromatic molecules pack together through offset or edge-to-face interactions.<sup>24, 26</sup> Diagrammatic representations of the packing motifs are shown in Figure 1.4.

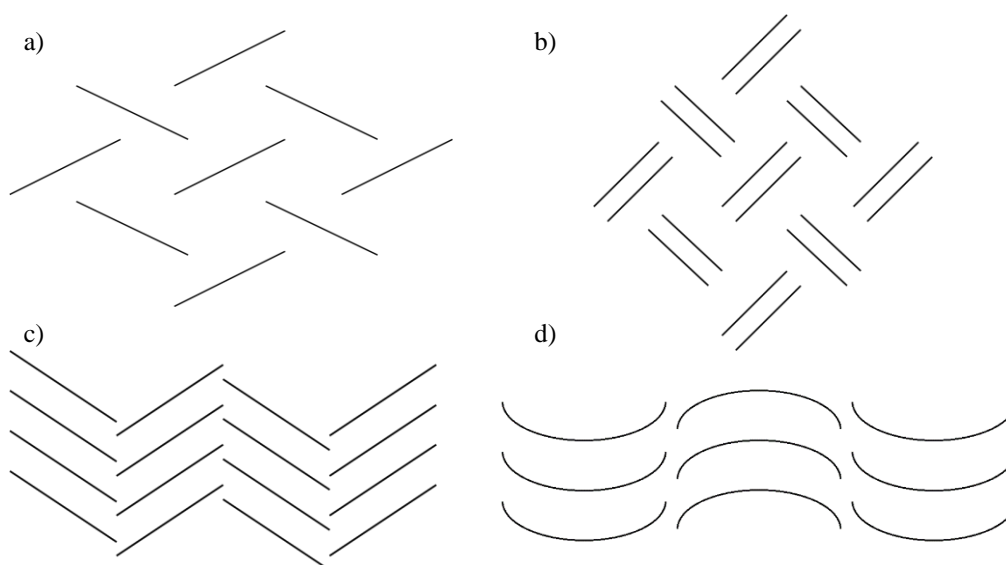


**Figure 1.4** The diagrammatic representations a) herringbone, b) sandwich herringbone, c)  $\gamma$ -motif and d)  $\beta$ -motif type packing. This image has been adapted from reference 26.

### 1.2.2.3. The hydrogen bond

The hydrogen bond is the most well-known and well-studied of all the intermolecular interactions due to its high directionality and strength, and is therefore often described as the “master-key” interaction in crystal engineering.<sup>20, 21</sup> Linus Pauling was the first to describe the hydrogen bond in 1931.<sup>27</sup> He defined it as a bond formed between a polarised hydrogen atom (due to its covalent connection to an electronegative atom X) and an acceptor atom A that has a lone pair of electrons or polarisable  $\pi$ -electrons.<sup>21, 28</sup> Margaret Etter broadened the definition of the hydrogen bond to:<sup>29</sup>

*“A hydrogen bond is an interaction that directs the association of a covalently bound hydrogen atom with one or more other atoms, groups of atoms, or molecules into an aggregate structure that is sufficiently stable to make it convenient for the chemist to consider it as an independent chemical species.”*

The definition of a hydrogen bond has been a much discussed topic in the crystal engineering community, to such an extent that the International Union of Pure and Applied Chemistry (IUPAC) put together a task team to define the hydrogen bond and determine the criteria that can be used to prove the presence of a hydrogen bond. The task group published the definition in 2011 and state that a hydrogen bond can be defined as follows:<sup>30</sup>

*“The hydrogen bond is an attractive interaction between a hydrogen atom from a molecule or a molecular fragment D–H in which D is more electronegative than H, and an atom or a group of atoms in the same or a different molecule, in which there is evidence of bond formation.”*

Evidence for the presence of a hydrogen bond depends largely on the electrostatics involved. The D–H bond must be polarised in order for the interaction between H···A to be classified as a hydrogen bond.<sup>30</sup> The distances and angles involved in a hydrogen bond are important since both the angle and distance of an interaction are indicative of its relative strength.<sup>30, 31</sup> Figure 1.5 shows the relation between the donor molecule and acceptor molecule of a hydrogen bond pair. The distance between the covalently linked hydrogen atom H and donor atom D is represented by  $r$ . The distance between H and the acceptor atom A is described by  $d$ . The distance Y represents the distance between the donor atom D and acceptor atom A. The donor angle ( $\angle$ DHA) is described by  $\theta$  and the acceptor angle ( $\angle$ HAX) by  $\phi$ .<sup>31</sup>

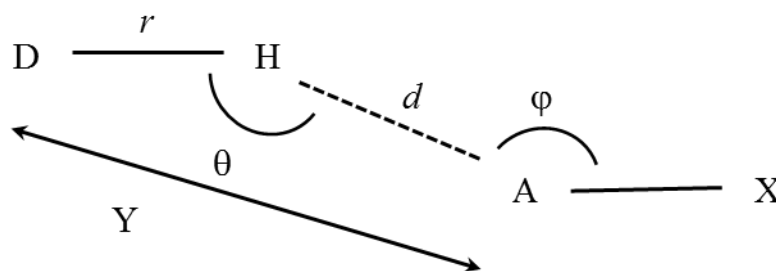


**Figure 1.5** The geometry and constituents of the hydrogen bond D–H···A–X and the important distances and angles involved. This image was adapted from reference 31.

For many years it was thought that a hydrogen bond is only possible if a highly electronegative acceptor atom, such as O, N or F, was combined with a –NHR or –OH group.<sup>10</sup> However, the possible combinations for hydrogen bond donor and acceptor pairs have vastly increased in the last few years as detection techniques, such as nuclear magnetic resonance (NMR) and infrared spectroscopy (IR), have improved with regard to the direct detection of hydrogen bonds.<sup>30, 32-34</sup> Possible acceptor atoms now include the remaining halogens, sulfur and even  $\pi$ -electron clouds.<sup>10</sup> Due to the wide range of possible donor-acceptor pairs, hydrogen bonds can be classified as very strong, strong or weak depending on how well they are able to determine and control supramolecular assembly.<sup>31</sup> Table 1.2

contains a summary of the average energy, bond distances and other properties of the three hydrogen bond classes.

**Table 1.2** Properties of very strong, strong and weak hydrogen bonds,  $D-H\cdots A$ . The information in this table has been adapted from references 21 and 31.

Property	Very strong	Strong	Weak
Examples	Strong acids/bases; proton sponge; HF complexes	Acids; alcohols; biological molecules	Minor components of bifurcated bonds; $C-H\cdots O$ , $O-H\cdots \pi$
Bond energy (kJ/mol)	60 - 120	16 - 60	<12
Bond lengths	$D-H \approx H\cdots A$	$D-H < H\cdots A$	$D-H \ll H\cdots A$
$D\cdots A$ (Y) range (Å)	2.2 - 2.5	2.5 - 3.2	3.0 - 4.0
$H\cdots A$ (d) range (Å)	1.2 - 1.5	1.5 - 2.2	2.2 - 3.0
Bonds shorter than van der Waals cutoff	100%	Almost 100%	30 - 80%
Angle ( $\theta$ ) range (°)	175 - 180	130 - 180	90 - 150
Effect on crystal packing	Dominant	Distinctive	Variable
Interaction type	Partially covalent	Mostly electrostatic	Electrostatic

One of the types of hydrogen bond interactions that play a very important structure directing role in the assembly of framework materials specifically in this study, is the formation of charge-assisted hydrogen bonds. A charge-assisted hydrogen bond consists of a donor atom and an acceptor atom that both carry an ionic charge which further enhances the already polarised hydrogen bond interaction, creating a stronger interaction.<sup>35, 36</sup> Charge-assisted hydrogen bonds are considered to be one of the strongest types of hydrogen bonds and their interaction energies usually fall within the 30 - 120 kJ/mol range.<sup>36</sup> It has been found that charge-assisted hydrogen bonds have shorter interaction distances,<sup>36</sup> which makes them an attractive synthon for the controlled and directed assembly of molecules in the solid state. This has been a particularly effective strategy in the construction of the hydrogen-bonded networks of the guanidinium sulfonates, which will be discussed in Section 1.5.4. This study makes specific use of the charge-assisted hydrogen bonds formed between carboxylic acids and pyridine derivatives due to the proton transfer from the acid to the base.

It is possible for a hydrogen atom to interact with more than one acceptor atom, especially in the case of weak hydrogen bonds as mentioned in Table 1.2. If a hydrogen atom hydrogen bonds to only one acceptor atom, it is seen as a simple hydrogen bond. If it hydrogen bonds to two or more acceptor atoms, it is described as a bifurcated or trifurcated hydrogen bond, respectively.<sup>37</sup> This concept is illustrated in Figure 1.6.

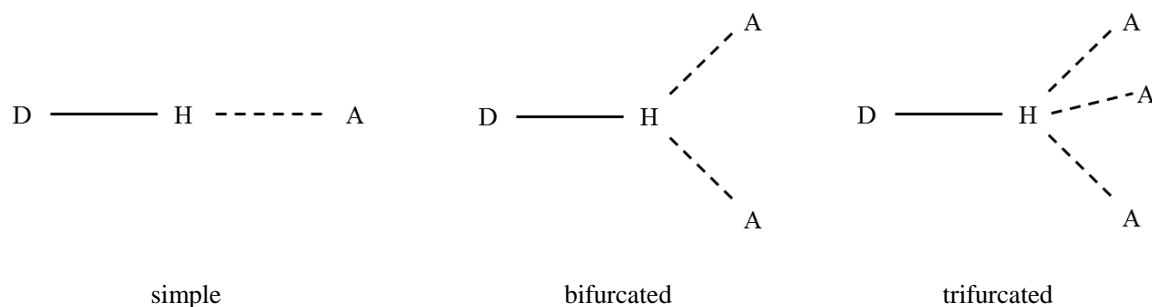


**Figure 1.6** The common hydrogen bond arrangements. It must be noted that the simple hydrogen bond is not always linear. This image has been adapted from reference 37.

Since hydrogen bonds can interact with different atoms and, on occasion, even more than one atom at a time, rules governing the order in which hydrogen bonds are preferentially formed have been proposed by Etter.<sup>29</sup> This is particularly important when choosing molecules and functional groups to employ in the design of a specific structure. If one set of interactions is dominant over another, yet the second interaction is the desired one, the dominant interaction will disrupt the formation of the second interaction. The first rule states that “*all good proton donors and acceptors are used in hydrogen bonding*”.<sup>29</sup> Good proton donors and acceptors in this sense predominantly refer to the very strong and strong hydrogen bond interactions listed in Table 1.2. The functional groups generally included in these classes are interactions between acids, bases, alcohols, amines, amides and carbonyls.<sup>7</sup> The second rule states that “*six-membered-ring intramolecular hydrogen bonds form in preference to intermolecular hydrogen bonds*”.<sup>29</sup> After all the good proton donor and acceptor atoms are involved in hydrogen bonding, intramolecular hydrogen bonds will first form before any other intermolecular hydrogen bonds. The third rule states that “*the best proton donors and acceptors remaining after intramolecular hydrogen-bond formation form intermolecular hydrogen bonds to one another*”.<sup>29</sup> This includes the weaker hydrogen bonds such as C—H···O and O—H···π interactions.<sup>7, 21, 31</sup> This hierarchy of hydrogen-bond formation holds for all neutral species. When ionic species are present, they of course take precedence over

any other possible hydrogen bond pairs due to the stronger hydrogen bond interaction between charged species.

### 1.2.3. Multicomponent systems

Crystallisation has long been used as a method to purify products of reactions, where a single component is crystallised or recrystallised from a suitable solvent to ensure the exclusion of impurities. However, in supramolecular chemistry, and more specifically crystal engineering, crystallisation has been used as a means to create multicomponent systems that consist of more than one type of molecule within the same crystal structure, using the various intermolecular interactions discussed in the previous section. Various terms are used to describe different types of multicomponent systems, such as solvates, salts, cocrystals and polymorphs, to name but a few.

During the crystallisation process the solvent of crystallisation can occasionally be included in the crystal structure. These solid-state host-guest complexes are known as *solvates*.<sup>38</sup> The solvent molecules are often included in cavities or channels and the bulk solid may exhibit interesting properties. When the included solvent is water, these complexes are referred to as *hydrates*. Host-guest systems will be discussed in more detail in Section 1.3.

Multicomponent systems in which proton transfer has occurred from an acid to a base, within the same structure, are termed *salts*. These structures therefore contain ionic species and are of particular importance to the work discussed in this thesis. Due to the proton transfer from acid to base the already polarised hydrogen bond is further polarised, leading to shorter interaction distances in many cases, and subsequently to stronger interactions.<sup>39</sup> It is generally accepted that salt formation will occur if the  $\Delta pK_a$  ( $\Delta pK_a = pK_a(\text{base}) - pK_a(\text{acid})$ ) of the reaction is greater than two or three.<sup>40</sup> While this is a good guideline to use, one must remember that  $pK_a$  is measured in solution, and therefore cannot always be accurately applied to the solid state. Ambiguity between salt and cocrystal formation arises in the region where  $\Delta pK_a$  is between zero and three and occasionally structures form that contain mixtures of ionised and unionised species.<sup>40</sup> Salt formation appears to have a somewhat disruptive effect on the formation of the most likely supramolecular synthons within a crystal structure.<sup>39</sup> This sometimes leads to the inclusion of a free or unionised acid,<sup>39</sup> which gives rise to new and unpredictable packing motifs in the solid state.

The term *cocrystal* has possibly been one of the most controversial terms put forward in the chemical crystallography community and has elicited much heated debate. Due to the discord concerning a specific definition of the term, many groups rather state what they understand a cocrystal to be and proceed to define it in terms of their work.<sup>38</sup> Aakeröy and Salmon<sup>41</sup> outlined three criteria to which they subscribe regarding the definition of a cocrystal, the first of which states that only crystals that are composed of neutral molecules will be defined as cocrystals, therefore excluding compounds that contain ions. The second condition states that only crystals that consist of reactants that are solids at ambient conditions will be defined as cocrystals. It has however been suggested that this condition be refined to rather state that no component should have played the role of the solvent of crystallisation.<sup>38</sup> Therefore solvates and hydrates and other such host-guest systems cannot be termed cocrystals. The third condition states that the components of a cocrystal should be neutral molecules present in well-defined stoichiometric quantities, which forms a structurally homogenous crystalline material. In general, most crystal engineers make use of these three criteria to some extent when defining cocrystals.

The term *polymorph* describes a chemical substance that can exist in more than one crystalline phase, i.e. different crystal structures that contain the same components in the same stoichiometry.<sup>38</sup> This has particular relevance to crystal engineering, since polymorphs often exhibit different properties, and therefore it could be possible to relate a solid state bulk property to a structure type or packing motif. Different types of polymorphism occur, such as *concomitant polymorphism*, which refers to instances where two or more polymorphs form in the same crystallisation vessel under the same crystallisation conditions.<sup>42</sup> *Conformational polymorphism* refers to conformationally flexible molecules that are able to adopt different conformations in the solid state.<sup>43</sup> Polymorphs are of particular interest in the pharmaceutical industry since a change in the crystal structure of a compound, or active pharmaceutical ingredient (API), often has ramifications for the properties of the compound, such as the solubility, stability and efficacy of the API.<sup>44</sup>

#### **1.2.4. Self-assembly and shape complementarity**

Molecular self-assembly was defined by Whitesides as “*the spontaneous association of molecules under equilibrium conditions into stable, structurally well-defined aggregates joined by noncovalent bonds*”.<sup>45</sup> Self-assembly relies on molecules recognising a molecular

complementarity and consequently aggregating through noncovalent interactions to form a thermodynamically stable supramolecular structure.<sup>21</sup> Due to aggregation relying on weaker noncovalent bonds it is possible for molecules to associate and disassociate reversibly in order to find the correct fit, in other words “self-healing” occurs when two molecules do not fit together perfectly, so that the most stable structure can be obtained.<sup>21</sup> In this sense a shape-match between molecules is also paramount to ensure a correct fit for maximum packing efficiency.<sup>46, 47</sup> Kitaigorodskii stated that crystals assemble according to the principle of close packing,<sup>48</sup> which implies that molecules will form the maximum number of contacts to ensure maximum packing efficiency and the minimum amount of void space in the solid-state structure. Host-guest chemistry particularly relies on molecular recognition and the close packing of molecules to minimise void space in the solid state.<sup>21, 46</sup> In this study we also rely on the process of molecular recognition to drive the assembly of molecules, but we aim to use highly directional interactions, such as charge-assisted hydrogen bonds and other interactions discussed in this section, to overcome the close packing of molecules to potentially allow for the formation of voids in the solid state.

### 1.3. Host-guest chemistry

Host-guest chemistry can trace its roots back to 1756, when Axel Crönstedt first described zeolites, and 1778 when Joseph Priestley first discovered clathrate hydrates.<sup>4</sup> Donald Cram<sup>4, 49</sup> has since then defined the relationship between host and guest as follows:

*“A host-guest relationship involves a complementary stereo-electronic arrangement of binding sites in host and guest... The host component is defined as an organic molecule or ion whose binding sites converge in the complex... The guest component as any molecule or ion whose binding sites diverge in the complex...”*

Since then the field of host-guest chemistry has expanded exponentially and can no longer only be restrained to organic molecules.

There are three core concepts that play an important role in host-guest chemistry, the first of which is the realisation by Paul Ehrlich in 1906 that molecules are unable to act if they do not first bind,<sup>50</sup> which is in essence the concept of a biological receptor. This implies that there first has to be a stable interaction between molecules before complexation can take place.



While studying receptor-substrate binding in 1894, Emil Fischer recognised that binding between molecules must be selective, and he introduced the *lock-and-key* concept.<sup>51</sup> This concept proposes that the guest molecule must have a steric fit and complementarity towards the host material. This type of *molecular recognition* explains why some host materials selectively include some guest molecules over others and forms the second core concept of host-guest chemistry.<sup>4, 51</sup> The third concept rests on the belief that there must be attraction or mutual affinity between the host and the guest for complexation to take place.<sup>4</sup>

Host guest chemistry therefore relies heavily on two principles, that of complementarity and preorganization.<sup>51</sup> In order for host and guest to recognise each other and form an assembly, there has to be shape and size complementarity along with the correct interplay of noncovalent interactions. This is however not always enough to drive complexation.<sup>51</sup> It is also necessary for conformationally flexible molecules to orientate themselves in such a way that a better fit is induced with the partner molecule. This is known as *preorganization*.<sup>51</sup> This could lead to the conformationally flexible molecule converting to a higher energy state in order to fit the partner molecule, but the sacrifice is worth it due to the complexation of the molecules forming a complex with a lower energy state.<sup>51</sup> One must therefore always be aware that the assembly of molecules is not a trivial exercise. There are various conditions that have to be satisfied and successful crystallisation is due to a careful balance between intermolecular interactions, fit and energy state.

Host-guest complexes in the solid state can broadly be divided into two classes, although there are no hard-and-fast rules.<sup>52</sup> Lattice-type inclusion compounds consist of host molecules which pack in such a way that cavities, channels or layers are formed that can accommodate guest molecules.<sup>53</sup> Examples of lattice inclusion compounds are clathrates.<sup>4</sup> The term “clathrate”, from the Latin word “clathratus”, means closed or surrounded from all sides.<sup>50</sup> In inclusion compounds such as clathrates the host interacts with guest molecules while in solution, but the true lattice inclusion compound only exists in the solid state. The second class of host-guest complexes form when a convex guest fits into the concave cavity of the host.<sup>53</sup> Cyclodextrins, carcerands, calixarenes and cyclophanes are all examples of hosts which form this type of host-guest complex.<sup>53</sup> What distinguishes these host-guest complexes from the lattice inclusion compounds is the fact that the host is a large rigid molecule that has an inherent cavity for a guest molecule. The host is not assembled *in situ*, but is preassembled through covalent synthesis and consequently the host-guest complex is able to exist in

solution and not only in the solid state. Figure 1.7 graphically represents the formation of the two classes of host-guest complexes.

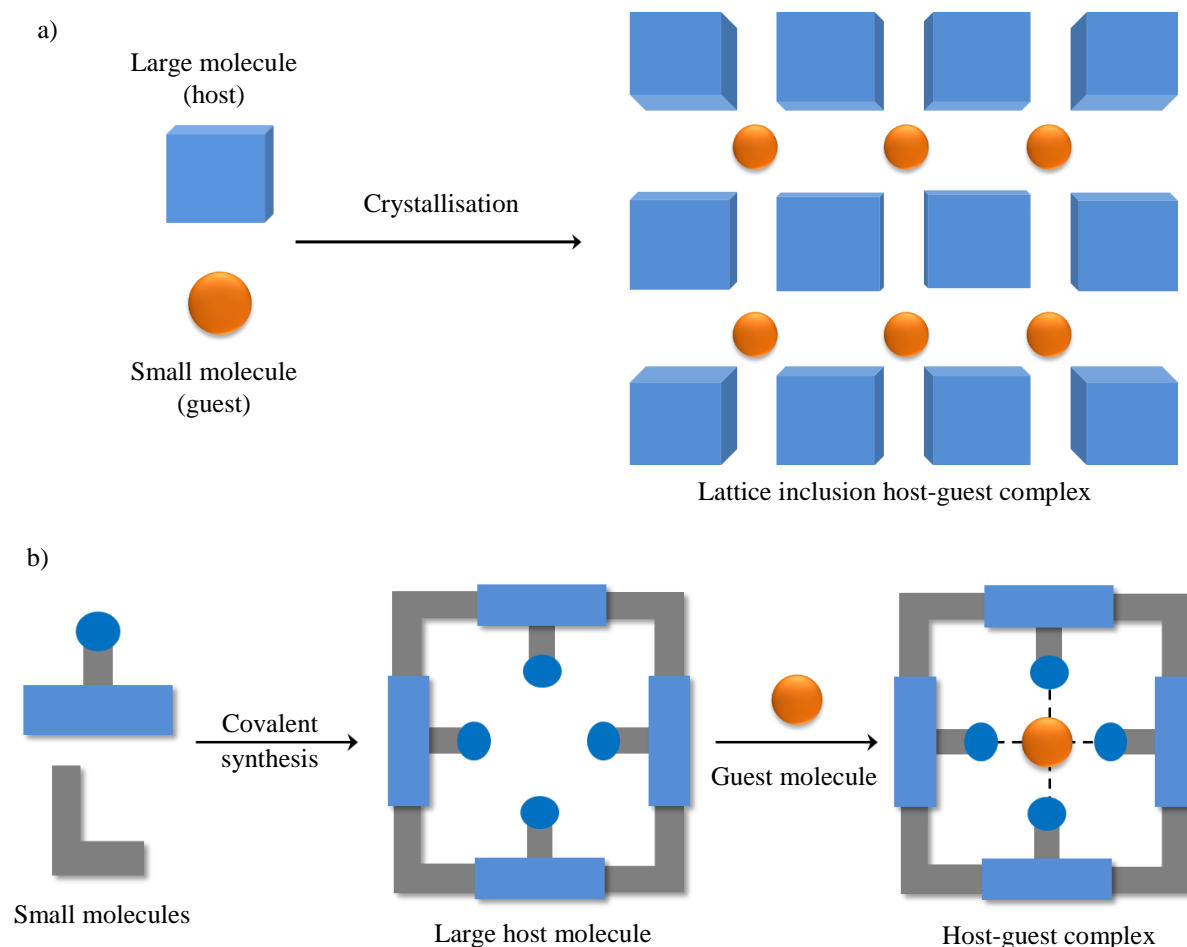
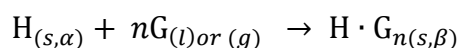


**Figure 1.7** The two main classes of host guest complexes. a) Lattice inclusion host-guest complex that only exists in the solid state. b) A rigid, covalently preassembled host molecule that encapsulates a guest molecule. This complex exists in both the solution and solid state. This image was adapted from reference 4.

A general formula for the formation of an inclusion compound<sup>54</sup> can be written as follows:



where  $\alpha$  represents the nonporous phase of the pure host H or the apohost,  $\beta$  is the phase of the host-guest complex and  $n$  is the host:guest ratio.<sup>54</sup>

The synthesis of an inclusion complex is usually performed by dissolving the host molecule in a particular solvent or liquid guest and allowing the solution to concentrate, often by slow evaporation. A noncompetitive solvent can be used, depending on the type of host molecule or other molecules present during the crystallisation process. However, one must bear in mind

that the noncompetitive solvent may influence the outcome of the final product due to the templating effect.<sup>55</sup> Different forms of the host-guest complex could then be generated due to the presence of a templating, noncompetitive solvent. In some cases single crystals can be grown by exposing the powdered host compound to the vapour of a solvent. The general process of formation of inclusion compounds and decomposition by heating is shown in Figure 1.8. There are three different scenarios that can occur upon heating of the  $\beta$ -phase. Firstly, decomposition can either yield the original  $\alpha$ -phase, or a new guest-free phase (c). The  $\beta$ -phase can undergo a phase transformation to yield a new  $\gamma$ -phase with new properties and this can also coincide with a change in the host:guest ratio (d). A third option is that the empty host  $\beta_0$  can be formed with the framework remaining intact.<sup>54</sup> This is of course the most sought-after product if the aim is to generate a potentially porous framework material.

Host-guest chemistry is a vast field of research with far-reaching real-world application. Host-guest complexes have been used as drug-delivery vehicles since they are able to encapsulate drug molecules without altering their properties.<sup>56-59</sup> Host-guest materials have been successfully used as sensing materials due to their inherent fluorescence properties or guest-triggered fluorescence.<sup>60, 61</sup> Introducing dye-molecules into host structures allows for the use of these materials in liquid-crystal displays (LCDs).<sup>62, 63</sup> Some host-guest systems are porous and have been used to store gases such as methane, carbon dioxide<sup>64</sup> and hydrogen,<sup>65</sup> which of course has many implications for carbon dioxide sequestration from the atmosphere and the future potential use of hydrogen as a fuel source. Host-guest complexes have been used to remove hazardous compounds from the environment, such as the capture of cesium<sup>66</sup> and carcinogenic aromatic amines<sup>67</sup> by *p-tert*-butylcalix[4]arene derivatives.

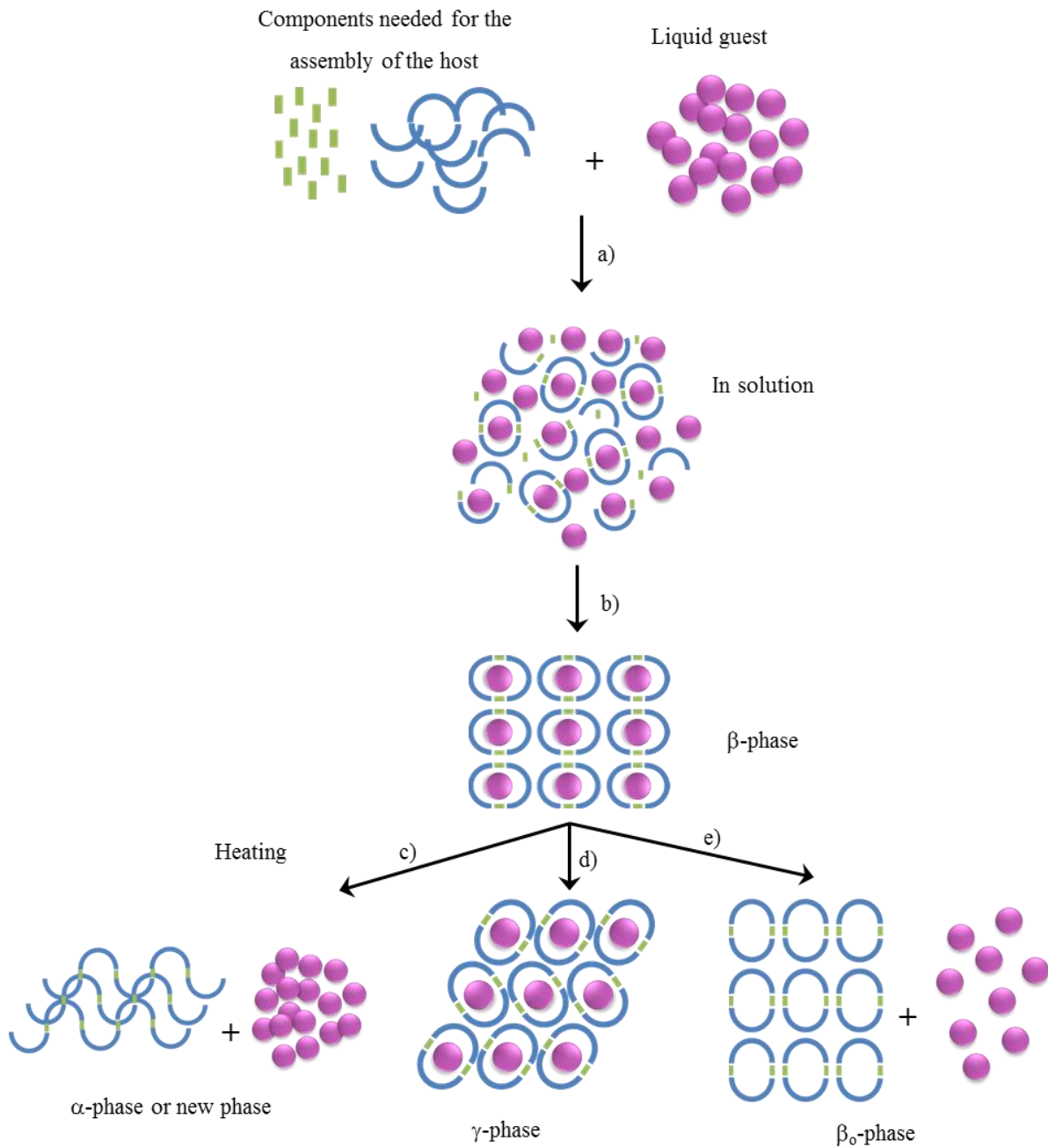


**Figure 1.8** The general process for the formation and thermal decomposition of inclusion compounds. This image has been adapted from reference 54.

## 1.4. Porosity

Of the many potential properties host-guest systems can possess, porosity has possibly been one of the best studied. Since molecules tend to close pack to ensure minimum void space is left in the crystal structure, obtaining crystals that are truly porous is quite rare.<sup>38</sup> Interest in the porosity of crystals is generally geared towards application in separation, heterogeneous catalysis, drug delivery, sensing and gas storage.<sup>68, 69</sup> The potential future use of hydrogen as a fuel source has also prompted much research into the controlled uptake and release of hydrogen, as well as the ability to safely store it.<sup>70</sup>

To determine whether a supramolecular structure is truly porous, Barbour<sup>70</sup> suggested in a paper entitled “*Crystal porosity and the burden of proof*” that two key aspects be met when claiming a host is porous. First of all, it must be shown that the host is permeable to either solvent or gas, since “porous” and “permeable” are inextricably linked. The host framework should remain essentially unaffected by the exchange, uptake or removal of the guest molecules and proof must therefore be supplied that the host framework integrity is not compromised. In short, a porous material can be defined as a material that allows the passage of another substance through its bulk dynamically.<sup>38</sup> There are different mechanisms for the movement of a guest through a framework material and therefore Barbour<sup>70</sup> identified three types of porosity:

### Virtual porosity

This is not true porosity and is simply a result of removing solvent molecules from the crystal structure model to make a structure appear porous.<sup>70</sup> This can also occur when a packing diagram is viewed in the capped-stick or ball-and-stick representations. A space filling diagram however takes into account the van der Waals radii of atoms and therefore gives a somewhat more accurate view of possible void space.

### Porosity without pores

This applies to crystals that contain discrete cavities yet are still able to allow a guest molecule to pass throughout the structure. This however implies that the host structure does not remain unaffected during the exchange process as molecules or layers have to move in order to accommodate the passage of the guest.<sup>70</sup>

## Conventional porosity

This is the type of porosity that zeolites possess and can be proven if the guest molecules can either be completely removed, or exchanged for other guests without the framework structure collapsing or significantly changing.<sup>70</sup>

Host-guest complexes can contain one-, two- or three-dimensional channels throughout the structure, and in the case of two- and three-dimensional channels they often interconnect to form networks of channels.<sup>38</sup> If the guest-accessible regions of the crystal are not interconnected, then these regions are referred to as cavities or (guest) pockets. The term void refers to cavities or pockets from which the guest molecule has been removed. A pore is an opening that refers to the window between neighbouring pockets that are connected to each other.<sup>38</sup>

When studying and discussing porous materials it is vital to know the size or volume of the channel or cavity. Computer programmes such as MSROLL<sup>71</sup> calculate the contact surface volumes whereas programmes such as PLATON<sup>72</sup> calculate the solvent accessible volumes. Both these programmes use a probe sphere of a chosen radius to sweep out the volume of a cavity or channel. The volume that is mapped to where the probe touches the van der Waals surfaces of the molecules that constitute the walls of the cavity is known as the *contact surface volume*.<sup>73, 74</sup> The centre of the probe traces a volume that is known as the *solvent accessible volume*<sup>73, 74</sup> and is generally used to indicate the theoretical presence of continuous channels and, in some cases, porosity. The result is highly dependent on the chosen probe radius, and therefore care must be taken to choose a sensible value. A hydrogen atom has a radius of 1.17 Å and therefore smaller values for the probe radius are meaningless. Generally probe radii between 1.4 and 1.7 Å are chosen.

## 1.5. Framework materials

There is no formal definition for the term “framework” in supramolecular chemistry. The Oxford dictionary<sup>75</sup> defines “framework” as an “*essential supporting structure...*” or “*a basic structure underlying a system*”, whereas The Free Dictionary<sup>76</sup> slightly expands on this definition by describing a framework as “*a structure for supporting or enclosing something else, especially a skeletal support*”. The term is also not exclusively used in conjunction with porous materials.<sup>77</sup> In most cases the term “framework” is used interchangeably with

“network” and refers to separate components that are interconnected *via* hydrogen bonds or coordination bonds (in metal-organic frameworks) in at least one direction in the solid state structure.<sup>78-81</sup> Ward<sup>36</sup> describes a network as an infinite structure in one, two or three dimensions. In the tartrate salts of organic diamines the interconnected sheets of tartaric and pillars of diamines are described as frameworks, even though they do not always form cavities or channels.<sup>82</sup> Pyridinium derivatives and L-malate derivatives also form infinite layers of anions with the cations acting as pillars to connect the layers, which Aakerøy and Nieuwenhuyzen described as two-dimensional frameworks.<sup>83</sup> For the purposes of this study, the term “framework” will therefore refer to an extended and interconnected structure, usually through hydrogen bonds, that forms the basic support for the crystal structure and contains guest molecules in cavities.

Framework materials can broadly be placed into three different categories: metal-organic frameworks, covalent organic frameworks and hydrogen bonded organic frameworks.

### 1.5.1. Metal-organic frameworks (MOFs)

In the field of supramolecular chemistry metal-organic frameworks (MOFs) need almost no introduction. They consist of metal centres connected to organic linkers through coordination bonds and form relatively rigid structures in the solid state that often include guest molecules in cavities or channels. Research into MOFs was originally inspired by the works of the Swedish mineralogist Axel Fredrik Crönstedt on the open framework aluminosilicate zeolite hosts.<sup>4, 84</sup> The term “zeolite” is derived from the Greek words “zeo” (to boil) and “lithos” (stone) due to the fact that zeolites release water (or any other guest) upon heating.<sup>38</sup> However, these large rigid structures are difficult to modify and their pore sizes cannot be easily controlled. MOFs, on the other hand, allow flexibility regarding the choice of components and the subsequent assembly of these components; the advantage being that it is not necessary to synthesise complicated, covalently-linked structures in order to generate a solid-state complex with the desired properties. Organic molecules serve as the linkers between metal nodes and due to the length of the linker it is possible to generate permanently porous solids that contain high surface areas while the metal-organic framework is stable enough to allow the removal of included guest molecules without collapse of the structure.<sup>84</sup> This concept is illustrated in Figure 1.9 where the length of the carboxylic acid linker determines the size of the pore, shown as a yellow sphere.<sup>85</sup>



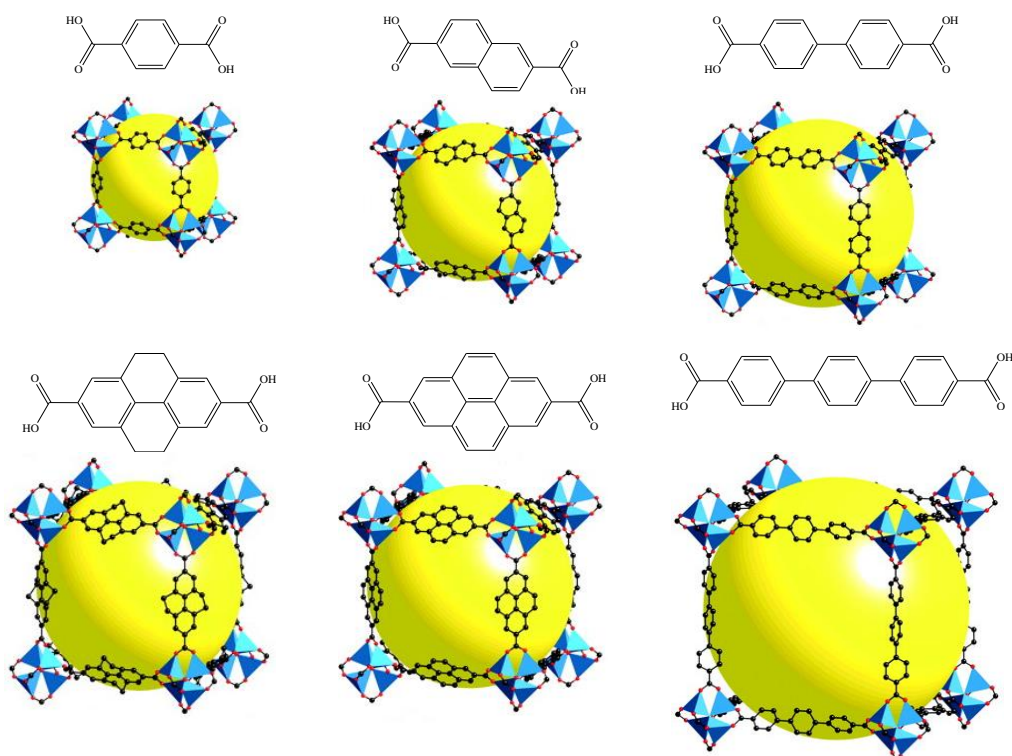


**Figure 1.9** MOFs formed by reacting carboxylic acids with Zn(II). The length of the carboxylic acid linker regulates the size of the pore (yellow sphere) and the subsequent porosity. This image has been adapted from reference 85.

Due to the great flexibility in the assembly of MOFs, various properties can be engineered into these materials. The hydrogen economy is of special importance currently due to the dwindling availability of carbon-based fossil fuels. To some extent MOFs have been able to reversibly include and store hydrogen gas.<sup>86</sup> This occurs through adsorption of hydrogen to the channels of MOFs, which allows hydrogen to be removed without the use of high temperatures as in the case of chemisorption where the hydrogen reacts with the functional groups in the walls of the framework, often irreversibly.<sup>65, 87</sup> MOFs have also been employed in the fields of sensing<sup>88</sup> and separation<sup>89-91</sup> due to their photoluminescent properties.<sup>88, 92</sup> The use of MOFs in drug delivery<sup>93-97</sup> has also caught our attention since one of the building blocks of this study is the pharmaceutically acceptable salt pamoic acid. If we could design a framework material that consists of only Generally Regarded as Safe (GRAS) materials and include a drug molecule into the structure, we could circumvent the problem MOFs could experience regarding toxicity due to the metals used in the frameworks. Biodegradable MOFs have however been developed to some extent.<sup>98</sup> MOFs have become an increasingly popular synthetic product for the aim of designing a myriad of materials with interesting properties and therefore recent reviews have surfaced in which possible design strategies to generate



porous materials are discussed.<sup>99, 100</sup> Guillerm *et al* even go so far as to suggest using a rare earth nonanuclear carboxylate-based cluster as a blueprint for the generation of other MOFs, to some success.<sup>101</sup> In a review amusingly entitled “*MOFs: Rise of the Ligands*” special investigation was made into ligands used to construct MOFs in order to optimally encode specific functions into these materials.<sup>102</sup> This means that recently more attention has been devoted to the organic part of the metal-organic framework by designing more elaborate and highly functionalised organic linkers. This allows more properties to be encoded into the MOF *via* the organic linker, such as luminescence<sup>92</sup> and chirality<sup>103</sup> which, in turn, could generate materials with the potential for non-linear optical activity due to the possible alignment of guest molecules by the chiral framework.

A special mention should also be made of a small subclass of metallated compounds called metallocycles.<sup>104-107</sup> These materials are not MOFs, but have been included because they contain metals. They are discrete units that consist of organic linkers and metal nodes that stack together to form either channels or cavities in the solid state. The design strategy of these systems was followed to some extent in this thesis. For the design of metallocycles, linkers are chosen according to their shape, generally C-shaped, to connect to the metal centres through imidazole moieties, forming a “doughnut-shaped” unit. In our case, the metal node was substituted with an organic heterocycle containing two nitrogen atoms. This concept is illustrated in Figure 1.10.

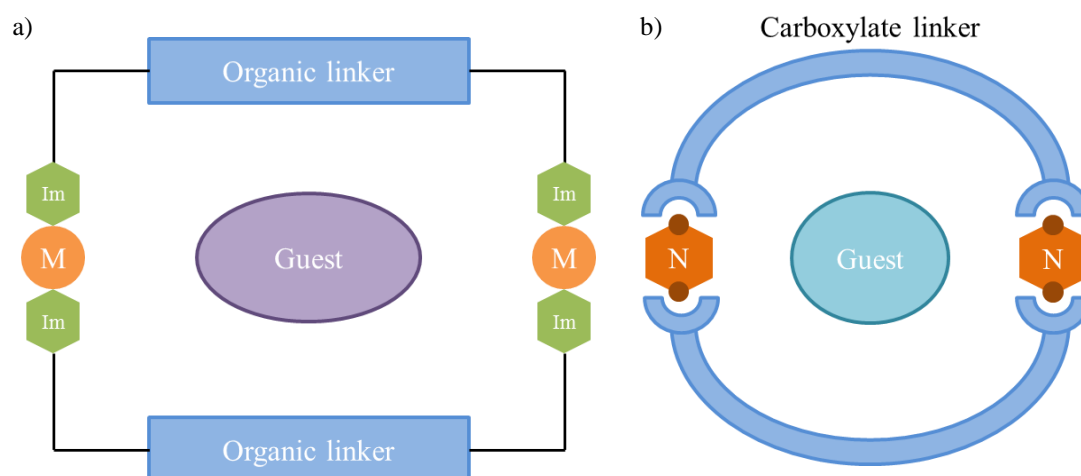


**Figure 1.10** The design strategy of a) metallocycles and b) the strategy used in this study. M refers to the metal centre, Im to the imidazole moiety and N to the N-heterocycle.

## 1.5.2. Covalent organic frameworks (COFs)

For a long time it was believed that the crystallisation of linked organic molecules into large covalently linked organic frameworks was a difficult endeavour, if not bordering on the impossible. However, in 2005 Côté *et al* reported a covalent organic framework that was synthesised through the condensation reaction of phenyldiboronic acid and hexahydroxy triphenylene.<sup>108</sup> The result was a rigid, covalently joined structure with pore diameters of 27 Å (Figure 1.11).

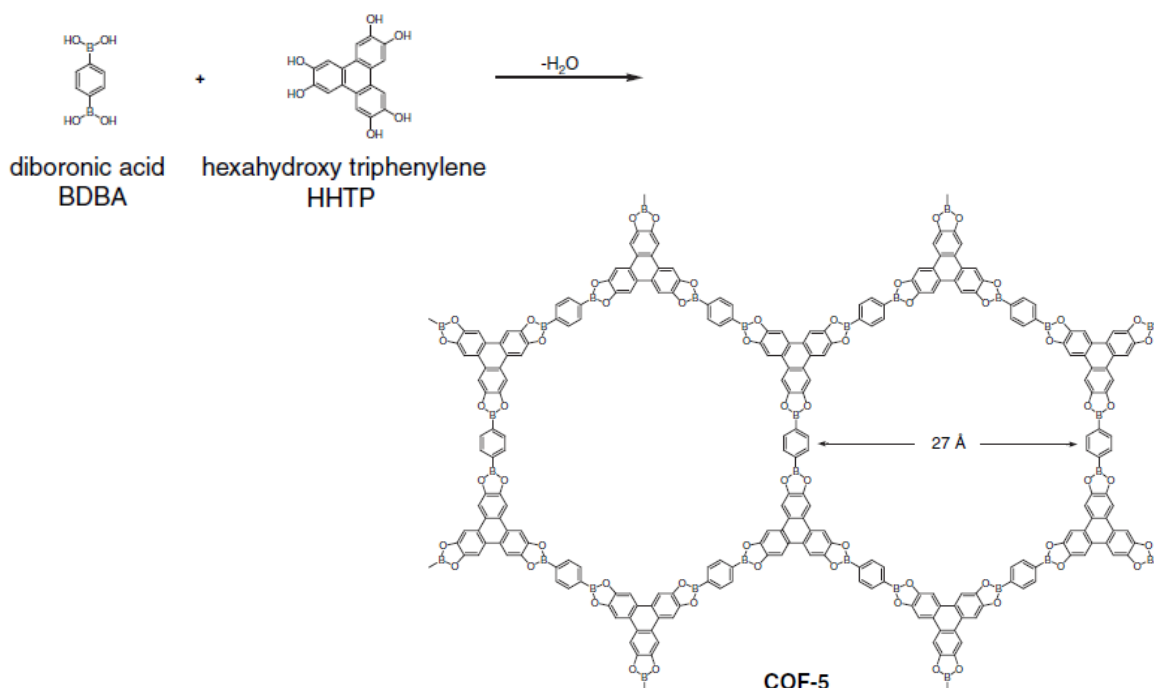


**Figure 1.11** The covalent organic framework generated by the condensation reaction between phenyldiboronic acid and hexahydroxy triphenylene with 27 Å pores. This image has been taken from reference 108.

The large cavities and channels of COFs and their highly porous character results in these materials having extremely low densities. The density of diamond is  $3.50 \text{ g/cm}^3$ , whereas the densities of COFs such as COF-108 have the lowest densities ever recorded<sup>109-111</sup> –  $0.17 \text{ g/cm}^3$ , lower even than some highly porous MOFs such as MOF-5.<sup>85</sup> COFs therefore showed improved gas sorption capabilities compared to MOFs and research into the field drastically expanded. Wan and co-workers incorporated  $\pi$ -conjugated systems into the starting materials for COFs such as 2,3,6,7,10,11-hexahydroxytriphenylene (HHTP) and pyrene-2,7-diboronic acid (PDBA), shown in Figure 1.12, which gave TP-COF (triphenylene and pyrene COF) luminescent and semiconducting properties.<sup>112</sup>

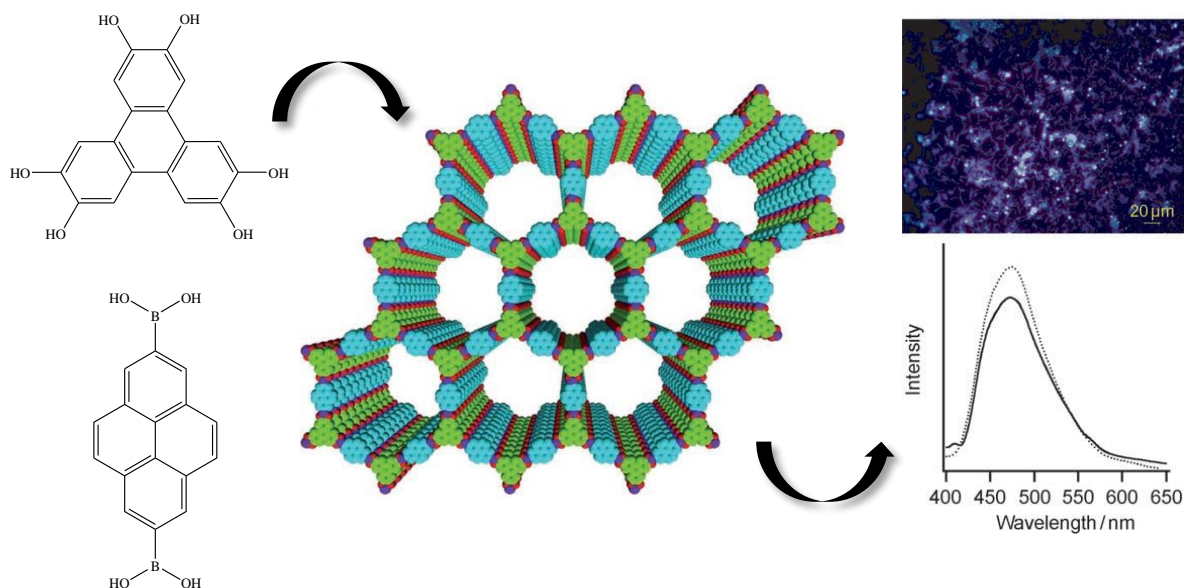


**Figure 1.12** The design, structure and luminescent properties of TP-COF. These images were taken from reference 112.

COFs have also been synthesised by the condensation reaction between hydrazine and formyl moieties and they also form the characteristic honeycomb structures of the boronic acid COFs with pore diameters of at least 28 Å.<sup>113</sup> Interesting functional groups such as the benzothiadiazole group were incorporated into starting materials to create 2D-NiPc-BTDACOF.<sup>114</sup> The incorporation of the benzothiadiazole group transformed the structure into an electron-transporting framework which is useful for photoconductivity in, for instance, solar cells.<sup>115-117</sup>

Recent research into COFs has centred around developing better strategies to synthesise the porous frameworks by studying the types of ligands used for synthesis and proposing three different mixed-ligand approaches to the design process, namely isostructural, heterostructural and truncated mixed ligand approaches.<sup>118</sup> The isostructural approach entails the use of two or more organic building blocks with the same size and linkage chemistry. In the heterostructural approach organic building blocks of different linkage geometry are chosen and in the truncated mixed ligand approach monomers with a different number of reactive groups are condensed, which in turn regulates the percentage of these two monomers throughout the structure.<sup>118</sup> The limiting feature of COFs which prohibits them from completely surpassing MOFs is the fact that they very rarely form single crystals of X-ray diffraction quality and most analyses have to be performed on powders. They also tend to

crystallise with starting materials present in the channels. Research has therefore focused on new and more reliable ways to generate these frameworks as crystalline materials. There have been attempts to discover solvent combinations that allow for the complete dissolution of the COF starting material since these do not readily dissolve and often precipitate with the product.<sup>119</sup> This has led to much better crystallisation conditions without the problem of unreacted monomer precipitating in the cavities of COFs due to the limited solubility of monomer and product. Liquid-assisted grinding techniques have also proved successful in producing COFs.<sup>120</sup>

### 1.5.3. Organic cages and nanoporous molecular crystals (NMCs)

Another class of inclusion compounds are formed by discrete, bulky molecules that are not able to pack efficiently in the solid state and therefore leave voids<sup>69</sup> (nanoporous molecular crystals, NMCs), or larger covalently linked molecular cages that cannot pack efficiently in the solid state and consequently also form voids in the solid state. These materials are strictly speaking not framework materials since they do not consist of an infinitely connected 3-D structure, but they have been included in this discussion since they are organic materials that can be engineered to have certain properties.

Nanoporous molecular crystals include compounds such as tris(*o*-phenylenedioxy)-cyclotriphosphazene (TPP, nr **5** in Figure 1.13) and *t*-butylcalix[4]arene (nr **1** in Figure 1.13).<sup>68</sup> TPP packs to form a highly symmetrical structure with channels in the solid state, whereas *t*-butylcalix[4]arene packs inefficiently due to its awkward shape. It has been shown that *t*-butylcalix[4]arene allows the passage of guest molecules through the bulk of its structure even though the material does not contain any continuous channels.<sup>70</sup> Nanoporous materials are particularly rare, but there is on-going research into this field.<sup>121, 122</sup>

Cage-type organic frameworks give the supramolecular chemist the choice between pre- or post-synthetic modification of the building blocks. This allows for a higher control of the properties that can be encoded into these materials.<sup>123</sup> Specific solvents have also been used effectively to control the crystallisation of the organic cages. Hasell and co-workers showed how the presence of 1,4-dioxane influences the crystallisation of the organic cage (**12**, **13** and **14** in Figure 1.13) and transforms it from a 2-D pore network to a 3-D diamondoid pore network.<sup>124</sup> Extensive research has been devoted to predicting the manner in which the

organic cages will crystallise, and Jones *et al* have made great strides towards reaching this goal.<sup>125</sup> Organic cage compounds have also shown promise for selective gas sorption, as shown by Mastalerz and co-workers with their salicylbisimine cage compound which contains high surface area and shows selective CO<sub>2</sub>/CH<sub>4</sub> adsorption.<sup>126, 127</sup> Figure 1.13 contains some of the known molecules either associated with NMCs or organic cage frameworks.<sup>122</sup>

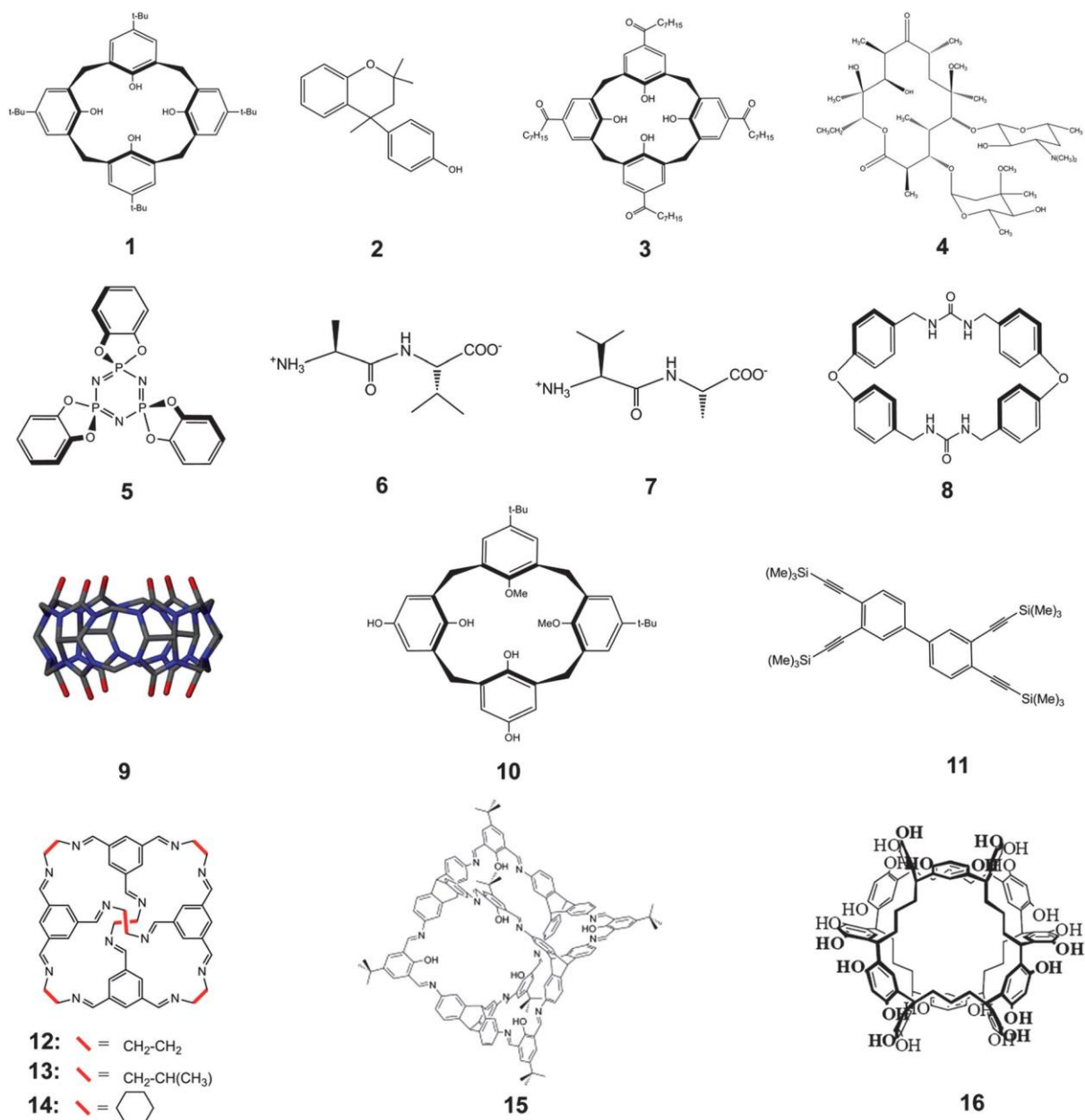


**Figure 1.13** Examples of molecules used to construct NMCs or cage-like organic frameworks. 1 – 4, 12: Porous structures with 0-D voids; 5 – 9, 13: Porous structures with 1-D channels; 14, 15: Porous structures with 3-D channels; 16: Amorphous materials. This image has been taken from reference 122.

### 1.5.4. Hydrogen-bonded organic frameworks (HOFs)

Although hydrogen-bonded organic frameworks (HOFs) have only recently become a popular research niche, the concept of using hydrogen bonds to form flexible networks was first introduced by Wuest and co-workers in 1988.<sup>128-130</sup> They predicted that a molecule with tetrahedral geometry and four “sticky sites” (hydrogen bonding sites) should form a cubic diamondoid framework in the solid state. Shortly thereafter the guanidinium sulfonate framework series was discovered and to date is probably the most beautiful body of work on using hydrogen bonds to control properties such as non-linear optics and pore size in the solid state.<sup>131, 132</sup> The guanidinium cations form hydrogen-bonded sheets while the sulfonate anions form the pillars that connect these sheets. Figure 1.14 contains a diagrammatic representation of the solid state structure of the guanidinium sulfonate frameworks. By varying the size and length of the disulfonate pillar it is possible to control the pore size of the framework.<sup>133</sup> Since the hydrogen bonds in the guanidinium sulfonates are formed between anions and cations, the interaction is much stronger than hydrogen bonds between neutral molecules, adding strength and stability to the framework structure. Due to the interactions between the host and the guest, the framework also has the ability to control the orientation of the guests within the channel, despite steric interactions between guests. They propose a mechanism whereby steric interactions between guests combined with the conformationally flexible sulfonate pillars act as “*synchronous molecular gears*” that communicate guest ordering from pore to pore.<sup>134, 135</sup> It was further discovered that the framework causes guest molecules to align along a polar axis, resulting in the potential for second harmonic generation and non-linear optical properties.<sup>136</sup>

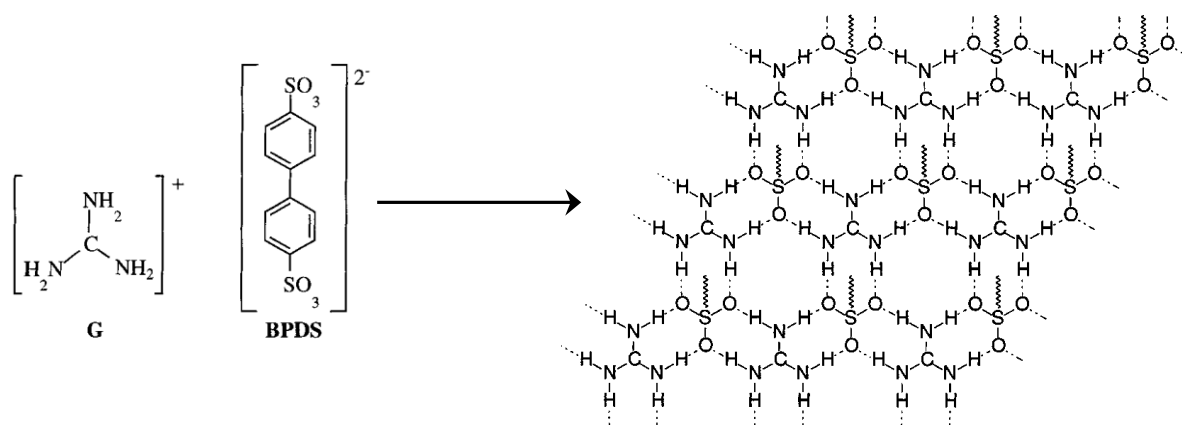


**Figure 1.14** A diagrammatic representation of the solid state structure of the guanidinium sulfonate frameworks with 4,4'-biphenyldisulfonate. This image has been taken from reference 134.

Intensive research has been conducted on the guanidinium sulfonates over the years, focusing on their inclusion capabilities and developing design strategies to predict the crystallisation patterns of these compounds.<sup>137-146</sup> The guanidinium sulfonates have made a large contribution towards understanding the packing of molecules in the solid state and how to tune the organic building blocks to design specific framework materials using only hydrogen bonds. A calix[4]arene has been functionalised on the upper rim with the sulfonate moieties in order to exploit the robust and highly directional interaction between the sulfonate anions and the guanidinium cations to form capsules that include guest molecules in the solid state.<sup>147</sup> Laser dyes have been included in the guanidinium sulfonate frameworks<sup>148</sup> and, most excitingly, radical compounds have also been included in these frameworks, which is important for information storage and quantum computing.<sup>149</sup>

One of the first HOFs proven to be permanently porous is HOF-1 which consists of melamine with one phenyl group in the place of one of the amine groups.<sup>150, 151</sup> This building block forms an extended hydrogen-bonded framework of neutral molecules (no charge-assisted hydrogen bonds are formed) with a pore diameter of 8.2 Å and shows high selectivity for ethylene and ethane gas absorption.<sup>150</sup> 2,6-diaminopurine has also proved to be a reliable building block for the formation of HOFs. In this case the organic building blocks are also neutral and do not make use of charge-assisted hydrogen bonds.<sup>152</sup> Various other HOFs consisting of neutral organic molecules that form hydrogen bonds have been identified,<sup>126, 153-155</sup> but our interest lies in frameworks that are generated through the use of charge-assisted hydrogen bonds. There are a few examples of these types of frameworks,<sup>61, 156, 157</sup> but only one charge-assisted HOF will be briefly discussed here. Recently Yamamoto and co-workers published a series of diamondoid porous organic salts<sup>158-161</sup> consisting of triphenylmethylamine and various sulfonic acids. The frameworks incorporate a combination of charge-assisted hydrogen bonds and neutral hydrogen bonds or  $\pi$ - $\pi$  stacking (Figure 1.15), thereby forming robust and highly stable diamondoid porous organic salts (*d*-POSs). Due to the flexibility the hydrogen bonds add to the structure, the frameworks are able to “breathe” to allow the exchange of guests and gases. If a fluorescent disulfonic acid is incorporated into the structure, not only does the framework retain its porous nature, but it also exhibits a tuneable fluorescent response to absorbed guest molecules (Figure 1.16).<sup>159</sup>



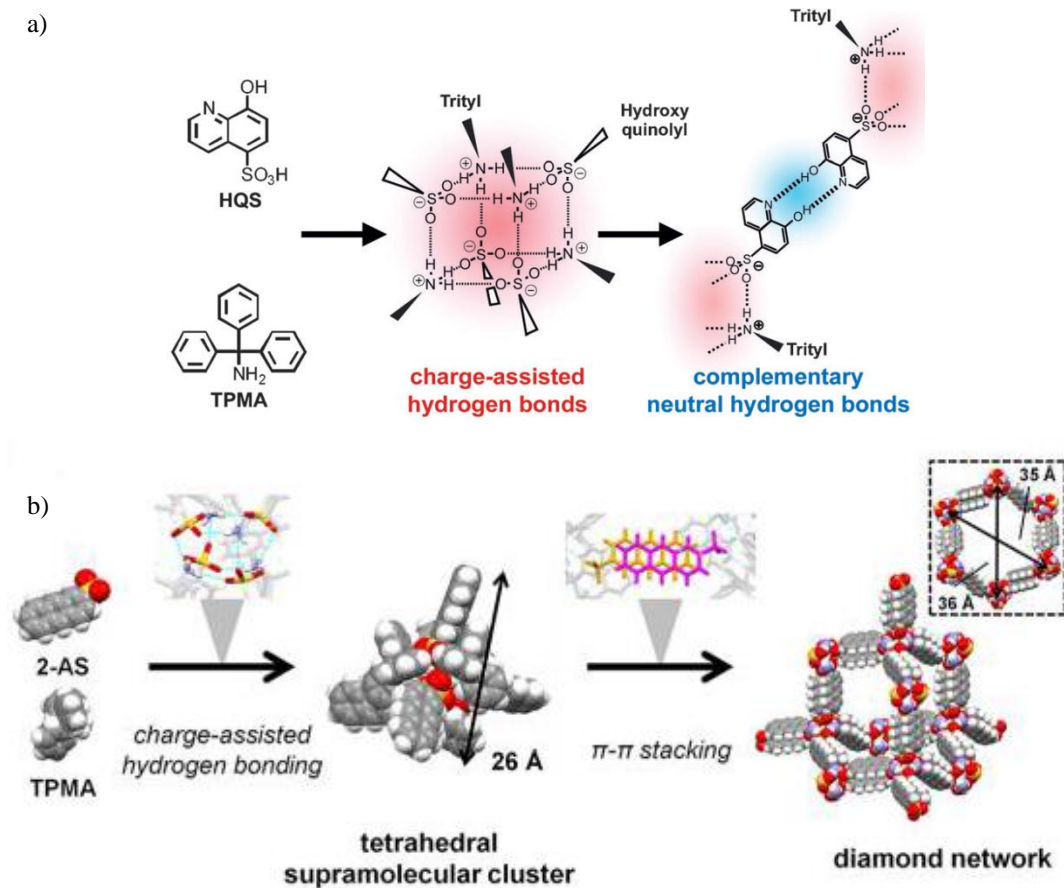


**Figure 1.15** The different combinations of interactions used in the synthesis of *d*-POSs. a) A combination of charge-assisted and neutral hydrogen bonds. b) A combination of charge-assisted hydrogen bonds and  $\pi$ - $\pi$  stacking. These images have been taken from references 160 and 161.

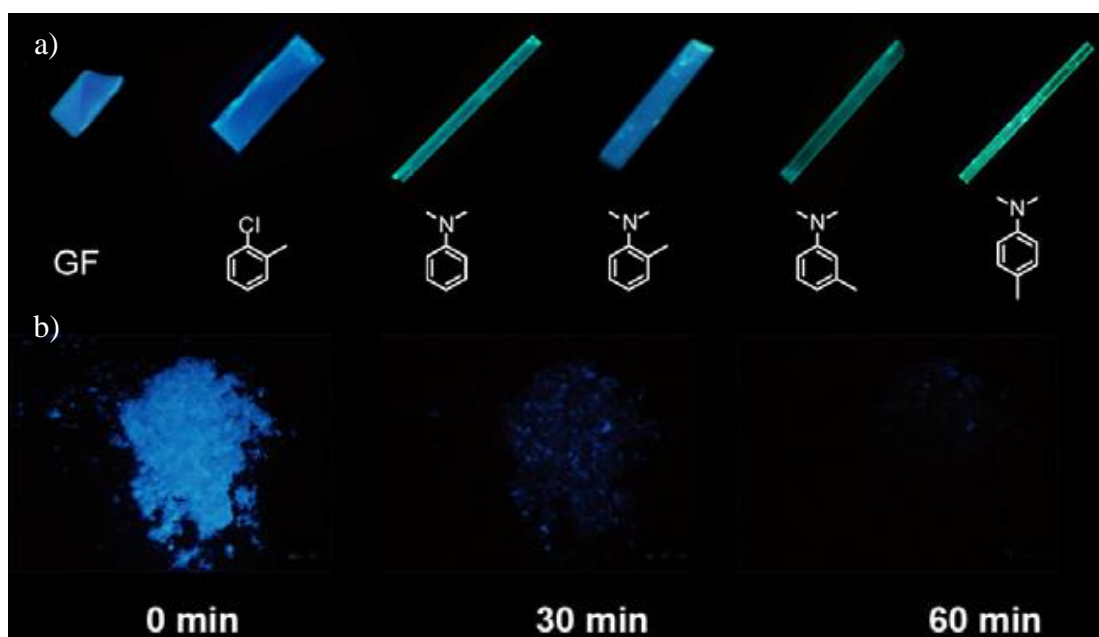


**Figure 1.16** The guest-dependent fluorescent properties of *d*-POS. a) Crystals under UV radiation with different guests (GF = guest-free). b) Diminishing fluorescence with the absorption of nitrobenzene. These images have been taken from reference 159.



## 1.6. Aim and scope of this study

The aim of this project is to use purely organic molecules to design and synthesise ionic organic framework materials based on carboxylate salts, with the intention of engineering interesting properties such as porosity, selectivity and non-linear optics into these materials. This study was inspired by a serendipitous discovery of a hydrogen-bonded organic framework, 3,4-lutidinium pamoate hemihydrate, with THF-filled channels in the solid state.<sup>162</sup> This framework will be discussed in detail in Chapter 2. We therefore wanted to investigate whether it was possible to purposely engineer similar ionic organic framework materials.

We specifically chose to work with only organic molecules due to the wide variety of molecules at our disposal. Organic molecules are often more soluble in common organic solvents, which increases the number of molecules that can be used to construct framework materials. It is also possible to incorporate different functional groups into one structure by the simple cocrystallisation of molecules. One set of functional groups can be used to direct the cocrystallisation of the molecules through synthons, while the remaining functional groups are available for potential post-synthetic modification. These functional groups can also serve as a coordination site for guest molecules, creating the potential for a guest-selective framework. It is therefore not necessary to use intensive synthetic procedures to create vast supramolecular assemblies as with COFs, but armed with an intelligent combination of small organic molecules it could be possible to create these assemblies. Without the need for long synthetic procedures it is also possible to perform many experiments in a shorter time frame. In other words, crystallisations can be used as a screening process to determine which molecules have the potential to form frameworks. Structures obtained from these crystallisations, whether they form frameworks or not, can also be used to help identify crystallisation patterns and structural features required for framework formation.

We intended to incorporate an ionic character into these framework materials through charge-assisted hydrogen bonds in order to lend greater stability to the framework. It has been shown in Section 1.5.4 that highly stable structures can be formed with the use of charge-assisted hydrogen bonds. The proton-transfer from acid to base further polarises the already electrostatic hydrogen bond, allowing for a stronger and more stable interaction, leading to

greater stability of the framework. By using charge-assisted hydrogen bonds as the glue to hold the framework together, we combine the strength of an ionic interaction with the flexibility of noncovalent interactions. In other words, the ionic interaction will lend stability to the framework upon guest removal, possibly allowing the framework to remain intact, while also allowing for greater flexibility of the framework in order to include different sized guests.

In this study we specifically chose to work with carboxylic acids in combination with various N-heterocycles. The interaction between carboxylic acids and pyridine derivatives is well established<sup>81, 163-167</sup> and is therefore a reliable supramolecular synthon to incorporate for the design of framework materials. This study primarily used dianions such as pamoic acid in combination with mono- and dication N-heterocycles. The choice of cation depended on the type of structural unit we wanted to employ. We attempted to cocrystallise a C-shaped dicarboxylic acid with a dication to form a circular unit as in the case of metallocycles (discussed in Section 1.5.1, Figure 1.10). These “doughnut-shaped” units could potentially stack together to form channels in the solid state. Another design strategy that was used during the course of this study was to limit the number of hydrogen-bond donor sites on the cation by using monocation species such as the isomers of lutidine and picoline and larger molecules such as 4-phenylpyridine. This restricts the number of hydrogen bonds that can form and therefore only the strongest, most reliable interactions are incorporated into the structure, which means one has a greater degree of control over the crystallisation process. Predicting the cocrystallisation of multicomponent systems is however in its infancy and more often than not crystal structures arise that even an experienced crystal engineer would not expect – the field of crystal engineering is never dull. Therefore we also attempted the cocrystallisation of various carboxylic acids and N-heterocycles that also contain other functional groups on the molecule. By doing so we could generate a library of compounds which we could study in order to determine interaction patterns and potentially identify structural features required for the formation of framework materials using carboxylic acids and N-heterocycles.

### 1.6.1. Brief overview of this thesis

**Chapter 2** will focus on the synthesis, structure and properties of a porous ionic organic framework discovered by our group. The framework is a 3,4-lutidinium pamoate hemihydrate

with THF-filled channels (framework **1**). Successful guest-exchange studies have been conducted with this framework and have shown that this framework exchanges the THF in the channels for a wide variety of guest molecules. Selectivity experiments have also been performed on this framework and the results will be discussed.

**Chapter 3** explores the kinetic behaviour of framework **1** during guest exchange with iodomethane and draws some conclusions regarding the mechanism of exchange and the relative ease with which exchange occurs.

**Chapter 4** discusses the attempts to design a second ionic framework material. The synthesis, structure and properties of a framework-like material, 4-phenylpyridinium pamoate that contains THF in restricted cavities, will be discussed. During the investigation into the second framework-like material, various other novel crystal structures were also discovered. These structures contribute valuable insight into the driving force behind crystallisation, the importance of the degree of ionisation of pamoic acid and the structure types most likely to form framework materials. These findings will be discussed in detail in this chapter.

**Chapter 5** discusses the third ionic framework material identified during the course of this study. This pyromellitic diimide carboxylate forms an extended 3-D framework structure with 3-picolylamine, with DMF molecules in interconnected solvent pockets. The interesting properties of this structure will be discussed, as well as the insights into framework formation in conjunction with other novel crystal structures obtained with pyromellitic diimide.

**Chapter 6** contains a discussion on the most important results from each chapter, concluding remarks and proposed future studies based on this work.

**Appendix A** contains information regarding the type of instruments used, experimental procedures and details on the processing and refinement of crystal structures.

On the attached CD are the CIF files for the structures discussed in this thesis, as well as Appendices B and C containing tables of crystallisations and  $^1\text{H}$  NMR spectra, respectively.

## 1.7. References

1. J. W. Steed, in *Encyclopedia of supramolecular chemistry*, eds. J. L. Atwood and J. W. Steed, Marcel Dekker, Inc., New York, 2004, vol. 2, pp. 1401 - 1411.
2. S. I. Stupp and L. C. Palmer, *Chem. Mater.*, 2014, **26**, 507-518.
3. J.-M. Lehn, *Angew. Chem., Int. Ed.*, 1988, **27**, 89.
4. J. W. Steed, J. L. Atwood and P. A. Gale, in *Supramolecular Chemistry: From Molecules to Nanomaterials*, eds. P. A. Gale and J. W. Steed, John Wiley & Sons, Ltd, United Kingdom, 1st edn., 2012, vol. 1, pp. 1 - 7.
5. L. F. Lindoy and I. M. Atkinson, in *Monographs in Supramolecular Chemistry*, ed. J. F. Stoddart, Royal Society of Chemistry, Cambridge, 1st edn., 2000, vol. 7.
6. J.-M. Lehn, *Angew. Chem., Int. Ed.*, 1990, **29**, 1304-1319.
7. G. Desiraju, J. J. Vittal and A. Ramanan, *Crystal engineering: a textbook*, World Scientific Publishing Co. Pte. Ltd., Singapore, 2011.
8. R. Pepinsky, *Phys. Rev.*, 1955, **100**, 971.
9. D. Braga, *Chem. Commun.*, 2003, 2751 - 2754.
10. C. B. Aakeroy, *Acta Crystallogr. B*, 1997, **B53**, 569 - 586.
11. A. Gavezzotti, *Acc. Chem. Res.*, 1994, **27**, 309-314.
12. G. R. Desiraju, *Angew. Chem., Int. Ed.*, 1995, **34**, 2311 - 2327.
13. M. J. Białek, J. K. Zaręba, J. Janczak and J. Zoń, *Cryst. Growth Des.*, 2013, **13**, 4039 - 4050.
14. G. Desiraju, *J. Mol. Struct.*, 2003, **656**, 5 - 15.
15. V. R. Thalladi, B. S. Goud, V. J. Hoy, F. H. Allen, J. A. K. Howard and G. R. Desiraju, *Chem. Commun.*, 1996, 401 - 402.
16. A. C. Larson and D. T. Cromer, *The Journal of Chemical Physics*, 1974, **60**, 185-192.
17. F. Allen, *Acta Crystallogr. B*, 2002, **58**, 380-388.
18. P. Bombicz, T. Gruber, C. Fischer, E. Weber and A. Kalman, *CrystEngComm*, 2014, **16**, 3646 - 3654.
19. T. Shattock, PhD Thesis, University of South Florida, 2007.
20. G. Desiraju, *Crystal engineering, the design of organic solids*, Elsevier, Amsterdam, 1989.

21. D. B. Varshey, J. R. G. Sander and T. Friščić, in *Supramolecular chemistry: from molecules to nanomaterials*, eds. P. A. Gale and J. W. Steed, John Wiley & Sons, Ltd., Chichester, 2012, vol. 1, pp. 9 - 24.
22. C. A. Hunter, K. R. Lawson, J. Perkins and C. J. Urch, *J. Chem. Soc., Perkin Trans. 2*, 2001, 651 – 669.
23. W. B. Jennings, B. M. Farrell and J. F. Malone, *Acc. Chem. Res.*, 2001, **34**, 885 - 894.
24. G. R. Desiraju and A. Gavezzotti, *Acta Crystallogr. B*, 1989, **45**, 473-482.
25. G. Desiraju and A. Gavezzotti, *Chem. Commun.*, 1989, 621 - 623.
26. L. Loots and L. J. Barbour, *CrystEngComm*, 2012, **14**, 300-304.
27. L. Pauling, *J. Am. Chem. Soc.*, 1931, **53**, 1367-1400.
28. L. Pauling, *The nature of the chemical bond and the structure of molecules and crystals; an introduction to modern structural chemistry*, Oxford University Press, Ithaca, NY, 1939.
29. M. C. Etter, *Acc. Chem. Res.*, 1990, **23**, 120 - 126.
30. E. Arunan, G. R. Desiraju, R. A. Klein, J. Sadlej, S. Scheiner, I. Alkorta, D. C. Clary, R. H. Crabtree, J. J. Dannenberg, P. Hobza, H. G. Kjaergaard, A. C. Legon, B. Mennucci and D. J. Nesbitt, *Pure Appl. Chem.*, 2011, **83**, 1637 – 1641.
31. G. Desiraju, in *Encyclopedia of supramolecular chemistry*, eds. J. L. Atwood and J. W. Steed, Marcel Dekker, Inc., New York, 2004, vol. 1, pp. 658 - 665.
32. J. Thar and B. Kirchner, *The Journal of Physical Chemistry A*, 2006, **110**, 4229-4237.
33. P. T. A. Galek, J. A. Chisholm, E. Pidcock and P. A. Wood, *Acta Crystallogr. B*, 2014, **70**, 91-105.
34. L. Nisius and S. Grzesiek, *Nat Chem*, 2012, **4**, 711-717.
35. D. Braga and F. Grepioni, in *Encyclopedia of supramolecular chemistry*, eds. J. L. Atwood and J. W. Steed, Marcel Dekker, Inc., New York, 2004, vol. 1, pp. 357 - 363.
36. M. D. Ward, in *Molecular networks*, ed. M. W. Hosseini, Springer-Verlag, Berlin, 2009, vol. 132, pp. 1 - 23.
37. C. B. Aakeröy and K. R. Seddon, *Chem. Soc. Rev.*, 1993, 397 - 407.
38. L. J. Barbour, D. Das, T. Jacobs, G. O. Lloyd and V. J. Smith, in *Supramolecular chemistry: from molecules to nanomaterials*, eds. P. A. Gale and J. W. Steed, John Wiley & Sons, Ltd., Chichester, 2012, vol. 6, pp. 2870 - 2903.
39. C. B. Aakeröy, M. E. Fasulo and J. Desper, *Molecular Pharmaceutics*, 2007, **4**, 317-322.

40. S. L. Childs, G. P. Stahly and A. Park, *Molecular Pharmaceutics*, 2007, **4**, 323-338.
41. C. B. Aakeroy and D. J. Salmon, *CrystEngComm*, 2005, **7**, 439-448.
42. J. Bernstein, *Polymorphism in Molecular Crystals*, Oxford University Press, New York, 2008.
43. D. Braga, F. Grepioni and L. Maini, *Chem. Commun.*, 2010, **46**, 6232 - 6242.
44. R. Hilfiker, F. Blatter and M. Von Raumer, ed. R. Hilfiker, John Wiley & Sons, Weinheim, 2006, p. 433.
45. G. Whitesides, J. Mathias and C. Seto, *Science*, 1991, **254**, 1312-1319.
46. E. R. T. Tiekink, in *Supramolecular chemistry: from molecules to nanomaterials*, eds. P. A. Gale and J. W. Steed, John Wiley & sons, Ltd., Chichester, 2012, vol. 6, pp. 2791 - 2828.
47. S. Turega, M. Whitehead, B. R. Hall, A. J. H. M. Meijer, C. A. Hunter and M. D. Ward, *Inorg. Chem.*, 2013, **52**, 1122-1132.
48. A. Kitaigorodskii, *Acta Cryst.*, 1965, **18**, 585-590.
49. D. J. Cram, *Angew. Chem., Int. Ed.*, 1986, **25**, 1039-1057.
50. Y. A. Dyadin and I. S. Terekhova, in *Encyclopedia of supramolecular chemistry*, eds. J. L. Atwood and J. W. Steed, Marcel Dekker, Inc., New York, 2004, vol. 1, pp. 253 - 260.
51. J. B. Wittenberg and L. Isaacs, in *Supramolecular chemistry: from molecules to nanomaterials*, eds. P. A. Gale and J. W. Steed, John Wiley & Sons, Ltd., Chichester, 2012, vol. 1, pp. 25 - 43.
52. E. Weber, in *Encyclopedia of supramolecular chemistry*, eds. J. L. Atwood and J. W. Steed, Marcel Dekker, Inc., New York, 2004, vol. 1, pp. 261 - 273.
53. L. R. Nassimbeni, in *Encyclopedia of supramolecular chemistry*, eds. J. L. Atwood and J. W. Steed, Marcel Dekker, Inc., New York, 2004, vol. 1, pp. 696 - 704.
54. L. R. Nassimbeni, *Acc. Chem. Res.*, 2003, **36**, 631-637.
55. H. Reuter, *Angew. Chem., Int. Ed.*, 1992, **31**, 1185 - 1188.
56. K. Higashi, H. Waraya, L. K. Lin, S. Namiki, M. Ogawa, W. Limwikrant, K. Yamamoto and K. Moribe, *Cryst. Growth Des.*, 2014, **14**, 2773-2781.
57. N. J. Hinks, A. C. McKinlay, B. Xiao, P. S. Wheatley and R. E. Morris, *Micropor. Mesopor. Mat.*, 2010, **129**, 330-334.
58. F. Ke, Y.-P. Yuan, L.-G. Qiu, Y.-H. Shen, A.-J. Xie, J.-F. Zhu, X.-Y. Tian and L.-D. Zhang, *J. Mater. Chem.*, 2011, **21**, 3843 - 3848.

59. Q.-D. Hu, G.-P. Tang and P. K. Chu, *Acc. Chem. Res.*, 2014, **47**, 2017-2025.
60. J. Ferrando-Soria, H. Khajavi, P. Serra-Crespo, J. Gascon, F. Kapteijn, M. Julve, F. Lloret, J. Pasán, C. Ruiz-Pérez, Y. Journaux and E. Pardo, *Adv. Mater.*, 2012, **24**, 5625-5629.
61. Y.-N. Li, L.-H. Huo, Z.-P. Deng, X. Zou, Z.-B. Zhu, H. Zhao and S. Gao, *Cryst. Growth Des.*, 2014, **14**, 2381-2393.
62. I. Kasianova, E. Kharatyian, A. Geivandov and S. Palto, *Liquid Crystals*, 2010, **37**, 1439-1451.
63. E. Şen, N. Kaya and A. Alicilar, *Journal of Molecular Liquids*, 2013, **186**, 33 - 38.
64. P. Sozzani, S. Bracco, A. Comotti, L. Ferretti and R. Simonutti, *Angew. Chem., Int. Ed.*, 2005, **44**, 1816-1820.
65. E. Klontzas, E. Tylianakis and G. E. Froudakis, *The Journal of Physical Chemistry Letters*, 2011, **2**, 1824-1830.
66. E. Hughes, J. Jordan and T. Gullion, *J. Phys. Chem. B*, 2001, **105**, 5887 - 5891.
67. S. Erdemir, M. Bahadir and M. Yilmaz, *Journal of Hazardous Materials*, 2009, **168**, 1170-1176.
68. J. R. Holst, A. Trewin and A. I. Cooper, *Nat Chem*, 2010, **2**, 915-920.
69. N. B. McKeown, *J. Mater. Chem.*, 2010, **20**, 10588-10597.
70. L. J. Barbour, *Chem. Commun.*, 2006, 1163-1168.
71. M. L. Connolly, *Science*, 1983, **221**, 709 - 713.
72. A. L. Spek, *PLATON, a multipurpose crystallographic tool*, Utrecht University, Utrecht, The Netherlands, 2005.
73. F. M. Richards, *Annual Review of Biophysics and Bioengineering*, 1977, **6**, 151-176.
74. M. L. Connolly, *J. Appl. Crystallogr.*, 1983, **16**, 548-558.
75. *The Oxford Dictionary*, <http://www.oxforddictionaries.com/definition/english/framework>, (Accessed online: August 2014) Oxford University Press, Oxford.
76. Framework, in *The American Heritage® Dictionary of the English Language*, Houghton Mifflin Company, 4th edn., 2009.
77. H. H.-M. Yeung, M. Kosa, M. Parrinello and A. K. Cheetham, *Cryst. Growth Des.*, 2013, **13**, 3705-3715.
78. A. K. Cheetham, C. N. R. Rao and R. K. Feller, *Chem. Commun.*, 2006, 4780-4795.



79. J.-H. Fournier, T. Maris and J. D. Wuest, *J. Org. Chem.*, 2004, **69**, 1762-1775.
80. S. Jin, M. Guo, D. Wang, S. Wei, Y. Zhou, Y. Zhou, X. Cao and Z. Yu, *J. Mol. Struct.*, 2012, **1020**, 70-82.
81. S. Jin, D. Wang, Y. Huang, H. Fang, T. Wang, P. Fu and L. Ding, *J. Mol. Struct.*, 2012, **1017**, 51-59.
82. D. M. M. Farrell, G. Ferguson, A. J. Lough and C. Glidewell, *Acta Crystallogr. B*, 2002, **58**, 272-288.
83. C. B. Aakeroy and M. Nieuwenhuyzen, *J. Am. Chem. Soc.*, 1994, **116**, 10983-10991.
84. M. H. Alkordi and M. Eddaoudi, in *Supramolecular chemistry: from molecules to nanomaterials*, eds. P. A. Gale and J. W. Steed, John Wiley & Sons, Ltd., Chichester, 2012, vol. 6, pp. 3087 - 3106.
85. M. Eddaoudi, J. Kim, N. Rosi, D. Vodak, J. Wachter, M. O'Keeffe and O. M. Yaghi, *Science*, 2002, **295**, 469-472.
86. J. R. Long and O. M. Yaghi, *Chem. Soc. Rev.*, 2009, **38**, 1213-1214.
87. H. W. Langmi, J. Ren, B. North, M. Mathe and D. Bessarabov, *Electrochimica Acta*, 2014, **128**, 368-392.
88. O. M. Yaghi, *Nat Mater*, 2007, **6**, 92-93.
89. J. L. C. Rowsell and O. M. Yaghi, *Micropor. Mesopor. Mat.*, 2004, **73**, 3-14.
90. X.-D. Zheng, M. Zhang, L. Jiang and T.-B. Lu, *Dalton Trans.*, 2012, **41**, 1786-1791.
91. D. Liu, J.-P. Lang and B. F. Abrahams, *J. Am. Chem. Soc.*, 2011, **133**, 11042-11045.
92. W. Zhao, J. Han, G. Tian and X.-L. Zhao, *CrystEngComm*, 2013, **15**, 7522-7530.
93. J. Della Rocca, D. Liu and W. Lin, *Acc. Chem. Res.*, 2011, **44**, 957-968.
94. P. Horcajada, C. Serre, G. Maurin, N. A. Ramsahye, F. Balas, M. Vallet-Regi, M. Sebban, F. Taulelle and G. Ferey, *J. Am. Chem. Soc.*, 2008, **130**, 6774 - 6780.
95. P. Horcajada, C. Serre, M. Vallet-Regi, M. Sebban, F. Taulelle and G. Ferey, *Angew. Chem., Int. Ed.*, 2006, **45**, 5974 - 5978.
96. M. Vallet-Regi, A. Rámila, R. P. del Real and J. Pérez-Pariante, *Chem. Mater.*, 2001, **13**, 308-311.
97. J. Y. An, S. J. Geib and N. L. Rosi, *J. Am. Chem. Soc.*, 2009, **131**, 8376 - 8377.
98. S. R. Miller, D. Heurtaux, T. Baati, P. Horcajada, J.-M. Greneche and C. Serre, *Chem. Commun.*, 2010, **46**, 4526 - 4528.



99. J. A. Martens, J. Jammaer, S. Bajpe, A. Aerts, Y. Lorgouilloux and C. E. A. Kirschhock, *Micropor. Mesopor. Mat.*, 2011, **140**, 2-8.
100. C. Dey, T. Kundu, B. P. Biswal, A. Mallick and R. Banerjee, *Acta Crystallogr. B*, 2014, **70**, 3-10.
101. V. Guillermin, J. WeselińskiŁukasz, Y. Belmabkhout, A. J. Cairns, V. D'Elia, WojtasŁukasz, K. Adil and M. Eddaoudi, *Nat Chem*, 2014, **6**, 673-680.
102. T.-H. Chen, I. Popov, W. Kaveevivitchai and O. Š. Miljanić, *Chem. Mater.*, 2014, **26**, 4322-4325.
103. Q. Tang, S. Liu, Y. Liu, S. Li, F. Ma, J. Li, S. Wang and C. Liu, *Dalton Trans.*, 2013, **42**, 8512-8518.
104. L. Dobrzańska, G. O. Lloyd, H. G. Raubenheimer and L. J. Barbour, *J. Am. Chem. Soc.*, 2006, **128**, 698 - 699.
105. L. J. Barbour, T. Jacobs, J. A. Gertenbach and D. Das, *Aust. J. Chem.*, 2010, **63**, 573 - 577.
106. T. Jacobs, PhD Thesis, Stellenbosch University, 2009.
107. S. V. Potts, PhD Thesis, Stellenbosch University, 2012.
108. A. P. Côté, A. I. Benin, N. W. Ockwig, M. O'Keeffe, A. J. Matzger and O. M. Yaghi, *Science*, 2005, **310**, 1166-1170.
109. H. M. El-Kaderi, J. R. Hunt, J. L. Mendoza-Cortés, A. P. Côté, R. E. Taylor, M. O'Keeffe and O. M. Yaghi, *Science*, 2007, **316**, 268-272.
110. H. Furukawa and O. M. Yaghi, *J. Am. Chem. Soc.*, 2009, **131**, 8875-8883.
111. J. R. Hunt, C. J. Doonan, J. D. LeVangie, A. P. Côté and O. M. Yaghi, *J. Am. Chem. Soc.*, 2008, **130**, 11872-11873.
112. S. Wan, J. Guo, J. Kim, H. Ihee and D. Jiang, *Angew. Chem., Int. Ed.*, 2008, **47**, 8826-8830.
113. F. J. Uribe-Romo, C. J. Doonan, H. Furukawa, K. Oisaki and O. M. Yaghi, *J. Am. Chem. Soc.*, 2011, **133**, 11478-11481.
114. X. Ding, L. Chen, Y. Honsho, X. Feng, O. Saengsawang, J. Guo, A. Saeki, S. Seki, S. Irlé, S. Nagase, V. Parasuk and D. Jiang, *J. Am. Chem. Soc.*, 2011, **133**, 14510-14513.
115. Y. Zhu, X. Meng, H. Cui, S. Jia, J. Dong, J. Zheng, J. Zhao, Z. Wang, L. Li, L. Zhang and Z. Zhu, *ACS Appl. Mater. Interfaces*, 2014, **6**, 13833 – 13840.
116. M. Dogru and T. Bein, *Chem. Commun.*, 2014, **50**, 5531-5546.

117. L. Chen, K. Furukawa, J. Gao, A. Nagai, T. Nakamura, Y. Dong and D. Jiang, *J. Am. Chem. Soc.*, 2014, **136**, 9806-9809.
118. D. N. Bunck and W. R. Dichtel, *Chem-Eur J*, 2013, **19**, 818-827.
119. B. J. Smith and W. R. Dichtel, *J. Am. Chem. Soc.*, 2014, **136**, 8783-8789.
120. G. Das, D. Balaji Shinde, S. Kandambeth, B. P. Biswal and R. Banerjee, *Chem. Commun.*, 2014, **50**, 12615-12618
121. M. Yoon, K. Suh, H. Kim, Y. Kim, N. Selvapalam and K. Kim, *Angew. Chem., Int. Ed.*, 2011, **50**, 7870-7873.
122. J. Tian, P. K. Thallapally and B. P. McGrail, *CrystEngComm*, 2012, **14**, 1909 - 1919.
123. M. Liu, M. A. Little, K. E. Jelfs, J. T. A. Jones, M. Schmidtman, S. Y. Chong, T. Hasell and A. I. Cooper, *J. Am. Chem. Soc.*, 2014, **136**, 7583-7586.
124. T. Hasell, J. L. Culshaw, S. Y. Chong, M. Schmidtman, M. A. Little, K. E. Jelfs, E. O. Pyzer-Knapp, H. Shepherd, D. J. Adams, G. M. Day and A. I. Cooper, *J. Am. Chem. Soc.*, 2014, **136**, 1438-1448.
125. J. T. A. Jones, T. Hasell, X. Wu, J. Bacsá, K. E. Jelfs, M. Schmidtman, S. Y. Chong, D. J. Adams, A. Trewin, F. Schiffman, F. Cora, B. Slater, A. Steiner, G. M. Day and A. I. Cooper, *Nature*, 2011, **474**, 367-371.
126. M. Mastalerz and I. M. Oppel, *Angew. Chem., Int. Ed.*, 2012, **51**, 5252-5255.
127. M. Mastalerz, M. W. Schneider, I. M. Oppel and O. Presly, *Angew. Chem., Int. Ed.*, 2011, **50**, 1046-1051.
128. M. Gallant, M. T. Phan Viet and J. D. Wuest, *J. Org. Chem.*, 1991, **56**, 2284 - 2286.
129. Y. Ducharme and J. D. Wuest, *J. Org. Chem.*, 1988, **53**, 5787 - 5789.
130. M. Simard, D. Su and J. D. Wuest, *J. Am. Chem. Soc.*, 1991, **113**, 4696-4698.
131. V. A. Russell, M. C. Etter and M. D. Ward, *Chem. Mater.*, 1994, **6**, 1206-1217.
132. V. A. Russell, M. C. Etter and M. D. Ward, *J. Am. Chem. Soc.*, 1994, **116**, 1941 - 1952.
133. V. A. Russell, C. C. Evans, W. Li and M. D. Ward, *Science*, 1997, **276**, 575 - 579.
134. J. A. Swift, A. M. Reynolds and M. D. Ward, *Chem. Mater.*, 1998, **10**, 4159 - 4168.
135. C. C. Evans, L. Sukarto and M. D. Ward, *J. Am. Chem. Soc.*, 1999, **121**, 320 - 325.
136. J. A. Swift and M. D. Ward, *Chem. Mater.*, 2000, **12**, 1501 - 1504.
137. D. J. Plaut, K. T. Holman, A. M. Pivovar and M. D. Ward, *J. Phys. Org. Chem.*, 2000, **13**, 858 - 869.

138. K. T. Holman, A. M. Pivovarov, J. A. Swift and M. D. Ward, *Acc. Chem. Res.*, 2001, **34**, 107 - 118.
139. K. T. Holman, S. M. Martin, D. P. Parker and M. D. Ward, *J. Am. Chem. Soc.*, 2001, **123**, 4421 - 4431.
140. R. Custelcean and M. D. Ward, *Angew. Chem., Int. Ed.*, 2002, **41**, 1724 - 1728.
141. A. D. Burrows, R. W. Harrington, M. F. Mahon and S. J. Teat, *Eur. J. Inorg. Chem.*, 2003, 1433 - 1439.
142. R. Custelcean and M. D. Ward, *Cryst. Growth Des.*, 2005, **5**, 2277 - 2287.
143. J. N. Voogt and H. W. Blanch, *Cryst. Growth Des.*, 2005, **5**, 1135 - 1144.
144. N. J. Burke, A. D. Burrows, M. F. Mahon and J. E. Warren, *Inorg. Chim. Acta*, 2006, **359**, 3497 - 3506.
145. M. J. Horner, K. T. Holman and M. D. Ward, *J. Am. Chem. Soc.*, 2007, **129**, 14640 - 14660.
146. K. Bouchmella, S. G. Dutremez, C. Guérin, J.-C. Longato and F. Dahan, *Chem-Eur J*, 2010, **16**, 2528 - 2536.
147. Y. Liu and M. D. Ward, *Cryst. Growth Des.*, 2009, **9**, 3859 - 3861.
148. A. C. Soegiarto and M. D. Ward, *Cryst. Growth Des.*, 2009, **9**, 3803 - 3815.
149. A. C. Soegiarto, W. Yan, A. D. Kent and M. D. Ward, *J. Mater. Chem.*, 2011, **21**, 2204 - 2219.
150. Y. He, S. Xiang and B. Chen, *J. Am. Chem. Soc.*, 2011, **133**, 14570-14573.
151. P. Li, Y. He, J. Guang, L. Weng, J. C.-G. Zhao, S. Xiang and B. Chen, *J. Am. Chem. Soc.*, 2014, **136**, 547-549.
152. P. Li, O. Alduhaish, H. D. Arman, H. Wang, K. Alfooty and B. Chen, *Cryst. Growth Des.*, 2014, **14**, 3634-3638.
153. X.-Z. Luo, X.-J. Jia, J.-H. Deng, J.-L. Zhong, H.-J. Liu, K.-J. Wang and D.-C. Zhong, *J. Am. Chem. Soc.*, 2013, **135**, 11684-11687.
154. X. Hou, Z. Wang, M. Overby, A. Ugrinov, C. Oian, R. Singh and Q. R. Chu, *Chem. Commun.*, 2014.
155. Y. Manjare, V. Nagarajan and V. R. Pedireddi, *Cryst. Growth Des.*, 2014, **14**, 723-729.
156. A. Comotti, S. Bracco, A. Yamamoto, M. Beretta, T. Hirukawa, N. Tohnai, M. Miyata and P. Sozzani, *J. Am. Chem. Soc.*, 2014, **136**, 618-621.
157. R. E. Meléndez and M. J. Zaworotko, *Supramol. Chem.*, 1997, **8**, 157-168.

158. A. Yamamoto, T. Hamada, I. Hisaki, M. Miyata and N. Tohnai, *Angew. Chem., Int. Ed.*, 2013, **52**, 1709-1712.
159. A. Yamamoto, T. Hirukawa, I. Hisaki, M. Miyata and N. Tohnai, *Tetrahedron Lett.*, 2013, **54**, 1268-1273.
160. A. Yamamoto, S. Uehara, T. Hamada, M. Miyata, I. Hisaki and N. Tohnai, *Cryst. Growth Des.*, 2012, **12**, 4600-4606.
161. A. Yamamoto, T. Hasegawa, T. Hamada, T. Hirukawa, I. Hisaki, M. Miyata and N. Tohnai, *Chem-Eur J*, 2013, **19**, 3006 – 3016.
162. H. Wahl, D. A. Haynes and T. le Roex, *Chem. Commun.*, 2012, **48**, 1775 - 1777.
163. B. R. Bhogala and A. Nangia, *New Journal of Chemistry*, 2008, **32**, 800-807.
164. A. D. Bond, *Chem. Commun.*, 2003, 250-251.
165. M. Du, Z.-H. Zhang, X.-J. Zhao and H. Cai, *Cryst. Growth Des.*, 2005, **6**, 114-121.
166. M. C. Grossel, A. N. Dwyer, M. B. Hursthouse and J. B. Orton, *CrystEngComm*, 2006, **8**, 123-128.
167. S. Varughese and V. R. Pedireddi, *Chem-Eur J*, 2006, **12**, 1597-1609.

## CHAPTER 2

### A POROUS IONIC FRAMEWORK BASED ON THE PAMOATE ION

The aim of this study is to use simple organic building blocks with substituents that have the ability to form charge-assisted hydrogen bonds with other molecules in order to construct complex structures that contain voids or channels in the solid state. Appropriate arrangement of molecules in the solid state is driven by using a combination of large bulky molecules, such as pamoic acid, that cannot pack efficiently, and the formation of highly directional hydrogen bonds that force the molecules to pack in a certain way.

The initial building blocks on which this study is based are of pamoic acid and the isomers of lutidine and picoline (Figure 2.1). Previous work in our group determined that various combinations of pamoic acid with these isomers are known to form a wide variety of solvates with THF, DMF and NMP.<sup>1-3</sup> We also investigated the effect water had on the products of crystallisation by carrying out cocrystallisations of pamoic acid with the isomers of lutidine and picoline in 1:1 solvent:H<sub>2</sub>O mixtures.<sup>4, 5</sup> From these studies we were able to identify certain robust structural features that arise from different combinations of anion, cation and solvent.

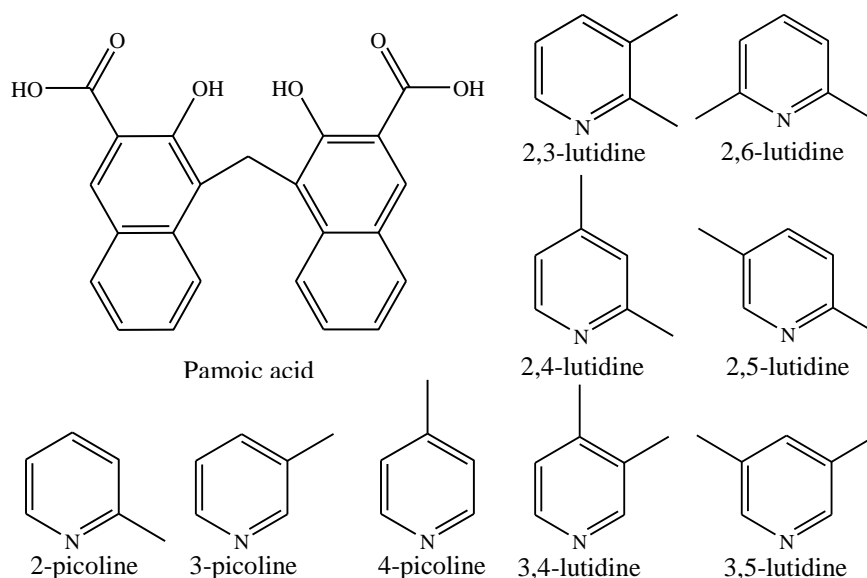


**Figure 2.1** The structures of pamoic acid and the isomers of lutidine and picoline.

Two main structure types were identified, termed **A** and **B**.<sup>3</sup> Structure type **A** is the most frequently occurring structure type and consists of singly deprotonated hydrogen-bonded pamoate chains with pendant lutidinium ions (Figure 2.2a). In structure type **B** the pamoate

ion is doubly deprotonated which allows two lutidinium ions to hydrogen bond to the pamoate ion, forming a base-acid-base unit (Figure 2.2b). The salts that form with structure type **A** tend to be isostructural despite the presence of different solvents, but in the case of **B** there is no isostructurality between salts that form the base-acid-base units. In each case the base-acid-base unit packs differently. We also identified two types of structures that incorporate water into the pamoate chain. In the first case (Figure 2.2c) the structure type **B** base-acid-base units are formed due to the doubly deprotonated pamoate ion, but the b-a-b units are connected to each other by hydrogen-bonded water molecules. The second hydrate contains the hydrogen-bonded pamoate chains with pendant lutidinium ions of structure type **A**, but the chain is interrupted by water molecules (Figure 2.2d) which then forms an extended 3-D hydrogen-bonded framework.<sup>6</sup> This structure is the focus of Chapter 2 and the structure of the framework and previous work done in our group on this framework will be discussed in Section 2.1.

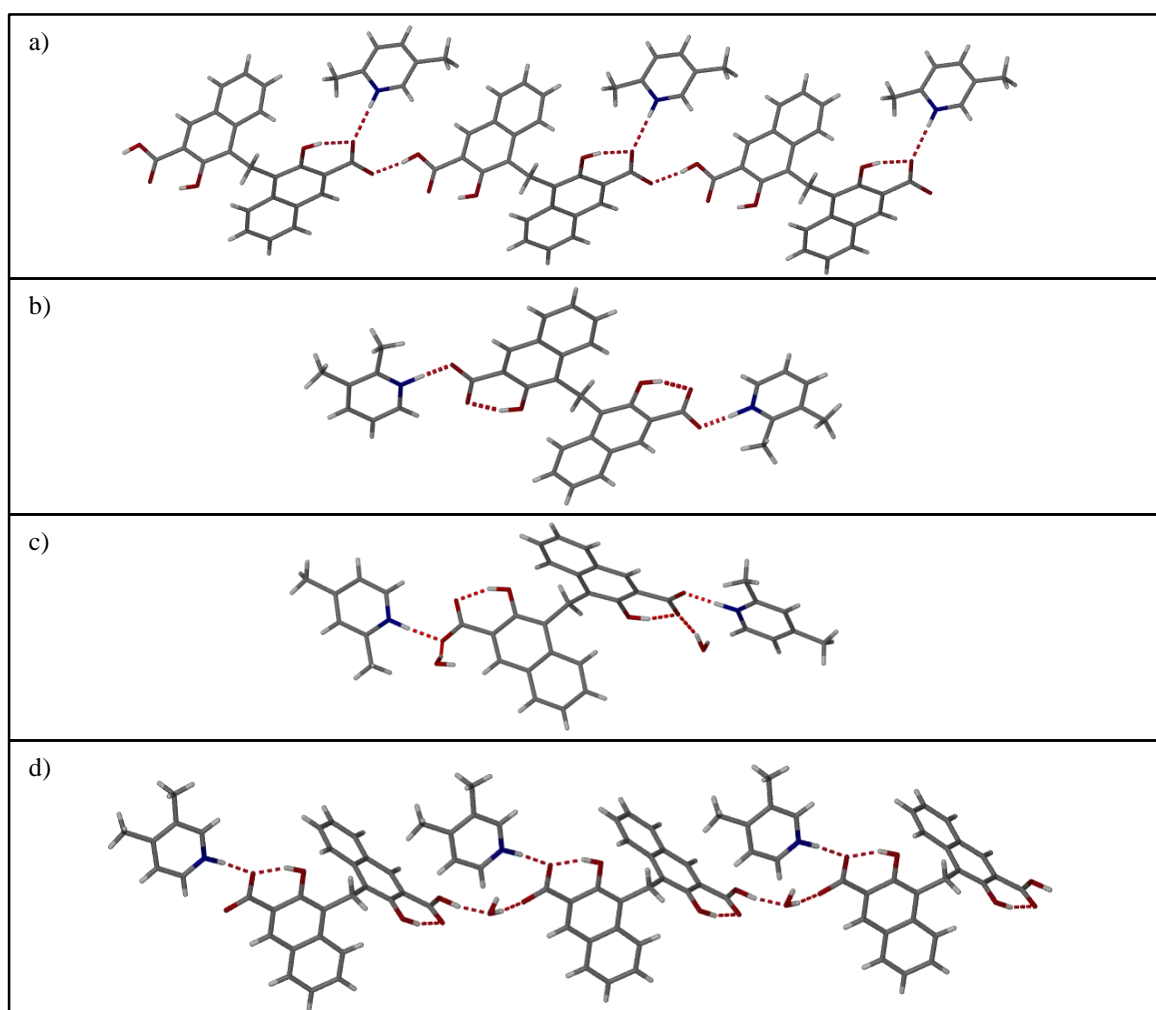


**Figure 2.2** The hydrogen-bonded units of the different structure types identified in the pamoate series. a) Structure type **A** (example shown here is TAPCIY). b) Structure type **B** (example shown here is TAPCOE). c) Structure type **B**, but water molecules connect the b-a-b units (the example shown here is BEVXUX). d) Structure type **A**, but water molecules disrupt the chain to form an extended hydrogen bonded framework (**1·THF**).

The 3,4-lutidinium pamoate hemihydrate (framework **1**) is interesting for two reasons. As was mentioned earlier, it is a hydrate structure which is unusual for the carboxylate salts of pyridinium-based cations.<sup>4</sup> Secondly, it forms an extended interconnected hydrogen-bonded network with large continuous channels that are filled with disordered THF molecules, which classifies it as a hydrogen-bonded organic framework (HOF). There are a number of HOFs found in the literature<sup>7-16</sup> but they are not nearly as prolific as MOFs and most of the discoveries have only recently occurred. These HOFs usually consist of two bulky molecules with hydrogen bond donor and acceptor sites and not all of them utilise the strong directional interaction of charge-assisted hydrogen bonds. Framework **1** is therefore quite rare since it is a hydrogen-bonded ionic organic framework that comprises three different components (3,4-lutidine, pamoic acid and water) that are able to form channels upon crystallisation. Further studies of this framework are therefore essential in order to better understand the drive behind the formation of this unique framework. We can then use this valuable information to design more of these types of frameworks and even fine-tune the design in order to make tailor-made frameworks with specific properties.

## 2.1. Synthesis and structure of framework **1**·THF

Crystals of **1**·THF can be grown by dissolving a 1:1 molar ratio of 3,4-lutidine and pamoic acid in a minimum amount of a 1:1 molar ratio of THF:H<sub>2</sub>O. It crystallises in the monoclinic space group *C2/c*. The asymmetric unit contains one pamoate ion, one 3,4-lutidinium ion, two THF molecules on special positions with half occupancy, and half a water molecule on a special position (Figure 2.3). Selected crystallographic data can be found in Table 2.1.

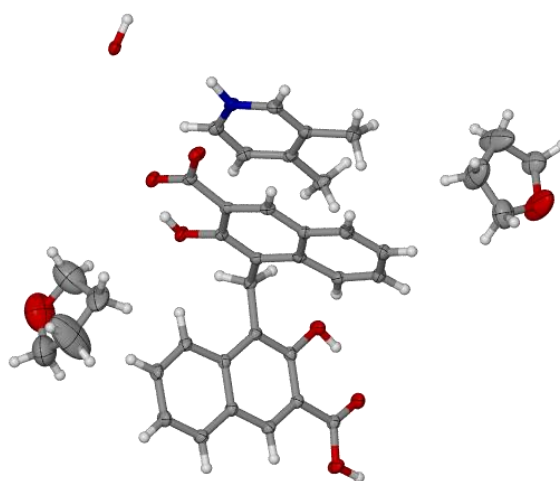


**Figure 2.3** The asymmetric unit of framework **1**. The thermal ellipsoids are drawn at 50% probability. The ellipsoids for the THF molecules are rather large due to the disorder of the molecules in the channel.

**Table 2.1** Selected crystallographic data for **1·THF**.

Parameters	1·THF
Stoichiometry (acid:base:solvent:water)	1:1:1:0.5
Chemical formula	C <sub>34</sub> H <sub>34</sub> NO <sub>7.5</sub>
Formula weight	576.62
Crystal system	Monoclinic
Space group	C2/c
Z	8
a/Å	22.117(1)
b/Å	19.857(1)
c/Å	14.615(8)
$\alpha^\circ$	90
$\beta^\circ$	115.240(1)
$\gamma^\circ$	90
Volume/Å <sup>3</sup>	5806.0(6)
Temperature/K	100(2)
$R_{\text{int}}$	0.0221
$R1 [I > 2\sigma(I)]$	0.0426

In this structure the pamoate ion is singly deprotonated which would usually, as was mentioned in the introduction, lead to the formation of structure type **A** with infinite hydrogen-bonded pamoate chains. However, a particularly interesting feature of this salt is the fact that it incorporates a water molecule into the structure. This water molecule plays a highly structure-directing role in the solid-state packing. It disrupts the usual pamoate chain by causing four pamoate ions to hydrogen bond to one water molecule. The COOH group on the pamoate ion is the hydrogen bond donor to the oxygen acceptor of the water molecule. The water molecule in turn is the hydrogen bond donor to the two deprotonated oxygen acceptors of the remaining pamoate ions (Figure 2.4a). Each of these pamoate-water units then hydrogen bonds to adjacent units to form an extended sheet (Figure 2.4a). The 3,4-lutidinium ions hydrogen bond to the pamoate ions *via* the remaining carboxylate oxygen atom, essentially locking the pamoate-water unit in place (Figure 2.4b), and disordered THF molecules fill the channels (Figure 2.4c). There are no hydrogen bonds between the THF molecules and the framework. The hydrogen bond parameters for **1·THF** are listed in Table 2.2.



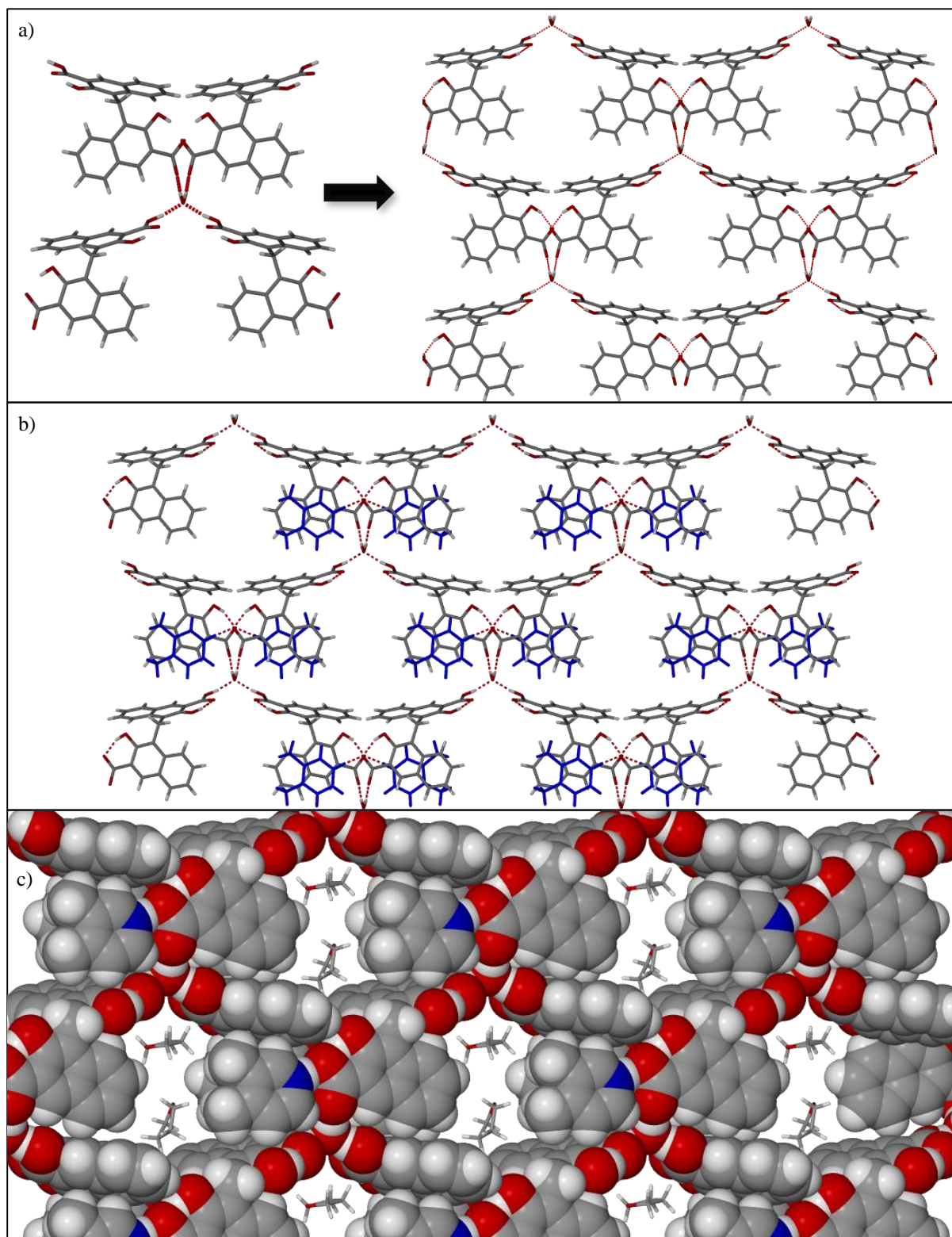


**Figure 2.4** a) Four singly deprotonated pamoate ions hydrogen bond to one water molecule, forming the basic unit of the sheet that forms the walls of the framework. These units hydrogen bond to one another through the pamoate ions of adjacent units. b) The lutidinium ions (blue) hydrogen bond to the pamoate ions *via* the remaining open carboxylate oxygen, essentially securing the units in their conformation. c) Disordered THF molecules then fill the channels, shown here in stick model and the framework in spacefill.

In general, neutron diffraction data is needed to accurately locate hydrogen atoms. However, we have included the hydrogen bond distances and angles between the donor/acceptor atom and the proton for completeness, since hydrogen atoms were located in the difference map in all structures discussed in this thesis and allowed to refine.

**Table 2.2** Hydrogen bond parameters for **1·THF**. D = donor atom, A = acceptor atom.

	<b>D–H (Å)</b>	<b>H···A (Å)</b>	<b>D···A (Å)</b>	<b>∠DHA (°)</b>
COOH···OH <sub>2</sub> <sup>a</sup>	0.96(2)	1.64(2)	2.595(1)	169(2)
H <sub>2</sub> O···OOC <sup>b</sup>	0.92(2)	1.68(2)	2.600(2)	172(2)
NH <sup>+</sup> ···OOC <sup>c</sup>	0.97(2)	1.73(2)	2.696(2)	176(2)
OH···O=C	0.89(2)	1.76(2)	2.591(2)	154(2)
OH···O=C (2)	0.921(3)	1.64(3)	2.517(1)	159(2)

<sup>a</sup>Symmetry operator: -x+1/2, -y+1/2, -z+1  
<sup>b</sup>Symmetry operator: x, -y, z+1/2  
<sup>c</sup>Symmetry operator: -x, -y, -z+1

In order to determine how large the channels of **1·THF** are, the *Void* function in Mercury<sup>17-20</sup> was used to map the contact surface and the solvent accessible surface of the space remaining when the THF molecules are deleted. The volume of a channel or void is determined by sweeping a spherical probe of a certain radius around the channel or cavity. The volume of the cavity swept out by the centre of the probe is defined as the solvent accessible surface<sup>21</sup> which is always smaller than that of the contact surface. The size of the probe must be chosen wisely as this will give valuable information regarding the potential porosity of a system. Generally probe radii of 1.4 to 1.7 Å are used to map voids, since using a probe radius smaller than the radius of a hydrogen atom (1.17 Å) will not produce any sensible information.<sup>21</sup> It is also important to remember that although the mapped *contact surface* may show that a system has connected channels it is possible that the contact surface of neighbouring voids may merge even though it is not possible for the probe to pass from one void to the next.<sup>21</sup> It is therefore better to consider the size and shape of the solvent accessible surface, since this surface will indicate whether it is possible for the probe to move from one cavity to the next. If the solvent accessible surfaces of two cavities are connected then solvent permeability should theoretically be possible.

In Figure 2.5 the mapped solvent accessible surface of framework **1·THF** is shown. With a probe radius of 1.4 Å the volume is calculated to be 331.59 Å<sup>3</sup>, 5.7% of the unit cell volume. In (a) and (b) the solvent accessible surface is shown viewed down the *a*-axis and *c*-axis, respectively, and it is clear that there are large cavities that are connected to each other, potentially allowing for the movement of solvent through the channels. In Figure 2.5c the framework is viewed down the *b*-axis, showing the long continuous 1-D channels along the *c*-axis. This view also shows that the voids are connected, indicating that solvent movement throughout the structure may be possible.

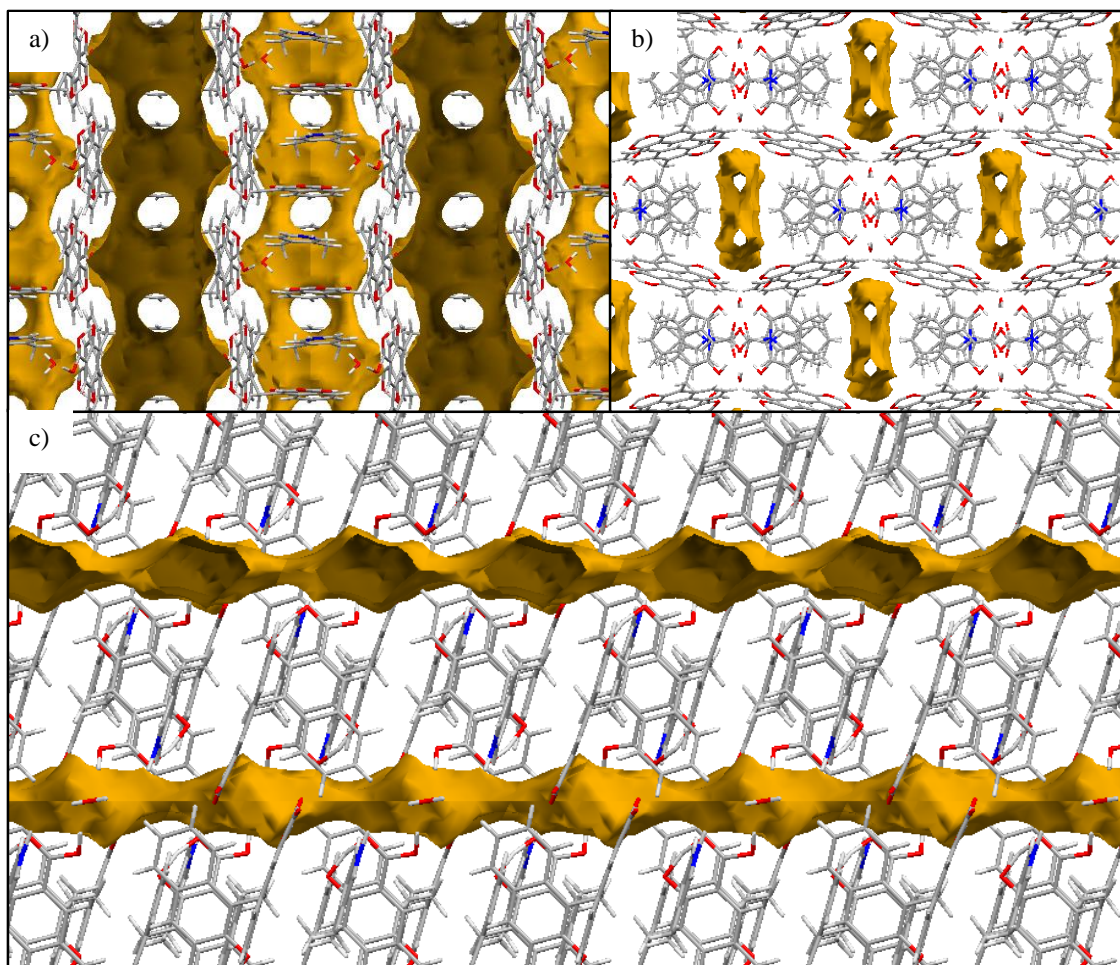


**Figure 2.5** a) The solvent accessible surface of **1·THF** viewed down the *a* axis. The cavities are clearly linked which indicates that the solvent could potentially move from cavity to cavity. b) The solvent accessible surface viewed down the *c* axis and down the channel. This view shows that there are large cavities that are connected to each other. c) The solvent accessible surface viewed down the *b* axis showing the long continuous channel the solvent molecules can move along.



### 2.1.1. The initial study of **1·THF**

Previously in our group<sup>6</sup> the permeability of **1·THF** was investigated by exposing dried crystals of **1·THF** to the solvent vapours of acetone, diethyl ether and acetone for approximately one week. <sup>1</sup>H NMR analysis confirmed that there was no THF present after one week and instead approximately one equivalent of the appropriate solvent had replaced the THF. Single-crystal data were collected of the framework after exchange with each solvent. It was not possible to model the diethyl ether in **1·Ether** satisfactorily, but SQUEEZE<sup>22</sup> analysis was performed and along with NMR results confirmed the presence of one diethyl ether molecule per asymmetric unit. In **1·Acetone** it was possible to model one molecule of acetone on a special position, but an appropriate model could not be obtained for the second molecule. SQUEEZE<sup>22</sup> and NMR analysis do however indicate the presence of one acetone molecule per asymmetric unit. In **1·DCM** two molecules of DCM on special positions could be modelled with a total occupancy of slightly less than one (which is also confirmed by NMR analysis). One molecule of DCM has been modelled as disordered with a partially occupied water molecule. In Figure 2.6 the structures of **1·Acetone** (left) and **1·DCM** (right) are shown and it is clear that the framework has retained its shape after exchange with the solvent. In each case there was no hydrogen bonding between the solvent and the framework. Selected crystallographic data for the four isostructural frameworks can be found in Table 2.3. Since it is possible for guest molecules to permeate through the bulk of the structure without altering the framework significantly, this framework can be classified as porous.

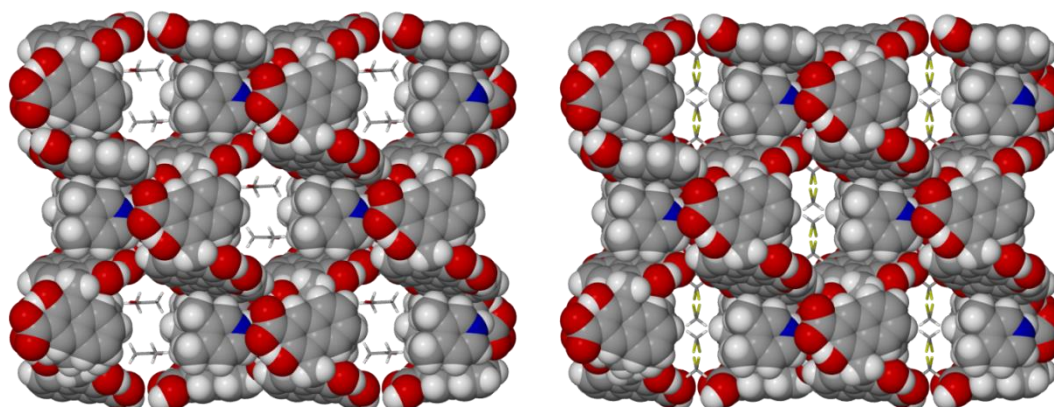


**Figure 2.6** The structures of **1·Acetone** on the left and **1·DCM** on the right. The framework is shown in spacefill representation and the solvent in stick representation.

**Table 2.3** Selected crystallographic information for the four isostructural framework materials.

Parameters	1·THF	1·Ether	1·Acetone	1·DCM
Stoichiometry (acid:base:solvent:H <sub>2</sub> O)	1:1:1:0.5	1:1:1:0.5	1:1:1:0.5	1:1:1:0.5
Chemical formula	C <sub>34</sub> H <sub>34</sub> NO <sub>7.5</sub>	C <sub>34</sub> H <sub>36</sub> NO <sub>7.5</sub>	C <sub>33</sub> H <sub>32</sub> NO <sub>7.5</sub>	C <sub>30.87</sub> H <sub>28.26</sub> C <sub>11.74</sub> NO <sub>6.76</sub>
Formula weight	576.62	578.64	562.60	582.99
Crystal system	Monoclinic	Monoclinic	Monoclinic	Monoclinic
Space group	<i>C2/c</i>	<i>C2/c</i>	<i>C2/c</i>	<i>C2/c</i>
Z	8	8	8	8
<i>a</i> /Å	22.117(1)	21.974(1)	22.12(2)	21.952(7)
<i>b</i> /Å	19.857(1)	19.909(1)	19.81(1)	19.780(7)
<i>c</i> /Å	14.615(8)	14.749(1)	14.75(1)	14.411(5)
$\alpha^\circ$	90	90	90	90
$\beta^\circ$	115.240(1)	114.287(1)	114.847(9)	114.883(4)
$\gamma^\circ$	90	90	90	90
Volume/Å <sup>3</sup>	5806.0(6)	5881.3(7)	5862(7)	5676(3)
Temperature/K	100(2)	100(2)	100(2)	100(2)
<i>R</i> <sub>int</sub>	0.0221	0.0330	0.0474	0.0827
<i>R</i> 1 [ <i>I</i> > 2σ( <i>I</i> )]	0.0426	0.0481	0.0554	0.1050

In order to determine whether the exchange occurs in a single-crystal to single-crystal fashion, crystals of **1·THF** were placed under a microscope and filmed while being exposed to the solvent vapours of diethyl ether, DCM and acetone. In Figure 2.7 crystals are shown before, during and after exchange with DCM and it is clear that no recrystallisation has taken place and that the exchange of THF for another solvent is a single-crystal to single-crystal process.

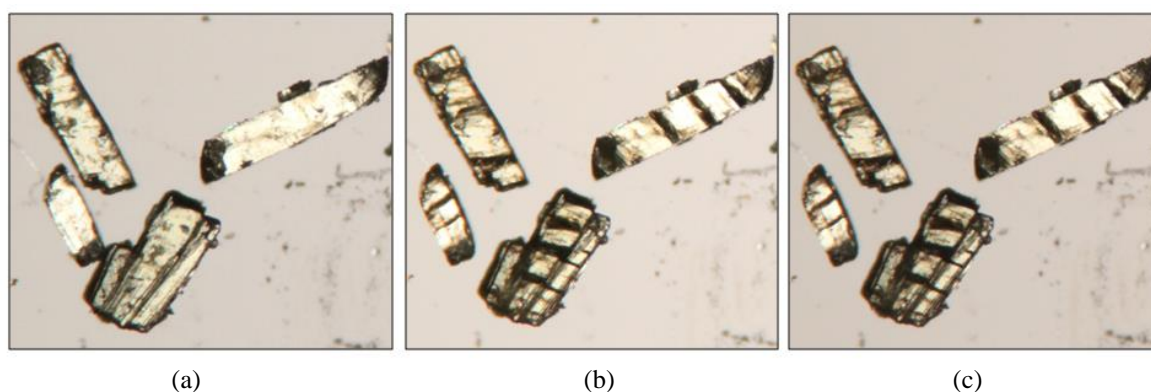


**Figure 2.7** a) Crystals of **1·THF** after removal from the mother liquor. b) Crystals after being exposed to DCM vapour for 12 hours. c) Crystals after exposure to DCM vapour for 24 hours.

To determine whether it was possible to remove the solvent from **1·THF** in order to leave empty channels without collapse of the structure the crystals of **1·THF** were immersed in supercritical CO<sub>2</sub> for one hour. Subsequent <sup>1</sup>H NMR analysis showed that only trace amounts of THF remained in the crystals and single crystal X-ray diffraction confirmed that the framework remained intact despite removal of a significant proportion of the solvent.<sup>6</sup>

It is possible to produce **1·THF** by mechanochemical synthesis.<sup>5</sup> An equimolar amount of 3,4-lutidine and pamoic acid (29 mg and 105 mg, respectively) were ground together with a mortar and pestle while adding approximately 5 drops of a 1:1 THF/H<sub>2</sub>O solution. The sample was ground until the powder became pale yellow. PXRD analysis indicated that **1·THF** had formed with some pamoic acid still present (Figure 2.8).

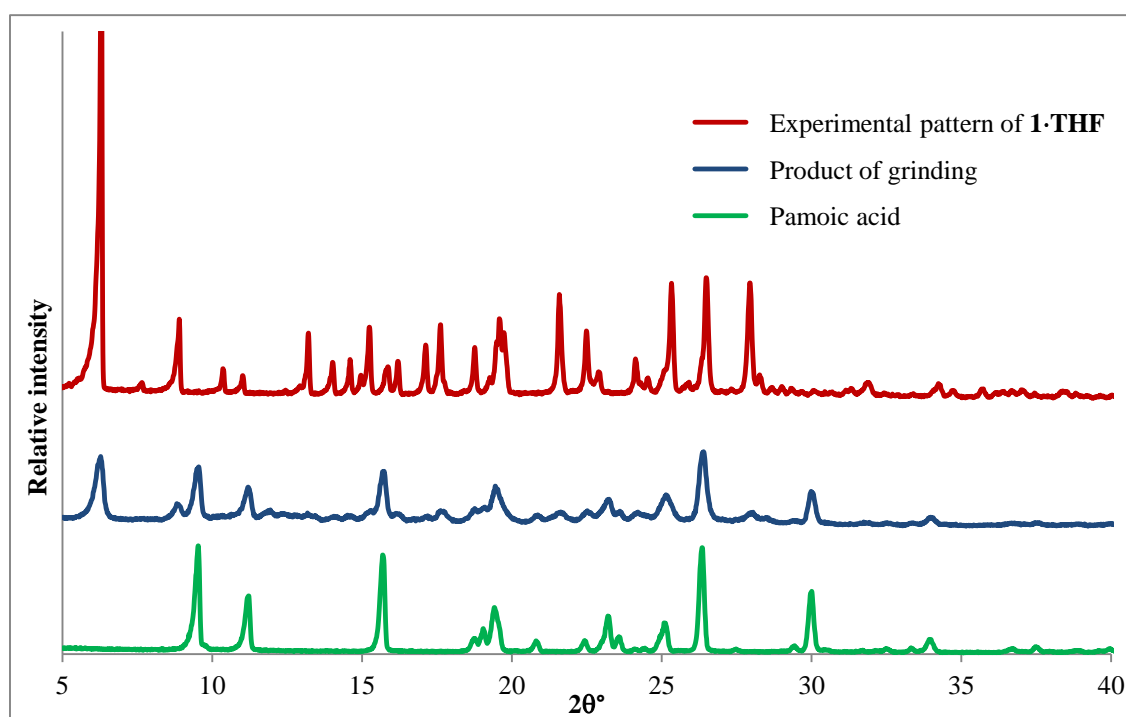


**Figure 2.8** PXRD analysis shows that it is possible to produce **1·THF** by grinding a stoichiometric amount of 3,4-lutidine and pamoic acid together with dropwise addition of THF/H<sub>2</sub>O. The conversion is however not complete since there are still some peaks belonging to pamoic acid present in the pattern of the ground product.

It should also be noted that two isostructural frameworks were obtained from crystallisations with 3- and 4-picoline. However, these two frameworks have not been included in this study since it has become increasingly difficult to isolate these crystals again.

At the start of the current study it was known that **1·THF** could be reproducibly crystallised from 1:1 THF:H<sub>2</sub>O solutions and that the THF in the channels could be exchanged for

acetone, diethyl ether and dichloromethane in a single-crystal to single-crystal fashion. We proceeded to characterise this material in significantly more detail.

## 2.2. Thermal behaviour

The thermal behaviour and stability of **1·THF** was investigated to determine whether it would be stable after the loss of solvent. Thermogravimetric analysis (TGA), differential scanning calorimetry (DSC) and variable temperature powder X-ray diffraction (VT PXRD) were used to investigate the thermal behaviour of the framework. The TGA results of **1·THF** show two distinct mass-loss steps, and DSC analysis show two endotherms that correspond to these mass loss steps. The first step starts at approximately 120 °C according to TGA (Figure 2.9) and corresponds to the loss of one THF molecule per asymmetric unit. The second step immediately follows the first and corresponds to the loss of one 3,4-lutidine and half a water molecule. The total mass loss comes to 33.0% (calculated 31.1%). The two mass loss steps can unfortunately not be isolated from each other and therefore the mass loss for each step cannot be accurately determined. The percentage loss for the first step is approximately 14.7% (calculated 12.5%) which roughly corresponds to the loss of one THF molecule per asymmetric unit.

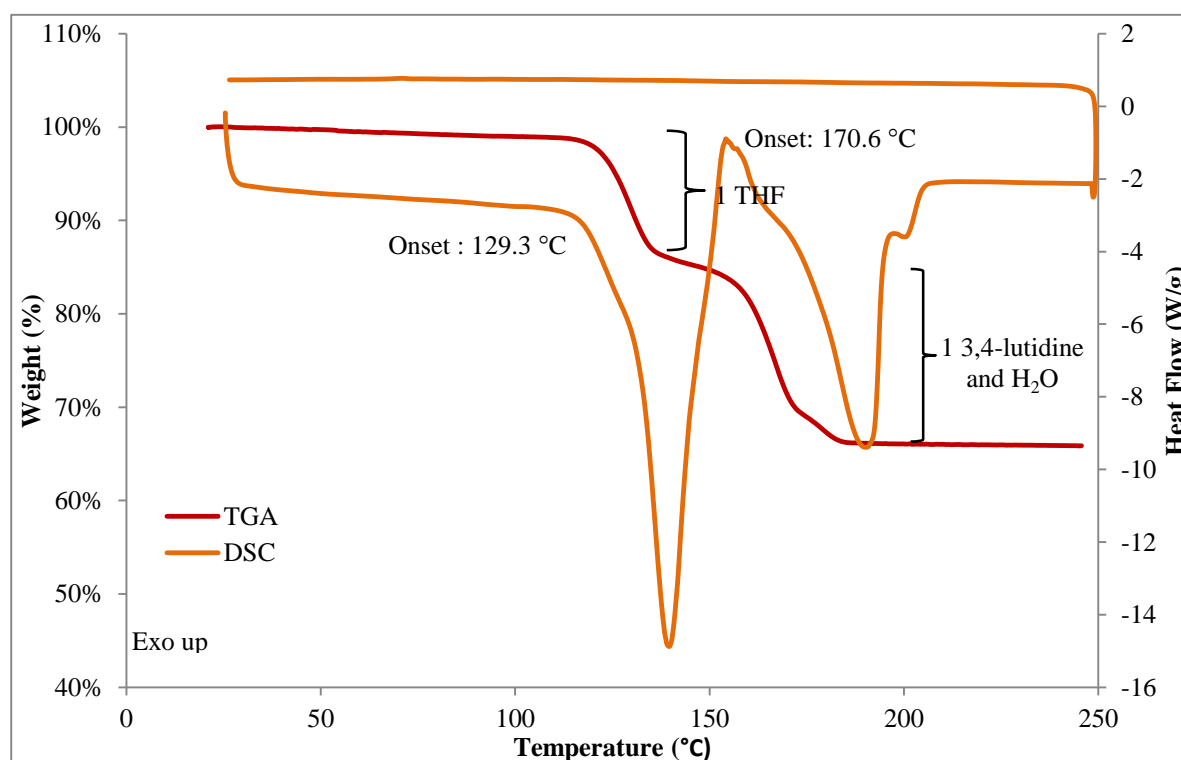


**Figure 2.9** The TG trace (shown in red) and the DSC trace (shown in orange) of **1·THF**. The total mass loss determined from TGA equals 33.0% (calculated 31.1%) and corresponds to the loss of one THF, one 3,4-lutidine and half a water molecule per asymmetric unit.

Variable temperature powder X-ray diffraction was performed on **1**·THF. The crystals were removed from the mother liquor, dried on filter paper and crushed to a fine crystalline powder. This ensures that preferred orientation of the small crystallites is minimised. The sample was then loaded into a 0.5 mm capillary, flame-sealed and spun. Powder patterns were collected at 10 °C intervals after 80 °C in order to capture what happens to the framework during the solvent loss process. According to TGA the solvent loss process starts at approximately 120 °C and the loss of 3,4-lutidine starts at approximately 150 °C (Figure 2.9). VT PXRD clearly shows that the framework remains intact up to 140 °C, since the powder pattern of **1** only changes at 150 °C (Figure 2.10). However, once the loss of 3,4-lutidine starts the framework undergoes dramatic changes, shown by the sudden change in the powder pattern at 150 °C. This shows that the 3,4-lutidinium ion plays an essential role in the stability of the framework. The previously mentioned notion that the 3,4-lutidinium ion that hydrogen bonds to the pamoate ion is in effect “locking” the structural unit into place appears to be validated. Once 3,4-lutidine is removed, the pamoate ion is reprotonated which changes the electrostatics of the carboxylate moiety, causing a decrease in the strength of the hydrogen bonds between the pamoate ions and water molecules which leads to the collapse of the structure. Further heating to 220 °C results in the evaporation of 3,4-lutidine, leaving only pamoic acid.

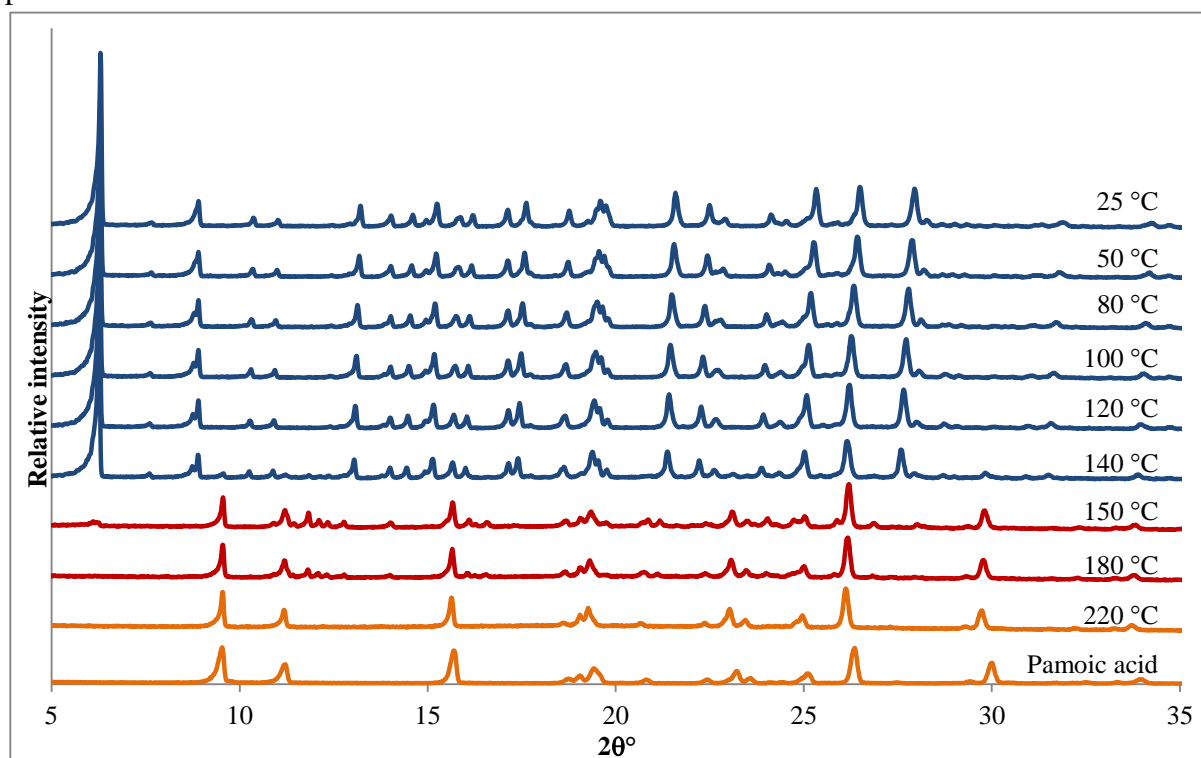


**Figure 2.10** The VT PXRD of **1**·THF. The framework remains intact during the loss of THF between 120 ° and 140 °C (as indicated by TGA). Once the loss of 3,4-lutidine starts the framework begins to collapse until only pamoic acid is left at 220 °C.



Since **1·THF** appears to remain stable after the loss of THF, further studies were conducted to determine whether the solvent could be removed to generate the apohost. Crystals of **1·THF** were dried and crushed on filter paper and placed in a Büchi oven at 90 °C and samples were taken and analysed after two hours, two and a half hours and three hours. A Büchi oven can simultaneously place a sample under dynamic vacuum and heat in order to remove the guest. Thermogravimetric analysis and powder diffraction analysis were performed on each of the samples (Figure 2.11 and Figure 2.12). TGA indicated a steady decrease in the overall mass loss (Figure 2.11) for each sample. PXRD data confirms that the framework remains intact after exposure to heat and vacuum (Figure 2.12). After three hours at 90 °C approximately half of the THF had been removed (indicated by the percentage mass loss from TGA), although there was some loss of crystallinity at this point as shown by the powder pattern in Figure 2.12 where intensity of the peaks has significantly decreased.

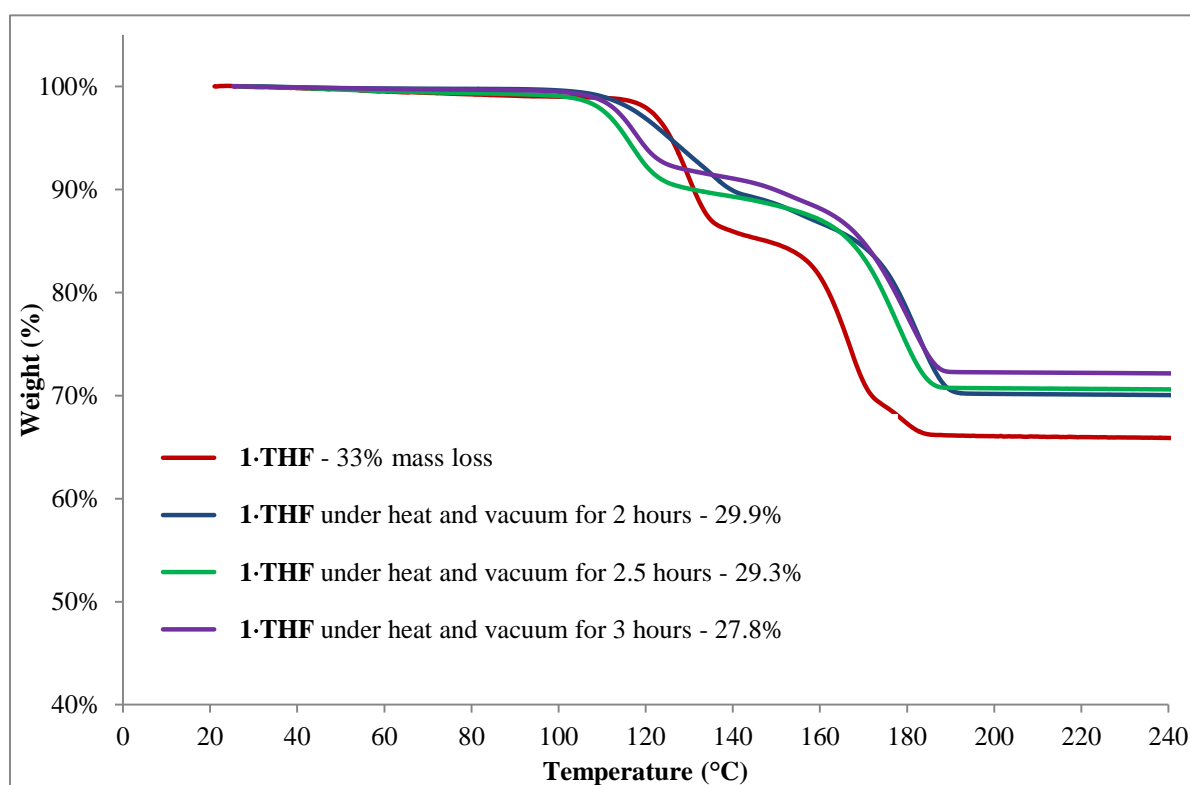


**Figure 2.11** TGA results showing the mass-loss profiles for each sample after exposed to vacuum and heat for two hours (blue), two and a half hours (green) and three hours (purple). There is a steady decrease in the overall mass loss for each sample. After three hours under vacuum and heat approximately half the THF had been removed.

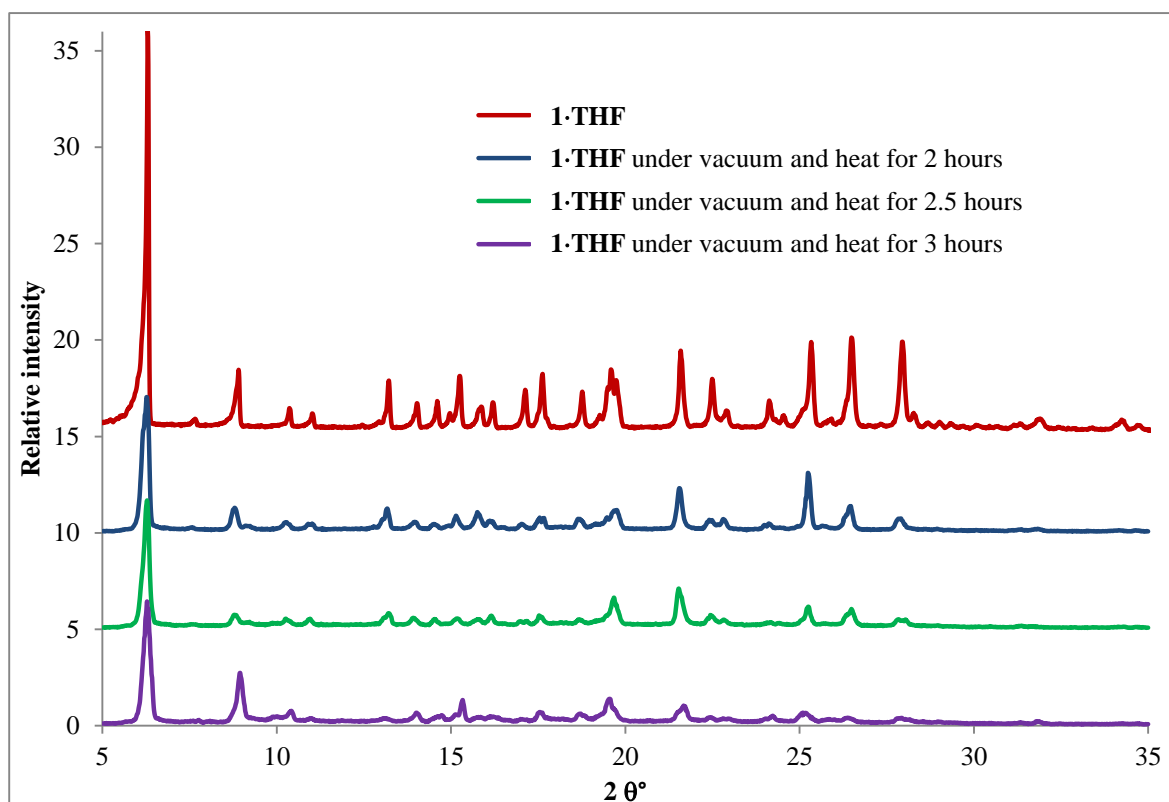


**Figure 2.12** PXRD analysis of the samples after exposure to heat and vacuum in the Büchi oven. The framework remains intact, but after three hours the sample starts to show loss in crystallinity indicated by the loss of intensity in the pattern.

Previous work in our group<sup>3, 6</sup>, as discussed in Section 2.1.1, has shown that **1·THF** can exchange THF for diethyl ether, dichloromethane and acetone. Diethyl ether is a much more volatile solvent (boiling point 34 °C) than THF with a boiling point of 66 °C. This encouraged us to determine whether it would be easier to remove the solvent from **1·Ether** rather than **1·THF**. Crystals of **1·Ether** were placed in a Büchi oven at 90 °C under vacuum and samples were analysed after one hour and 40 minutes, two hours 50 minutes and three hours. TGA indicated that significant loss of solvent had occurred after 2 hours and 50 minutes: a total mass loss of only 23.4% occurred compared to the usual loss of 30.2% for **1·Ether** (Figure 2.13). After three hours (purple trace in Figure 2.13) TGA indicates that there is no more ether present in the crystal structure, but visual inspection of the crystals show that they are either opaque or very cracked and striated. PXRD analysis (Figure 2.14) shows that the bulk sample is a mixture of pamoic acid and **1·Ether**. Crystals of **1·Ether** were also placed under vacuum and heated to 100 °C for one hour and 20 minutes. The crystals unfortunately appeared opaque and very yellow, which is reminiscent of pamoic acid. A faint odour of lutidine was also detected which indicated that loss of 3,4-lutidine and subsequent collapse of the framework had started to occur.

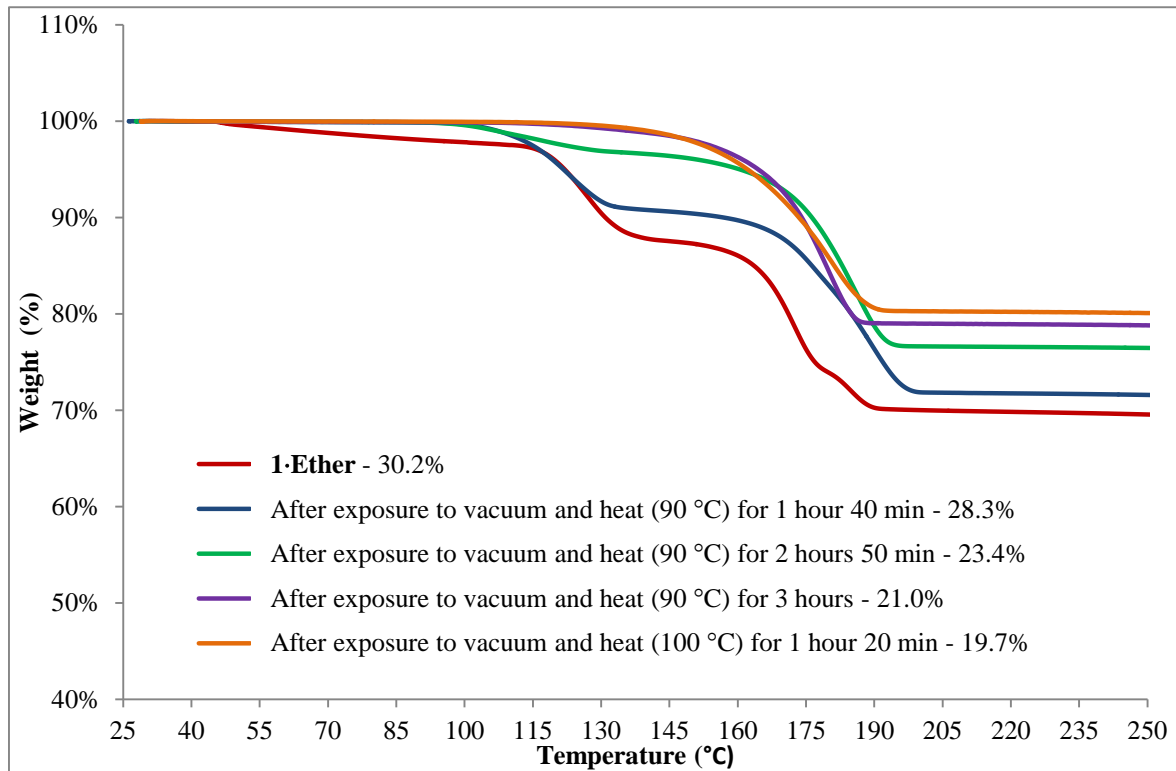


**Figure 2.13** TGA traces of **1-Ether** after exposure to vacuum and heat at 90 °C and 100 °C. After three hours at 90 °C (purple trace) and 1 hour 20 min at 100 °C the framework has started to collapse.

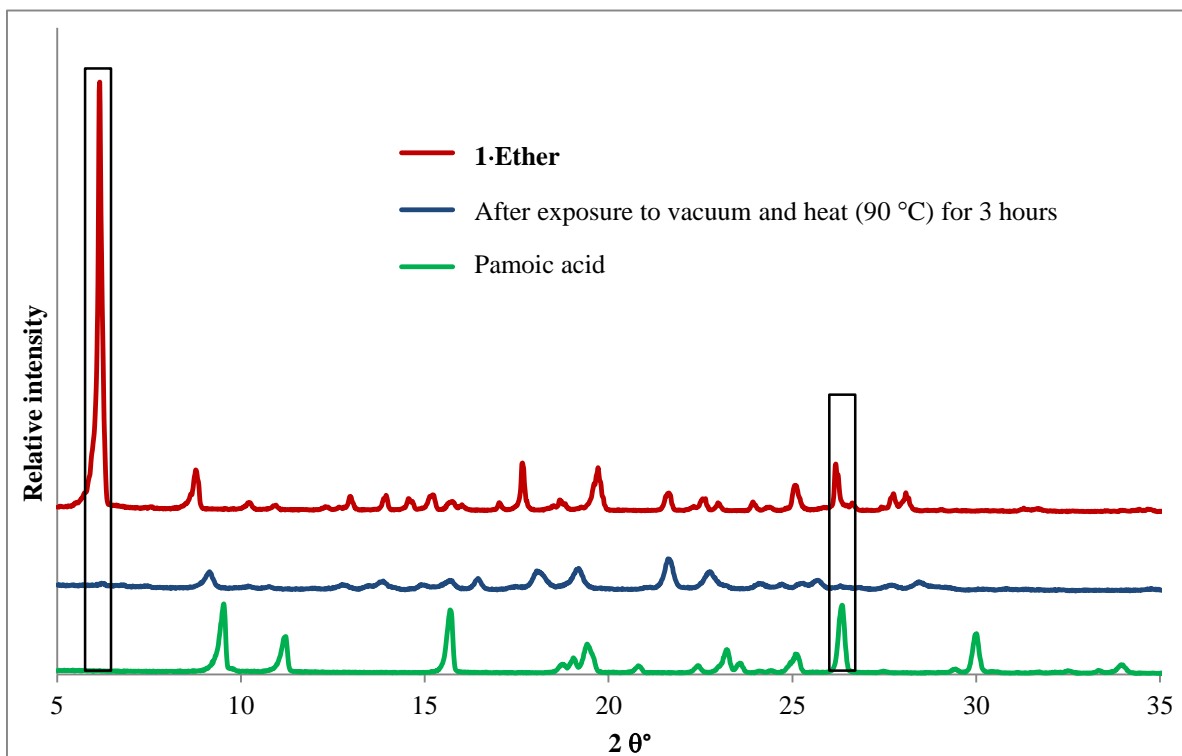


**Figure 2.14** PXRD of **1-Ether** after exposure to vacuum and heat at 90 °C for three hours. The structure has started to collapse as is seen by the disappearance of the indicated peaks in the pattern.

### 2.3. Exchange studies with framework 1

Previous work done in our group<sup>6</sup> discussed in Section 2.1.1 has already shown that **1·THF** exchanges the THF in the channels for diethylether, dichloromethane and acetone in a single-crystal to single-crystal fashion when exposed to the vapour of these solvents. For the current study the range of compounds was expanded in order to compile a list of compounds that undergo exchange with **1·THF** and to determine whether there is any selectivity for certain compounds.

Crystals of the **1·THF** were taken from the mother liquor and dried on filter paper. The crystals were placed in a glass vial that was then placed in a larger jar. The larger jar was filled with approximately one millilitre of the desired solvent and sealed with a lid as well as parafilm. This was left for approximately one week after which the crystals were analysed by NMR, PXRD, TGA and in some cases Fourier transform infrared spectroscopy (FTIR). All successful and unsuccessful exchanges are listed in Table 2.4.

**1·THF** undergoes solvent exchange with a wide variety of solvents. For easier reading, the work will be divided into five sections. In Section 2.3.1 the successful exchanges that have supporting single crystal X-ray diffraction (SCD) data will be discussed. In Section 2.3.2 the successful exchanges that we were unable to obtain SCD data for will be discussed along with other supporting data. In Section 2.3.3 the unsuccessful exchanges with **1·THF** will be discussed. Section 2.3.4 contains the results of step-wise exchange experiments, where crystals of **1·THF** were sequentially exposed to five different solvents. Section 2.3.5 contains the results of attempted solvent exchange by immersing crystals of **1·THF** in the relevant solvent.

**Table 2.4** Vapour exchange experiments with **1·THF**. Successful exchange of the THF in **1·THF** for the first 14 solvents/compounds in the table have all been confirmed by single-crystal X-ray diffraction. Unfortunately, for the remaining 7 compounds it was not possible to collect single-crystal X-ray diffraction data as the crystals were either too small or did not diffract sufficiently to collect a full dataset. Other methods were therefore used to confirm whether exchange had taken place.

Solvent/solid	Framework name/product	Analyses performed
<i>Successful exchanges</i>		
Acetone	1·Acetone	NMR, PXRD, TGA, SCD
Benzene	1·Benzene	NMR, PXRD, TGA, SCD
Chloroform	1·Chloroform	NMR, PXRD, TGA, SCD
Dichloromethane	1·DCM	NMR, PXRD, TGA, SCD
Diethyl ether	1·Ether	NMR, PXRD, TGA, SCD
1,4-dioxane	1·Dioxane	NMR, PXRD, TGA, SCD
Ethanol (EtOH)	1·EtOH	NMR, PXRD, TGA, SCD
<i>n</i> -hexane	1·Hexane	NMR, PXRD, TGA, SCD
Iodine	1·Iodine	NMR, PXRD, TGA, SCD
Methanol (MeOH)	1·MeOH	NMR, PXRD, TGA, SCD
1-propanol (PrOH)	1·PrOH	NMR, PXRD, TGA, SCD
Pyrazine	1·Pyrazine	NMR, PXRD, TGA, SCD
Toluene	1·Toluene	NMR, PXRD, TGA, SCD
Iodomethane	1·MeI	NMR, PXRD, TGA, SCD
Acetonitrile	-	NMR, PXRD, TGA
Benzonitrile	-	NMR, PXRD, TGA, IR
Naphthalene	-	NMR, PXRD, TGA, IR
1-ethyl-pyrrolidone	-	NMR, PXRD
N-methylpyrrolidone (NMP)	-	NMR, PXRD, TGA
<i>p</i> -xylene	-	NMR, PXRD
<i>m</i> -xylene	-	NMR, PXRD
<i>Unsuccessful exchanges</i>		
Cyclohexane	Unchanged <b>1·THF</b>	NMR, PXRD, TGA
Cyclohexanone	Unchanged <b>1·THF</b>	NMR, PXRD, TGA
2-pyrrolidone	Unchanged <b>1·THF</b>	NMR, PXRD
Aniline	New compound	NMR, PXRD, TGA
Morpholine	New compound	NMR, PXRD
Dimethylformamide	Mixture of SIQCIF <sup>a</sup> and TAPDAR <sup>b</sup>	NMR, PXRD, TGA
Pyridine	Pyridinium pamoate salt (TABMAK)	NMR, PXRD

<sup>a</sup> Pamoic acid/DMF solvate; <sup>b</sup> 3,4-lutidinium pamoate DMF solvate

### 2.3.1. Successful exchanges with **1·THF** and supporting SCD data

In this section the relevant PXRD and TGA data of the structures after solvent exchange with **1·THF** will first be discussed. In the subsection 2.3.1.1 the crystal structure of each exchange product will be discussed.

The compounds listed in Table 2.4 that successfully exchange with the THF in **1·THF** do not have much in common. These compounds do not have general similarity in shape, they all have varying boiling points, dipole moments, and densities and yet they are all able to exchange with the THF in the channels of **1·THF** in a single-crystal to single-crystal fashion. There are many examples of single-crystal to single-crystal solvent exchange,<sup>23</sup> but these mostly only occur in MOFs and COFs due to their strong coordination and covalent bonds that are able to keep the structure intact upon removal or exchange of the solvent. Organic inclusion compounds often revert to different structures upon exposure to another solvent since it is relatively easy to disrupt the weaker intermolecular interactions that hold these inclusion compounds together and form a different structure with lower energy.<sup>24-26</sup> However, due to the charge-assisted hydrogen bonding in the framework of **1·THF**, lending it greater strength and stability, it is possible to exchange the guest in the channels without collapse of the framework.

After exchange with the relevant solvent the bulk of the crystals were analysed by <sup>1</sup>H NMR, TGA and PXRD. NMR analysis (Appendix C) confirmed the presence and relative ratio of each solvent in the framework and PXRD analysis, shown in Figure 2.15, confirmed that the structure of the framework was retained after exchange. There are very slight differences between the powder patterns, but this is due to the presence of the different guests in the channels as some have different implications for the symmetry of the crystal. For instance, chloroform is not on a special position whereas most of the other solvents are, and therefore this symmetry element is lost from the structure and **1·Chloroform** now conforms to the space group  $P2_1/c$ .\*

---

\*Tables of crystallographic data can be found at the end of Section 2.3.1 in Table 2.5 and Table 2.6. Hydrogen bond parameters for all the frameworks can be found in Appendix C.

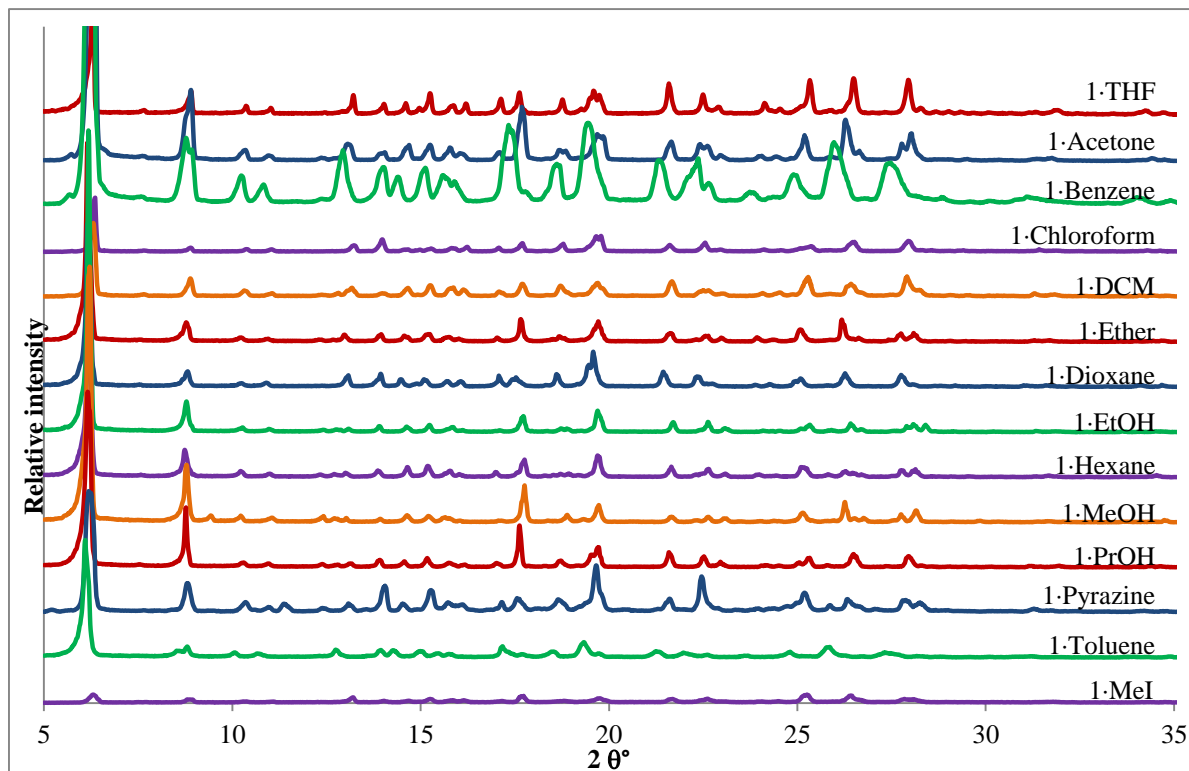


**Figure 2.15** PXRD patterns of crystals of **1·THF** after exchange with the solvent indicated. All of the patterns closely resemble that of the original structure, indicating that the original framework is retained upon exchange.

Thermal analysis of most of the exchanged structures show well-defined two-step mass loss profiles similar to those of the original framework, **1·THF**, shown in Figure 2.16. Solvents such as methanol, ethanol, iodomethane and diethyl ether show substantial mass loss from room temperature, but the thermal profile is still similar to that of **1·THF**. Two of the structures however exhibit quite a different mass loss profile, shown in Figure 2.17. For 1,4-dioxane and pyrazine no two-step mass loss profile is observed. Instead, solvent loss and framework degradation all appear to have merged into one step. This could mean that these particular solvents have a much stronger interaction with the framework and that the loss of these solvents then leads to the structural collapse of the framework in each case. This is however strange since no strong interactions such as hydrogen bonds form between the guests and the framework in each case. We cannot therefore say with certainty what exactly occurs in the framework during the desolvation of 1,4-dioxane and pyrazine.

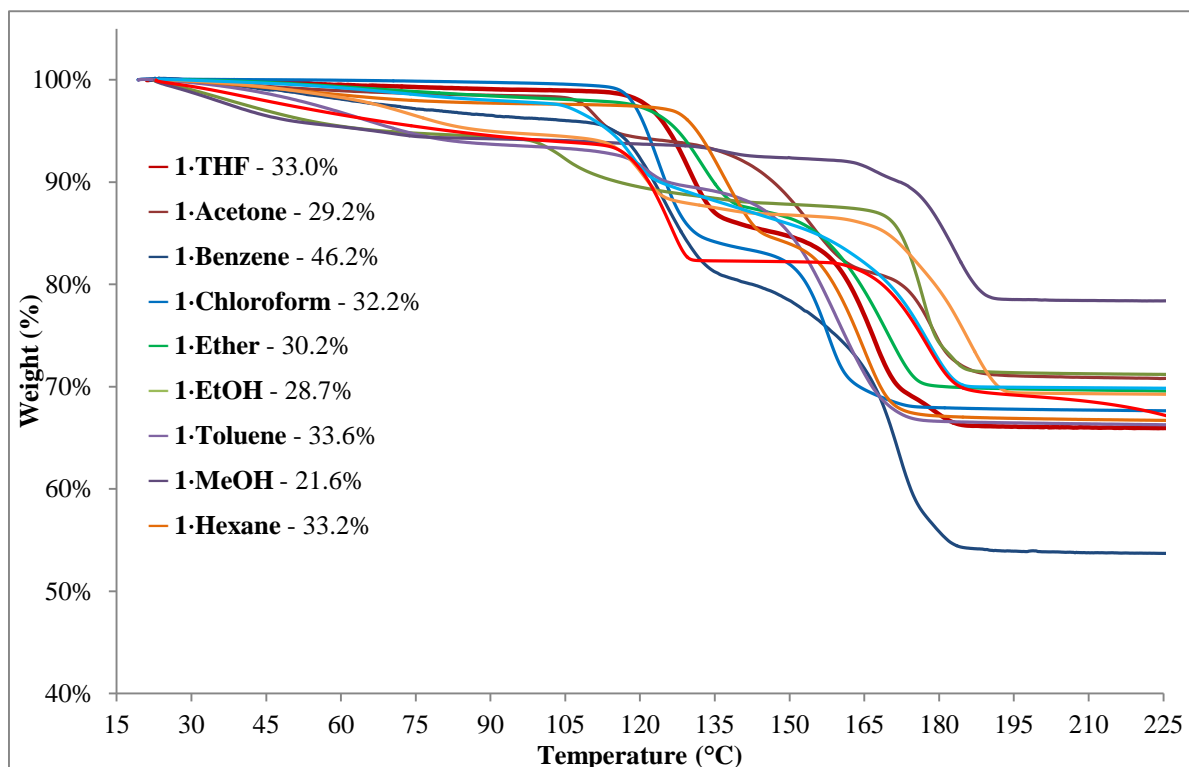


**Figure 2.16** The exchanged structures that have two-step mass loss profiles similar to that of **1·THF**. Solvents such as methanol, ethanol, iodomethane and diethyl ether show substantial solvent loss from room temperature.

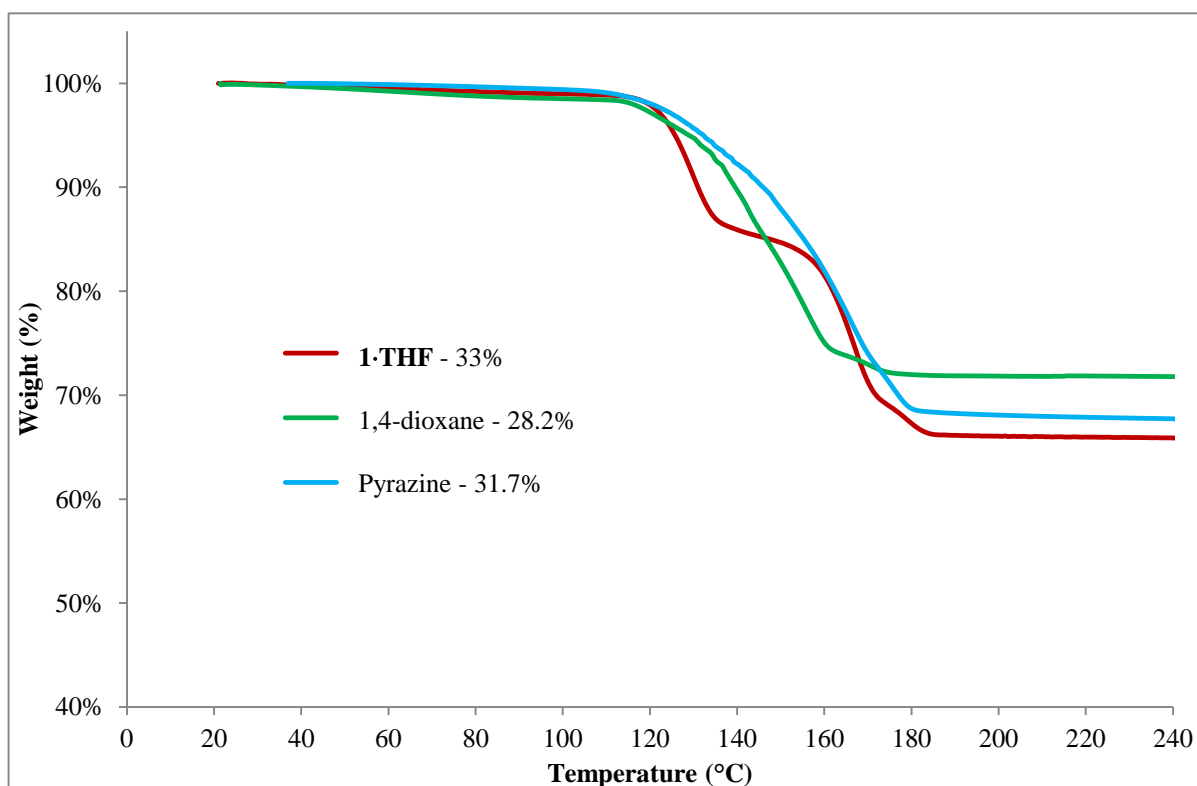


**Figure 2.17** The thermal mass loss profiles of crystals after exchange with 1,4-dioxane and pyrazine. These traces do not follow the characteristic two-step mass loss profile of the original **1·THF** framework. This could mean that these compounds experience a stronger interaction with the framework, causing the loss of solvent and framework degradation to merge into one overall step.



### 2.3.1.1. Discussion of crystal structures

This section contains the crystal structure descriptions of the successful exchanges discussed in 2.3.1. The structures of **1·Acetone**, **1·DCM** and **1·Ether** will however not be described in this section as they have been discussed in Section 2.1.1. In all cases the framework remained the same, therefore only the guest modelling and orientation will be described for each structure. PLATON<sup>27, 28</sup> SQUEEZE<sup>29</sup> analysis was also used in some cases to infer the presence of the guest if it was not possible or difficult to model. In some structures a THF molecule has been modelled. In these instances it is possible that the exchange of the guest for THF was not yet complete in some crystals. When a suitable crystal was selected for SCD collection the crystal in which exchange was not yet complete was inadvertently selected since it was possibly in a better condition than the other crystals. Exchange of the THF for a different guest does tend to leave the crystals intact but severely striated. NMR results do however indicate that complete exchange occurs for the bulk material.

#### a) **1·Chloroform**

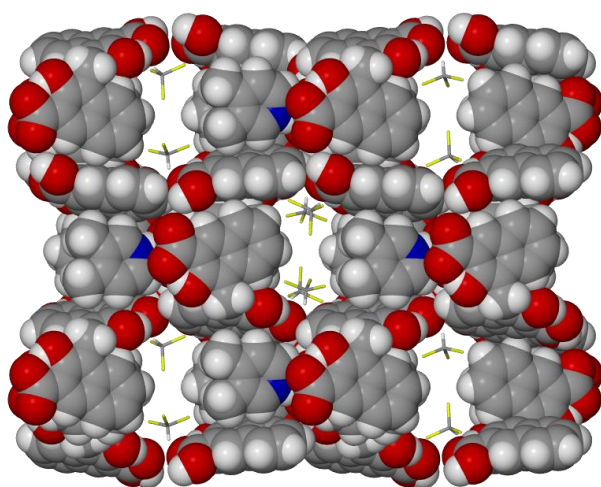


**Figure 2.18** The packing diagram of **1·Chloroform** viewed down the *c* axis.

**1·Chloroform** is the only structure that, in contrast to the original **1·THF**, conforms to the space group  $P2_1/c$ . In all other cases the crystals after exchange remain in the original space group  $C2/c$ . This loss of symmetry is due to the chloroform molecule that is no longer on a special position. In **1·Chloroform** the asymmetric unit consists of two pamoate ions, two 3,4-lutidinium ions, one water molecule and two fully occupied chloroform molecules.

In other words the asymmetric unit has essentially doubled due to the loss of the mirror plane. In Figure 2.18 the packing diagram of **1·Chloroform** is shown down the *a* axis with the chloroform molecules oriented in four different symmetry-related positions. The centre channel shows how the four positions overlap within the channel.

## b) 1·Dioxane

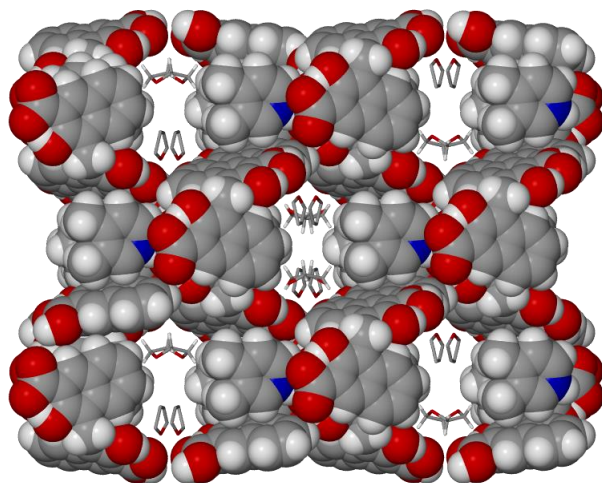


**Figure 2.19** The packing diagram of **1·Dioxane** viewed down the *c* axis.

In **1·Dioxane** there is one molecule of 1,4-dioxane and one molecule of THF, both on special positions, in the asymmetric unit. The 1,4-dioxane molecule is disordered over two positions and in Figure 2.19 the two possible positions of the 1,4-dioxane molecule are shown. It either lies with both oxygen atoms pointing up or both pointing down. The molecule is therefore in the boat conformation within the channel, possibly due to the shape of the

pocket in which the 1,4-dioxane molecule resides. The second guest molecule in both cases is generated through symmetry.  $^1\text{H}$  NMR results of the crystals exposed to 1,4-dioxane indicate that there is not one full molecule of 1,4-dioxane present per asymmetric unit. There were also still traces of THF in the NMR spectrum, although one THF peak and the peak for 1,4-dioxane overlap. SQUEEZE analysis of the empty structure calculated there to be 285 electrons in the solvent accessible volume, or 36 per asymmetric unit. This does not equate to full occupancy of 1,4-dioxane, which is why the second molecule has been modelled as THF.

## c) 1·MeOH

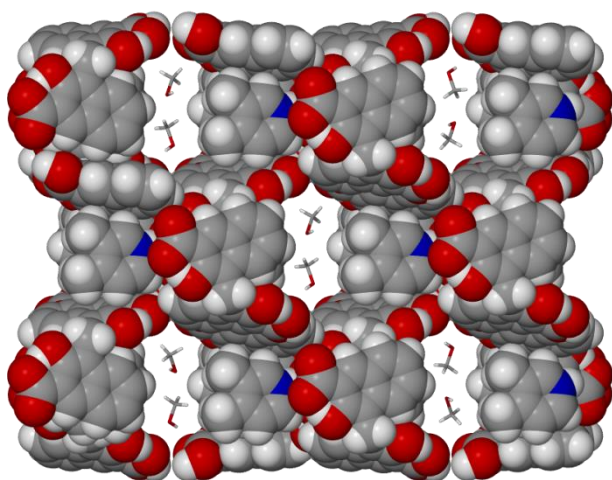


**Figure 2.20** The packing diagram of **1·MeOH**, viewed down the *c* axis.

In **1·MeOH** two methanol molecules have been modelled on special positions. According to  $^1\text{H}$  NMR analysis there is one methanol molecule per asymmetric unit, but SQUEEZE analysis indicates that there are 40 electrons per asymmetric unit, which is equal to approximately two methanol molecules per asymmetric unit (36 electrons). There is however some residual electron density observed around the

methanol molecules which could indicate the presence of disordered THF in the structure.

This would account for the higher electron count calculated from SQUEEZE analysis. Very large thermal ellipsoids are also observed for the methanol molecules, indicating that the methanol is highly disordered within the structure. This is probably because the molecule is so small and the channel in comparison so much larger, allowing space for the methanol molecules to constantly move around in the channel. In Figure 2.20 the different positions of the methanol molecules related through an inversion centre are shown.

#### d) 1·EtOH

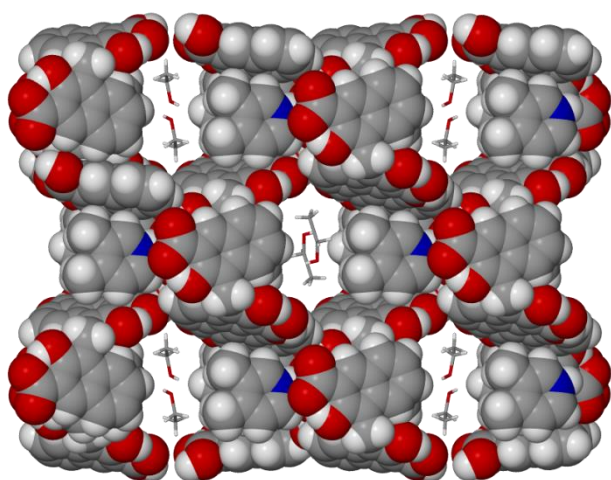


**Figure 2.21** The packing diagram of **1·EtOH**, viewed down the *c* axis.

In each position the hydroxyl groups of the ethanol molecules are orientated perpendicular to the *c*-axis and the length of the channel, whereas the alkyl chain is slightly angled along the length of the channel.

#### e) 1·PrOH

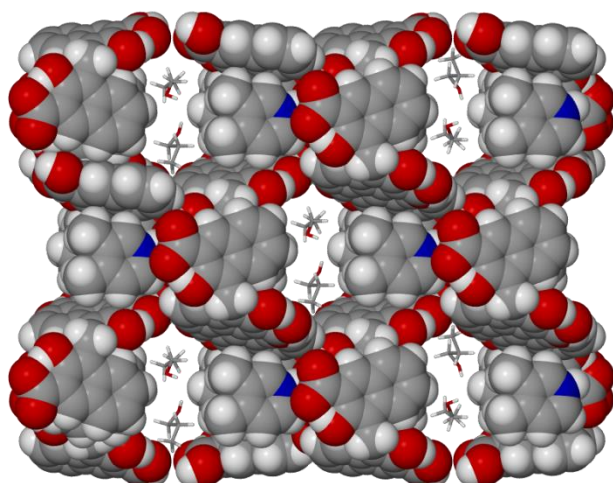


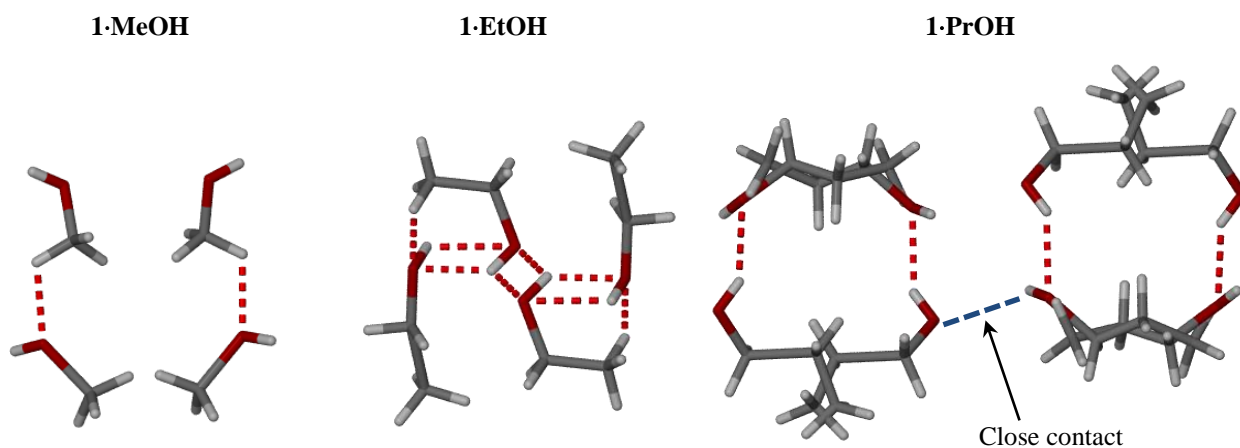
**Figure 2.22** The packing diagram of **1·PrOH**.

In **1·EtOH** there are two unique molecules of ethanol modelled on special positions. For this structure the  $^1\text{H}$  NMR and SQUEEZE analyses are in agreement with each other, indicating the presence of one ethanol molecule per asymmetric unit. The thermal ellipsoids of the two modelled molecules are rather large, indicating that there is a lot of movement of the ethanol molecules within the structure. The different orientations of the ethanol molecules are

The crystal structure of **1·PrOH** contains two unique molecules of 1-propanol on special positions. NMR and SQUEEZE analysis also confirm the presence of one 1-propanol molecule per asymmetric unit. In Figure 2.22 the different orientations of the 1-propanol molecules are shown. In each orientation the 1-propanol molecule is angled down the length of the channel, i.e.

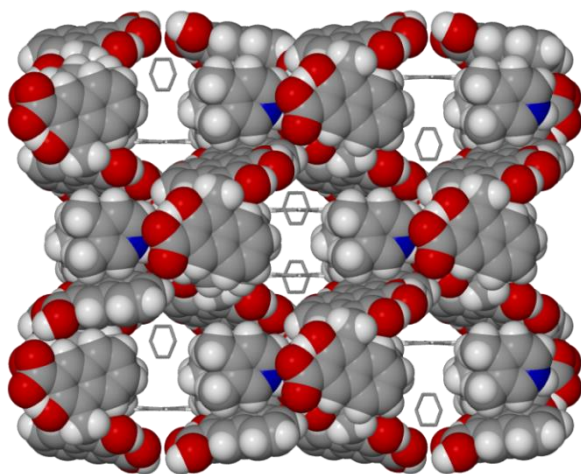
parallel to the  $c$  axis. This is possibly due to the longer alkyl chain of 1-propanol that does not allow for the same perpendicular arrangement as seen in **1·MeOH** and **1·EtOH**. There was no investigation into the inclusion of longer chain alcohols, but it would be interesting to determine in future studies if the length of the alkyl chain determines the orientation within the channel.

It is also important to note that no hydrogen bonding occurs between the alcohols and the framework. There are however varying degrees of weak hydrogen bond formation between the solvent molecules themselves (Figure 2.23). The methanol molecules in **1·MeOH** hydrogen bond to each other in a head-to-tail fashion, whereas the ethanol molecules in **1·EtOH** hydrogen bond to each other *via* the hydroxyl groups to form an extended chain down the channel. In **1·PrOH** the 1-propanol molecules form dimers *via* the hydroxyl groups and the dimers pack alongside one another down the channel.



**Figure 2.23** The hydrogen bond motifs found between the methanol, ethanol and 1-propanol molecules of **1·MeOH**, **1·EtOH** and **1·PrOH**, respectively. The methanol molecules form head-to-tail hydrogen bonds, while the ethanol molecules interact through head-to-head hydrogen bonds to form extended chains down the channel. The 1-propanol molecules form hydrogen bonded dimers that stack next to each other down the channel.

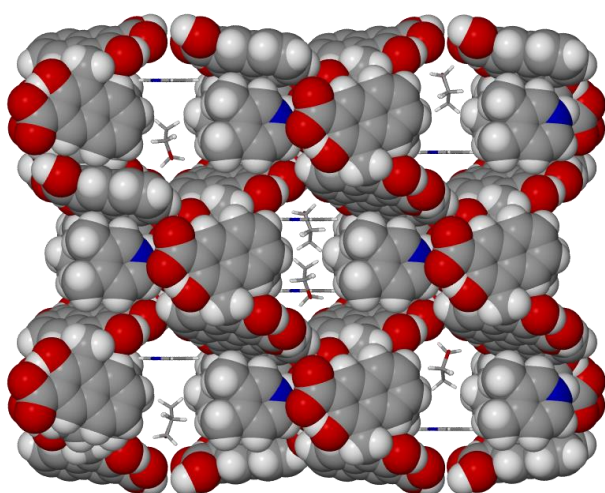


**f) 1-Benzene**

**Figure 2.24** The packing diagram of **1-Benzene**, viewed down the *c* axis.

One benzene molecule could be modelled on a special position with ease. However, no satisfactory model could be obtained for the second molecule. It is possible to model the second molecule as a benzene molecule on a special position where half of the molecule is completed by symmetry. It is however not possible to model any hydrogen atoms on this molecule and it appears as if it is disordered with another molecule that could either be a THF

molecule or another benzene molecule.  $^1\text{H}$  NMR and SQUEEZE analysis unfortunately do not shed any light on this perplexing matter. Results from both analyses suggest that there is not a full benzene molecule per asymmetric unit. SQUEEZE analysis of the structure where the second guest molecule has been removed indicates that there are 20 electrons present in the asymmetric unit. This is equal to either half a benzene molecule or half a THF molecule, since benzene has 42 electrons and THF has 40 electrons.

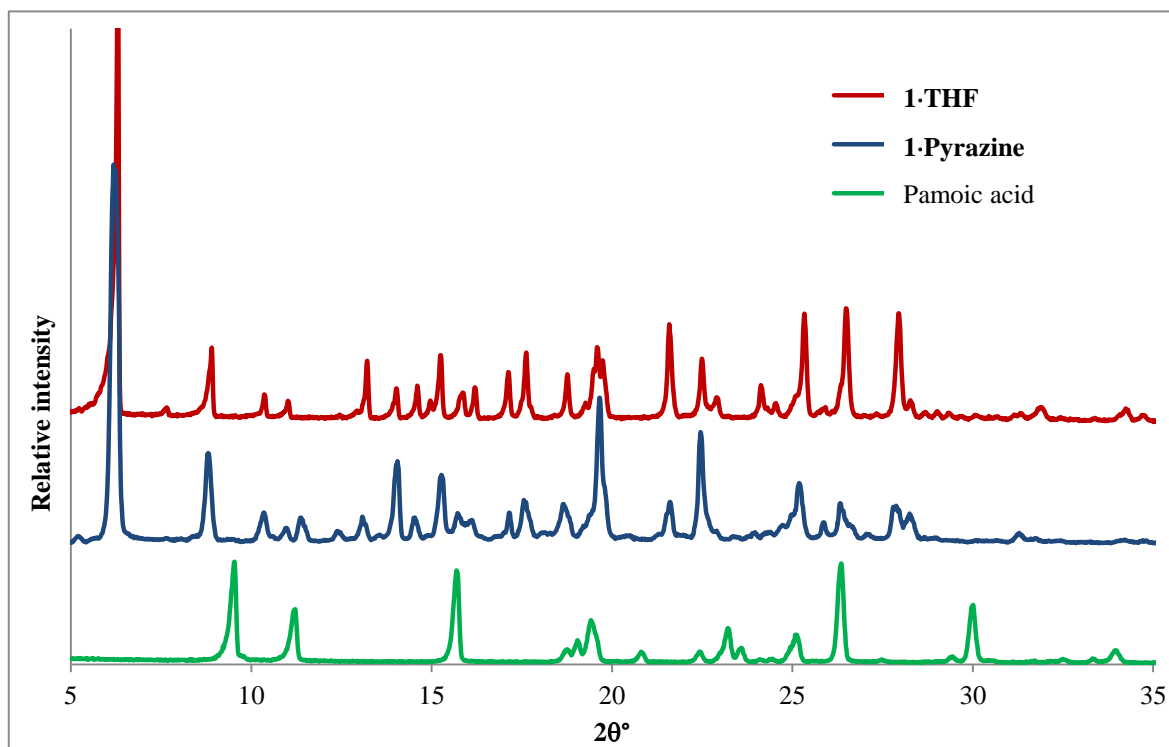
**g) 1-Pyrazine**

**Figure 2.25** The packing diagram of **1-Pyrazine**, viewed down the *c* axis.

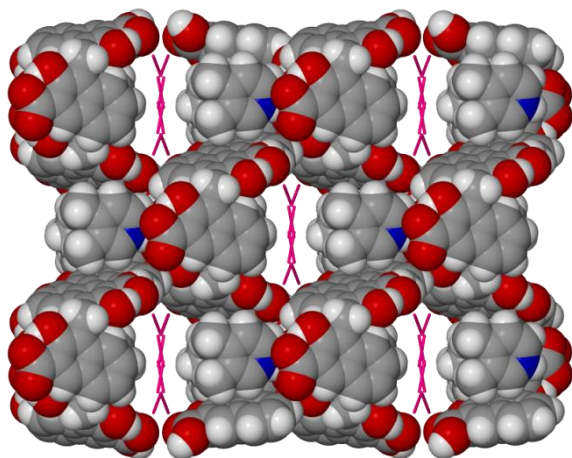
One of the exciting discoveries about **1-THF** is that it is possible to exchange the THF in the channels for volatile solids such as pyrazine and iodine. There are very few reports in which pyrazine is included in a structure by exposing the structure to pyrazine vapour. In one study pyrazine was used as a templating agent to increase the pore size of a MOF<sup>30</sup> by adding a specific molar equivalent to the crystallisation. In a study by Balász *et al.* pyrazine was

successfully encapsulated within a cyclic calix[4]arene diamide receptor.<sup>31</sup> To the best of our knowledge **1·Pyrazine** appears to be the first ionic organic framework to include pyrazine in the crystal structure *via* guest exchange.

One pyrazine molecule and one THF molecule have been modelled on special positions. The pyrazine and THF molecules lie perpendicular to each other as is seen in Figure 2.25. Prolonged exposure to pyrazine tends to turn crystals opaque, which is possibly why a crystal was unintentionally selected that still contained THF in the channels. PXRD analysis of crystals of **1·Pyrazine** did however confirm that the structure of the framework was retained despite crystals appearing opaque upon visual inspection (Figure 2.26). <sup>1</sup>H NMR analysis (Appendix C) also indicates that almost complete exchange with pyrazine occurs with only trace amounts of THF observed in the spectrum.



**Figure 2.26** The powder patterns of **1·THF** and **1·Pyrazine** indicating that the framework structure was retained upon exchange despite crystals going opaque after prolonged exposure to pyrazine vapour.

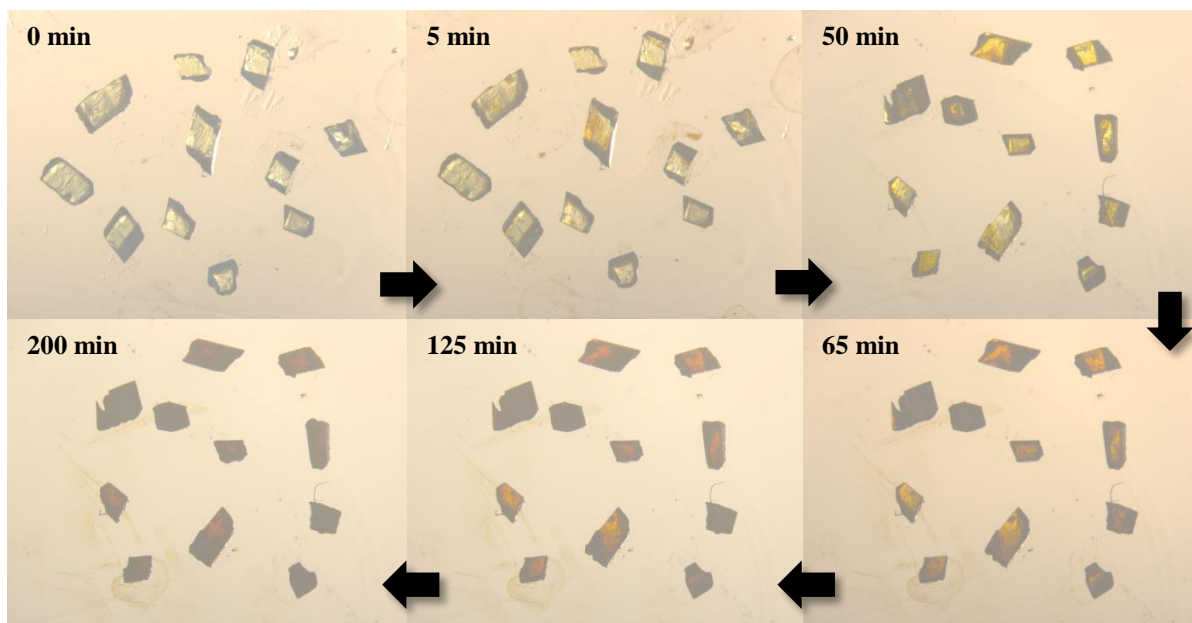
h) **1·Iodine**

**Figure 2.27** The packing diagram of **1·Iodine** viewed down the *c* axis.

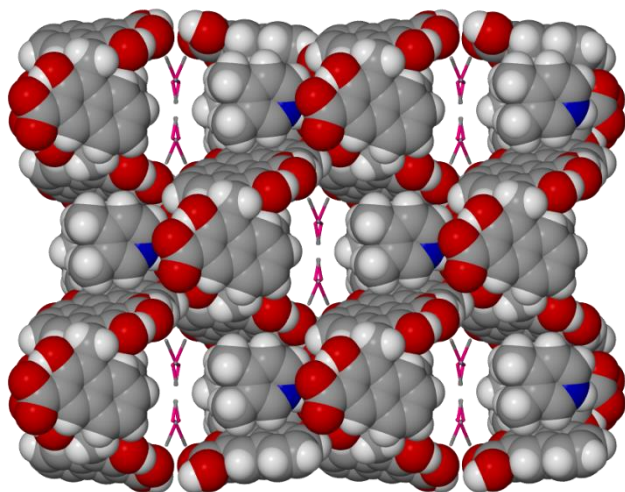
Iodine uptake in framework materials such as MOFs<sup>32, 33</sup> and organic framework materials<sup>34, 35</sup> has been reported fairly recently and often, but to our knowledge has not yet been reported for an ionic organic framework. In **1·Iodine** two molecules of iodine have been modelled in the asymmetric unit where the occupancy of the molecules has been allowed to refine. SQUEEZE analysis infers the presence of 0.9 iodine molecules per asymmetric unit (99 electrons

whereas iodine has 106 electrons). The lower than expected occupancy could be due to the loss of iodine while searching for a suitable crystal for SCD analysis. As can be seen in Figure 2.27, the iodine molecules spiral along the *b* axis and fill the channel.

There is a gradual change in the colour of crystals of **1·THF** exposed to iodine vapour (Figure 2.28). The crystals are initially colourless and upon exposure to iodine vapour the colour gradually starts to change from the edges of the crystal until the entire crystal is purple. Upon prolonged exposure the crystals start to degrade.

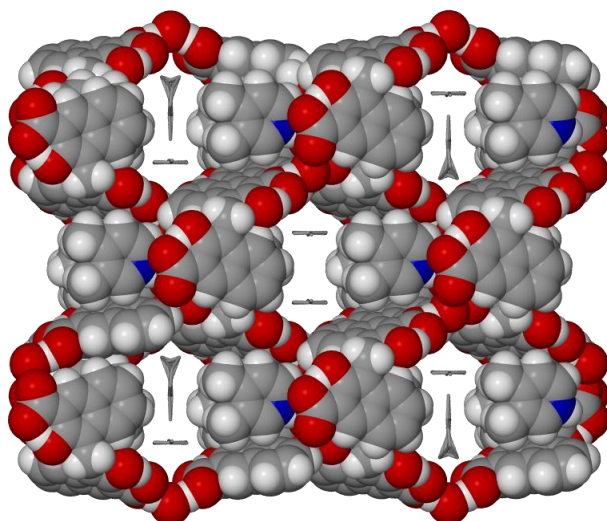


**Figure 2.28** The crystals of **1·THF** exposed to iodine vapour for four hours. The crystals darken from the edges of crystal, gradually spreading to the centre.

**i) 1·MeI****Figure 2.29** The packing diagram of **1·MeI**.

**1·THF** was exposed to iodomethane in order to determine the kinetics of exchange of the framework. This work will be discussed in Chapter 3. In **1·MeI** four molecules of iodomethane have been modelled with the sum occupancy of one. NMR and SQUEEZE analysis confirm that there is one iodomethane molecule per asymmetric unit. The thermal ellipsoids of the iodomethane molecules are quite large, indicating that there is a lot

of movement of the iodomethane molecules within the channel. The methyl hydrogen atoms for iodomethane have not been modelled.

**j) 1·Toluene****Figure 2.30** The packing diagram of **1·Toluene**.

In **1·Toluene** one molecule of toluene could be modelled on a special position. No satisfactory model could however be obtained for the second molecule. It seems as though the second toluene molecule is disordered over two positions, sharing the methyl group. SQUEEZE and NMR analysis confirm the presence of one toluene molecule per asymmetric unit. There also appear to be C-H... $\pi$  interactions between the toluene

molecules in the channel (Figure 2.30) where one toluene molecule lies flat along the channel and the other lies perpendicular to it.



### k) **1·Hexane**

For **1·Hexane** no good model could be obtained for the guest in the channel. Some of the modelled electron density appears to extend down the channel but the disorder makes it difficult to model the guest properly. It could be that the long disordered alkyl chain of *n*-hexane disturbs the translational symmetry of the structure. The periodicity of the guest does therefore not match the periodicity of the framework and makes it extremely difficult to model the guest. **1·Hexane** could be an example of an *incommensurately modulated structure*.<sup>36</sup> In modulated structures there are atoms or molecules that are shifted with respect to neighbouring atoms or molecules.<sup>36</sup> This causes a loss in the three-dimensional translational symmetry of the structure.<sup>36</sup> In this case the translational symmetry of the framework and *n*-hexane do not match, causing it to be incommensurate. <sup>1</sup>H NMR analysis of crystals of **1·Hexane** indicate the presence of 0.3 molecules of *n*-hexane per asymmetric unit, which is further supported by SQUEEZE analysis that also indicate that *n*-hexane is not present in the channels at full occupancy.

**Table 2.5** Selected crystallographic information for the exchanges with **1·THF**.

	<b>1·THF</b>	<b>1·Acetone</b>	<b>1·DCM</b>	<b>1·Ether</b>	<b>1·Chloroform</b>	<b>1·Dioxane</b>	<b>1·MeOH</b>	<b>1·EtOH</b>
Stoichiometry (acid:base:solvent:water)	1:1:1:0.5	1:1:1:0.5	1:1:1:0.5	1:1:1:0.5	1:1:1:0.5	1:1:1:0.5	1:1:1:0.5	1:1:1:0.5
Chemical formula	C <sub>34</sub> H <sub>34</sub> NO <sub>7.5</sub>	C <sub>33</sub> H <sub>32</sub> NO <sub>7.5</sub>	C <sub>30.87</sub> H <sub>28.26</sub> C <sub>11.74</sub> NO <sub>6.76</sub>	C <sub>34</sub> H <sub>36</sub> NO <sub>7.5</sub>	C <sub>62</sub> H <sub>54</sub> Cl <sub>6</sub> N <sub>2</sub> O <sub>13</sub>	C <sub>33</sub> H <sub>30</sub> NO <sub>7.75</sub>	C <sub>31</sub> H <sub>30</sub> NO <sub>7.5</sub>	C <sub>32</sub> H <sub>32</sub> NO <sub>7.5</sub>
Formula Weight	576.62	562.60	582.99	578.64	1247.77	564.58	536.56	550.61
Crystal System	Monoclinic	Monoclinic	Monoclinic	Monoclinic	Monoclinic	Monoclinic	Monoclinic	Monoclinic
Space group	<i>C2/c</i>	<i>C2/c</i>	<i>C2/c</i>	<i>C2/c</i>	<i>P2<sub>1</sub>/c</i>	<i>C2/c</i>	<i>C2/c</i>	<i>C2/c</i>
Z	8	8	8	8	4	8	8	8
<i>a</i> /Å	22.117(1)	22.12(1)	21.952(7)	21.974(1)	14.586(1)	22.105(2)	21.973(7)	22.086(2)
<i>b</i> /Å	19.857(1)	19.81(1)	19.780(7)	19.909(1)	19.829(1)	19.940(2)	19.800(7)	19.782(1)
<i>c</i> /Å	14.615(8)	14.75(1)	14.411(5)	14.749(1)	20.742(2)	14.742(1)	14.519(5)	14.585(1)
$\alpha^\circ$	90	90	90	90	90	90	90	90
$\beta^\circ$	115.240(1)	114.847(9)	114.883(4)	114.287(1)	104.343(1)	115.242(1)	114.443(4)	114.304(1)
$\gamma^\circ$	90	90	90	90	90	90	90	90
Volume/Å <sup>3</sup>	5806.0(6)	5862(7)	5676(3)	5881.3(7)	5812.2(7)	5877.7(1)	5751(3)	5807.4(7)
Temperature/K	100(2)	100(2)	100(2)	100(2)	100(2)	100(2)	100(2)	100(2)
<i>R</i> <sub>int</sub>	0.0221	0.0474	0.0827	0.0330	0.0308	0.0276	0.0300	0.0281
<i>R</i> <sub>1</sub> [ <i>I</i> > 2σ( <i>I</i> )]	0.0426	0.0554	0.1050	0.0481	0.0798	0.0816	0.0853	0.0872

**Table 2.6** Selected crystallographic data (continued) for the exchanges with **1·THF**.

	<b>1·PrOH</b>	<b>1·Benzene</b>	<b>1·Pyrazine</b>	<b>1·Iodine</b>	<b>1·MeI</b>	<b>1·Toluene</b>	<b>1·Hexane</b>
Stoichiometry (acid:base:solvent:water)	1:1:1:0.5	1:1:1:0.5	1:1:1:0.5	1:1:1:0.5	1:1:1:0.5	1:1:1:0.5	1:1:1:0.5
Chemical formula	C <sub>33</sub> H <sub>33</sub> NO <sub>7.5</sub>	C <sub>36</sub> H <sub>29</sub> NO <sub>6.5</sub>	C <sub>34</sub> H <sub>32</sub> N <sub>2</sub> O <sub>7</sub>	C <sub>60</sub> H <sub>52</sub> I <sub>1.57</sub> N <sub>2</sub> O <sub>13</sub>	C <sub>30.77</sub> H <sub>26</sub> I <sub>0.99</sub> NO <sub>6.50</sub>	C <sub>36.24</sub> H <sub>25</sub> NO <sub>6.5</sub>	C <sub>35</sub> H <sub>26</sub> NO <sub>6.5</sub>
Formula Weight	563.60	579.63	580.64	1208.58	639.20	578.44	564.60
Crystal System	Monoclinic	Monoclinic	Monoclinic	Monoclinic	Monoclinic	Monoclinic	Monoclinic
Space group	<i>C2/c</i>	<i>C2/c</i>	<i>C2/c</i>	<i>C2/c</i>	<i>C2/c</i>	<i>C2/c</i>	<i>C2/c</i>
Z	8	8	8	4	8	8	8
<i>a</i> /Å	22.152(6)	22.094(4)	22.050(3)	22.094(3)	22.040(2)	21.992(7)	22.139(3)
<i>b</i> /Å	19.852(6)	20.011(4)	19.967(3)	19.900(2)	19.803(2)	20.034(6)	19.812(2)
<i>c</i> /Å	14.576(4)	14.700(3)	14.616(2)	14.636(3)	14.597(2)	14.690(5)	14.663(2)
$\alpha$ /°	90	90	90	90	90	90	90
$\beta$ /°	115.428(3)	115.097(3)	115.233(2)	115.028(2)	114.718(2)	114.703(4)	115.089(1)
$\gamma$ /°	90	90	90	90	90	90	90
Volume/Å <sup>3</sup>	5789(3)	5885.7(2)	5821.0(1)	5830.9(1)	5787.2(1)	5880(3)	5824.7(1)
Temperature/K	100(2)	100(2)	100(2)	100(2)	100(2)	100(2)	100(2)
<i>R</i> <sub>int</sub>	0.0584	0.0457	0.0282	0.0475	0.0247	0.0415	0.0350
<i>R</i> 1 [ <i>I</i> > 2σ( <i>I</i> )]	0.0897	0.0904	0.0681	0.1566	0.1122	0.0960	0.0886

### 2.3.2. Successful exchanges with 1·THF where no SCD data could be obtained

Of the 21 successful guest exchanges with 1·THF, 14 could be characterised by SCD. Unfortunately we were unable to obtain SCD data for the remaining seven exchanges, listed in Table 2.7.

**Table 2.7** Successful exchanges with 1·THF for which no SCD data could be obtained.

Compound exposed to 1·THF	Supporting data
Acetonitrile	NMR, PXRD, TGA
Benzonitrile	NMR, PXRD, TGA, IR
Naphthalene	NMR, PXRD, TGA, IR
1-ethyl-pyrrolidone	NMR, PXRD
N-methylpyrrolidone (NMP)	NMR, PXRD, TGA
<i>p</i> -xylene	NMR, PXRD
<i>m</i> -xylene	NMR, PXRD

In Figure 2.31 the powder patterns of crystals of 1·THF after exchange with the indicated compound are shown. In all cases the framework structure remained intact, but there was a significant loss in crystallinity as is illustrated by the decrease in the intensity of the powder patterns, as well as the broad peaks seen in the powder pattern after exchange with naphthalene.

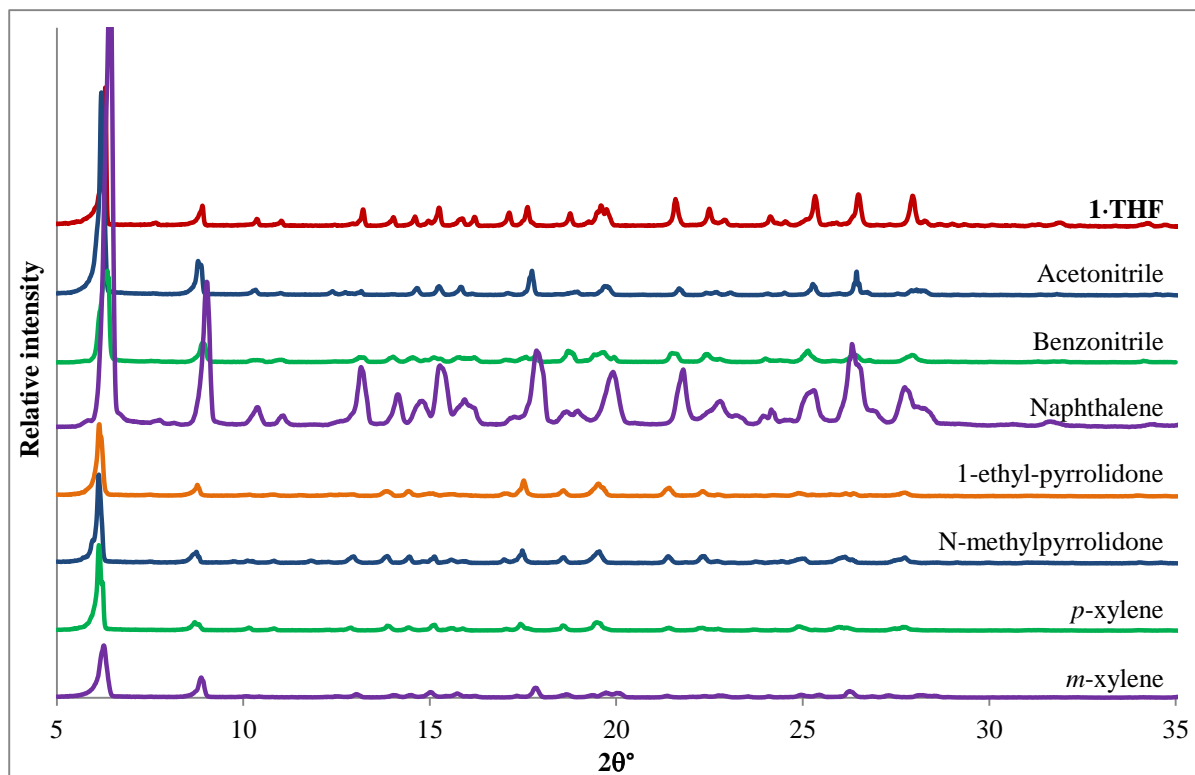


**Figure 2.31** PXRD analysis of crystals of **1·THF** after exposure to the indicated compound. The framework structure was retained in all cases, but there is a significant loss in crystallinity evidenced by the decreased intensity of the patterns and the broad peaks seen for the crystals of **1·THF** after exposure to naphthalene.

$^1\text{H}$  NMR analysis (Appendix C) confirmed the presence of the relevant guest in each of the structures as well as the stoichiometric ratio. In the case of exchange with acetonitrile full 1:1 exchange occurred and there were no THF peaks in the NMR spectrum. For *m*-xylene half a molecule was present per asymmetric unit and no THF peaks were observed in the NMR spectrum. In the case of the remaining exchanges there were varying ratios of guest:THF present per asymmetric unit. Very little benzonitrile had exchanged over the space of a week: the benzonitrile:THF ratio was only 0.2:0.8. These exchanges appear to take place over a much longer time period than the exchanges discussed in Section 2.3.1. It was also necessary to do these exchange experiments at slightly elevated temperatures in order to start the exchange process. PXRD analysis indicated that the framework remained intact after each exchange. Single crystals after exposure to the vapour of these compounds were of very poor quality and not suitable for SCD analysis. Table 2.8 contains a summary of the NMR results.

Thermal analysis of the crystals after exchange with the relevant compound, shown in Figure 2.32, mostly resembled the two-step mass loss profile of the original **1·THF**. However, crystals that have been exposed to benzonitrile do not have the same mass loss profile as the original structure. Here the loss of guest and 3,4-lutidine have merged into one step, which is

reminiscent of the mass loss profiles of **1-Pyrazine** and **1-Dioxane** (Section 2.3.1). The calculated percentage mass loss was determined with the aid of the NMR results and correlates well with the experimental mass loss percentages for each exchange. The TGA results are also summarised in Table 2.8.

**Table 2.8** Selected results of the NMR and TG analysis of crystals of **1-THF** exposed to the relevant solvent.

Compound	NMR ratio (guest:THF) per asymmetric unit	TGA results (per asymmetric unit)	
		Calculated % loss	experimental % loss
Acetonitrile	1:0	27.2	26.3
Benzonitrile	0.2:0.8	31.8	30.9
Naphthalene	0.7:0.3	35.5	31.1
N-methylpyrrolidone	0.75:0.25	33.4	31.9

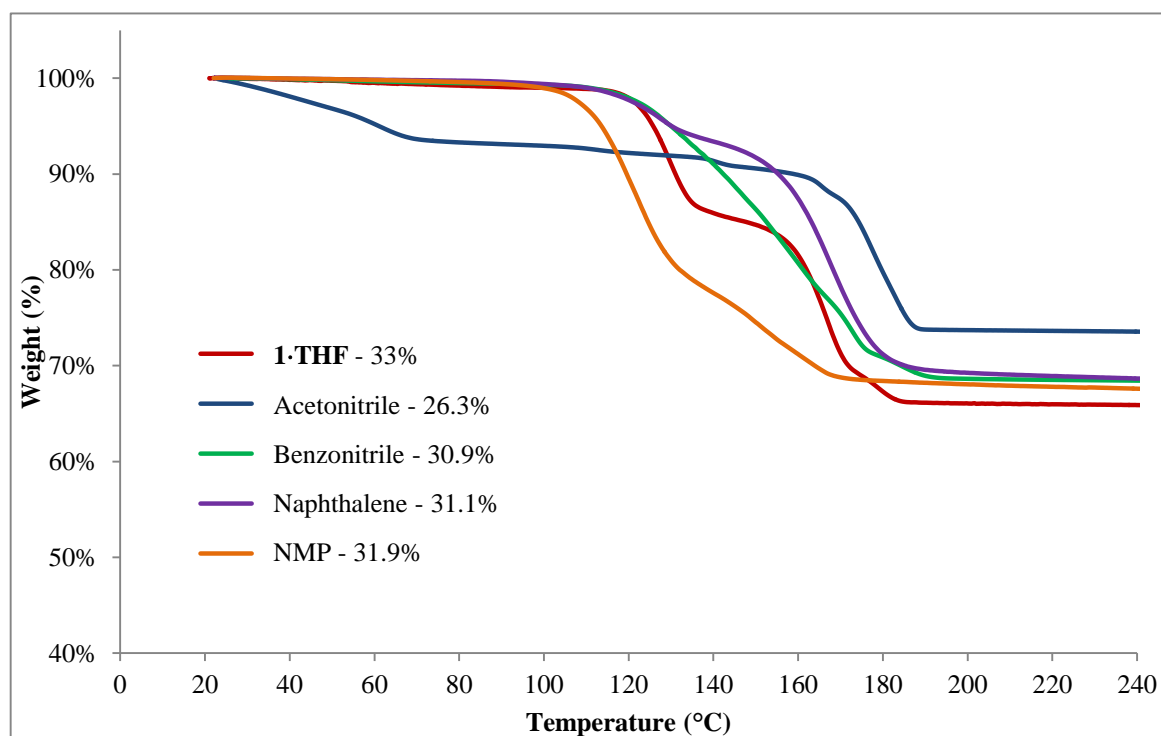


**Figure 2.32** Thermogravimetric analysis of the crystals of **1-THF** after exchange with the indicated solvent. Acetonitrile, naphthalene and NMP exhibit two-step mass loss profiles similar to that of THF. Benzonitrile however does not - in this case the loss of solvent and lutidine have merged into one step, similar to the mass loss profiles of **1-Pyrazine** and **1-Dioxane**.

To further confirm the presence of benzonitrile and naphthalene in the framework FTIR analysis was performed on the crystals after exchange. In Figure 2.33 the IR spectra of **1·THF** before exchange is compared to the spectra of the crystals after exchange with benzonitrile and naphthalene. The spectra are practically identical except for a small peak at approximately  $2220\text{ cm}^{-1}$  in the benzonitrile spectrum that is not seen in the spectrum of **1·THF** (Figure 2.33(ii)). This stretch is in the region where the  $-\text{C}\equiv\text{N}$  stretch is usually observed.<sup>37</sup> This is however a very small peak, which supports the NMR evidence that very little benzonitrile undergoes exchange with **1·THF**. The spectrum of the naphthalene exchange does not clearly indicate whether naphthalene is present in the crystals or not. This is possibly due to the fact that naphthalene only contains aromatic rings, much like pamoic acid and therefore it is not possible to separate which stretches belong to naphthalene and which to pamoic acid. The aromatic stretches are usually observed between  $1600$  and  $1475\text{ cm}^{-1}$ .<sup>37</sup> The only small difference between the spectrum of the naphthalene structure and that of **1·THF** is that a peak at approximately  $2380\text{ cm}^{-1}$  has slightly shifted and the splitting is different (Figure 2.33(i)). We are however unable to draw any conclusive results from the spectrum of the naphthalene exchange.

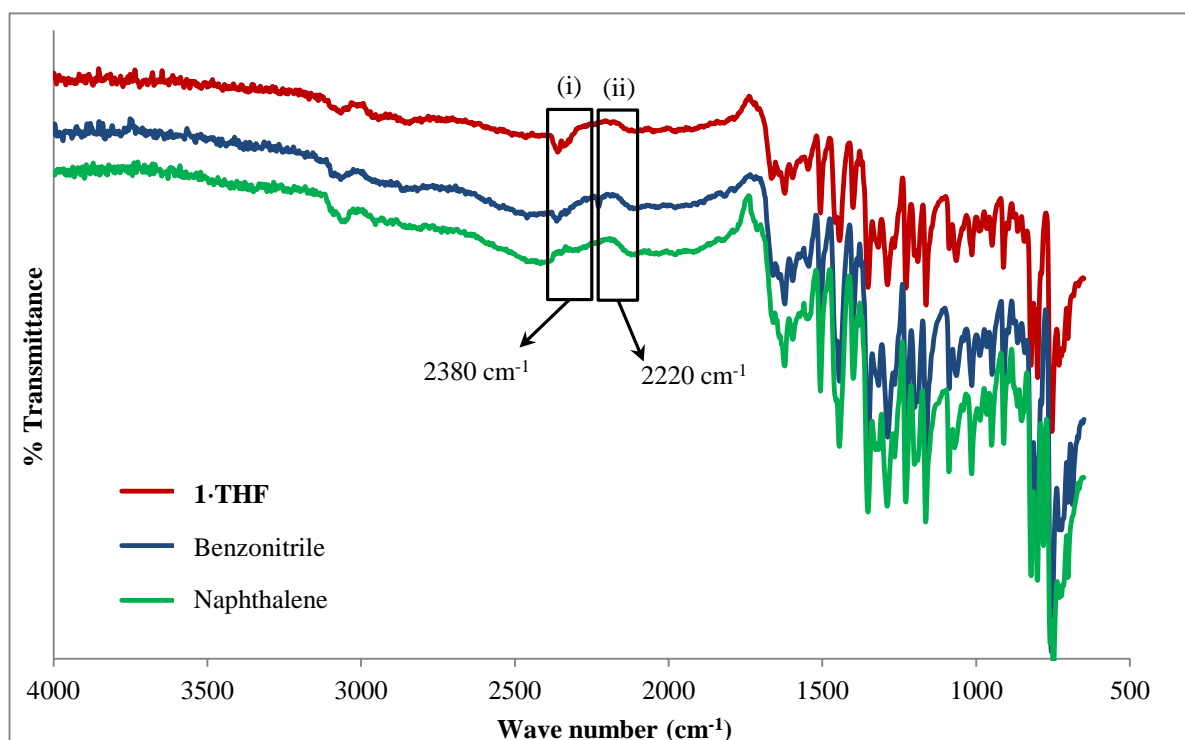


**Figure 2.33** The infrared spectra of **1·THF**, and crystals of **1·THF** after exposure to benzonitrile and naphthalene. A peak in the naphthalene spectrum at  $2380\text{ cm}^{-1}$  (i) has shifted slightly compared to the peak in the spectrum of **1·THF**. Otherwise the spectra of **1·THF** and exchange with naphthalene appear to be identical and we cannot draw any conclusions regarding the presence of naphthalene in the framework. The peak at  $2220\text{ cm}^{-1}$  (ii) in the spectrum of exchange with benzonitrile is in the region of the nitrile stretch and is not present in the spectrum of **1·THF**. This indicates that benzonitrile is present in the framework, but as indicated by the low intensity of the peak, not in a large amount.

### 2.3.3. Unsuccessful exchanges with 1·THF

There are a few cases where no exchange takes place with 1·THF. These are listed again in Table 2.9.

**Table 2.9** A summary of the unsuccessful exchanges with 1·THF and the resultant products.

Solvent	Product	Analyses performed
Cyclohexane	Unchanged 1·THF	NMR, PXRD, TGA
Cyclohexanone	Unchanged 1·THF	NMR, PXRD, TGA
2-pyrrolidone	Unchanged 1·THF	NMR, PXRD
Aniline	New compound	NMR, PXRD, TGA
Morpholine	New compound	NMR, PXRD
Dimethylformamide	Mixture of SIQCIF and TAPDAR	NMR, PXRD, TGA
Pyridine	Pyridinium pamoate salt (TABMAK)	NMR, PXRD

When 1·THF is exposed to cyclohexane, cyclohexanone or 2-pyrrolidone no exchange takes place and the original 1·THF structure is retained. This was confirmed by <sup>1</sup>H NMR and PXRD analysis. It could be that cyclohexane and cyclohexanone are simply too big for the channel, but this is not the case for 2-pyrrolidone. This molecule does not have the methyl group that N-methylpyrrolidone (NMP) has, yet NMR and PXRD analysis suggests that NMP does exchange with THF. It could be that 2-pyrrolidone is not volatile enough to generate a vapour pressure high enough to allow for exchange to take place. The boiling point of 2-pyrrolidinone is significantly higher than that of NMP: 251 °C compared to 202 °C. NMP has a vapour pressure of approximately 8 mmHg at 20 °C,<sup>38</sup> therefore one could safely assume that the vapour pressure of 2-pyrrolidone would be even lower. It is therefore possible that the vapour pressure of 2-pyrrolidone is too low and that is why exchange does not take place.

In some cases the solvent has the ability to interact with the constituents of the framework to form a different compound. When 1·THF is exposed to the vapour of pyridine it forms the known pyridinium pamoate salt (CSD-TABMAK<sup>39</sup>). When exposed to the vapour of DMF the crystals that were produced gave a powder pattern of rather poor quality and it is not possible to say with absolute certainty whether the pattern matches to any known structure with pamoic acid. The powder pattern appears to be a mixture of the pamoic acid/DMF solvate (CSD-SIQCIF<sup>40</sup>) and the 3,4-lutidinium pamoate DMF solvate (CSD-TAPDAR<sup>3</sup>) and



it seems plausible that DMF could convert **1·THF** to any of these two structures. In the case of exposure to the vapours of aniline and morpholine new compounds are formed that do not match the powder patterns of any of the known cocrystals, salts or solvates with pamoic acid. It is suspected that since pyridine had the ability to transform **1·THF** into the pyridinium pamoate salt that aniline and morpholine also converted the framework to the pamoate salt of these compounds. This could be a  $pK_a$  effect that allows for proton transfer to occur from the 3,4-lutidinium ion to the pamoate ion, allowing pamoic acid to react with pyridine, aniline or morpholine. The powder patterns of these compounds are shown in Figure 2.34.

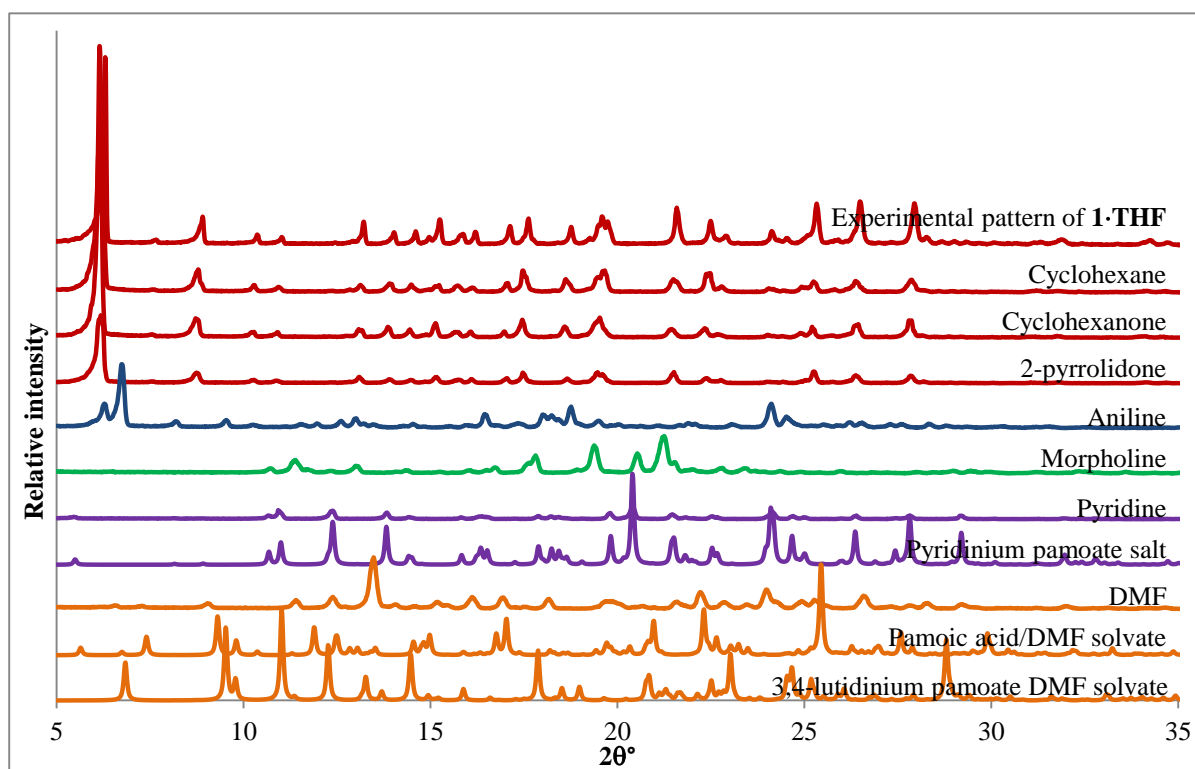


**Figure 2.34** The powder patterns of the solvents that did not undergo exchange with **1·THF** (cyclohexane, cyclohexanone and 2-pyrrolidone) and the solvents that changed the original **1·THF** structure (aniline, morpholine, pyridine and DMF). Exposure to pyridine leads to the collapse of the framework and the conversion to the pyridinium pamoate salt TABMAK. Exposure to DMF leads to the formation of a mixture of what could be the pamoic acid/DMF solvate (SIQCIF) and the 3,4-lutidinium pamoate DMF solvate (TAPDAR).

As part of future work with framework **1** it should be investigated whether cyclohexane, cyclohexanone and 2-pyrrolidone may exchange with the THF in **1·THF** at higher temperatures, as was the case with some compounds discussed in Section 2.3.2.

### 2.3.4. Step-wise exchanges with 1·THF

It is also possible to do step-wise exchanges with framework **1**. Crystals of **1·THF** were dried and placed in a glass vial, which was in turn placed in a larger jar containing approximately 1 ml acetone. The jar was capped and sealed with parafilm. The crystals were left for approximately five days under an atmosphere of acetone vapour, after which a sample of approximately 20 mg was taken from the glass vial for PXRD (Figure 2.35) and NMR (Figure 2.36) analysis which confirmed that full exchange had taken place and the framework was still intact. For each of the subsequent exchanges, the crystals were exposed to the solvent vapour for approximately five days. Each solvent exchanged completely for the next. The order was as follows: THF → acetone → benzene → chloroform → diethyl ether → DCM. After the fifth exchange from diethyl ether to DCM, the crystals started to look opaque and severely striated.

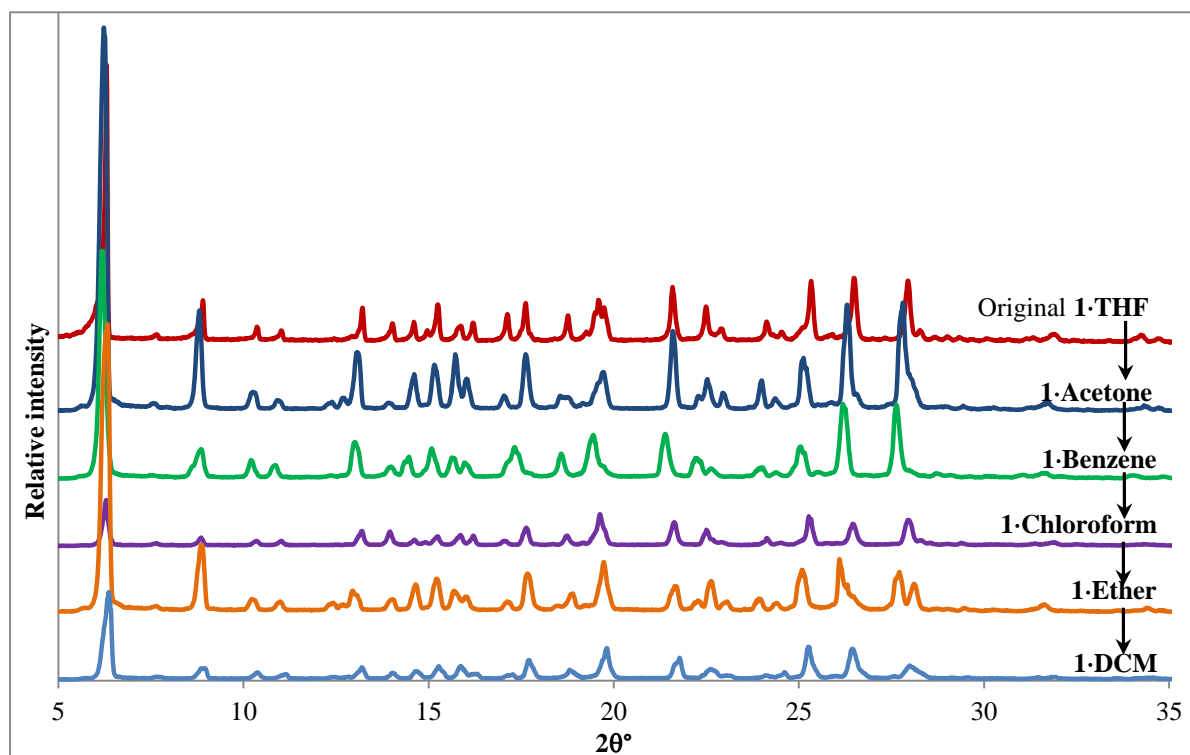


**Figure 2.35** The powder patterns of the crystals after step-wise exchange with the desired solvent.

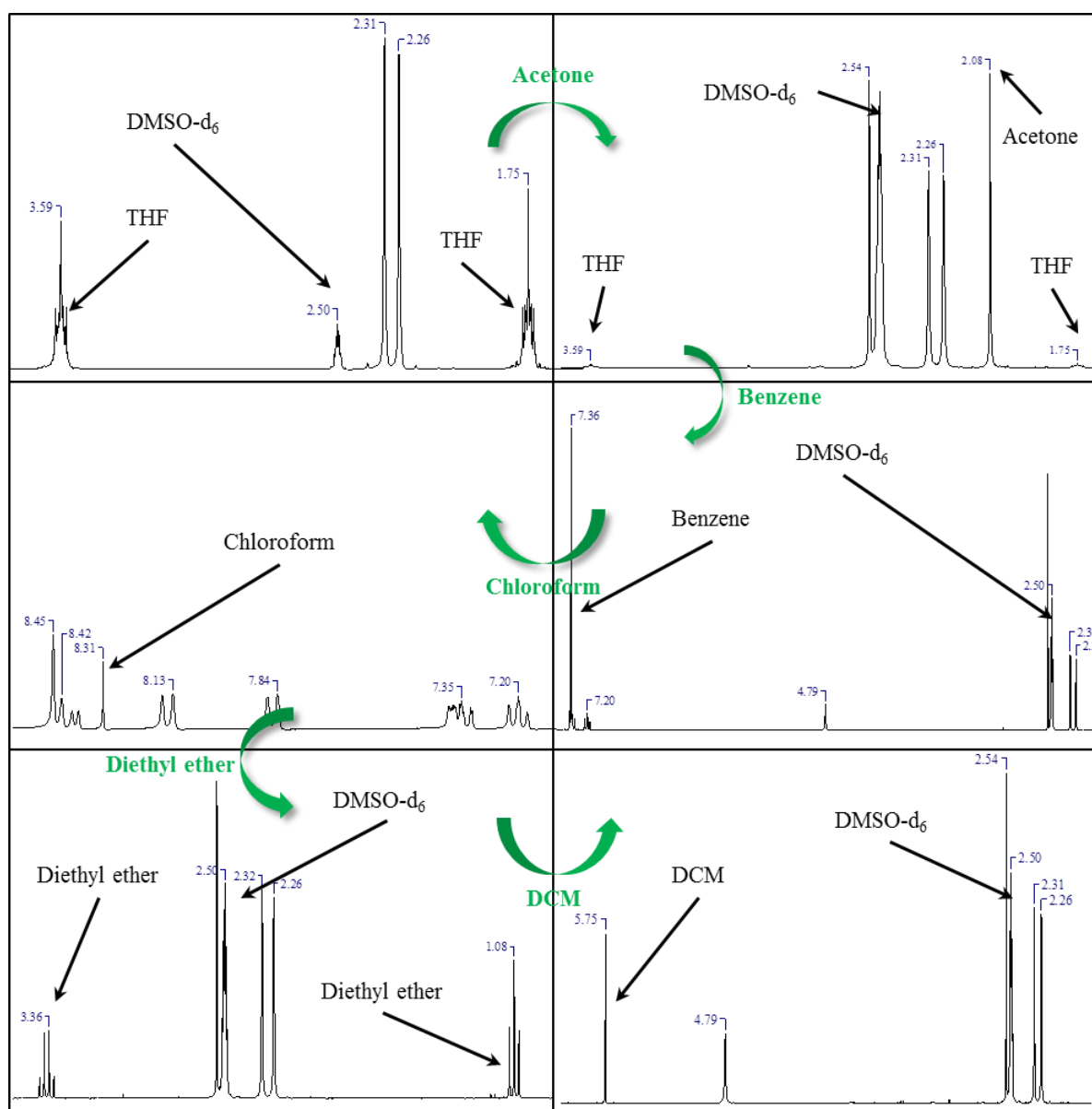


**Figure 2.36** The  $^1\text{H}$  NMR results after step-wise exchange with the appropriate solvent, starting at the top left with the spectrum of  $1\cdot\text{THF}$ . In each case complete exchange occurred.

It is also possible to regenerate  $1\cdot\text{THF}$  by exposing the crystals of  $1\cdot\text{Chloroform}$  to THF vapour. This was confirmed by NMR and PXRD analysis. It has not been determined whether this is possible for  $1\cdot\text{Pyrazine}$  and  $1\cdot\text{Iodine}$ , but it seems unlikely since these crystals drastically deteriorate after prolonged exposure to pyrazine and iodine, respectively.

### 2.3.5. Exchange by immersion of crystals in various solvents

We investigated whether it was possible to exchange the THF in  $1\cdot\text{THF}$  by immersing the crystals in the solvent of choice. In doing so it is possible to gain insight into how robust the framework is when directly exposed to solvent and how strong the hydrogen bonding in the

framework is. If the hydrogen bonding within the framework is of sufficient strength and the framework is the more favourable than any new structure that could potentially form, then **1·THF** will be less likely to dissolve to form a different structure.

Crystals of **1·THF** were removed from the mother liquor, dried on filter paper and placed in a glass vial. A thin layer of the appropriate solvent was added, enough to only cover the crystals. The vial was sealed with a cap and parafilm. After two days the crystals were analysed by  $^1\text{H}$  NMR (Appendix C), which confirmed in each case that exchange had taken place, and PXRD, which confirmed that the framework structure had been retained. In Figure 2.37 the powder patterns of the crystals are shown after exchange. When crystals of **1·THF** are exposed to acetonitrile and methanol new structures are formed. In the case of acetonitrile a 3,4-lutidinium pamoate acetonitrile solvate forms which will be further discussed in Section 2.5. Suitable crystals for SCD could not be obtained from methanol, but due to the similarity of the powder pattern to that of the acetonitrile solvate it is possible that an isostructural methanol solvate was formed.

It seems as though framework **1** is a very stable structure that easily allows for the permeation of various solvents through the channels.

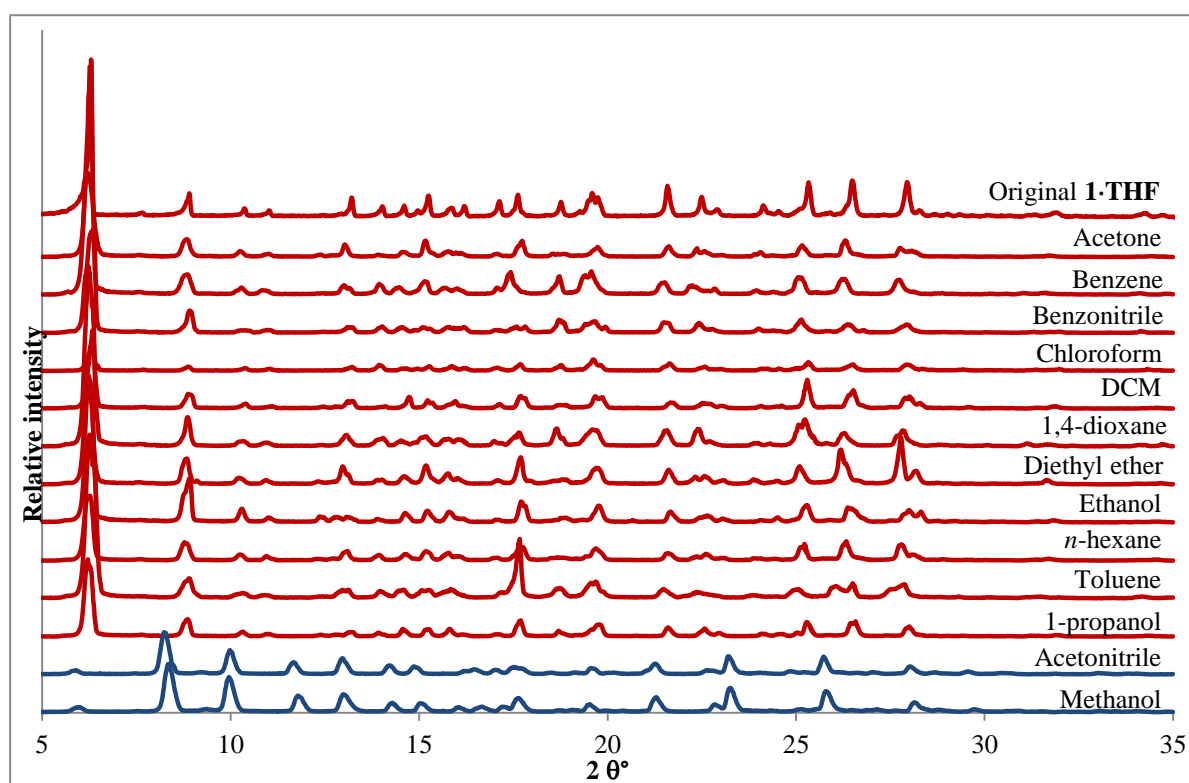


**Figure 2.37** The powder patterns of crystals of **1·THF** after immersion in various solvents. The structure of the framework was retained except when the crystals were immersed in acetonitrile and methanol.

## 2.4. Competition experiments

Competition experiments were performed with **1·THF** to determine whether the framework exhibited any selectivity towards certain solvents. If the framework does show selectivity it could lay the foundation for future research into possibly using this material for purification or separation purposes. One would expect that preference would be shown to a solvent molecule that fits the channel the best. Therefore doing selectivity experiments could lend insight into which solvent molecules have a better shape-fit in the channels of the framework.

Since it is possible to exchange the original THF in **1·THF** by immersing the crystals in the solvent or by simply exposing the crystals to the vapour of the solvent, two different types of competition experiments were performed with **1·THF**. The first set of experiments was performed with 1:1 molar mixtures of solvents to which crystals of **1·THF** were exposed to the vapour of the solvent mixture. This does however not imply that the vapour phase will contain a 1:1 molar mixture of the solvents due to the difference in the partial pressures of the various solvents. The aim was to expose **1·THF** to a mixture of solvent vapours whilst mimicking the environment during vapour exchange experiments with pure solvents, i.e. room temperature and atmospheric pressure, to investigate whether the framework shows any preference for certain solvents. The results will be discussed in Sections 2.4.1 and 2.4.2. The second set of experiments involved setting up 1:1 molar mixtures of solvents and then immersing the crystals of **1·THF** directly in the solvent mixtures for approximately two days. The results of these experiments will be discussed in Section 2.4.4.

### 2.4.1. Competition experiments with mixed solvent vapours

Crystals of **1·THF** were exposed to mixed solvent vapours for approximately one week, after which the crystals were analysed by  $^1\text{H}$  NMR to determine the ratio of the solvents present in the crystals. The results are tabulated in Table 2.10. The solvent combinations were chosen according to their similarity in size and shape to determine whether the framework has any selectivity specifically for one solvent over another when they are roughly the same size and shape. Preliminary results show that there is the possibility of selectivity for some solvents over others. Vapour pressure diagrams<sup>38, 41</sup> of each of the solvents used were plotted to determine whether or not some solvents were in excess in the vapour phase (Figure 2.38). In a mixture of chloroform/DCM the DCM was in excess; in benzene/toluene the benzene was in excess; in ethanol/methanol the methanol was in excess; in acetonitrile/diethyl ether the

diethyl ether was in excess; and in 1,4-dioxane/NMP the 1,4-dioxane was in excess. Using this information in combination with the results from the vapour competition experiments allows us to draw some conclusions regarding the selectivity of the framework. The relative vapour pressures of the pure solvents of each mixture at 20 °C have also been included in Table 2.10.

**Table 2.10** Results of the exposure of **1**·THF to mixed vapours of selected solvents and the approximate vapour pressure of each pure solvent at 20 °C.

Solvent mixture (1:1 A:B)	Percentage solvent A	Percentage solvent B	Vapour pressure at 20 °C (A:B) in mmHg
Chloroform/DCM	64	36	175:350
Acetone/DMSO		No longer framework <b>1</b>	
Benzene/toluene	41	59	70:23
Ethanol/methanol	77	23	43:93
Acetonitrile/diethyl ether	15	85	70:435
1,4-dioxane/NMP	79	21	32:8

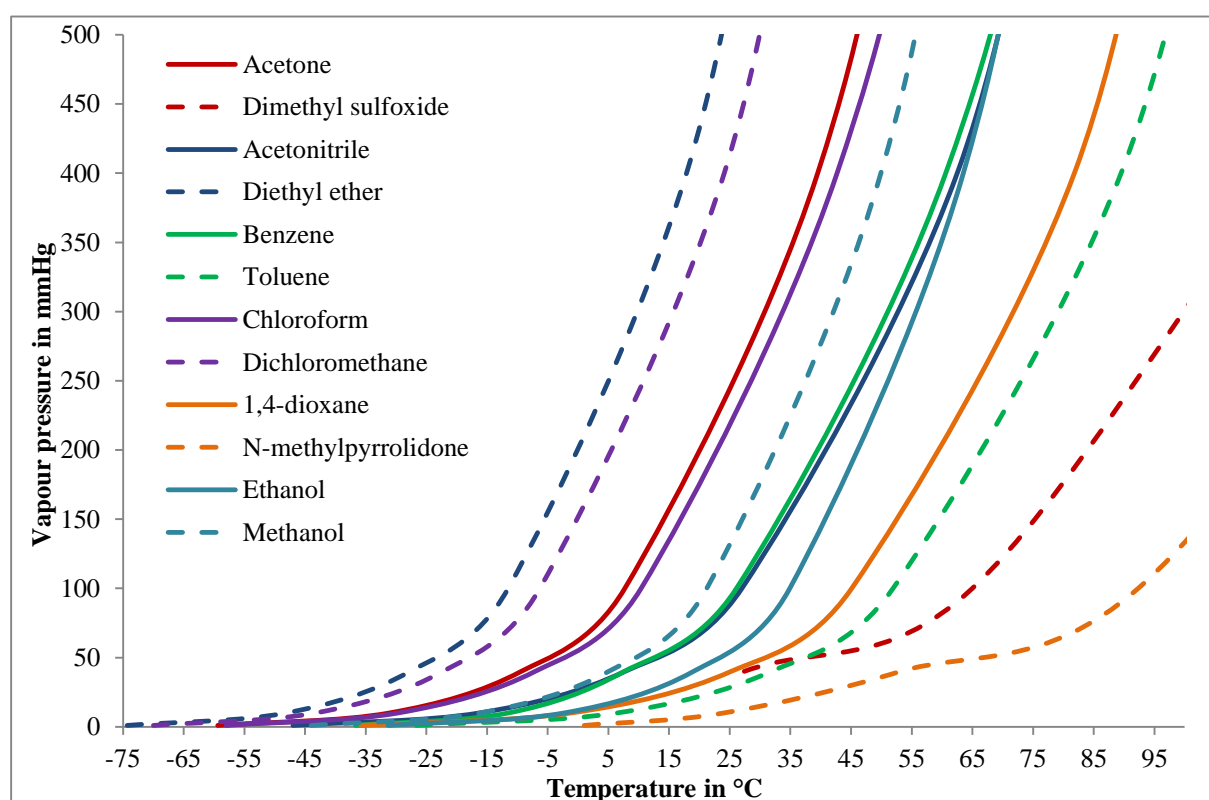


**Figure 2.38** The vapour pressures of pure solvents at various temperatures. Values were obtained from the *CRC Handbook of Chemistry and Physics*, 66<sup>th</sup> and 85<sup>th</sup> edition.<sup>27, 28</sup>

There is unfortunately no value for the vapour pressure of DMSO at 20 °C since the first recorded value for the vapour pressure of DMSO from the *CRC handbook of chemistry and physics* is only at 27 °C. This does however imply that the vapour pressure of DMSO is very low at 20 °C – much lower than that of acetone.

PXRD analysis of the crystals after exposure to the mixed solvent vapours (Figure 2.39) shows that when crystals of **1·THF** are exposed to a mixture of acetone/DMSO vapours, the framework converts to a structure that appears to be isostructural to a 3,4-lutidinium pamoate acetone solvate that will be discussed in Section 2.5. It is suspected that this is an isostructural DMSO solvate since NMR analysis indicated a much larger portion of DMSO present in the sample than acetone. No crystals of SCD quality could be obtained of this suspected DMSO solvate for further analysis.

These results indicate that **1·THF** selectively exchanges for chloroform over dichloromethane, toluene over benzene, ethanol over methanol, diethyl ether over acetonitrile and 1,4-dioxane over NMP.

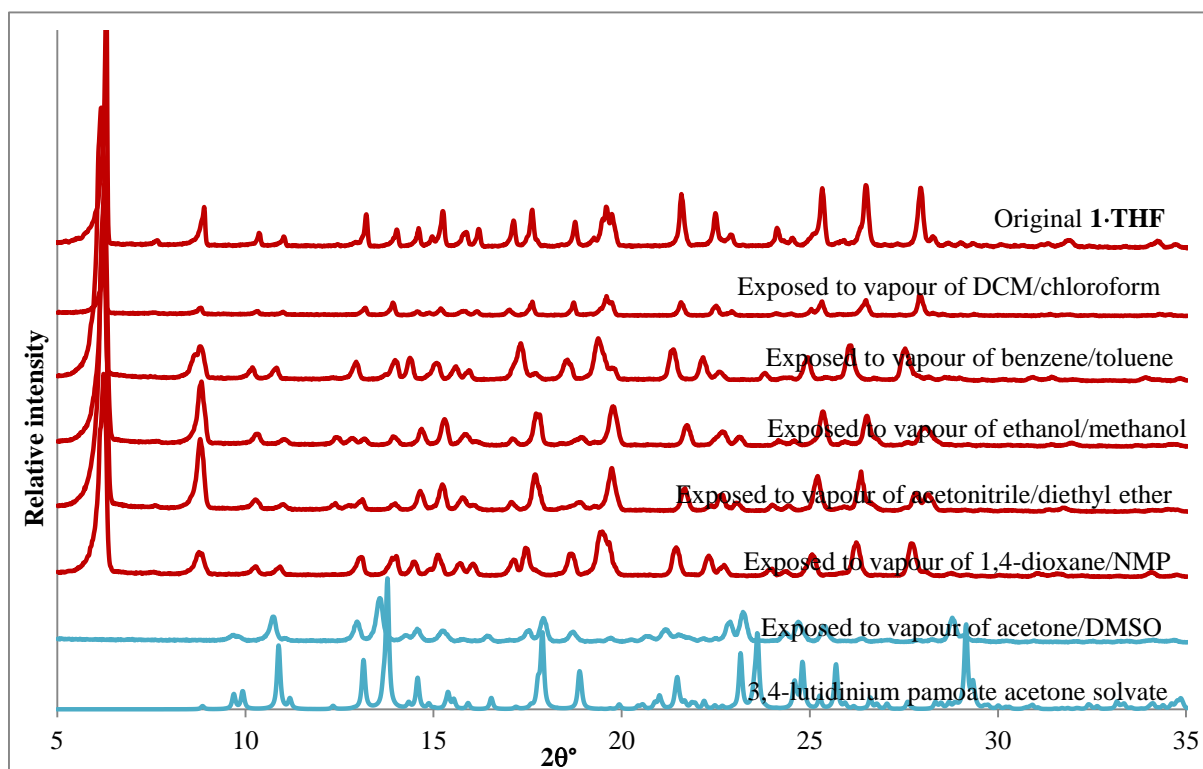


**Figure 2.39** The powder patterns of crystals after exposure to the mixed solvent vapours. When crystals of **1·THF** are exposed to a vapour mixture of acetone/DMSO a new structure is formed.

It is very interesting to note that in most cases the solvent with the lower vapour pressure is the one included in the framework structure, except with mixtures of acetonitrile/diethyl ether

and 1,4-dioxane/NMP. In these two instances the vapour pressures of diethyl ether and 1,4-dioxane are much higher and a larger percentage of these solvents have been included in framework **1**. It is however not possible to conclude whether diethyl ether and 1,4-dioxane are selectively included simply due to their higher vapour pressures or whether the framework **1** shows actual selectivity for these solvents. This was further investigated and will be discussed in Section 2.4.4 where crystals of **1**·THF were directly immersed in the solvent mixtures, thus eliminating the influence of vapour pressure and the amount of each solvent in the vapour phase.

### 2.4.2. Competition experiments with vapour mixtures of varying benzene/toluene fractions

In order to conclusively determine whether framework **1** is selective for certain solvents it is necessary to vary the ratio of the solvent mixtures that the framework is exposed to. This will indicate whether the framework simply absorbs whichever solvent is in excess or whether the framework exhibits true selectivity by preferably including solvent A over solvent B even at low fractions of solvent A.

The experiment is however not completely straightforward when the aim is to expose the crystals of **1**·THF to only the vapour of the solvent mixtures. The fraction of solvent present in the liquid phase is not always directly related to the fraction present in the vapour phase, unless one is dealing with an *ideal solution*.

Raoult's law states that the partial pressure of each of two components in a solution is directly proportional to the vapour pressure of the pure substance  $P_i^*$  and the mole fraction of each component in the liquid,  $x_i$ .<sup>42</sup> The partial pressure of each component is then given by

$$P_i = x_i P_i^* \quad (2.1)$$

where  $i$  is either component A or B. The total pressure over the solvent mixture can be expressed as

$$P_{total} = x_A P_A^* + x_B P_B^* \quad (2.2)$$

where  $x_A + x_B = 1$ .<sup>42</sup> This is strictly however only applicable to ideal solutions. The benzene/toluene mixture is the only solution that closely resembles an ideal solution. In an



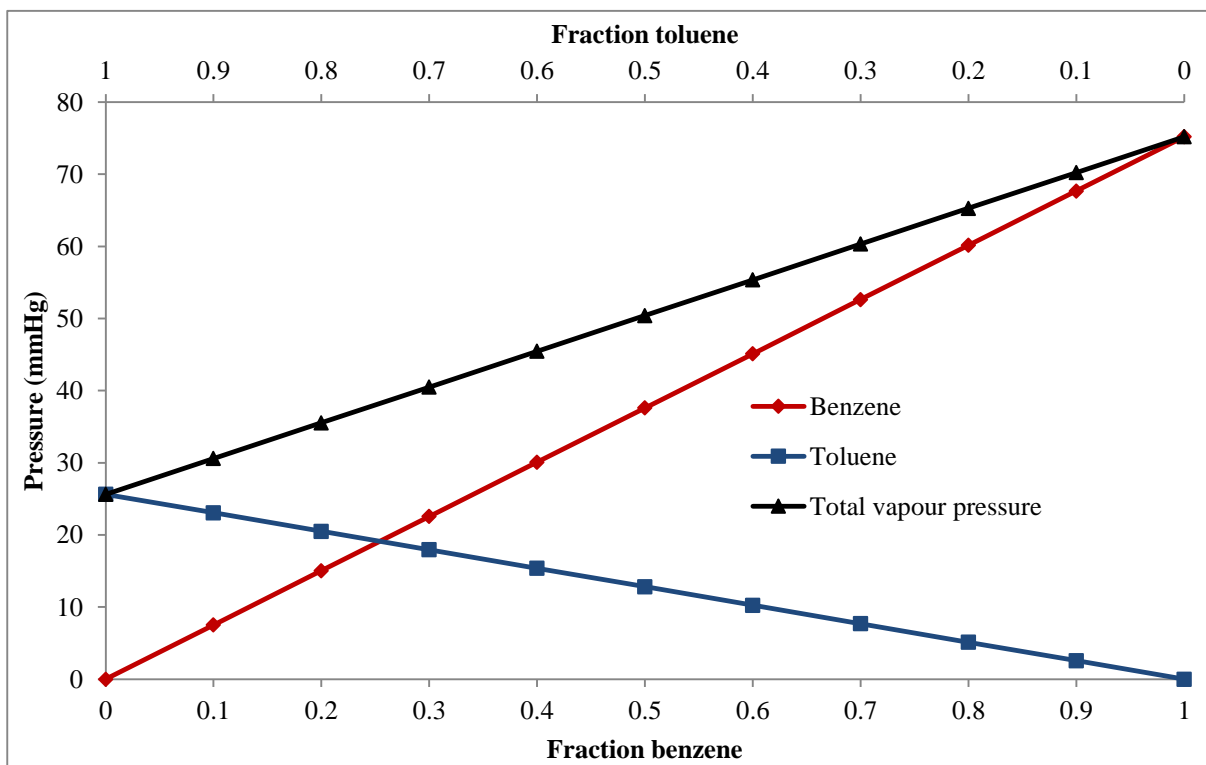
ideal solution the forces between A-B are the same as those of A-A and B-B.<sup>42</sup> If the attractive forces between A-B are stronger than A-A or B-B, more molecules will remain in solution and the vapour pressure will be lower than expected. If the repulsive forces between A-B are stronger, more molecules will be in the vapour phase and the vapour pressure will be higher than expected. In the case of benzene/toluene the two molecules are very similar in size, shape and chemical properties and therefore this solution obeys Raoult's law. Further vapour competition experiments were therefore performed with benzene/toluene where the molar fraction of benzene: toluene ranged from 0 to 1 in increments of 0.1. With the Antoine equation<sup>42</sup>

$$\ln \frac{P(T)}{\text{Pa}} = A(1) - \frac{A(2)}{\frac{T}{K} + A(3)} \quad (2.3)$$

it is possible to calculate the vapour pressure,  $P(T)$ , of the pure components at 20 °C (the temperature at which the exchange took place). The terms  $A(1)$ ,  $A(2)$  and  $A(3)$  are component-specific parameters. There are two sets of parameters for calculation of vapour pressure: one set for calculation of vapour pressure of a component up to the normal boiling point and a second set for calculations above the boiling point to the critical point of the component.<sup>43, 44</sup> For these experiments the first set of parameters were used since the experiments were performed below the boiling points of toluene and benzene. These values were then used in equation 2.1 to determine the partial pressure of each component in the vapour phase. Table 2.11 and Figure 2.40 contain the results of these calculations. Toluene has a much lower vapour pressure at each mole fraction since benzene is the more volatile of the two solvents.

**Table 2.11** The table lists the mole fraction of benzene (B) and toluene(T) and the subsequent partial vapour pressure of each using equations 2.1 – 2.3.

Mole fraction benzene	$P_B = x_B P_B^*$ (mmHg)	Mole fraction toluene	$P_T = x_T P_T^*$ (mmHg)	Sum of pressures (mmHg)
1.0	75.20	0.0	0.0	75.20
0.9	67.68	0.1	2.56	70.24
0.8	60.16	0.2	5.13	65.29
0.7	52.64	0.3	7.69	60.33
0.6	45.12	0.4	10.26	55.37
0.5	37.60	0.5	12.82	50.42
0.4	30.08	0.6	15.38	45.46
0.3	22.56	0.7	17.95	40.51
0.2	15.04	0.8	20.51	35.55
0.1	7.52	0.9	23.07	30.59
0.0	0.00	1.0	25.64	25.64

**Figure 2.40** A visual representation of the data in Table 2.11. Toluene has a much lower vapour pressure at all fractions compared to benzene since benzene is the more volatile solvent.

From the values in Table 2.11 and Figure 2.40 it is possible to calculate the actual fraction of each solvent present in the vapour phase by dividing each vapour pressure by the sum total of the combined vapour pressures, as shown in Table 2.12.

**Table 2.12** Calculation of the fractions of benzene and toluene present in the vapour mixture.

Vapour pressure of benzene(mmHg)	Vapour pressure of toluene(mmHg)	Sum of pressures (mmHg)	Fraction of benzene in vapour phase ( $X_{benzene}$ )	Fraction of toluene in vapour phase ( $X_{toluene}$ )
75.20	0.0	75.20	1.00	0.00
67.68	2.56	70.24	0.96	0.04
60.16	5.13	65.29	0.92	0.08
52.64	7.69	60.33	0.87	0.13
45.12	10.26	55.37	0.81	0.19
37.60	12.82	50.42	0.75	0.25
30.08	15.38	45.46	0.66	0.34
22.56	17.95	40.51	0.56	0.44
15.04	20.51	35.55	0.42	0.58
7.52	23.07	30.59	0.25	0.75
0.00	25.64	25.64	0.00	1.00

The fraction of toluene in the vapour phase ( $X_{toluene}$ ) is plotted against the fraction present in the crystals ( $Z_{toluene}$ ). The selectivity coefficient  $K_{toluene:benzene}$  can then be calculated as

$$K_{toluene:benzene} = \left( \frac{Z_{toluene}}{Z_{benzene}} \right) \times \left( \frac{X_{benzene}}{X_{toluene}} \right) \quad (2.4)$$

where  $X_{toluene} + X_{benzene} = 1$ .<sup>45</sup> The results in Figure 2.41 indicate that **1·THF** exhibits selectivity for toluene over all fractions. This is particularly interesting since toluene has a much lower partial vapour pressure than benzene, indicating quite a strong affinity for toluene over benzene. What is also interesting is that toluene is slightly larger than benzene and one would presume that it would be more difficult for the larger molecule with a more bulky methyl substituent to enter the channel.

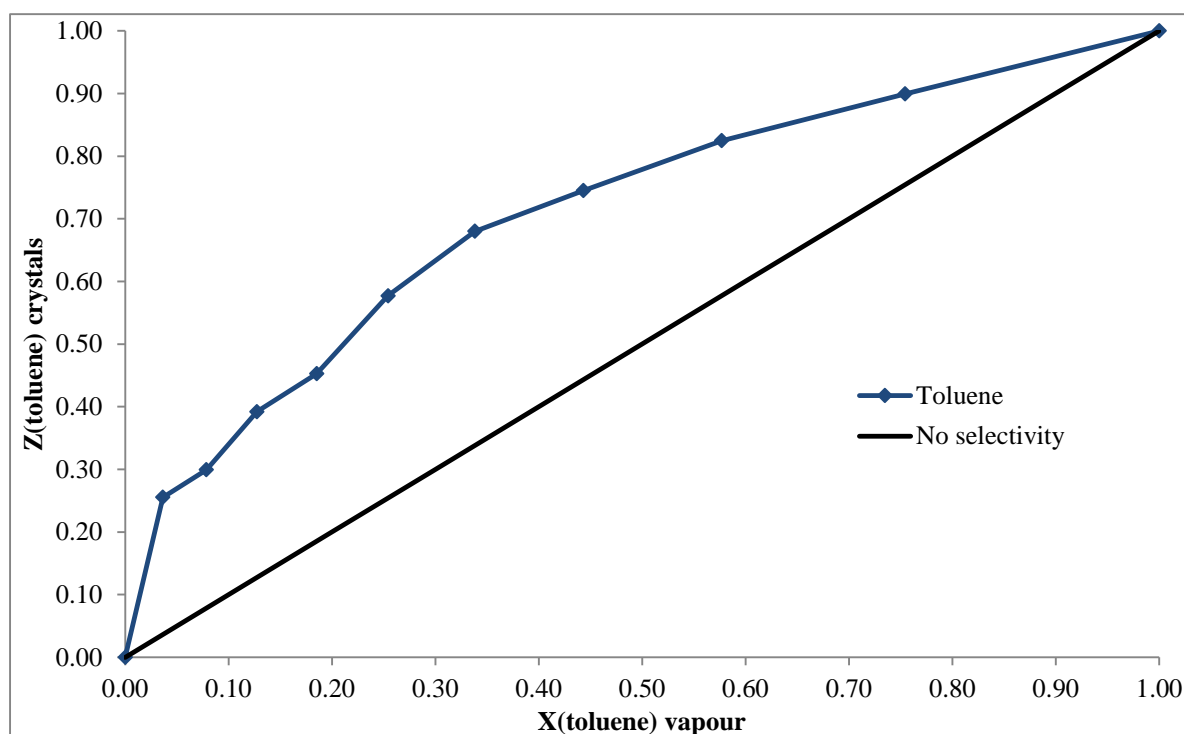


**Figure 2.41** The results of competition experiments between fractions of benzene/toluene ranging from 0 to 1. The crystals were exposed to the vapour of these solvent mixtures. **1·THF** appears to show selectivity for toluene.

### 2.4.3. Competition experiments with crystals immersed in varying fractions of benzene/toluene

We further investigated competition experiments with benzene/toluene mixtures to determine whether the same selectivity trend occurs in solution as in the vapour phase. The solvent fractions of benzene/toluene ranged from 0 to 1 with 0.1 increments. Freshly dried crystals of **1·THF** were immersed in the solvent mixtures for two days after which  $^1\text{H}$  NMR analysis was used to determine the relative ratio of the solvents present in the crystals.  $Z_{\text{toluene}}(\text{crystals})$  was plotted against  $X_{\text{toluene}}(\text{solution})$  and the results are shown in Figure 2.42. The framework once again shows selectivity towards toluene over all fractions. The selectivity for toluene does however appear to be somewhat more pronounced in Figure 2.41, where crystals were exposed to the vapour mixture, than in Figure 2.42, where crystals were immersed in the solvent mixtures. This is however due to the fact that the vapour pressure of toluene is much lower than that of benzene at all fractions. When the fraction of toluene in the crystals ( $Z_{\text{toluene}}$ ) is then plotted against the fraction of toluene in the vapour phase ( $X_{\text{toluene}}$ ) the selectivity effect is more pronounced because toluene is included even though it has a much lower fraction present in the vapour phase than benzene. It is however clear that **1·THF**

selectively exchanges for toluene over benzene over all fractions of toluene/benzene, whether crystals of **1·THF** are exposed to the vapour mixture or directly immersed in the solvent.

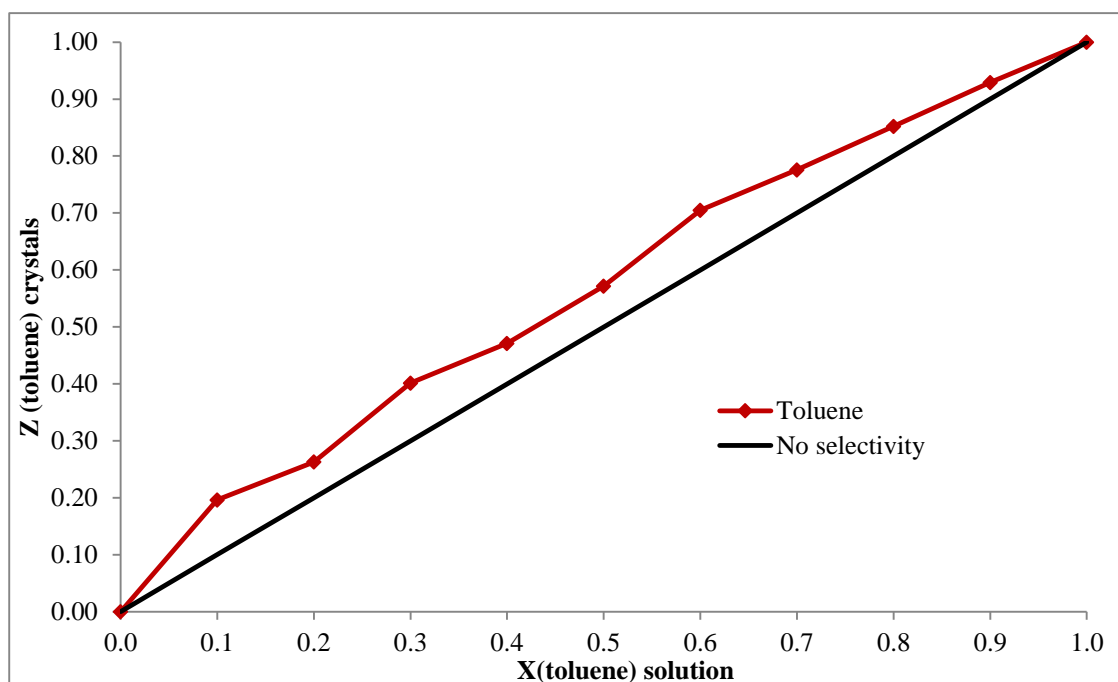


**Figure 2.42** The selectivity curve of crystals of **1·THF** immersed in fractions of benzene/toluene mixtures ranging from 0 to 1. Again it seems that **1·THF** is selective towards toluene.

#### 2.4.4. Competition experiments with crystals immersed in 1:1 solvent mixtures

Further competition experiments were done by immersing the freshly dried crystals of **1·THF** in 1:1 solvent mixtures. The crystals were covered by a thin layer of solvent. After two days the crystals were removed from the solvent, dried on filter paper and analysed by  $^1\text{H}$  NMR. PXRD analysis was also performed on each sample to ensure that the crystals were still that of framework **1**. **1·THF** exchanges the THF in the channels for such a wide variety of solvents that the number of possible solvent combinations for competition experiments is rather large. Therefore initially only combinations with acetone (Table 2.13) and acetonitrile (Table 2.14) were investigated, which already amounts to 20 solvent combinations only in a 1:1 molar ratio. Future work will certainly expand on the range of solvent combinations initially investigated in this study and will include varying the fractions of the solvents in each combination to further confirm whether or not the framework displays selectivity. It would also be interesting to investigate whether other solvent combinations with acetone cause crystals of **1·THF** to convert to different structures as was seen with a vapour mixture of

acetone/DMSO (Section 2.4.1). The same effect was seen when crystals of **1·THF** were immersed in either acetonitrile or methanol.

The results listed in Table 2.13 of 1:1 solvent mixtures with acetone suggest that in only three out of eight experiments is acetone the preferred solvent for inclusion. This is excluding the three instances where the framework converts to a different structure upon exposure to the solvent mixture. Acetone is only the preferred solvent when the mixture contains acetonitrile, chloroform or dichloromethane. This result is also particularly interesting since the same trend is seen when crystals of **1·THF** are immersed in 1:1 solvent mixtures with acetonitrile (Table 2.14) – acetonitrile is the preferred solvent only when the mixture also contains chloroform or dichloromethane. The powder patterns in Figure 2.43 and Figure 2.44 show that the framework structure was retained except in mixtures of acetone/alcohol and mixtures with acetonitrile/alcohol. In the case of mixtures with acetone, **1·THF** converts to a 3,4-lutidinium pamoate acetone solvate and in the case of mixtures with acetonitrile, **1·THF** converts to a 3,4-lutidinium pamoate acetonitrile solvate. These two structures will be discussed in greater detail in Section 2.5.

**Table 2.13** The results of competition experiments of in which crystals of **1·THF** were immersed in 1:1 solvent mixtures with acetone.

Solvent mixture with acetone (1:1)	Percentage of acetone in the crystals	Percentage solvent B in the crystals
Acetonitrile	71	29
Benzene	31	69
Chloroform	82	18
Diethyl ether	40	60
Dichloromethane	84	16
1,4-dioxane	29	71
Ethanol		No longer framework <b>1</b>
Methanol		No longer framework <b>1</b>
Toluene	25	75
<i>n</i> -hexane	48	52
1-propanol		No longer framework <b>1</b>

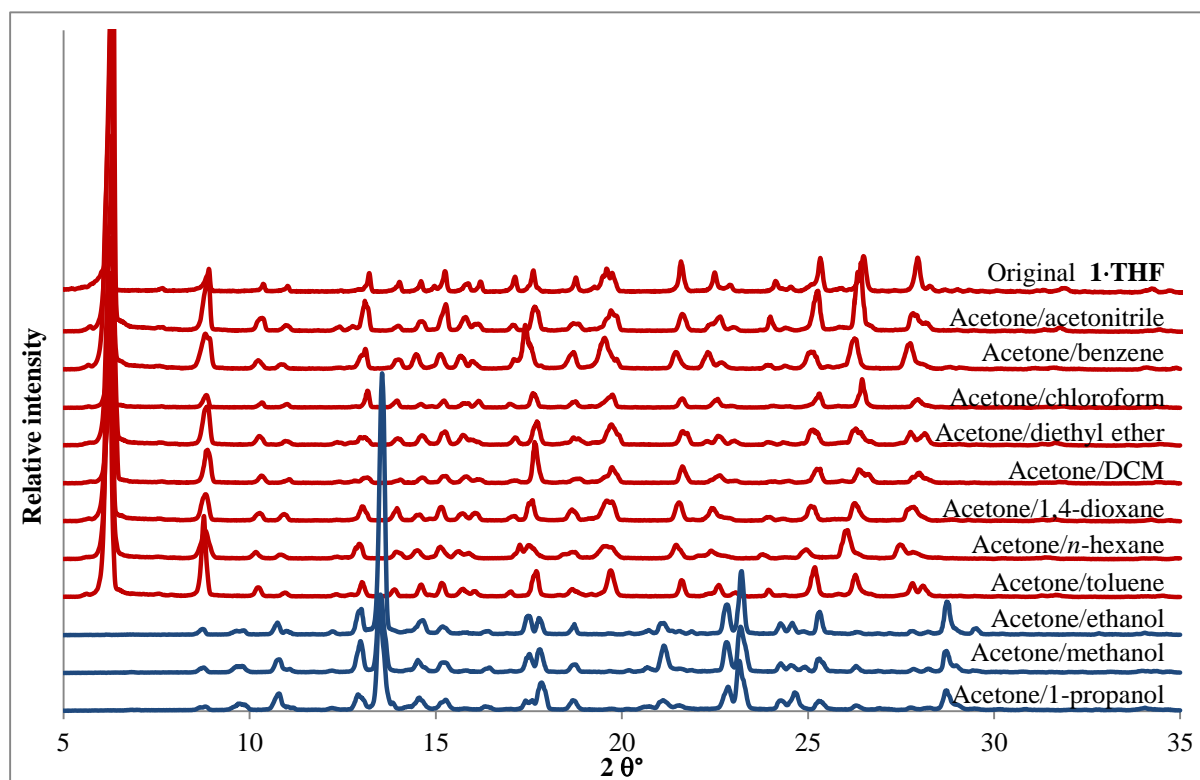


**Figure 2.43** The powder patterns of competition experiments in which crystals of **1·THF** were immersed in 1:1 molar ratio mixtures with acetone. When crystals are immersed in acetone/ethanol, acetone/methanol or acetone/1-propanol the framework converts to a new 3,4-lutidinium pamoate acetone solvate.

**Table 2.14** The results of competition experiments in which crystals of **1·THF** were immersed in 1:1 solvent mixtures with acetonitrile.

Solvent mixture with acetonitrile (1:1)	Percentage acetonitrile in the crystals	Percentage of solvent B in the crystals
Benzene	15	85
Chloroform	54	46
Diethyl ether	13	87
Dichloromethane	60	40
1,4-dioxane	12	88
Ethanol		No longer framework <b>1</b>
Methanol		No longer framework <b>1</b>
Toluene	5	95
1-propanol		No longer framework <b>1</b>

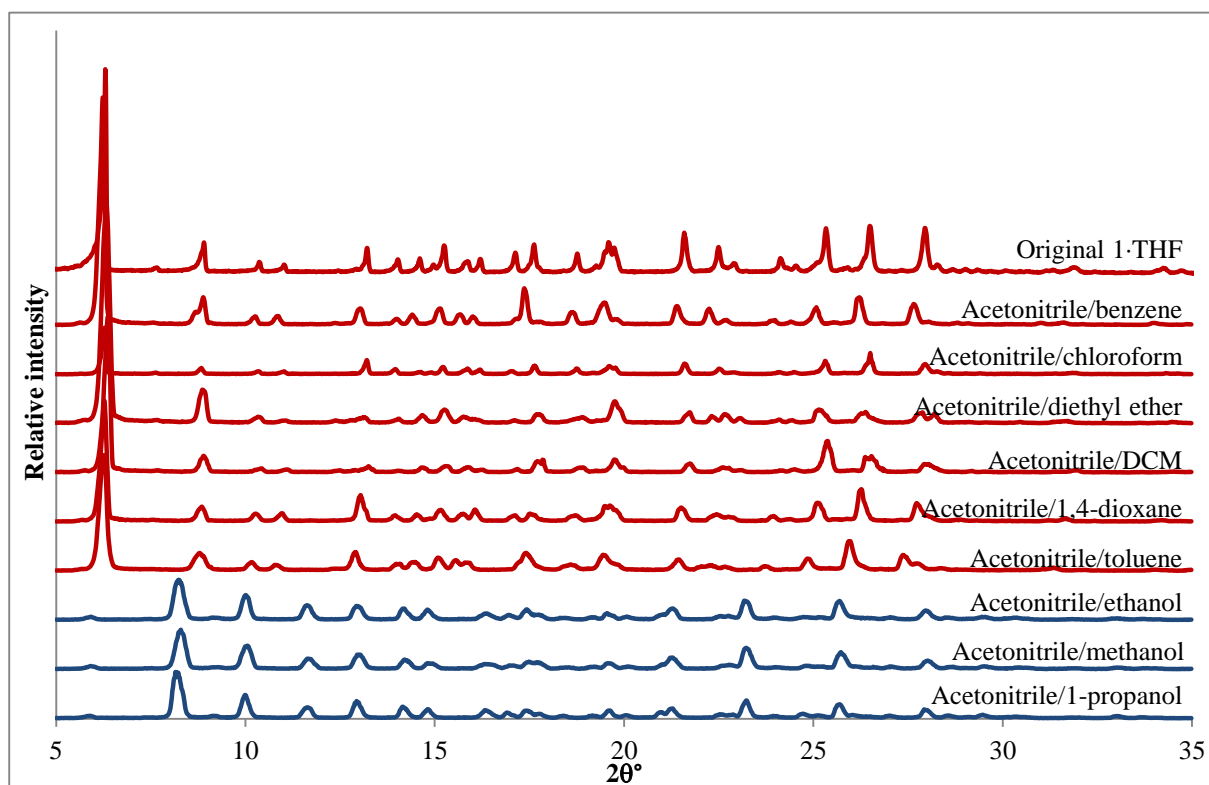


**Figure 2.44** The powder patterns of competition experiments in which crystals of **1·THF** were immersed in 1:1 molar ratio mixtures with acetonitrile. When crystals are immersed in acetonitrile/ethanol, acetonitrile/methanol or acetonitrile/1-propanol framework **1** converts to a 3,4-lutidinium pamoate acetonitrile solvate.

It is interesting to note that **1·THF** selectively excludes chlorinated solvents and acetonitrile when there is a choice of solvents, but includes these solvents when exposed to the pure vapour. This could be due to unfavourable electrostatic interactions between the chlorinated molecules/acetonitrile and the framework. This could imply that the channel has an environment more suited to apolar molecules and therefore the inclusion of molecules with a dipole, such as acetonitrile, dichloromethane and chloroform, are less favoured due to incompatible interactions with the framework.

## 2.5. The effect of immersion in certain solvents on framework **1**

As was mentioned in the previous section, immersion in solvents like acetonitrile and mixtures of acetone or acetonitrile with methanol, ethanol and 1-propanol causes framework **1** to recrystallise as a different structure. Figure 2.45 shows the PXRD patterns of **1·THF** compared to **1·THF** after immersion in the indicated solvent or solvent mixture. When **1·THF** is immersed in acetonitrile, methanol or combinations of acetonitrile and an alcohol, the framework changes to the same structure in each case (**AA**). When **1·THF** is immersed in combinations of acetone with an alcohol, a different structure type emerges (**AcA**). The



structures of the crystals after immersion were determined, and their simulated powder patterns are shown in Figure 2.45 for comparison.

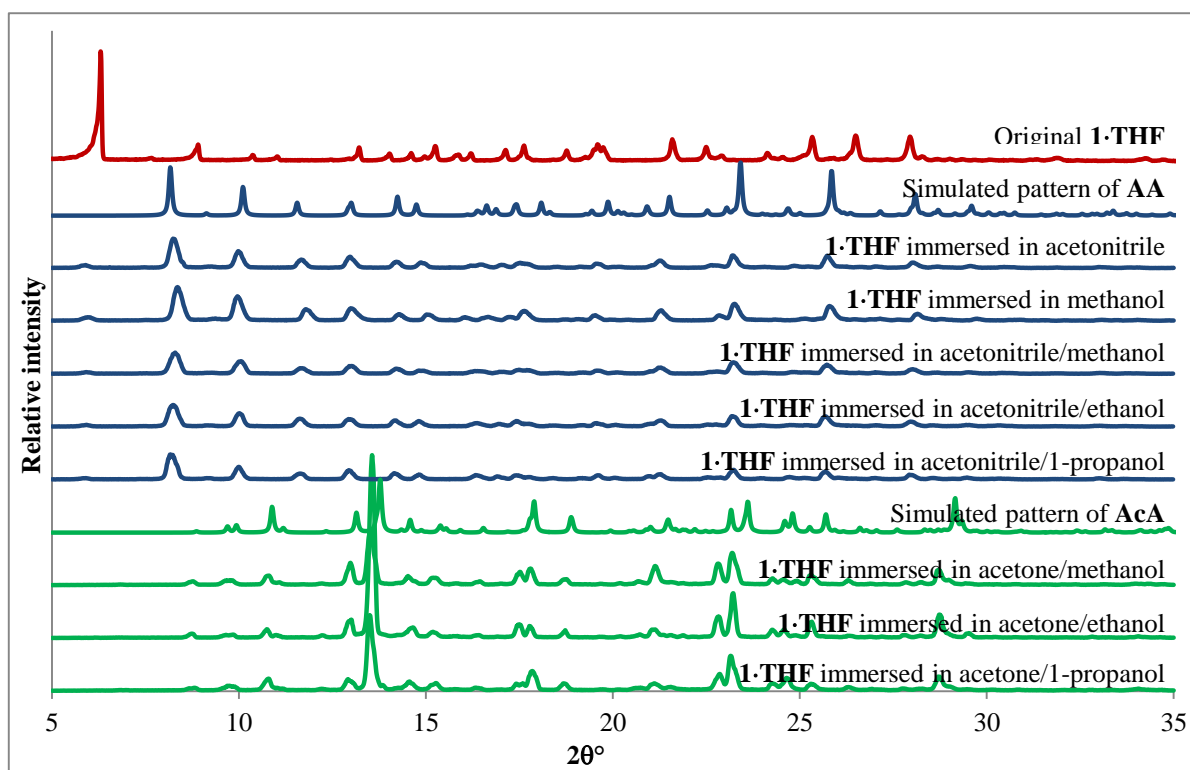


**Figure 2.45** The powder patterns of **1·THF** after immersion in certain solvents or solvent combinations that cause it to change to two different structure types. The simulated patterns of the new structures, **AA** and **AcA**, are also included.

The structure (**AA**) grown from acetonitrile/alcohol mixtures is a 3,4-lutidinium pamoate acetonitrile solvate that is in the space group  $I4_1cd$ , which is a non-centrosymmetric polar space group. There is one pamoate ion, singly deprotonated, one 3,4-lutidinium ion and one acetonitrile molecule in the asymmetric unit. In this structure the pamoate ions form a spiral hydrogen-bonded chain (Figure 2.46a) with pendant 3,4-lutidinium ions (Figure 2.46b). In (c) the spiral chain is viewed head-on with the acetonitrile molecules shown to spiral around the chain, the four-fold symmetry wonderfully illustrated.

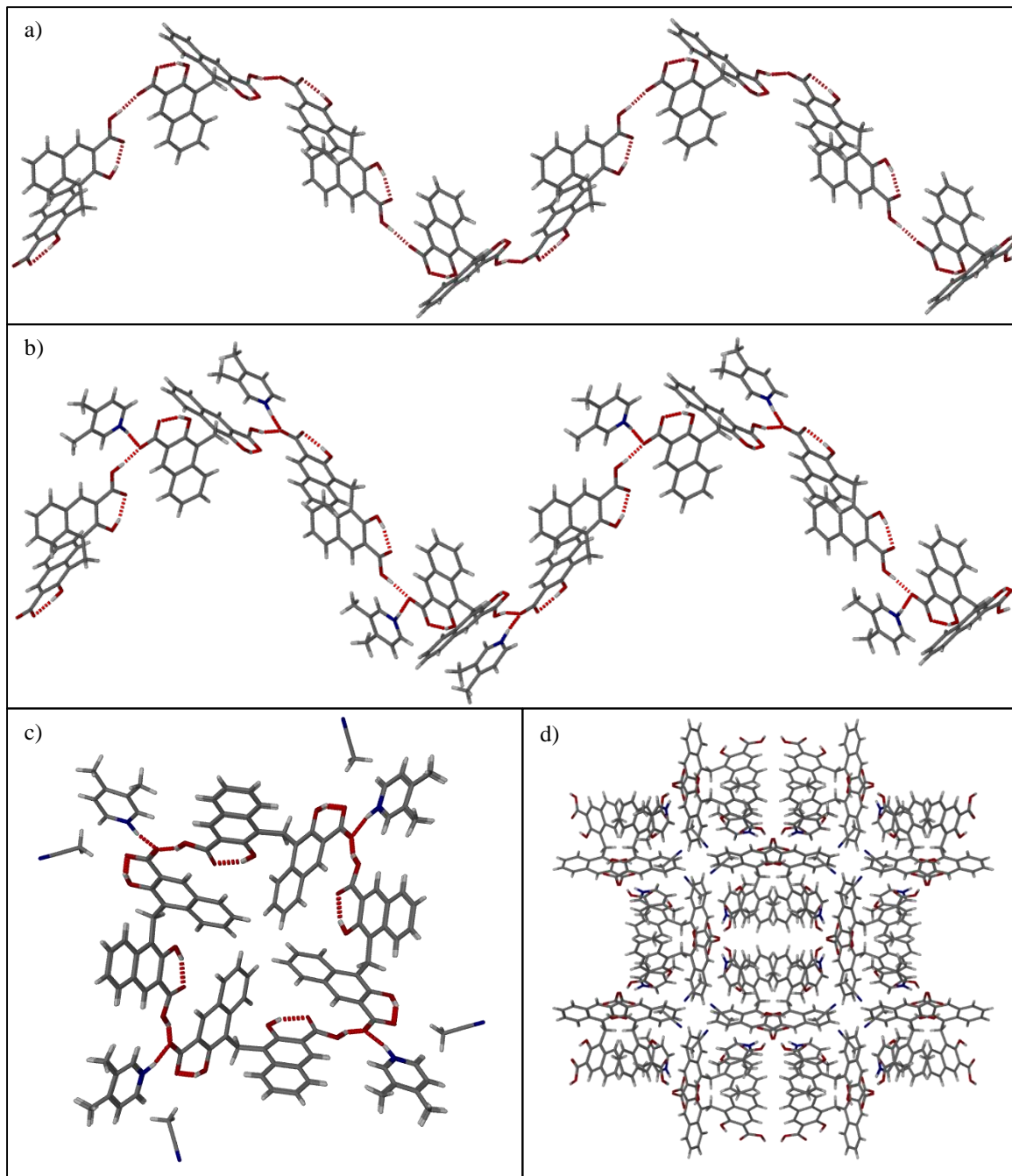


**Figure 2.46** The hydrogen bond motifs and packing diagram of AA. a) The pamoate ions form a spiral hydrogen bonded chain. b) The 3,4-lutidinium ions hydrogen bond to the chain. c) The spiral is shown head-on with the acetonitrile molecules around it. d) The packing diagram shown down the *c* axis.

The very interesting feature of this host-guest material is the fact that the acetonitrile molecules spiral throughout the structure, all aligned in the same direction along the *c* axis and therefore forming a polar axis. Figure 2.47a illustrates how the acetonitrile molecules are aligned in a head-to-tail fashion in the spiral. In Figure 2.48 the acetonitrile spirals are shown in the *ac*-plane, where it is clear that the nitrogen atoms of the acetonitrile molecules face the same direction along the *c* axis.

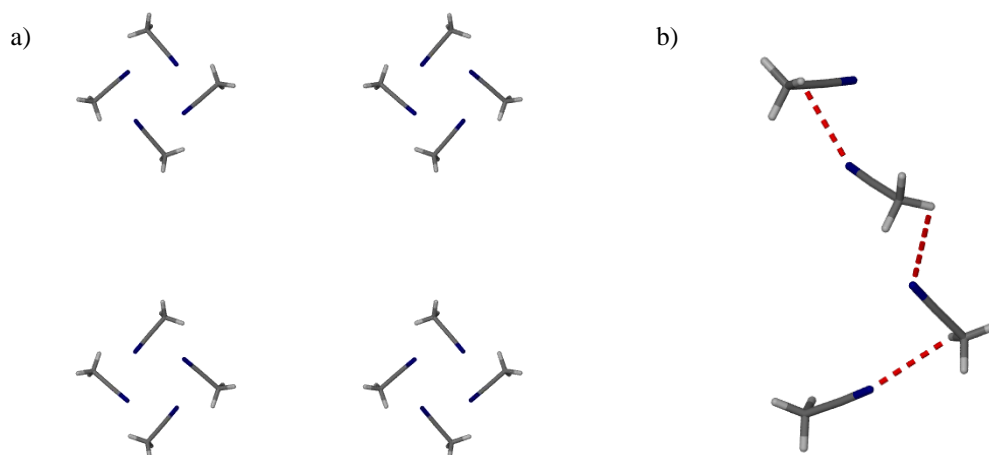


**Figure 2.47** Acetonitrile spirals in **AA**. a) The head-to-tail spiral of the acetonitrile molecules viewed down the *c*-axis. b) The contact formed between the nitrogen atom of one molecule and the hydrogen atom of a neighbouring molecule.

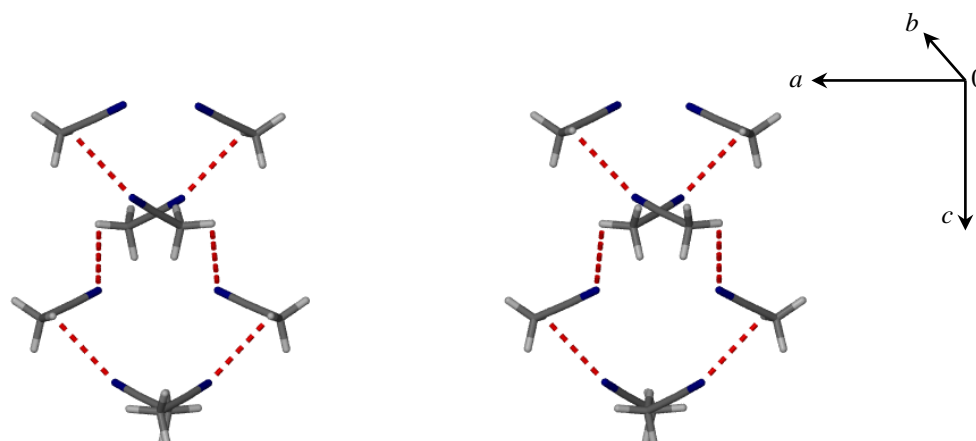


**Figure 2.48** The acetonitrile spirals in the *ac*-plane that show how the molecules all face the same direction along the *c* axis.

The second structure grown from acetone/alcohol mixtures (**AcA**) is in the space group  $P2_1/c$ . There is one singly deprotonated pamoate ion, one 3,4-lutidinium ion and one acetone molecule in the asymmetric unit. The pamoate ion forms a hydrogen-bonded chain with pendant lutidinium ions (Figure 2.49a). Acetone molecules fill the spaces in between adjacent chains (Figure 2.49b). Selected crystallographic data and hydrogen bond parameters for **AA** and **AcA** can be found in Table 2.15 and Table 2.16, respectively, at the end of this section (pages 97 and 98).

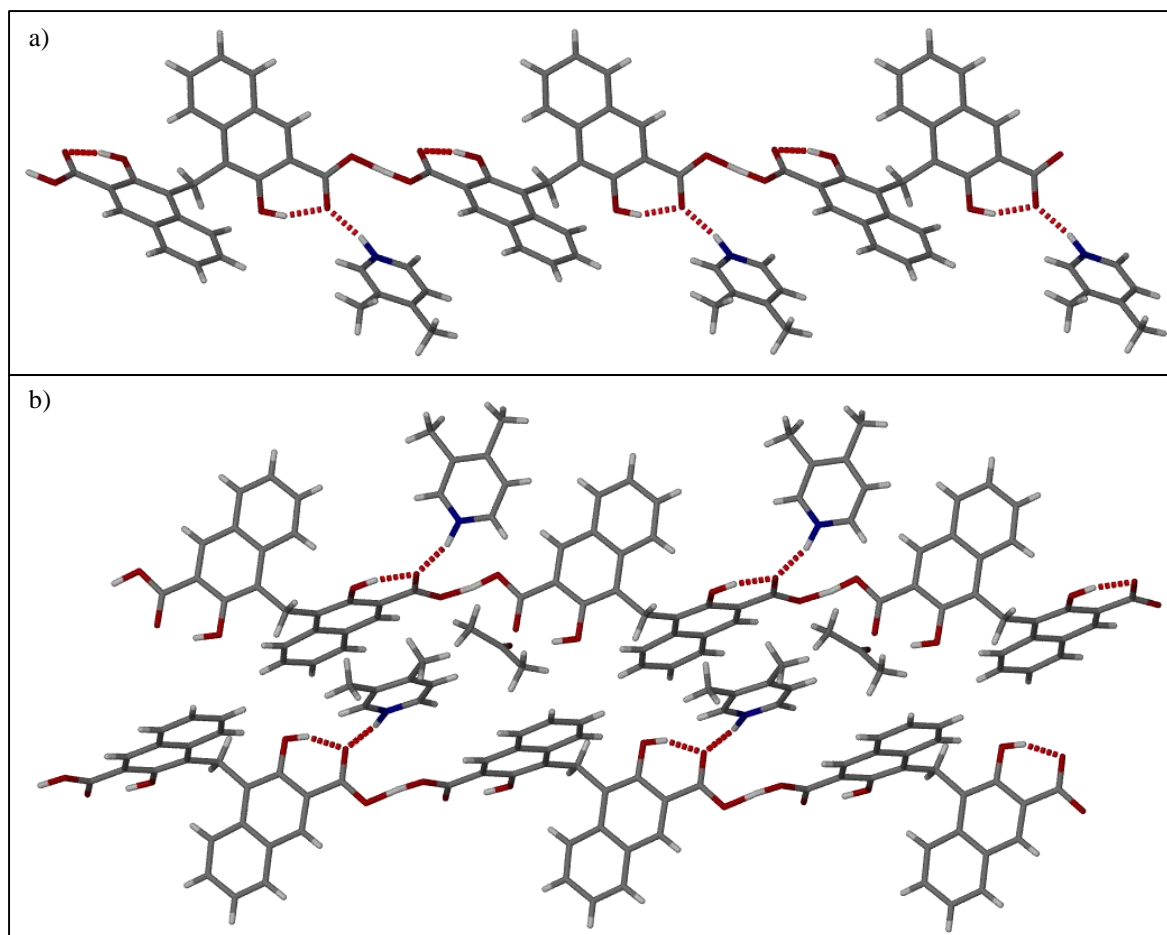


**Figure 2.49** a) The hydrogen bonded chains of pamoate ions with pendant lutidinium ions. b) Acetone molecules fill the spaces in between adjacent chains.

In both **AA** and **AcA** the change in structure from **1·THF** is not single-crystal to single-crystal. Crystals of **1·THF** were placed in a 1:1 molar mixture of acetone/ethanol since this particular mixture resulted in the best crystals of **AcA**. The crystals were filmed for one day. Crystals of **1·THF** are shown in the first frame in Figure 2.50. After one hour most of the crystals have started to dissolve since they are smaller in the second frame. After two hours new crystals have started to grow already and after three and a half hours the crystals have substantially increased in size. After approximately two days all the crystals have transformed to **AcA**, as verified by PXRD analysis.

The same conversion of **1·THF** to a different structure is also observed when crystals of **1·THF** are immersed in methanol. Unfortunately no suitable crystals could be obtained for SCD analysis, but it is presumed that a methanol solvate isostructural to **AA** forms, since the powder pattern is similar to that of **AA** (Figure 2.45).

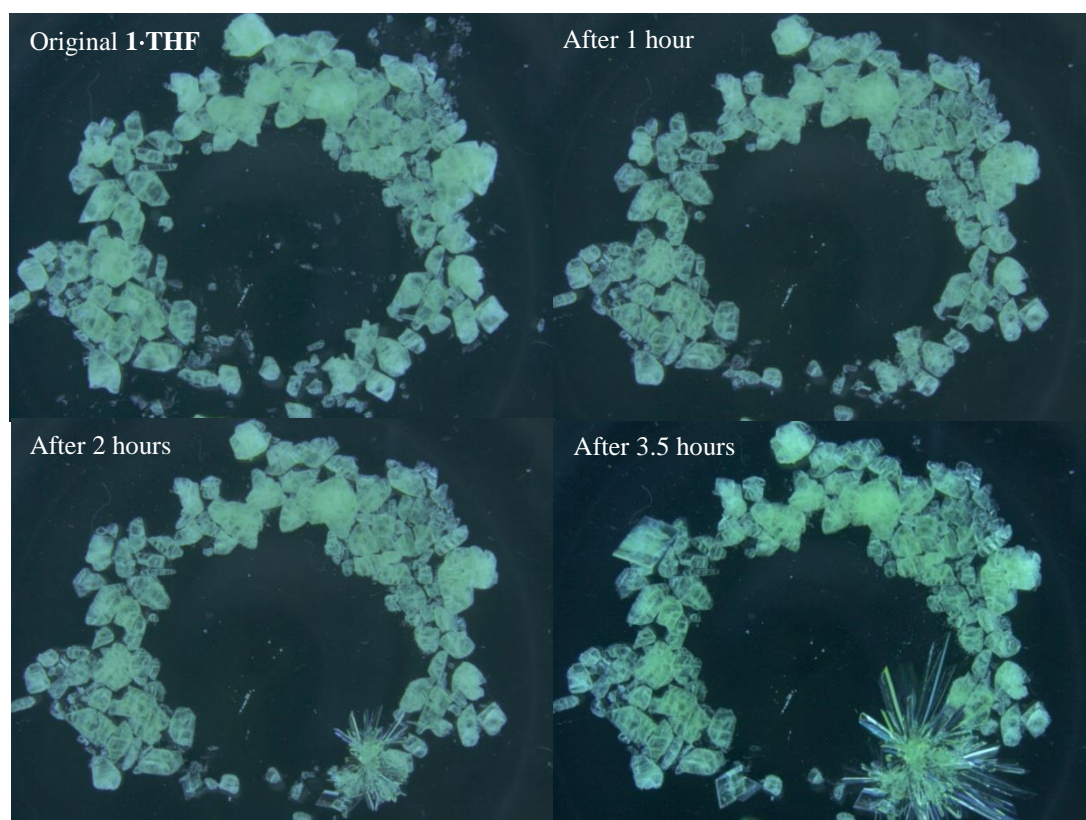


**Figure 2.50** The progression of crystals of **1·THF** immersed in acetone/ethanol converting to **AcA**. Some of the crystals have started to dissolve after one hour. After two hours new crystals have started to grow.

The combination of acetone or acetonitrile with any of the alcohols possibly allows the crystals to dissolve (the crystals do not readily dissolve in any other solvent except DMSO). The degree of ionisation of pamoate ion also does not change from **1·THF** to **AA** or **AcA**. In both structures the pamoate ion remains singly deprotonated which leads to the formation of hydrogen-bonded pamoate chains. It is possible that the favourable alignment of the acetonitrile molecules in **AA** drives the packing of the structure.

**Table 2.15** Selected crystallographic data for **AA** and **AcA**.

Parameters	AA	AcA
Stoichiometry (acid:base:solvent)	1:1:1	1:1:1
Chemical formula	C <sub>32</sub> H <sub>28</sub> N <sub>2</sub> O <sub>6</sub>	C <sub>33</sub> H <sub>31</sub> NO <sub>7</sub>
Formula weight	536.58	553.61
Crystal system	Tetragonal	Monoclinic
Space group	<i>I4<sub>1</sub>cd</i>	<i>P2<sub>1</sub>/c</i>
Z	16	4
<i>a</i> /Å	30.610(6)	13.808(2)
<i>b</i> /Å	30.610(6)	12.846(2)
<i>c</i> /Å	11.367(2)	16.866(3)
$\alpha^\circ$	90	90
$\beta^\circ$	90	110.401(2)
$\gamma^\circ$	90	90
Volume/Å <sup>3</sup>	10651(5)	2804.0(8)
Calculated density/g.cm <sup>-3</sup>	1.338	1.311
Temperature/K	173(2)	100(2)
<i>R</i> <sub>int</sub>	0.0372	0.0312
<i>R</i> 1 [ <i>I</i> > 2σ( <i>I</i> )]	0.0280	0.0685

**Table 2.16** Hydrogen bond parameters for **AA** and **AcA**.

	<b>D–H (Å)</b>	<b>H...A (Å)</b>	<b>D...A (Å)</b>	<b>∠DHA (°)</b>
<b>AA</b>				
O1-H1O...O4 <sup>a</sup>	1.01(4)	1.54(4)	2.525(3)	162(3)
O3-H3O...O2	0.89(4)	1.73(4)	2.570(3)	154(3)
N1-H1N...O4 <sup>b</sup>	0.98(5)	1.72(5)	2.674(3)	165(4)
O6-H6O...O5	0.90(5)	1.70(5)	2.535(3)	154(4)
<sup>a</sup> y-1/2, -x+1, z+3/4; <sup>b</sup> -y+1/2, x, z-1/4				
<b>AcA</b>				
O1-H1O...O4 <sup>c</sup>	1.08(3)	1.37(3)	2.447(2)	170(3)
O3-H3O...O2	0.92(3)	1.71(3)	2.574(2)	156(2)
N1-H1N...O5 <sup>d</sup>	0.96(3)	1.81(3)	2.716(2)	157(2)
O6-H6O...O5	0.89(3)	1.71(3)	2.551(2)	155(3)
<sup>c</sup> x-1, y, z; <sup>d</sup> x, -y+3/2, z+1/2				



## 2.6. Conclusions and future work

A detailed investigation into the porosity of the 3,4-lutidinium pamoate hemihydrate THF framework was carried out and the results were discussed in this chapter. It was determined that 21 solvents can undergo exchange with **1·THF**. For 14 of these solvents it was possible to obtain single crystal data of the exchanged structures. For the remaining 7 it was only possible to confirm the presence of the solvent in the structure by  $^1\text{H}$  NMR analysis and whether the integrity of the framework was maintained by PXRD analysis. **1·THF** is also able to exchange the THF in the channels for volatile solids such as pyrazine and iodine. To the best of our knowledge this is the first example of an ionic organic hydrogen-bonded framework including volatile solids such as pyrazine and iodine through guest exchange. To some extent it was also shown that naphthalene is able to enter the channels of **1·THF**, but unfortunately this could not unequivocally be proven by single crystal X-ray diffraction.

There appears to be no common property between the solvents that undergo exchange that could shed light on the requirements a potential guest has to meet in order for exchange with the THF in **1·THF** to take place. The list of compounds is a surprisingly random collection of aromatic compounds, long alkyl chains, alcohol groups with alkyl chains of different lengths and small volatile solids such as iodine. There is no shape similarity between these compounds either! Solvents that are not able to exchange are cyclohexane, cyclohexanone and 2-pyrrolidone. This is somewhat strange since cyclohexane is approximately the same size as 1,4-dioxane which is able to enter the channel and 2-pyrrolidone is slightly smaller than N-methylpyrrolidone, which is also able to enter the channels of **1·THF**. This could have two explanations: either the solvent is too big or the vapour pressure of the solvent is too low and not enough solvent molecules are present in the vapour phase to drive the exchange process. Cyclohexane is quite a volatile solvent<sup>38</sup> with a vapour pressure of 77 mmHg at 20 °C, therefore in this case it is possible that cyclohexane is simply too big. The fact that it is roughly the same size and shape as 1,4-dioxane does however question whether it really is just a size mismatch. It is possible that due to the hydrophobic nature of cyclohexane there is no favourable interaction with the ionic framework and thus exchange does not take place. Why then is *n*-hexane able to exchange? In this case shape could be the determining factor. It would be easier for a long alkyl chain to enter the channel since it can stretch down the channel, minimising possible contact with the framework. Cyclohexane however is a six-membered ring that has to fill the entire cavity in all directions in order to fit, which causes



unfavourable interactions with the framework. The case of 2-pyrrolidone is an example of the vapour pressure being too low for exchange to take place. NMP has a boiling point of 202 °C and a vapour pressure of approximately 8 mmHg at 20 °C whereas 2-pyrrolidone has a boiling point of 251 °C and a vapour pressure possibly even lower than that of NMP. Due to the low vapour pressure of 2-pyrrolidone, not enough solvent molecules are present in the vapour phase in order to drive the exchange process.

With regard to the step-wise exchanges discussed in Section 2.3.4, it would be interesting to investigate whether it would be possible to exchange the contents of the channel of **1** for one of the solvents that do not undergo exchange (Section 2.3.3) if one starts with a framework that contains a guest other than THF. In other words expose crystals of, e.g. **1·Chloroform** to cyclohexane and determine whether exchange takes place. This would demonstrate how much of an influence the guest has on the environment within the channel and whether it can alter the environment in the channel enough to allow the exchange of a guest that could previously not undergo exchange with **1·THF**.

The selectivity of **1·THF** was investigated by performing competition experiments. Crystals of **1·THF** were exposed to vapour mixtures of solvents and the results indicate that the framework does exhibit selectivity. **1·THF** selectively exchanges for chloroform over DCM, toluene over benzene and ethanol over methanol even though the solvents that are selectively exchanged for have much lower vapour pressures than their counterparts. This indicates that the framework has a strong preference for some guests over others. Only in two cases did the preferred guest have a higher vapour pressure, namely in the case of diethyl ether/acetonitrile and 1,4-dioxane/NMP where the solvent with the higher vapour pressures, i.e. diethyl ether and 1,4-dioxane, were selectively exchanged for.

Further investigations into the selectivity for solvents in the vapour phase included a study of the selectivity of **1·THF** when exposed to varying vapour fractions of benzene/toluene. The resultant selectivity curve showed marked preference for toluene over benzene over all fractions of benzene/toluene. This is an interesting result since one would expect the smaller, more volatile guest to be selectively included. Although the framework includes a wide range of compounds seemingly indiscriminately, there do appear to be certain interactions present between guest and framework that cause the framework to selectively include some guests over others. Upon studying the crystal structures of **1·Benzene** and **1·Toluene**, even though

not all of the solvent could be adequately modelled, some answers did arise. Due to the perpendicular orientation of the toluene molecules with respect to each other in the channel there appear to be C–H $\cdots$  $\pi$  interactions (edge-to-face) between the toluene molecules. The same type of interaction is not seen between benzene molecules. The interactions between the toluene molecules could therefore induce a *cooperative* exchange effect, where as soon as one toluene molecule is included the rest follow suit. This could be studied further computationally by calculating the guest-guest interaction energy for benzene and toluene and in this way determine if the interaction energy between guest molecules is higher for toluene.

Further competition studies were also carried out by immersing the crystals of **1·THF** in 1:1 solvent mixtures with acetone and acetonitrile. The results indicated that the framework selectively excludes chloroform, dichloromethane and acetonitrile when in the presence of other guests. Only when crystals of **1·THF** are immersed in mixtures of the chlorinated solvents with acetonitrile is acetonitrile preferred. It is not clear whether it is the polarity of the molecules that cause them to have a less favourable interaction with the framework. The dipole moments of a few compounds are compared in Table 2.17. Acetone and acetonitrile have very large dipoles, which could explain why they are often selectively excluded by the framework when exposed to vapour mixtures with these solvents. This could imply that the environment within the channel is more apolar/hydrophobic and the introduction of highly polarised molecules disturbs the electrostatics of the framework.

**Table 2.17** Dipole moments of selected compounds in Debye units

Compound	Dipole moment (D, Debye units)
Benzene	0
Toluene	0.34
1,4-dioxane	0.45
Diethyl ether	1.15
1-propanol	1.58
Dichloromethane	1.60
Iodomethane	1.64
Ethanol	1.69
Methanol	1.7
THF	1.75
Chloroform	1.90
Acetone	2.88
Acetonitrile	3.93

Further investigation into the selectivity of **1·THF** is necessary in order to better understand the exchange process. It would be interesting to determine whether the solvent already occupying the channel has any influence on the selectivity of the framework. The selectivity of the *empty* framework should therefore also be investigated in future. This could give us valuable information regarding the interactions at play during the exchange process and whether there are interactions between different guest molecules that determine selectivity or whether it is the framework that determines selectivity. As of yet we have not established how to completely empty **1·THF**.

It has also been shown that when crystals of **1·THF** are immersed in acetonitrile, methanol or acetonitrile/alcohol mixtures, the crystals are able to dissolve and recrystallise as a high symmetry acetonitrile solvate in which the acetonitrile molecules align along the *c* axis, forming a polar alignment. This structure definitely warrants further investigation since it could potentially have interesting properties such as second harmonic generation. The reason why these particular solvent combinations cause **1·THF** to recrystallise could be the collaborative polarity of the solvent mixtures that allows the crystals to dissolve. These crystals do not easily dissolve in many solvents. Pamoate chains are reformed upon recrystallisation, but it is probably the favourable alignment of the acetonitrile molecules that drives the formation of the high symmetry compound.

From the results discussed in this chapter it is clear that **1·THF** is a robust ionic organic framework and that the incorporation of charge-assisted hydrogen bonds lends great stability to the framework. Since **1·THF** is such a unique framework, further investigations were conducted into the exchange of guests in order to better understand this process. These investigations will be discussed in the next chapter.

## 2.7. References

1. D. A. Haynes, W. Jones and W. D. S. Motherwell, *CrystEngComm*, 2005, **7**, 538-543.
2. D. A. Haynes, Z. F. Weng, W. Jones and W. D. S. Motherwell, *CrystEngComm*, 2009, **11**, 254-260.
3. H. Wahl, D. A. Haynes and T. le Roex, *CrystEngComm*, 2011, **13**, 2227-2236.
4. D. A. Haynes, W. Jones and W. D. Samuel Motherwell, *CrystEngComm*, 2005, **7**, 342-345.
5. H. Wahl, D. A. Haynes and T. le Roex, *CrystEngComm*, 2013, **15**, 2450-2455.
6. H. Wahl, D. A. Haynes and T. le Roex, *Chem. Commun.*, 2012, **48**, 1775 - 1777.
7. M. Mastalerz and I. M. Opperl, *Angew. Chem., Int. Ed.*, 2012, **51**, 5252-5255.
8. A. I. Cooper, *Angew. Chem., Int. Ed.*, 2012, **51**, 7892-7894.
9. Y. He, S. Xiang and B. Chen, *J. Am. Chem. Soc.*, 2011, **133**, 14570-14573.
10. X.-Z. Luo, X.-J. Jia, J.-H. Deng, J.-L. Zhong, H.-J. Liu, K.-J. Wang and D.-C. Zhong, *J. Am. Chem. Soc.*, 2013, **135**, 11684-11687.
11. P. Li, O. Alduhaish, H. D. Arman, H. Wang, K. Alfooty and B. Chen, *Cryst. Growth Des.*, 2014, **14**, 3634-3638.
12. P. Li, Y. He, J. Guang, L. Weng, J. C.-G. Zhao, S. Xiang and B. Chen, *J. Am. Chem. Soc.*, 2014, **136**, 547-549.
13. A. Yamamoto, T. Hasegawa, T. Hamada, T. Hirukawa, I. Hisaki, M. Miyata and N. Tohnai, *Chem-Eur J*, 2013, **19**, 3006 – 3016.
14. A. Yamamoto, T. Hamada, I. Hisaki, M. Miyata and N. Tohnai, *Angew. Chem., Int. Ed.*, 2013, **52**, 1709-1712.
15. A. Yamamoto, T. Hirukawa, I. Hisaki, M. Miyata and N. Tohnai, *Tetrahedron Lett.*, 2013, **54**, 1268-1273.
16. A. Yamamoto, S. Uehara, T. Hamada, M. Miyata, I. Hisaki and N. Tohnai, *Cryst. Growth Des.*, 2012, **12**, 4600-4606.
17. I. J. Bruno, J. C. Cole, P. R. Edgington, M. Kessler, C. F. Macrae, P. McCabe, J. Pearson and R. Taylor, *Acta Crystallogr. B*, 2002, **B58**, 389 - 397.
18. C. F. Macrae, I. J. Bruno, J. A. Chisholm, P. R. Edgington, P. McCabe, E. Pidcock, L. Rodriguez-Monge, R. Taylor, J. van de Streek and P. A. Wood, *J. Appl. Crystallogr.*, 2008, **41**, 466 - 470.
19. C. F. Macrae, P. R. Edgington, P. McCabe, E. Pidcock, G. P. Shields, R. Taylor, M. Towler and J. van de Streek, *J. Appl. Crystallogr.*, 2006, **39**, 453 - 457.

20. R. Taylor and C. F. Macrae, *Acta Crystallogr. B*, 2001, **B57**, 815 - 827.
21. L. J. Barbour, *Chem. Commun.*, 2006, 1163-1168.
22. A. L. Spek, *J. Appl. Crystallogr.*, 2003, **36**, 7 - 13.
23. M. P. Suh and Y. E. Cheon, *Aust. J. Chem.*, 2006, **59**, 605-612.
24. M. R. Caira, T. le Roex, L. R. Nassimbeni and E. Weber, *Cryst. Growth Des.*, 2006, **6**, 127 - 131.
25. L. Nassimbeni, H. Su and L. Patel, *J. Chem. Crystallogr.*, 2014, **44**, 190-193.
26. L. R. Nassimbeni, H. Su and T.-L. Curtin, *Supramol. Chem.*, 2012, **24**, 344 - 349.
27. A. L. Spek, *J. Appl. Crystallogr.*, 2003, **36**, 7-13.
28. A. L. Spek, *PLATON, a multipurpose crystallographic tool*, Utrecht University, Utrecht, The Netherlands, 2005.
29. P. van der Sluis and A. L. Spek, *Acta Crystallogr., Sect. A: Found. Crystallogr.*, 1990, **46**, 194 - 201.
30. T. Panda, P. Pachfule and R. Banerjee, *Chem. Commun.*, 2011, **47**, 7674-7676.
31. B. Balázs, A. Grün, I. Bitter and G. Tóth, *Magn. Reson. Chem.*, 2008, **46**, 707-712.
32. A. K. Chaudhari, S. Mukherjee, S. S. Nagarkar, B. Joarder and S. K. Ghosh, *CrystEngComm*, 2013, **15**, 9465-9471.
33. Z. Wang, Y. Zhang, M. Kurmoo, T. Liu, S. Vilminot, B. Zhao and S. Gao, *Aust. J. Chem.*, 2006, **59**, 617-628.
34. C. Pei, T. Ben, S. Xu and S. Qiu, *J. Mater. Chem. A*, 2014, **2**, 7179-7187.
35. X. Xiao, W. Li and J. Jiang, *Inorg. Chem. Commun.*, 2013, **35**, 156-159.
36. L. J. Barbour, D. Das, T. Jacobs, G. O. Lloyd and V. J. Smith, in *Supramolecular chemistry: from molecules to nanomaterials*, eds. P. A. Gale and J. W. Steed, John Wiley & Sons, Ltd., Chichester, 2012, vol. 6, pp. 2870 - 2903.
37. L. Pavia, G. M. Lampman, G. S. Kriz and J. R. Vyvyan, *Introduction to spectroscopy*, 4th edn., Brooks/Cole, California, 2001.
38. D. R. Lide, ed., *CRC handbook of chemistry and physics, Internet version, 2005* <<http://www.hbcnetbase.com>>CRC Press, Boca Raton, FL, 2005.
39. A. C. Blackburn, A. J. Dobson and R. E. Gerkin, *Acta Crystallogr. C*, 1996, **52**, 1269.
40. M. Du, C.-P. Li, X.-J. Zhao and Q. Yu, *CrystEngComm*, 2007, **9**, 1011-1028.
41. R. C. Weast, ed., *CRC handbook of chemistry and physics*, 66th edn., CRC Press, Boca Raton, FL, 1985.

42. T. Engel and P. Reid, *Thermodynamics, statistical thermodynamics, & kinetics*, 3rd edn., Pearson Education, Inc., Boston, 2010.
43. N. A. Lange and J. A. Dean, eds., *Lange's Handbook of chemistry*, McGraw-Hill, California, 1979.
44. C. L. Yaws and H.-C. Yang, *Hydrocarbon Processing*, 1989, **68**, 65 – 68.
45. A. M. Pivovar, K. T. Holman and M. D. Ward, *Chem. Mater.*, 2001, **13**, 3018-3031.

# CHAPTER 3

## KINETIC STUDIES ON FRAMEWORK 1

---

Host complexes such as metal-organic frameworks, covalent organic frameworks and, more recently, hydrogen-bonded organic frameworks have been widely studied for their abilities to encapsulate or release various molecules.<sup>1-8</sup> It is therefore important to investigate the kinetics of solvent inclusion or guest exchange for these materials in order to better understand the mechanisms involved during these processes. If these processes are better understood we take a step towards being able to regulate them which, among others, is particularly sought after in the pharmaceutical industry for the controlled released of drug molecules in the body.<sup>9-13</sup> This also allows us to better understand the factors that stabilise a framework material in the absence of solvent. If we better understand these stabilisation factors we are better equipped to develop similar materials of which we can finely tune the properties we desire.

Despite the fact that these systems have been so widely studied, the kinetics involved have yet to be studied in all but a few cases.<sup>14</sup> Decomposition kinetics of inorganic compounds have been extensively studied over the years<sup>15, 16</sup> and in the last 20 years inclusion and desolvation kinetics of host-guest compounds have been investigated.<sup>14, 17-21</sup> There has been investigation into the kinetics of guest exchange<sup>22-27</sup> but reported data and procedures are few and far between, possibly due to the complexity of the experimental procedure and the associated interpretation of data due to the complex interactions between heterogeneous compounds, such as a solid and a gas or a solid and guest molecules in the vapour phase.<sup>14, 17, 18, 28, 29</sup>

Reaction kinetics are studied in order to determine the rate equation that describes the reaction and hence identify the mechanism of the reaction. This information can then be used to possibly predict the behaviour of the compound under certain conditions.<sup>28</sup> The rate of a solid-state reaction can be described by the following equation:<sup>30</sup>

$$\frac{d\alpha}{dt} = Ae^{-(E_a/RT)}f(\alpha) \quad (3.1)$$

where  $A$  is the pre-exponential or frequency factor,  $E_a$  is the activation energy,  $T$  is the absolute temperature,  $R$  is the gas constant,  $f(\alpha)$  is the specific model used to describe the reaction and  $\alpha$  is the conversion fraction or extent of reaction.<sup>30</sup> In homogeneous reactions the



increase or decrease in the concentration of reactants or products are measured,<sup>28</sup> but in heterogeneous reactions between a solid and a gas or vaporised guest molecules the change in concentration of reactants or products cannot be used, and therefore the reaction is monitored by the extent of reaction ( $\alpha$ ). The extent of the reaction is measured by the mass loss (or gain, depending on the type of kinetic experiment)

$$\alpha = \frac{(m_0 - m_t)}{(m_0 - m_f)} \quad (3.2)$$

where  $m_0$  is the initial mass,  $m_t$  is the mass at time “ $t$ ” and  $m_f$  is the final mass.<sup>28</sup> A graph of  $\alpha$  versus time plots at fixed temperatures can then be used to determine the kinetic model that best describes the data.

Kinetic models can be grouped into four categories depending on the shape of the curve: acceleratory, deceleratory, linear or sigmoidal models.<sup>30</sup> Examples of curves describing these models are shown in Figure 3.1. For acceleratory models the reaction rate increases as the reaction progresses, whereas deceleratory models experience a decrease in the reaction rate as the reaction progresses. For linear models the rate remains constant and for sigmoidal models there is a bell-shaped relationship between rate and the extent of the reaction.<sup>30</sup>

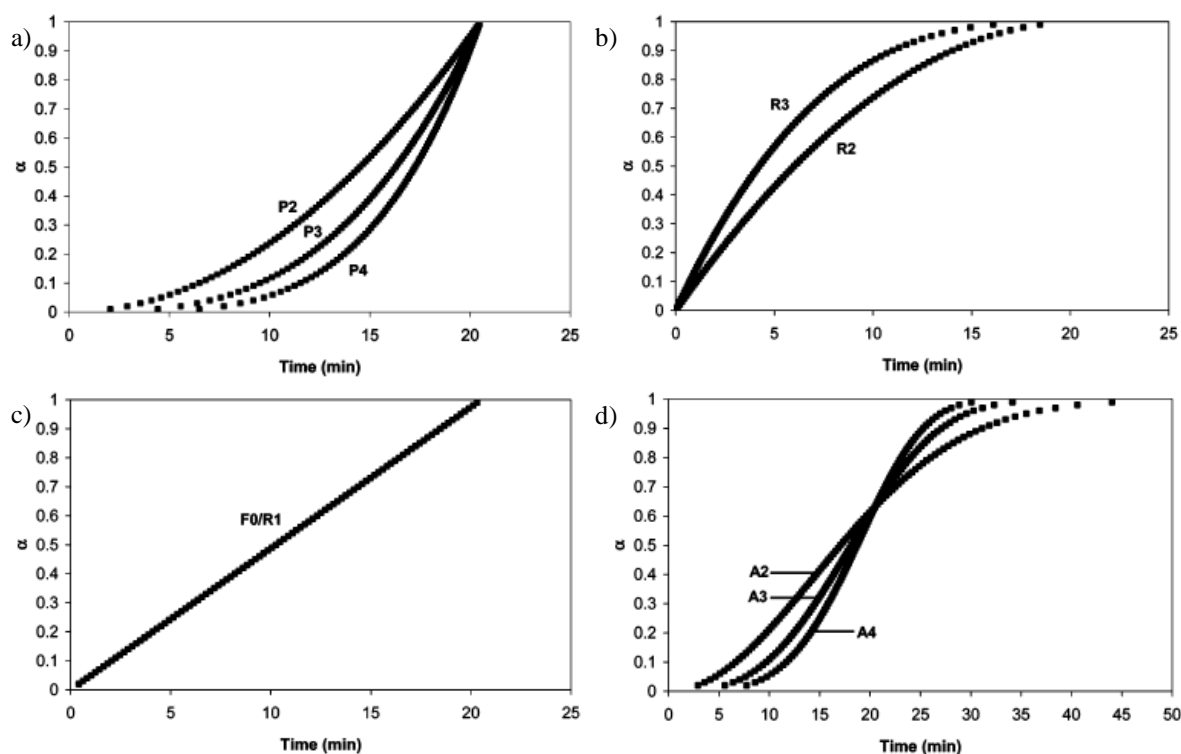


**Figure 3.1** Examples of the four kinetic models described by  $\alpha$ -time plots, namely a) acceleratory b) deceleratory c) linear and d) sigmoidal. These images have been taken from reference 30. In Table 3.1 the models P, R, F0 and A are listed.

The four models shown in Figure 3.1 are then further divided into nucleation, geometrical contraction, diffusion and reaction-order models which are described by various rate equations, listed in Table 3.1. In this table the rate equation is expressed in the integral form  $g(\alpha) = kt$  from which the rate constant  $k$  can then be determined.

**Table 3.1** The rate equations used in the kinetic analysis of solid-state reactions. The table has been adapted from references 28 and 30.

Model	$g(\alpha) = k(t' - t_0) = kt$
<i>Acceleratory <math>\alpha</math>-time curves (nucleation model)</i>	
Power law (P2)	$\sqrt{\alpha}$
Power law (P3)	$\sqrt[3]{\alpha}$
Power law (P4)	$\sqrt[4]{\alpha}$
<i>Sigmoid <math>\alpha</math>-time curves (nucleation model)</i>	
Avrami-Erofeev (A2)	$\sqrt{[-\ln(1 - \alpha)]}$
Avrami-Erofeev (A3)	$\sqrt[3]{[-\ln(1 - \alpha)]}$
Avrami Erofeev (A4)	$\sqrt[4]{[-\ln(1 - \alpha)]}$
Avrami Erofeev (An)	$\sqrt[n]{-\ln(1 - \alpha)}$
Prout-Tompkins (B1)	$\ln[\alpha/(1 - \alpha)]$
<i>Deceleratory <math>\alpha</math>-time curves</i>	
Geometrical contraction models	
Contracting area (R2)	$1 - \sqrt{1 - \alpha}$
Contracting volume (R3)	$1 - \sqrt[3]{1 - \alpha}$
Diffusion models	
1-D diffusion (D1)	$\alpha^2$
2-D diffusion (D2)	$(1 - \alpha)\ln(1 - \alpha) + \alpha$
3-D diffusion – Jander (D3)	$[1 - \sqrt[3]{1 - \alpha}]^2$
Ginstling-Brounshtein (D4)	$1 - (2/3)\alpha - (1 - \alpha)^{2/3}$
Reaction-order models	
Zero-order (F0/R1)	$\alpha$
First-order (F1)	$-\ln(1 - \alpha)$
Second-order (F2)	$[1/(1 - \alpha)] - 1$
Third-order (F3)	$[1/(1 - \alpha)^2] - 1$

The  $\alpha$ -time curves are fitted to each of the rate equations listed in Table 3.1 in order to determine which model best describes the reaction. This is done by substituting each value of  $\alpha$  into the rate equation  $g(\alpha)$  to give values  $F$  at time  $t$ . In this study it was done manually through Microsoft Excel and by using a program called *Alphatime* written by Professor Len Barbour. The plot of  $F(\alpha)$  versus time should produce a straight line of the form  $y = mx + c$  with a high correlation coefficient,  $r$ . The slope of the curve is equal to the rate constant  $k$ . It is necessary to obtain  $\alpha$ -time curves at different fixed temperatures in order to determine the effect of temperature on the rate of the reaction. The Arrhenius equation<sup>31</sup> is then used to calculate the activation energy  $E_a$  and the pre-exponential or frequency factor  $A$ :

$$k = Ae^{-E_a/RT}. \quad (3.3)$$

The activation energy  $E_a$  describes the energy barrier to the reaction<sup>32</sup> and is expressed in units of energy, usually kJ/mol.<sup>31</sup> The pre-exponential factor  $A$  describes the frequency of the situation which may lead to the formation of product.<sup>32</sup> The unit of  $A$  is usually the same as that of the rate constant<sup>31</sup> which in this study is  $\text{min}^{-1}$ .  $R$  is the gas constant ( $8.314 \text{ J mol}^{-1}\text{K}^{-1}$ ) and  $T$  is the temperature in Kelvin. In order to determine the values of  $E_a$  and  $A$  the natural logarithm of equation 3.3 yields

$$\ln(k) = -\frac{E_a}{R} \frac{1}{T} + \ln(A) \quad (3.4)$$

where a plot of  $\ln(k)$  versus  $T^{-1}$  should yield a straight line in the form  $y = mx + c$ . The slope of the line is equal to  $-E_a/R$  and the y-intercept is equal to  $\ln(A)$ .<sup>31</sup>

There is some controversy regarding the application of the Arrhenius equation to heterogeneous reactions, but Brown and Galway<sup>33</sup> argue that the parameters  $E_a$  and  $A$  do have practical importance and give quantitative information regarding the temperature dependence of solid-state reactions and especially the temperature dependence of the Arrhenius parameters  $E_a$  and  $A$ .

Since framework **1** is one of only a few ionic organic framework materials, it is essential to try to understand the mechanisms involved in guest inclusion and exchange. We attempted to study the desolvation kinetics of **1**·THF but this proved to be unsuccessful and the reasons for that will be discussed in Section 3.1. Obtaining results for the exchange kinetics of **1**·THF

was also not without obstacles and the successful procedure and subsequent results will be discussed in Section 3.2.

### 3.1. Attempted studies of the desolvation kinetics of **1·THF**

Thermal analysis of **1·THF**, which was discussed in Section 2.2 of Chapter 2, shows that decomposition of **1·THF** occurs in two well-defined steps (Figure 3.2). The first mass loss step correlates to the loss of one THF molecule per asymmetric unit and the second step to the loss of 3,4-lutidine and water.

The desolvation kinetics of inclusion compounds can be measured by isothermal thermogravimetric analysis where solvent loss is measured over a range of fixed temperatures.<sup>32</sup> In the case of **1·THF** we attempted to isolate the first mass loss step in order to study the desolvation kinetics before collapse of the framework structure.

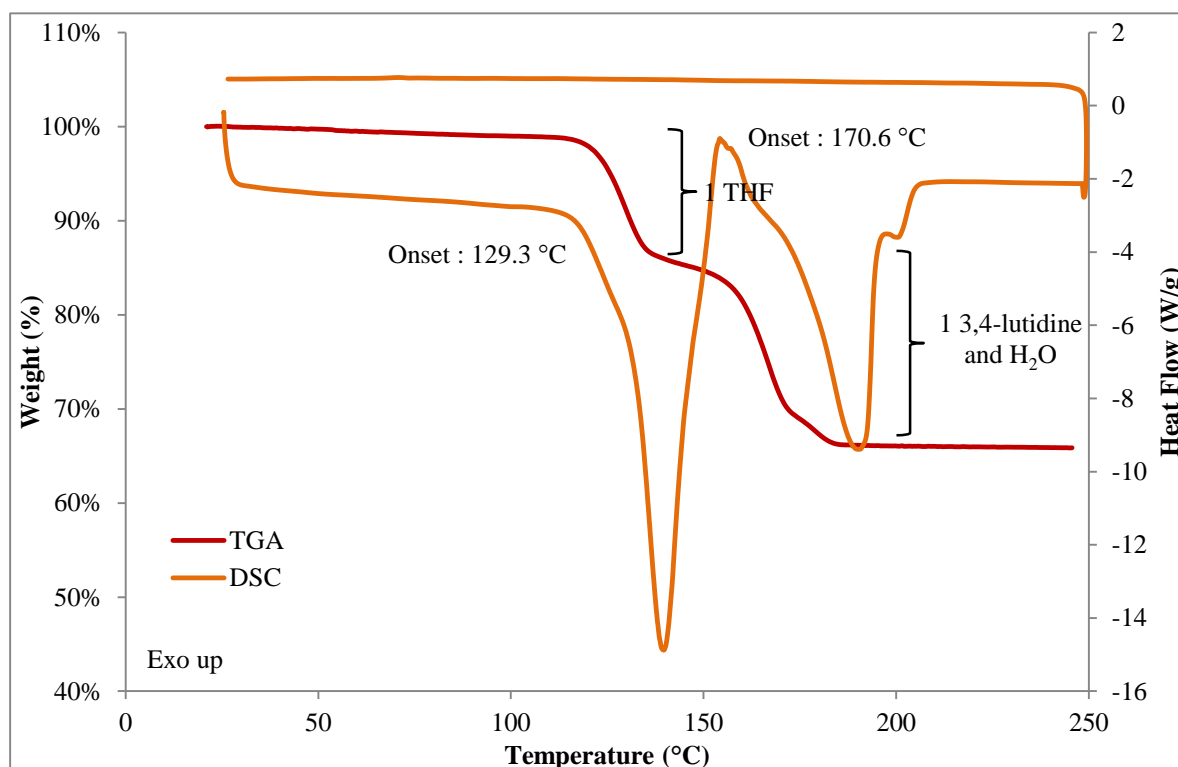


**Figure 3.2** The TG and DSC analysis of **1·THF**, showing two well-defined mass loss steps. The first mass loss correlates to the loss of one THF molecule per asymmetric unit.

Thermogravimetric analysis was used to heat crystals of **1·THF** to a specified temperature and then hold the sample at this temperature until the complete loss of THF occurred. Crystals

of **1·THF** were kept at isothermal temperatures of 95, 100, 105, 107, and 110 °C. Higher temperatures such as 112, 115 and 120 °C were also tested, but complete loss of THF had already occurred before the instrument reached the chosen isothermal temperature. It is unfortunately not possible to equilibrate the instrument at a specific temperature before the sample is added. The temperature of the furnace drastically drops when it has to be lowered to place the sample on the sample pan and then the sample has to be heated to the specified temperature again. At temperatures lower than 95 °C solvent loss does not occur or takes place at such a slow rate that desolvation could potentially continue over a few days. Figure 3.3 shows the isothermal mass loss profiles at different temperatures. It is quite clear that desolvation occurs much faster at higher temperatures, which is expected since the solvent molecules obtain more energy allowing them to escape the channels faster. It is also noticeable that the mass loss profiles never reach a plateau once complete loss of THF has occurred. This implies that the two distinct mass loss steps observed in Figure 3.2 are not completely isolated from one another and that loss of 3,4-lutidine follows closely after loss of THF. This unfortunately has negative implications for further studies into the kinetics of desolvation of **1·THF**. For an accurate interpretation of the data it is necessary to measure the solvent loss step between two plateaus, one before solvent loss starts and one after solvent loss is complete.

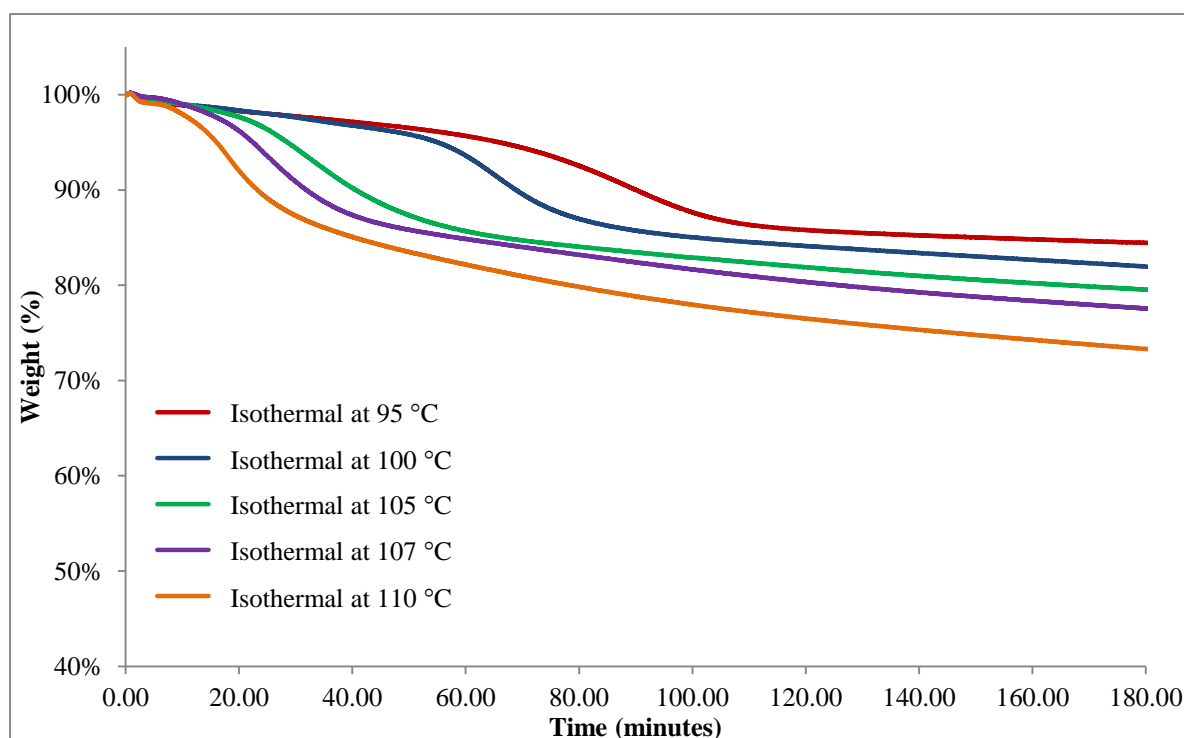


**Figure 3.3** The mass loss profiles of **1·THF** at different isothermal temperatures. After loss of THF there is a steady decrease in the mass of the sample, indicating the onset of the next mass loss step, i.e. loss of 3,4-lutidine.

The  $\alpha$ -time curves of the desolvation of **1·THF** were plotted using equation 3.1 where the mass loss is converted to  $\alpha$ , the extent of the reaction, as shown in Figure 3.4. From this graph it is also evident that desolvation occurs faster at higher temperatures since the extent of the reaction is closer to completion in a shorter time. Unfortunately, no kinetic model could be found that accurately described the desolvation step of **1·THF**. This is due to the fact that the loss of THF is too closely followed by the loss of 3,4-lutidine and therefore the loss of THF cannot be isolated for kinetic study.

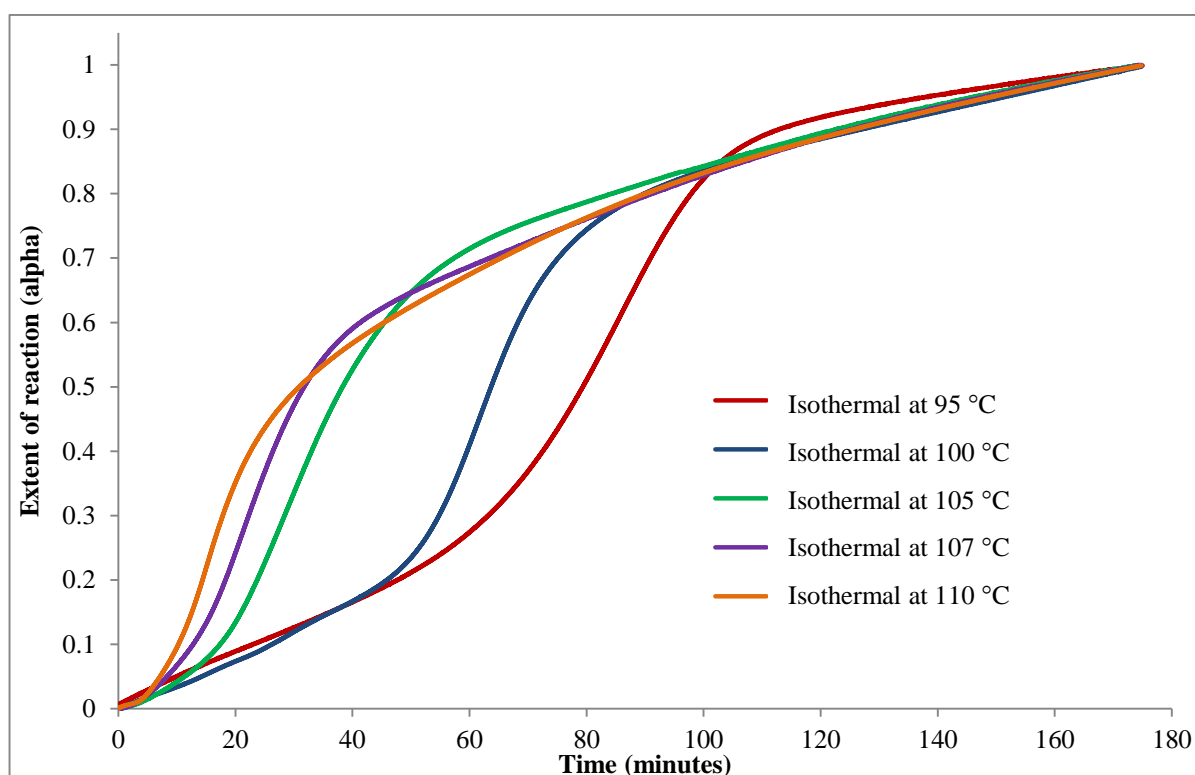


**Figure 3.4** The  $\alpha$ -time plots at different fixed temperatures of the isothermal solvent loss of THF from **1·THF**.

The possibility of using one of the isostructural solvates of **1·THF** discussed in Chapter 2 for kinetic analysis was investigated, but the same problem was encountered: the desolvation step and loss of 3,4-lutidine occur too close together to allow for accurate kinetic analysis. **1·Ether** and **1·DCM** appeared to be promising due to the wide separation between the two mass loss steps in the TGA (Figure 3.5), but closer inspection of the TG trace shows that the mass steadily decreases after desolvation. There is also significant mass loss from room temperature which also makes these compounds unsuitable for isothermal analysis.

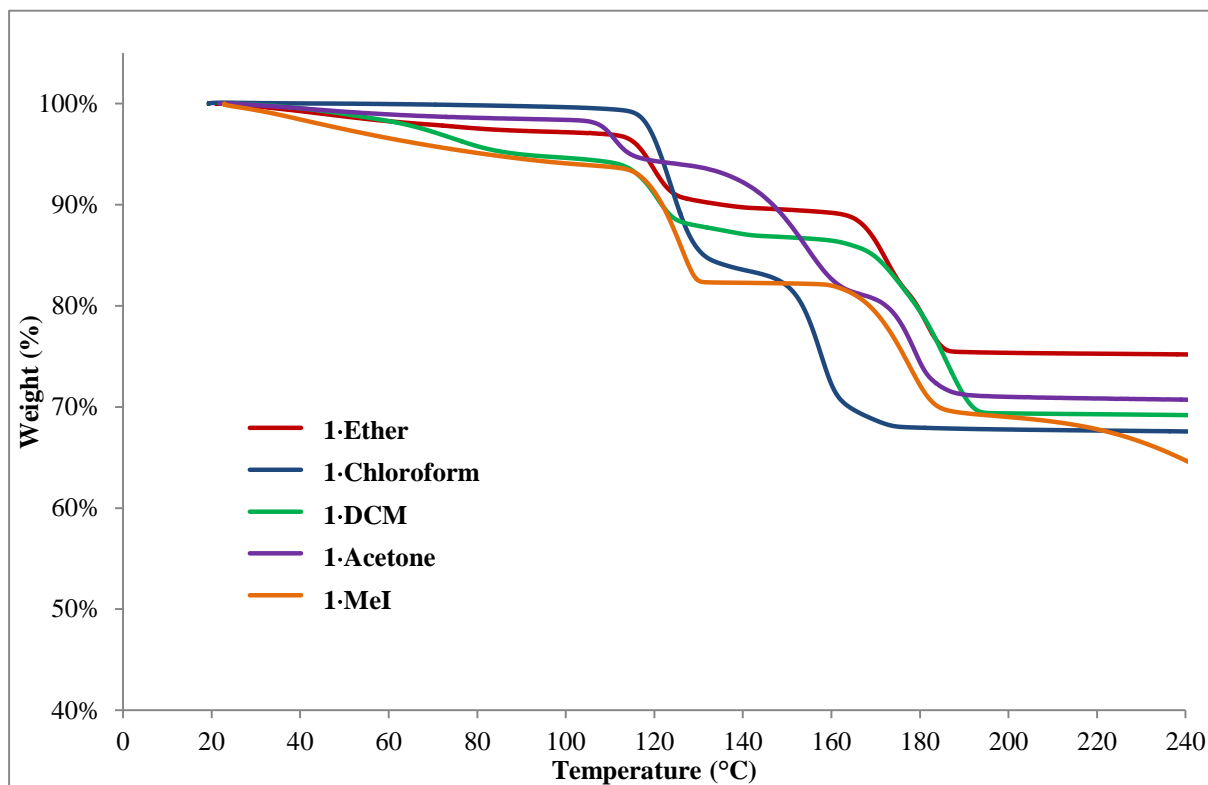


**Figure 3.5** The TG traces of other solvates of framework **1** considered for the kinetics of desolvation study.

**1·MeI** however appears to have a steady plateau between the loss of iodomethane and the loss of 3,4-lutidine. There is unfortunately a steady decrease in mass from room temperature, indicating that iodomethane is easily lost from the crystals at room temperature (Figure 3.6). Isothermal analysis of **1·MeI** (Figure 3.7) shows that a substantial amount of iodomethane is lost in each case even before the set temperature for isothermal analysis is reached. The mass of iodomethane lost during each isothermal experiment is also not consistent. For temperatures from 85 – 100 °C only approximately 10% of iodomethane is lost where the total amount of iodomethane lost during the first step should be closer to 17.7% (Figure 3.6). This could indicate that a large portion of iodomethane is lost during sample preparation and during equilibration at the correct temperature, which implies that kinetic studies of this compound are also not possible. This was confirmed by plotting the  $\alpha$ -time curves for each isothermal experiment (Figure 3.8). There also appears to be a low signal-to-noise ratio in the plots for 85, 90 and 95 °C. This is potentially due to the very long measurement time and instability of the baseline of the TG over such long analysis times.<sup>33</sup> The results could also not be fitted to any kinetic laws.



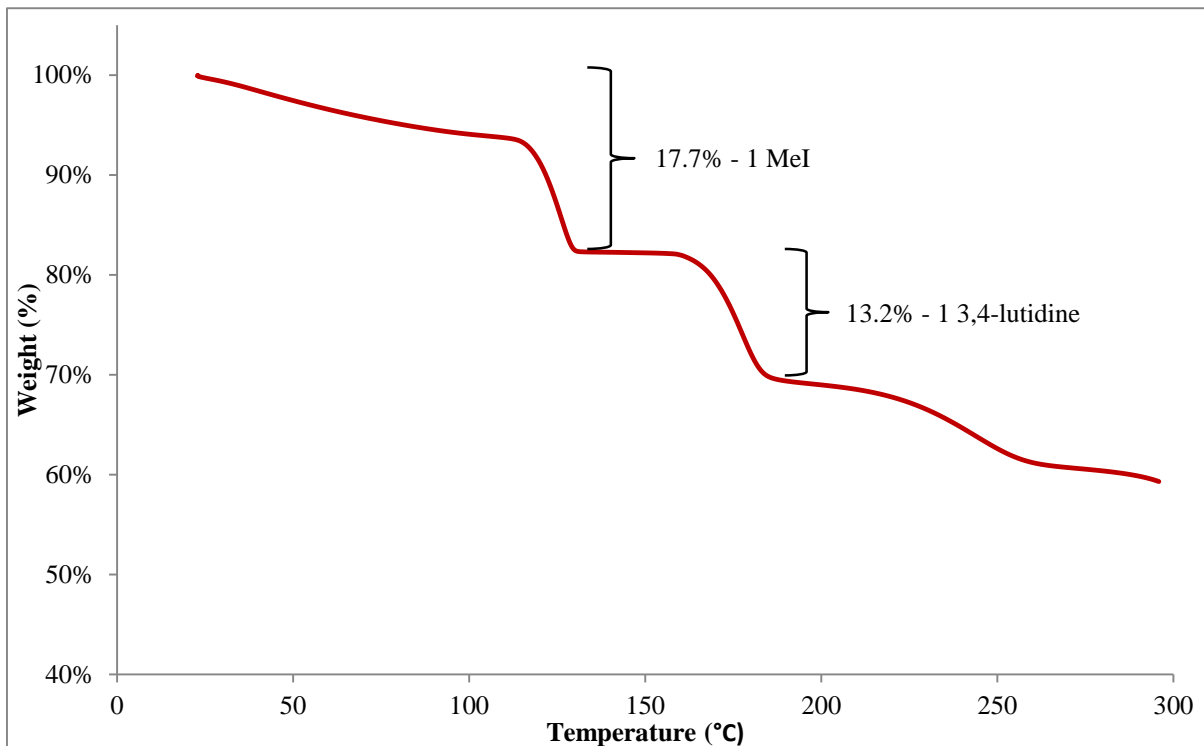


**Figure 3.6** The thermal mass-loss profile of **1-MeI**. There is good separation between the loss of MeI and 3,4-lutidine but significant solvent loss occurs from room temperature.

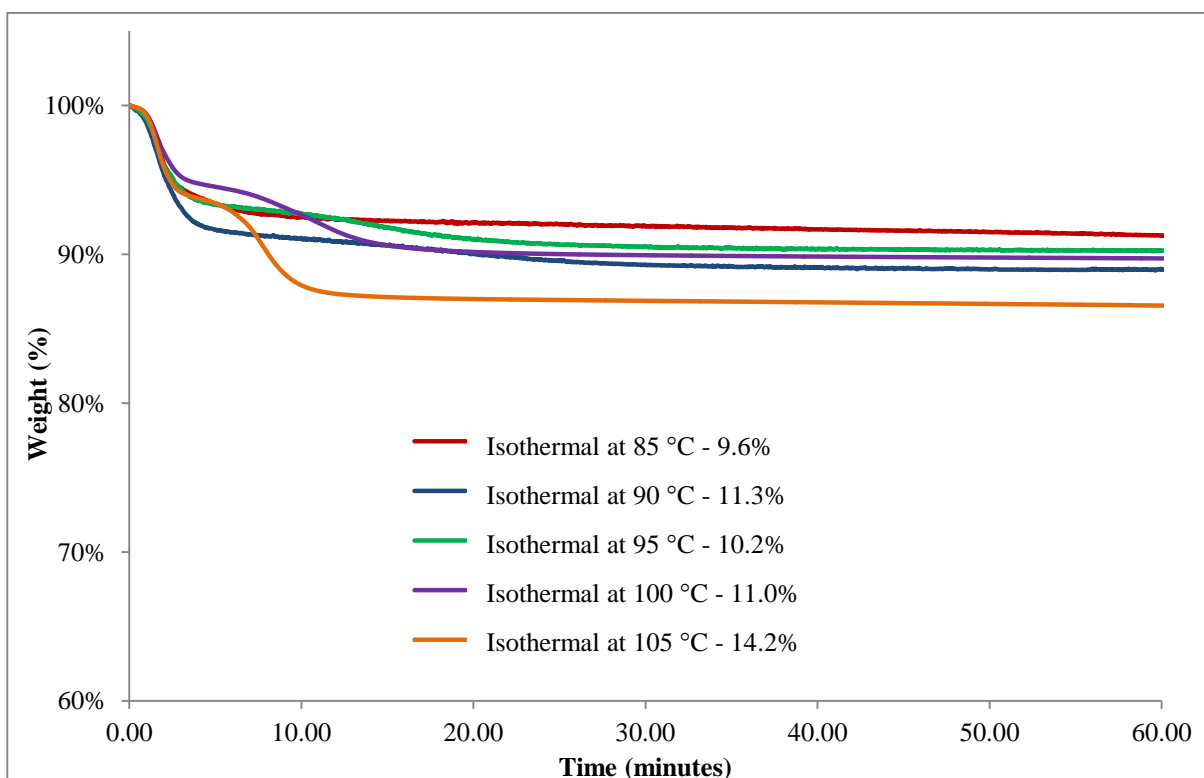


**Figure 3.7** The isothermal TG experiments with **1-MeI**. The mass loss of each experiment is indicated and it is interesting to observe that significantly less iodomethane has been lost at 85, 90, 95 and 100 °C. This could imply that during sample preparation a large portion of iodomethane was already lost before recording of the data began.

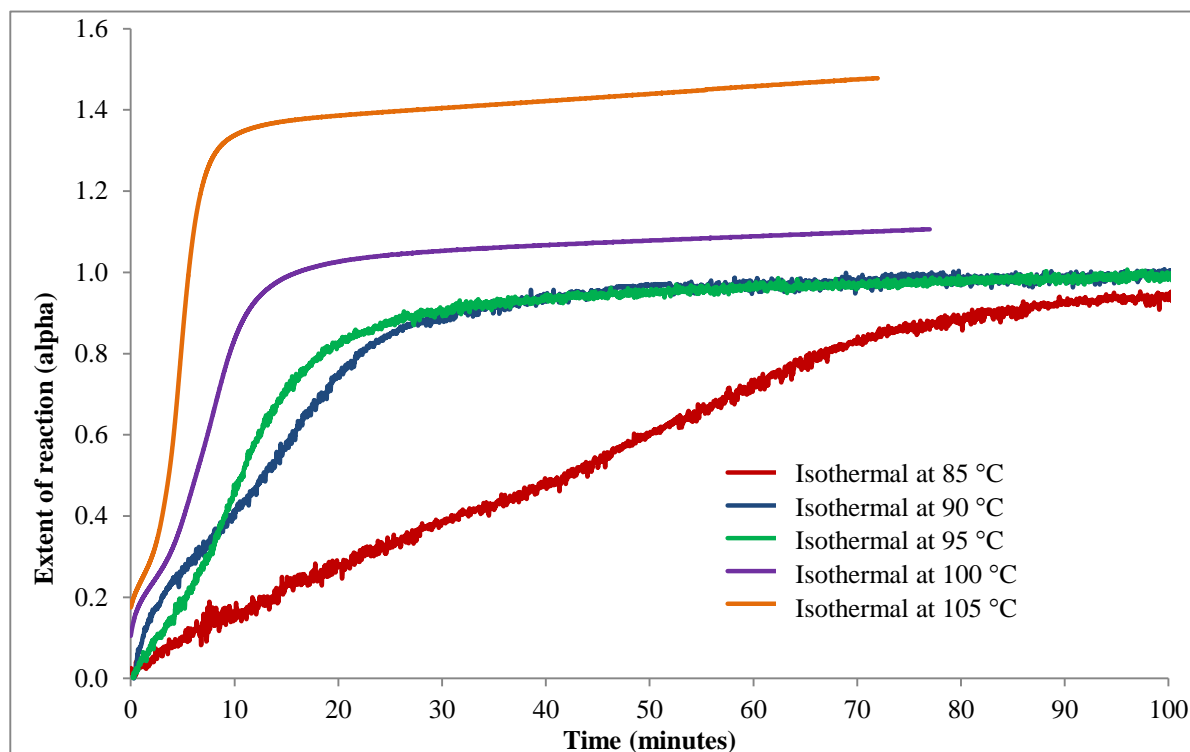


**Figure 3.8** The alpha-time plots for the isothermal TG experiments with **1-MeI**. There appears to be a lot of noise in plots of 85, 90 and 95 °C. This is potentially due to the very long measurement time and instability of the baseline of the TG over the long analysis times. The  $\alpha$ -time plots could not be fitted to any kinetic laws.

Although it was not possible to study the desolvation kinetics of **1·THF** or any of its derivatives, we attempted to obtain kinetic data on the exchange of one solvent for another with **1·THF**.

### 3.2. Studies on the kinetics of exchange with **1·THF**

In order to study the kinetics of the exchange which occurs when crystals of **1·THF** are exposed to the vapour of a different solvent, it is necessary to measure the change in weight of the sample. The solvent to which the crystals of **1·THF** are exposed therefore has to be a solvent that contains heavy atoms in order to induce a substantial and measurable increase in the weight of the sample. For this reason the solvent of choice for this study was iodomethane. Due to the presence of the heavy atom iodine, iodomethane has a molecular weight of 141.94 g/mol which would cause a weight increase of 2.422 mg for a 20 mg sample since **1·THF** undergoes a 1:1 exchange with iodomethane. This is an adequate amount of weight gain to be measured on a very sensitive balance.

### 3.2.1. First experimental setup for the kinetic study of **1·THF**

The first device used to attempt to study the exchange kinetics of **1·THF** was an instrument designed by Professor Luigi Nassimbeni at the University of Cape Town.<sup>34</sup> The instrument is illustrated in Figure 3.9. It consists of a sample plate (D) that is placed on the balance pan (B). A large brass cylinder (C) is placed around the sample plate. A brass panhandle lid (E) is placed on top to seal off the sample from the solvent wells. The brass cylinder with well holes (F) is placed on top of the panhandle lid and covered with a lid (G). The lid and cylinder have holes for a thermometer to fit into. The six-place balance on which the brass setup is assembled is located within a large temperature controlled box (Figure 3.9c). The temperature is regulated by means of light bulbs and fans.

Crystals of **1·THF** were dried and crushed on filter paper to ensure that no THF was present on the surface of the crystals and that they were all roughly of equal size. A sample of approximately 100 mg was placed in the sample plate. The brass components were then assembled around the sample ensuring that the panhandle lid (E) separated the solvent chamber from the sample chamber. The well holes of the brass cylinder F were filled with a total approximate volume of 4 ml iodomethane. The setup was allowed to equilibrate at the desired temperature but equilibration times were kept to a minimum since iodomethane is a very volatile solvent which easily evaporates. Once the temperature had stabilised the panhandle lid E was removed and recording of the data began.

Measurements were recorded at 25, 30 and 35 °C, with and without sample present in the sample plate. The sample-free experiments served as a control to ensure that the mass gain in the sample was genuine and not due to the condensation of iodomethane on the sample plate. Unfortunately there was significant solvent deposition on the sample plate which meant that it was not possible to determine the gain in weight of the sample due to exchange of THF for iodomethane. This is illustrated in Figure 3.10 where the change in mass over time has been recorded without any crystals of **1·THF** in the sample plate. The large decrease in mass initially is due to the panhandle lid being removed from the brass setup.

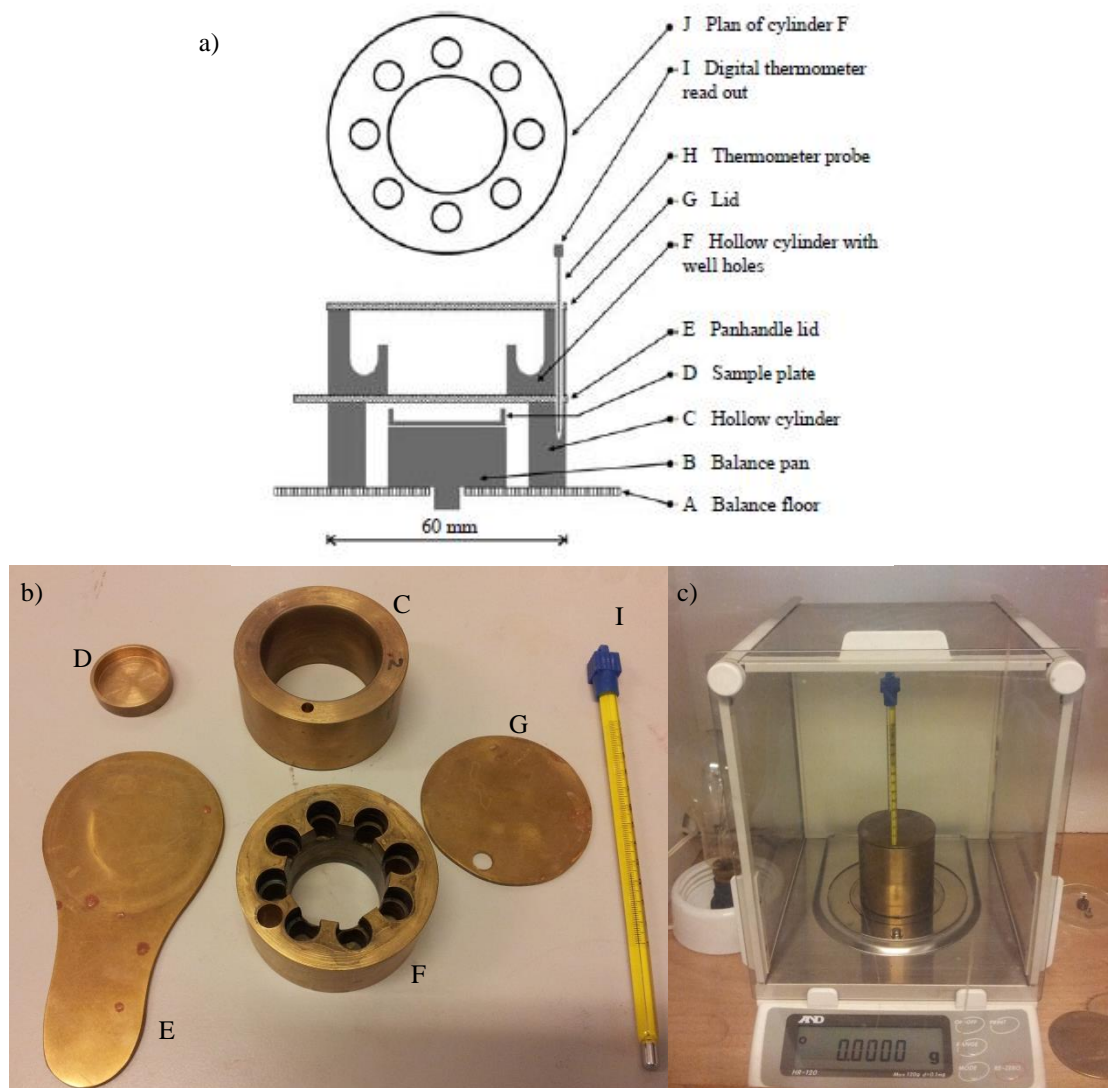


**Figure 3.9** a) A diagrammatic representation of the instrumental setup. This diagram has been reproduced from reference 34. b) A photograph of the different components. c) The balance is located within a temperature-controlled box. The temperature is controlled by means of light bulbs (heating) and fans (cooling).

Iodomethane is a very volatile solvent (comparable to diethyl ether) with a boiling point in the range of 41 – 43 °C. A large volume of iodomethane is also needed to fill the wells of the brass cylinder and it is suspected that due to the slight differences in temperatures of the well hole cylinder and the sample plate the large vapour volume of iodomethane easily condenses on the sample plate, causing the increase in mass. Even when less iodomethane was added to the solvent wells the same problem occurred. It was therefore not possible to use this instrumental setup to study the kinetics of exchange of **1-THF**.

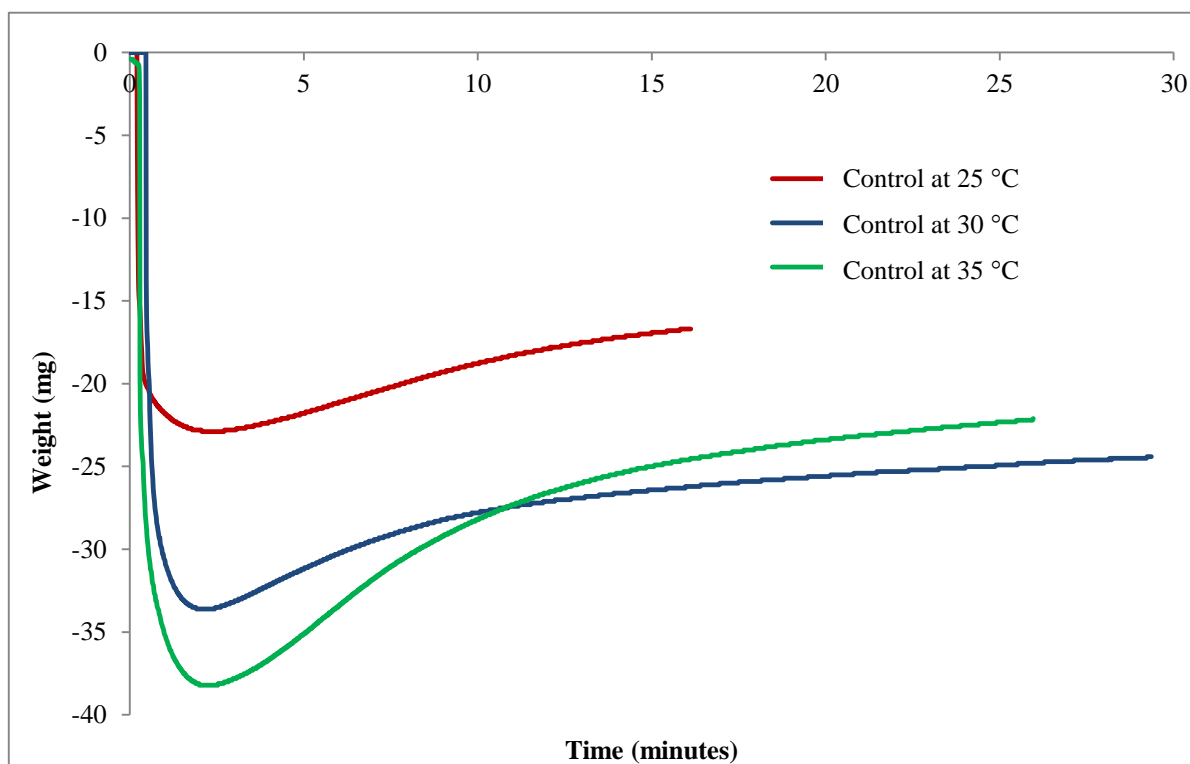
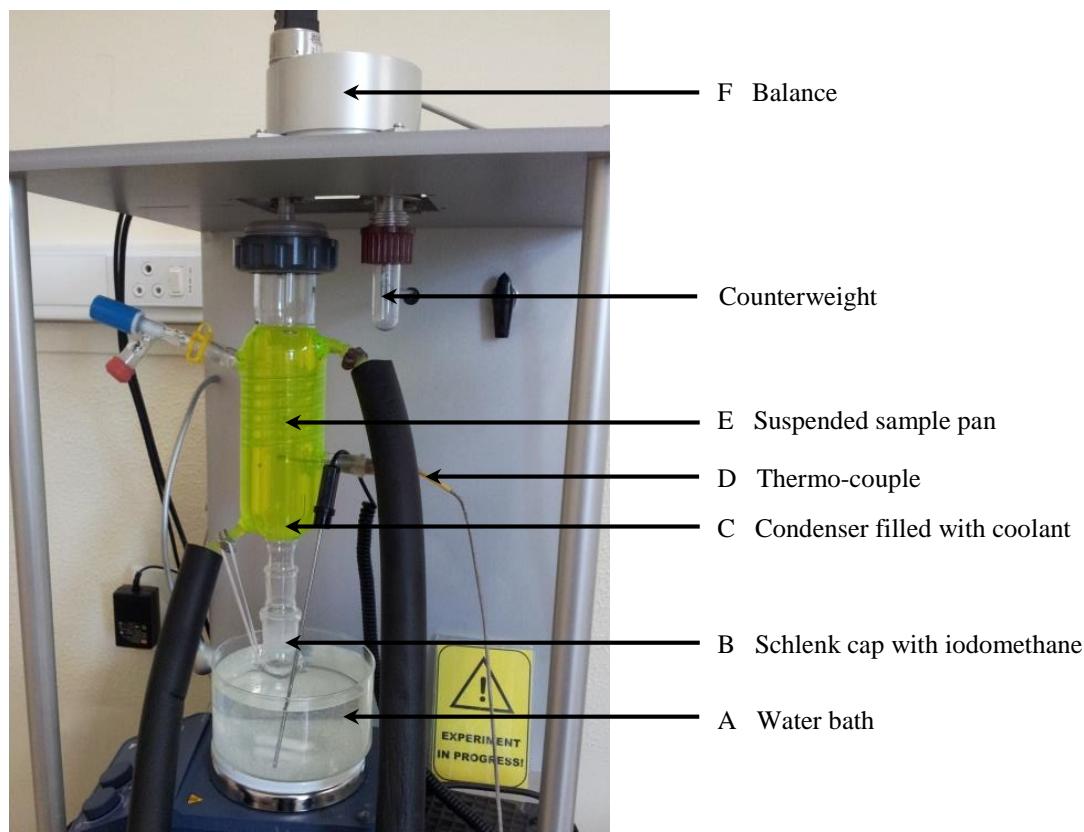


**Figure 3.10** The plot of weight versus time for control experiments without any crystals of **1·THF** in the sample plate. There is a significant increase in weight of the sample plate indicating that iodomethane has condensed on the sample plate.

### 3.2.2. Successful study of kinetics of exchange with **1·THF**

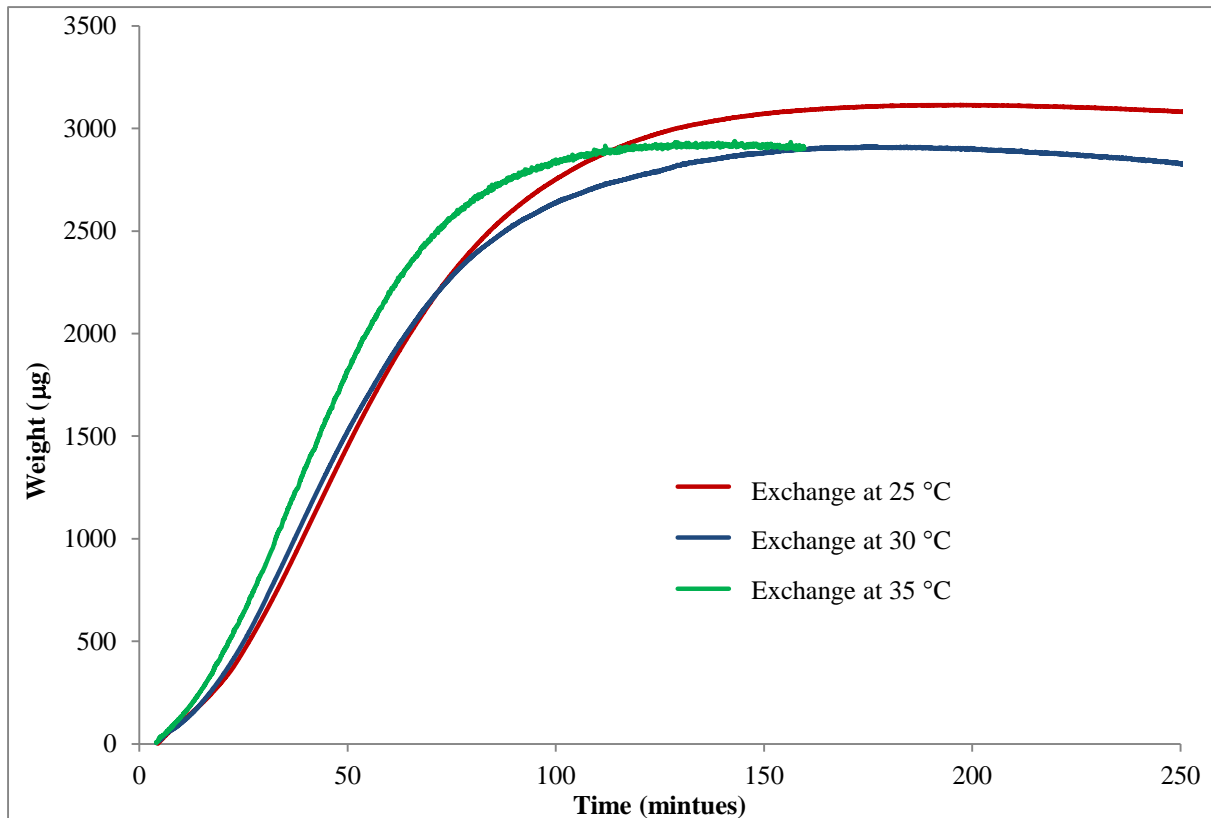
A successful study of the exchange kinetics of **1·THF** was performed on an instrument designed by Professor Len Barbour that consists of an automated magnetic suspension balance.<sup>29</sup> This instrument, shown in Figure 3.11, is designed to study the gas-solid interactions between a solid crystalline material and the vapours of a solvent or solid by measuring the increase in the sample mass as a function of time or vapour pressure. The desired solvent or solid is placed in the Schlenk cap (B) and the temperature of the compound in B can be regulated with a water bath (A) if necessary. The atmosphere surrounding the sample pan is temperature controlled by a condenser filled with coolant (C). The sample pan (E) is suspended in this temperature-controlled cylinder. A thermo-couple (D) reads the temperature directly below the sample pan. Usually with this instrument experiments are performed under vacuum to eliminate the effect air molecules could have on the exchange process or prohibit the host from absorbing nitrogen from the atmosphere and therefore competing with the absorption of the guest being investigated. In our case we conducted experiments at atmospheric pressure since all the exchange reactions we have performed and studied were done at atmospheric pressure. Samples of crushed and dried crystals of **1·THF**

ranged between 15 and 20 mg and were exposed to the vapour of approximately 0.5 ml iodomethane. Measurements were taken twice at 25, 30 and 35 °C in order to improve the accuracy of the results.



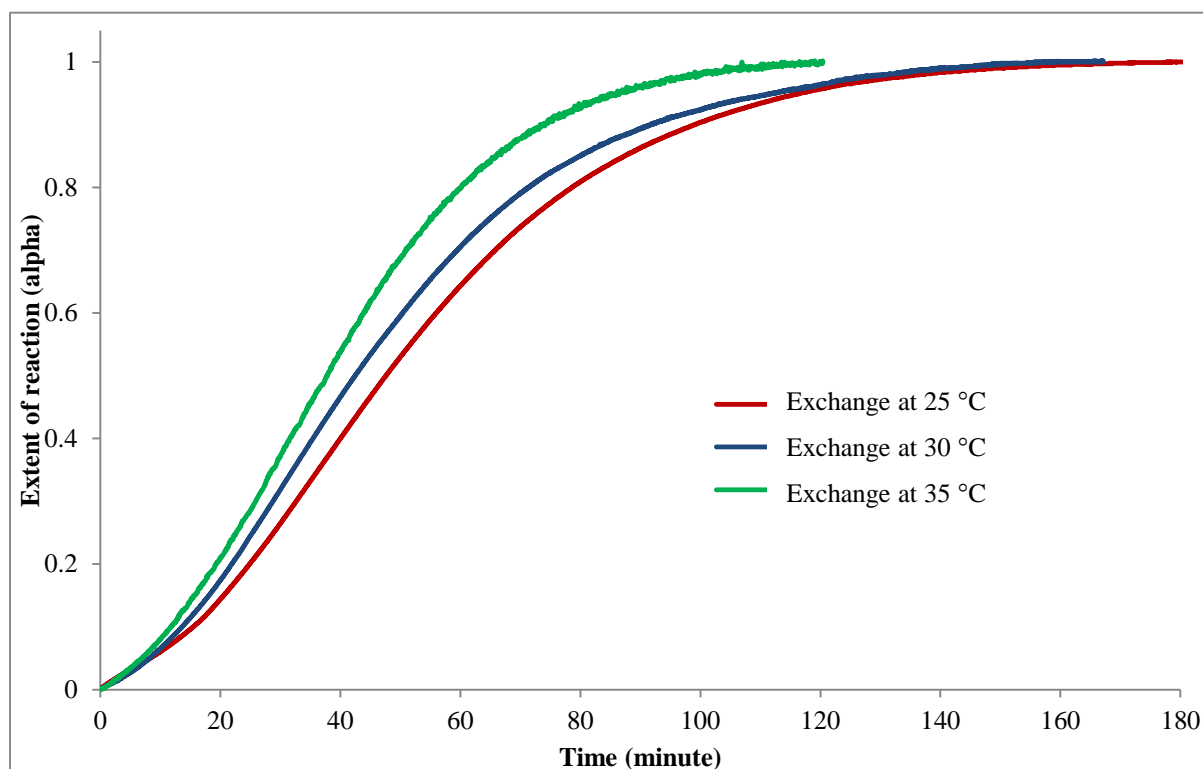
**Figure 3.11** The instrumentation used to measure the change in weight of a sample of 1·THF when exposed to the vapour of iodomethane.

Figure 3.12 shows the increase in weight of the sample in micrograms over time when exposed to the vapour of iodomethane at different temperatures. Once complete exchange has taken place the weight stabilises, but after prolonged exposure the weight of the sample starts to decrease again. This is possibly due to the crystals deteriorating after prolonged exposure to the vapour and then starting to release the iodomethane again, causing a decrease in the weight. However, this could also be due to surface THF that has started to evaporate which, in turn, influences the weight of the sample. It is also clear that the exchange occurs faster as the temperature increases. This could be due to the higher vapour pressure of iodomethane at higher temperatures. Full exchange is then reached in a shorter period.



**Figure 3.12** The increase in weight of a sample of **1·THF** over time when exposed to the vapour of iodomethane at different temperatures. The exchange appears to occur faster as the temperature increases.

A plot of  $\alpha$  versus time was plotted at each isothermal temperature using equation 3.1, and these are shown in Figure 3.13. The  $\alpha$ -time plots resemble both the deceleratory and sigmoidal kinetic models shown in Figure 3.1, although the deceleratory model would possibly better describe the exchange reaction since the initial reaction is fast, but as the reaction nears completion the reaction rate decelerates.



**Figure 3.13** The  $\alpha$ -time plots of crystals of **1·THF** exposed to iodomethane at different temperatures. These plots resemble both sigmoidal and geometrical models due to the shape of the curves.

Various rate laws, which are listed in Table 3.1, were fitted to the  $\alpha$ -time curves using the program *Alphatime*. It was found that two rate laws fit the data quite well, which is often the case for solid-state kinetics.<sup>14</sup> The rate laws were fitted to the data between  $\alpha=0.05$  and  $\alpha=0.95$  in order to determine which model described the data best with the highest correlation coefficient over the broadest range of  $\alpha$ . The first rate law that fitted the data is one of the sigmoidal models, A2 Avrami-Erofe'ev,

$$\sqrt{-\ln(1 - \alpha)} \quad (3.5)$$

and the second rate law is one of the deceleratory geometrical models R3, contracting volume,

$$1 - \sqrt{(1 - \alpha)}. \quad (3.6)$$

The plots for the Avrami-Erofe'ev model A2 are shown in Figure 3.14 with linear regression lines fitted to each plot with the indicated correlation coefficient. The plots for the geometrical model R3 are shown in Figure 3.15 with a linear regression line fitted to each of the plots with the indicated correlation coefficient,  $r$ .



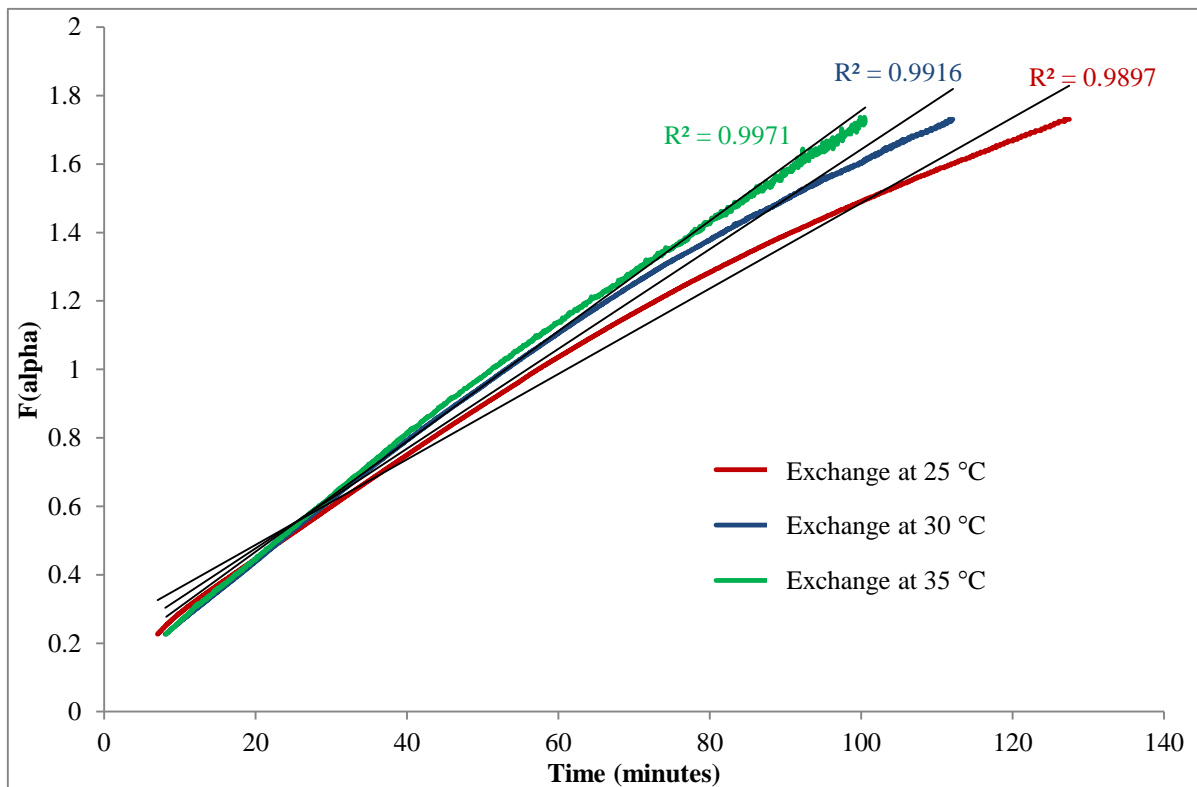


**Figure 3.14** The linear plots generated by the Avrami-Erofe'ev model A2. The linear regression lines are represented by the black lines.

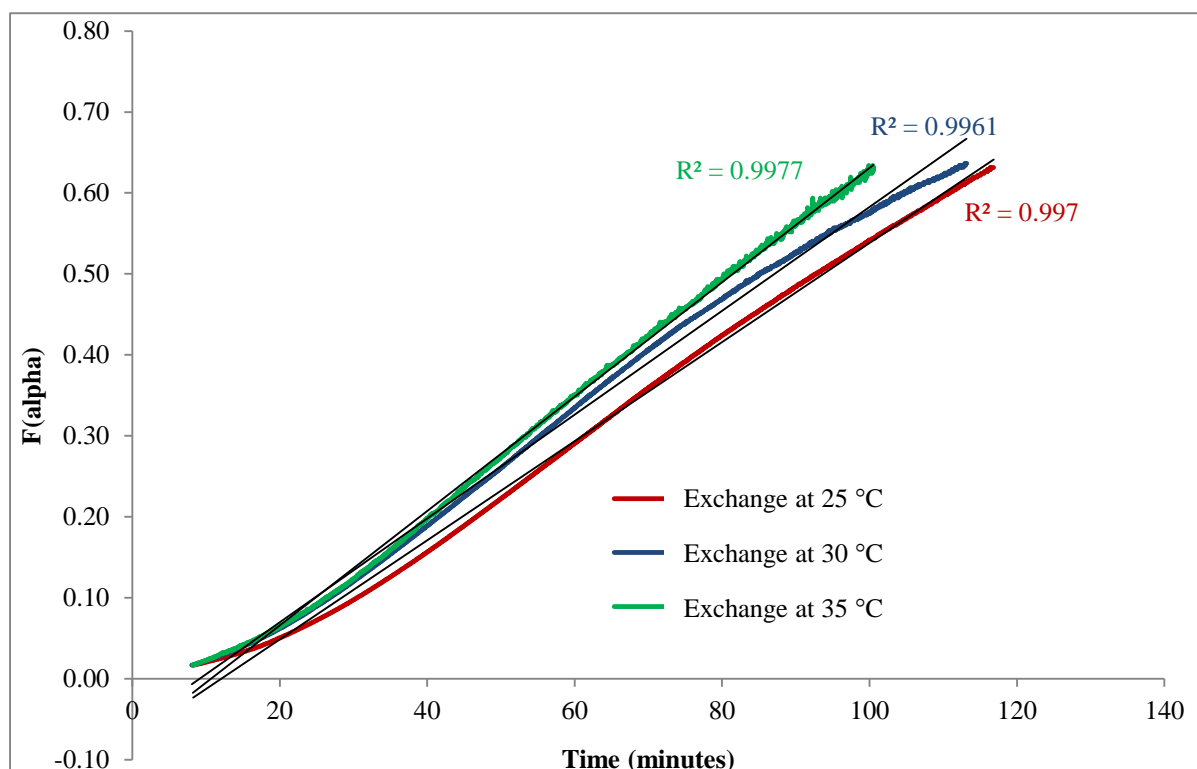


**Figure 3.15** The linear plots generated by the geometrical model R3 describing contracting volume. The black lines represent the linear regression lines.

The R3 model appears to have a slightly better fit to the data, indicated by the slightly higher correlation coefficients of the linear regression line of each plot in Figure 3.14.

The equation of each linear regression line is of the form  $y = mx + c$  where  $m$ , the slope of the curve, is the rate constant  $k$ . The rate constants from each plot are summarised in Table 3. 2. It is evident that the standard deviation for the R3 model is less than that of the A2 model, indicating that the R3 model for contracting volume is a slightly better description of the exchange process with iodomethane. This implies that the rate of exchange is dependent on the volume of the particle exposed to the vapour of iodomethane.

**Table 3. 2** The rate constant  $k$  at each temperature for the two models that best fit the data.

	R3 – contracting volume		A2 – Avrami-Erofe'ev	
	$k$ (min <sup>-1</sup> )	Standard deviation	$k$ (min <sup>-1</sup> )	Standard deviation
25 °C	0.005825	±0.0004	0.01325	±0.0011
30 °C	0.006909	±0.0007	0.01575	±0.0017
35 °C	0.007707	±0.0009	0.01764	±0.0022

The Arrhenius equation (3.3) and the natural logarithm thereof (3.4) were used to determine the activation energy  $E_a$  and the pre-exponential factor  $A$ . A plot of  $\ln(k)$  versus  $T^{-1}$  yields a straight line with a correlation coefficient of 0.9866 (Figure 3.16). The slope of the curve is equal to  $E_a/R$  and the intercept is equal to  $\ln(A)$ . From the graph the activation energy was calculated to be 21.41 kJ/mol and  $A$  was calculated to be 33.10 min<sup>-1</sup>. This means that for iodomethane to exchange for the THF in the channels of **1·THF** an energy barrier of 21.41 kJ/mol must be overcome before exchange can take place. This value seems rather small since the thermal energy available at room temperature (298 K), expressed as  $kT$ , which is the product of the Boltzmann constant  $k$  and the temperature  $T$ , is 2.479 kJ/mol.<sup>35</sup> This energy barrier is therefore high enough to inhibit loss of THF from room temperature, due to the low thermal energy of 2.479 kJ/mol available at room temperature. However, when **1·THF** is exposed to iodomethane, the energy barrier is low enough for exchange to take place, where the high concentration of iodomethane molecules in the atmosphere drive the exchange process.

The regression line fits the data fairly well which indicates that the results are fairly accurate. To further increase the accuracy of this plot the measurements of weight gain over time at 25,

30 and 35 °C should be repeated at least once more since these experiments were only repeated twice. It would also improve the data to measure the increase of weight over time at 20 and 15 °C. At higher temperatures the reaction may occur too fast to accurately measure the weight gain and the boiling point of iodomethane is nearly reached. This could lead to a lot of solvent condensation on the sample pan or the surface of the crystals due to the extremely high vapour pressure. However, these results are sufficient to draw some conclusions regarding the exchange mechanism of **1·THF** with iodomethane.

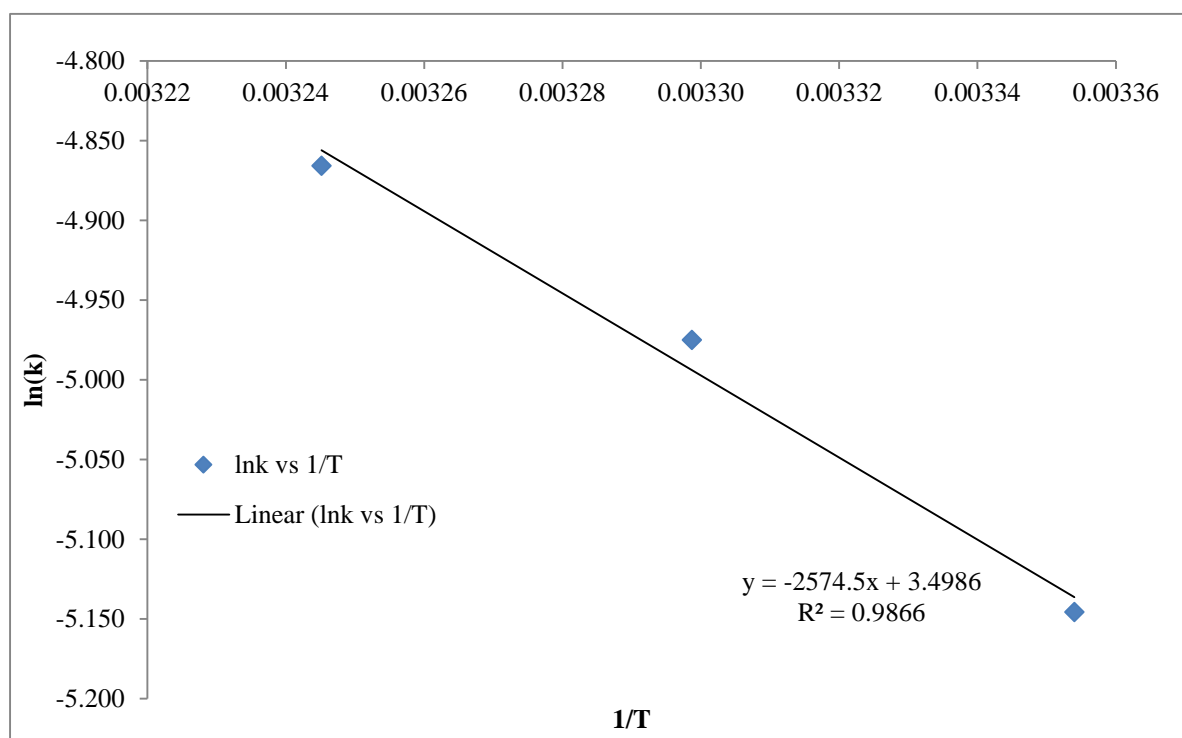


**Figure 3.16** The plot of  $\ln(k)$  versus  $T^{-1}$  which yields a straight line with a correlation coefficient of 0.9866. The slope of the curve is equal to  $-E_a/R$  and the y-intercept is equal to  $\ln(A)$ .

### 3.3. Discussion and interpretation of the kinetic data of **1·THF**

In this study the rate of exchange of **1·THF** with iodomethane was determined by measuring the increase in weight of a sample of **1·THF** during exposure to iodomethane vapour at three fixed temperatures, 25, 30 and 35 °C. It was determined that the rate law of contracting volume  $1-(1-\alpha)^{1/2}$  describes the exchange process the best. The rate law at each temperature was calculated and indicated that the rate of the reaction increases at higher temperatures due to the increase in the rate constant  $k$  in the order  $k_{25} < k_{30} < k_{35}$ . These data were used to plot a

graph of  $\ln(k)$  versus  $T^{-1}$  and the activation energy  $E_a$  and the pre-exponential factor  $A$  were calculated to be 21.41 kJ/mol and 33.10 min<sup>-1</sup>, respectively. This implies that for the exchange of THF for iodomethane in **1·THF** an energy barrier of 21.41 kJ/mol must first be overcome before the exchange can take place. It is unfortunately difficult to compare these results to similar systems in the literature since these types of studies for hydrogen-bonded framework materials are far in the minority. There are a few studies that report the rate constants and activation energies involved in guest exchange for large dimer molecules that encapsulate small guest molecules.<sup>20, 36-41</sup> There is also another report of a M<sub>4</sub>L<sub>6</sub> tetrahedral host where the rate constants and activation energies for different guests are reported.<sup>22</sup> These studies will be used to compare results obtained in this study to determine whether exchange occurs faster and more easily in **1·THF** and also to attempt to describe a possible mechanism for guest exchange of **1·THF** based on the acquired kinetic results.

Rate constants have been reported for guest exchange in hydrogen-bonded dimer molecules. These values are listed in Table 3.3. **1·THF** has one of the slower guest exchange rate constants of the compounds listed in Table 3.3. This is possibly due to the mechanism of guest exchange. The kinetic model that best describes the exchange process of **1·THF** and iodomethane is the contracting volume model, which means that the rate of exchange is dependent on the volume of the particle exposed to the vapour. This means that the exchange rate could be slower due to the time it takes for iodomethane to permeate throughout a large crystal. The kinetic studies of the compounds listed in Table 3.3 have been conducted in the solution state which could better facilitate the interaction between host and guest. As was mentioned before, it is rather difficult to compare this study to other similar studies since the rate of guest exchange is not often studied. More often than not the rate of encapsulation of a guest into the apohost (empty host) is studied rather than the exchange process of one guest for another. It is however important to study this process since framework **1** has the fascinating ability to exchange the THF in the channels for a wide variety of solvents and understanding what mechanism drives this is invaluable. As was discussed in Chapter 2.5.3, framework **1** appears to selectively exclude chlorinated solvents such as chloroform and dichloromethane in a solvent mixture. This would imply that iodomethane, it being a halogenated guest and having a dipole moment, would also be less favoured by **1·THF** for guest exchange. This could explain why the rate of exchange appears to be rather slow.

**Table 3.3** The guest exchange rate constants of hydrogen bonded dimer molecules in comparison with **1·THF**.

Hydrogen bonded host	Guest	Rate constant (s <sup>-1</sup> ) at 25 °C
<b>1·THF</b>	Iodomethane	0.35
Glycoluril host <b>IV</b> <sup>20, 36, 41</sup>	Ethane	0.56
Tetra urea calix[4]arene Host <b>V</b> <sup>20, 39</sup>	Benzene	0.47
Cavitand porphyrin host <b>VI</b> <sup>20, 40</sup>	Ethylene	0.6
Imide calix[4]resorcinarene host <b>VII</b> <sup>20, 38</sup>	Benzene	0.25
Gallium 1,5-bis(2',3'-dihydroxybenzamido)naphthalene host <sup>22</sup> [Ga <sub>4</sub> L <sub>6</sub> ] <sup>12-</sup>	PEt <sub>4</sub> <sup>+</sup>	0.003
	NEt <sub>4</sub> <sup>+</sup>	0.009
	NMe <sub>2</sub> Pr <sub>2</sub> <sup>+</sup>	4.4
	NPr <sub>4</sub> <sup>+</sup>	1.4

### 3.4. Supporting studies for the kinetic model of **1·THF**

In order to further study the exchange process attempts were made to follow the exchange of **1·THF** with iodomethane in single crystals. From these results it would then be possible to confirm that the exchange of one solvent for another does not occur *via* the apohost structure but rather through the inclusion of one guest and the expulsion of the other guest simultaneously. In addition it would be possible to determine whether the framework undergoes great change during the guest exchange process.

A small crystal of **1·THF** was selected since the smaller crystals appear to undergo less structural damage during the exchange process. The crystal was then carefully glued to a glass fibre and care was taken to avoid covering the crystal in glue and potentially inhibiting exchange. This was done with four crystals of **1·THF**. Each crystal was exposed to the vapour of 0.1 ml iodomethane for a specific time period (one hour, two hours, four hours and six hours) by placing the crystal and glass fibre in a jar that was sealed with a lid and parafilm (Figure 3.17). All of these exchanges were performed at 25 °C.

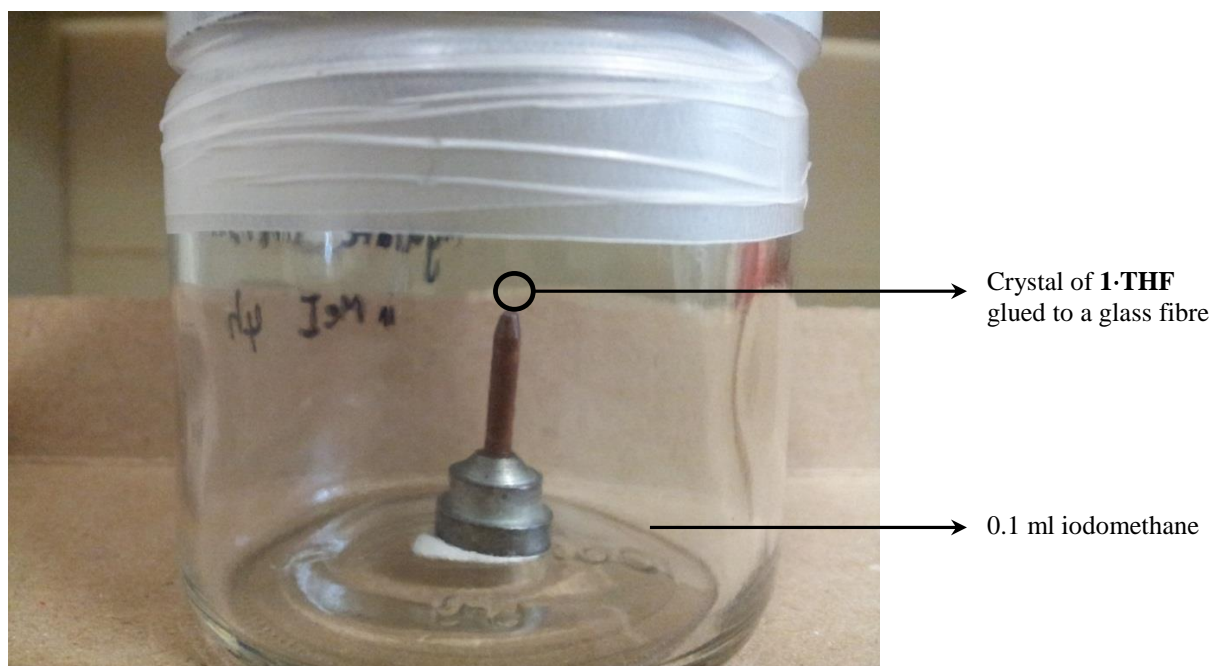


**Figure 3.17** The experimental setup of a single crystal of **1·THF** exposed to iodomethane for 1 hour, 2 hours, 4 hours and 6 hours.

It was possible to solve the structures collected after one and two hours of exposure to iodomethane, but not the structures collected after exposure for four and six hours. During the exchange the crystals had cracked, causing them to form two domains for which the individual reflections could not be separated in order to solve the structures. Photographs of the crystals are shown in Figure 3.18.

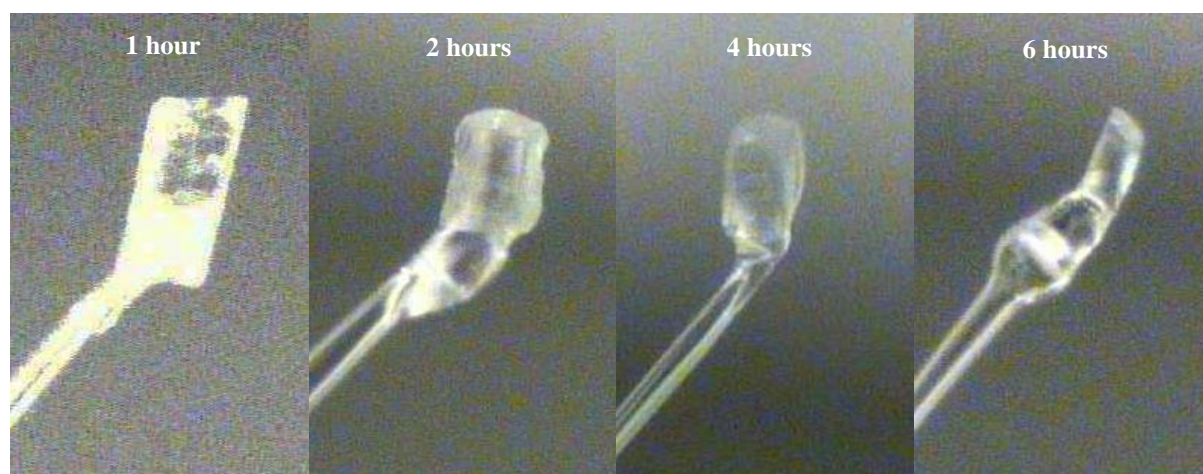


**Figure 3.18** Different crystals of **1·THF** after exposure to iodomethane at 25 °C for 1 hour, 2 hours, 4 hours and 6 hours, respectively.

The solvent molecules could not be adequately modelled in the structures after exposure to iodomethane for one hour (**1·MeI\_1h**) and two hours (**1·MeI\_2h**). It was however possible to compare the PLATON<sup>42</sup> SQUEEZE<sup>43</sup> results of the two structures to that of the original



**1·THF** and the structure after full exchange with iodomethane, **1·MeI**. These results along with selected crystallographic data for the crystal structures are summarised in Table 3.4. It is notable that the crystal mosaicity is much higher after longer exposure to iodomethane, except in the case of the fully exchanged structure **1·MeI**. The unit cell parameters also do not change significantly between the different structures. The length of the *c*-axis hardly varies which is expected since the channels are down the length of the *c*-axis so no lengthening or shortening of this axis is expected to accommodate the inflow of a guest. There is a slight shortening of the *a*-axis, while the length of the *b* axis seems to vary during exchange. These slight changes in the length of the *a* and *b* axes are possibly due to the framework slightly adjusting in order to facilitate movement of the guest molecules.

The SQUEEZE results of the structures in Table 3.4 show how the electron count changes during the exchange process. Although the results of SQUEEZE analysis are not always infallible it is another method of obtaining a glimpse of what is occurring in the crystal structure during guest exchange. According to SQUEEZE analysis the original **1·THF** structure contains 44 electrons in the asymmetric unit. This correlates fairly well with the number we expect, since a THF molecule has 40 electrons. SQUEEZE analysis of the **1·MeI** structure calculates there to be 69 electrons per asymmetric unit, which is relatively close to the electron count of one iodomethane molecule (62 electrons). It is therefore possible to obtain results that can to some degree indicate what is occurring in the crystal structure during exchange. SQUEEZE analysis for **1·MeI\_1h** indicates that there are 55 electrons in the asymmetric unit. This could equate to half a THF molecule (20 electrons) and half an iodomethane molecule (31 electrons), in other words a 50% presence of each solvent in the crystal after one hour of exposure to iodomethane vapour. One could argue that the 55 electrons in **1·MeI\_1h** could just be one THF molecule, but upon solving the structure there is a residual electron density peak that is too high for a partially occupied oxygen molecule of THF, which indicates that there certainly is iodomethane present in the structure. SQUEEZE analysis of **1·MeI\_2h** indicates that there are 80 electrons present in the asymmetric unit. This is a large increase from the previous structure, indicating that there is definitely more iodomethane present in this structure. In this case it could equate to a quarter of a THF molecule (10 electrons) and one iodomethane molecule (62 electrons), i.e. 25% occupancy of the THF molecules in the crystal structure and fully occupied iodomethane molecules. This structure is at greater than full occupancy, which could also explain why the crystal mosaicity is higher in this structure than the previous structure. This could also indicate that the

exchange process has not yet reached equilibrium. In **1·MeI** all the THF has been replaced by iodomethane. In this case the crystal had suffered very little structural damage which is probably because the exchange was performed at a lower temperature, causing less structural damage to the crystal due to a slower exchange process. These results also confirm that the inflow of iodomethane and outflow of THF occur simultaneously and not *via* the formation of the apohost<sup>27</sup> since both solvent molecules are present in the crystal structure during the initial stages of exchange.

**Table 3.4** Selected crystallographic data for exchange experiments with **1·THF** and iodomethane.

	<b>1·THF</b>	<b>1·MeI_1h</b>	<b>1·MeI_2h</b>	<b>1·MeI_4h</b>	<b>1·MeI_6h</b>	<b>1·MeI</b>
Crystal system	Monoclinic	Monoclinic	Monoclinic			Monoclinic
Space group	<i>C2/c</i>	<i>C2/c</i>	<i>C2/c</i>			<i>C2/c</i>
<i>a</i> /Å	22.1174(13)	22.0503(8)	21.996(48)			22.0399(23)
<i>b</i> /Å	19.8568(12)	19.8214(7)	19.8431(43)			19.803(2)
<i>c</i> /Å	14.6154(8)	14.5772(7)	14.6072(32)	Could not be solved	Could not be solved	14.5966(16)
$\alpha$ /°	90	90	90			90
$\beta$ /°	114.6154(8)	115.065(1)	114.570(3)			114.718(2)
$\gamma$ /°	90	90	90			90
Volume/Å <sup>3</sup>	5806.0(6)	5771.23	5798.30			5787.15
Temperature/K	100(2)	100(2)	100(2)	100(2)	100(2)	100(2)
Crystal mosaicity/°	0.49	0.55	0.69	0.74	0.62	0.52
Crystal dimensions/mm	0.144x 0.163 x0.386	0.164x0.232 x0.459	0.106x0.186 x0.254	0.112x0.146 x0.262	0.089x0.091 x0.289	0.258x0.294 x0.490
SQUEEZE e <sup>-</sup> count (per asymmetric unit)	44	55	80	-	-	69

The single crystal data were further supported by thermogravimetric analysis of the exchange process. Fresh crystals of **1·THF** were removed from the mother liquor, dried on filter paper and placed in a glass vial. The glass vial was placed in a larger jar with approximately 0.5 ml iodomethane and sealed with a cap and parafilm. The temperature around the jar was kept between 22 and 25 °C and exchange was allowed to take place for 5 minutes after which a



sample of approximately 11 mg was taken for TG analysis. This was repeated for time periods of 15 minutes, 45 minutes, 1 hour, 2 hours, 24 hours and 48 hours. The thermal mass-loss profiles for each exchange for a certain time period are shown in Figure 3.19 as well as the mass-loss profile for the original **1·THF** for comparison. It is clear from the graph that there is a general increase in the percentage mass loss as the exposure time to iodomethane increases. This is due to more iodomethane being present in the crystals after longer exposure to iodomethane. After 2 hours the exchange process has almost reached completion since the mass loss for crystals fully occupied with iodomethane is 17.7%, depending on the amount lost at room temperature during sample preparation.

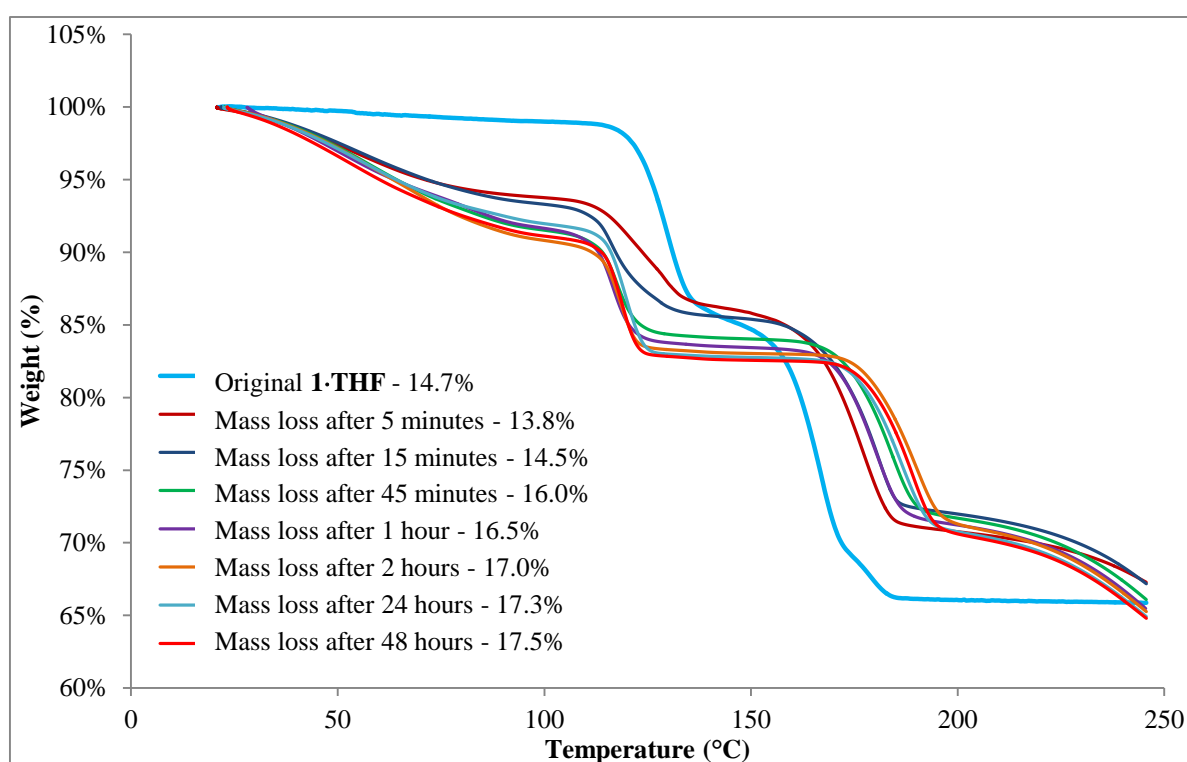


**Figure 3.19** The thermal mass-loss profiles of exchanges of the THF in **1·THF** with iodomethane after exposure to iodomethane after specific time intervals. There is a clear increase in the mass loss percentage as the exposure time to iodomethane increases.

The mass loss percentages after one and two hours of exposure are 16.5% and 17.0%, respectively. In the case of exposure for one hour, the mass loss percentage is equal to the loss of 0.4 iodomethane molecules and 0.6 THF molecules per asymmetric unit (calculated 16.55%). The occupancies of the two molecules are therefore 40% and 60%, respectively, which roughly correlates to the results of SQUEEZE analysis of **1·MeI\_1h** which showed that the occupancy was approximately 50:50 for iodomethane and THF. In the case of exposure to iodomethane for 2 hours the mass loss percentage is equal to the loss of half an iodomethane molecule and half a THF molecule (calculated 17.5%), whereas SQUEEZE analysis inferred

the presence of 0.25 THF molecules and a fully occupied iodomethane molecule per asymmetric unit. The discrepancies between the TGA and SQUEEZE results could be due to the quality of the single crystal X-ray diffraction data, since for sensible SQUEEZE results it is necessary to obtain really good data. The take-home message from these experiments is that the influx of iodomethane occurs at the same time as the outflow of THF and that the exchange process does not occur through the generation of the empty structure. This is expected since the framework contains large channels that would allow for the uninhibited exchange of one guest for another. To some extent this could explain why the rate constant of the reaction is slow when compared to other host compounds: one guest has to be “pushed out” by the incoming guest. The kinetic study is also further complicated since two processes are occurring simultaneously.

### 3.5. Conclusions and future work

In this chapter the kinetic studies of **1·THF** were discussed. We attempted to obtain kinetic information on the desolvation of **1·THF** as well as information regarding the exchange process of another solvent for the THF in **1·THF**. It was not possible to obtain kinetic data on the desolvation of **1·THF** since the loss of THF from the structure is quickly followed by the start of the loss of 3,4-lutidine. Since these two mass loss steps could not be isolated from each other during isothermal thermogravimetric analysis, it was not possible to obtain an  $\alpha$ -time plot for the first step on its own. It was also not possible to determine the kinetics of desolvation of any of the other solvates of **1** discussed in Chapter 2. In each case the two mass loss steps for solvent and 3,4-lutidine were too close to each other, or the complex started losing solvent from room temperature, which would make accurate kinetic analysis difficult.

The kinetic law that best describes the exchange of the THF in **1·THF** with iodomethane was identified to be the model of contracting volume. The volume of the particle therefore determines the rate of exchange. This model does seem to describe the exchange process well, since the framework does not undergo great structural changes in order to accommodate new guests or to expel the existing guest. The size of the crystals must therefore be the rate limiting factor. If the framework had to bend and stretch in order to allow the entry of guests, as with some dimer molecules<sup>20, 37, 39</sup> and tetrahedral host compounds<sup>22</sup>, the deformation of the framework would have been rate limiting and a different model would have been applicable. Single crystal data were collected at specific time intervals during the exchange

process with iodomethane and this also confirmed that there is no significant change in the unit cell parameters of the different crystals at different stages of exchange. The SCD also suggest that the inflow of iodomethane and outflow of THF occur simultaneously since both molecules are present (at different occupancies) within the crystal structure at various stages during the exchange process. It is however important to remember that guest exchange is a difficult process to study kinetically, since two processes (the inflow and outflow of guest molecules) are occurring simultaneously. It is therefore not possible to unambiguously assign a kinetic model to the exchange process, but the current study does give some insight as to how guest exchange may take place.

Since the same kinetic model could be applied to the exchange process at different temperatures it was possible to calculate the activation energy  $E_a$  from the Arrhenius equation (equations 3.3 and 3.4). It was calculated to be 21.41 kJ/mol, which is a surprisingly low barrier that has to be overcome in order for exchange to take place. To bring the value of 21.41 kJ/mol into perspective, compare it to the strength of a strong hydrogen bond which can range from 80 – 120 kJ/mol.<sup>44</sup> The low activation energy of 21.41 kJ/mol is possibly due to the fact that there are no hydrogen bonds between the framework and the guest in the channel. The guest molecules are only stabilised by weak van der Waals forces for which the strength of the interaction is generally less than 5 kJ/mol.<sup>21</sup> Therefore an activation energy of 21.41 kJ/mol allows for easy exchange with a different guest, but provides enough of an activation barrier to prohibit the desolvation of THF at room temperature. The loss of THF only starts at approximately 120 °C according to the thermal analysis results (Figure 3.2).

The kinetics of exchange of the wide array of solvents that **1·THF** exchanges for should certainly be investigated. It would be interesting to determine what the influence of the guest is on the rate constant  $k$ , especially since **1·THF** shows selectivity for some solvents (discussed in Chapter 2.4). In future it would be of interest to investigate whether the rate constant increases for solvents that **1·THF** selectively includes. **1·THF** has also been shown to selectively exclude chlorinated solvents such as chloroform and dichloromethane when these solvents are present in a solvent mixture. It would therefore be interesting to determine whether the rate constants would be much slower for these particular solvents and whether this exchange rate is faster, slower or the same as that of iodomethane. If the rate constant is the same as that of iodomethane it would imply that the framework not only selectively

excludes chlorinated solvents, but selectively excludes halogenated solvents. This would lead to some insight regarding the electrostatics of the channel of framework **1**.

A problem however arises regarding the recording of the exchange data with other solvents. Iodomethane was specifically chosen due to the presence of the heavy atom iodine, which allowed us to measure the weight increase of the sample with a sensitive balance. This would not be possible with the other solvents that do not have this heavy atom. This would even be difficult with chloroform and dichloromethane. One would therefore have to turn to a combination of DSC and  $^1\text{H}$  NMR analysis to track the extent of the reaction over time. DSC analysis has been employed to study the enclathration process of some inclusion compounds<sup>14, 21, 24, 27</sup> and NMR analysis has also been used to study the encapsulation of guest molecules into large dimers.<sup>20, 37-39</sup>

A proposed method would be to expose crystals of **1·THF** to the desired solvent in a sealed jar at different fixed temperatures. Samples should then be taken at specific time intervals for analysis. In each case the weight of the sample must be known as accurately as possible. Using DSC analysis to track the extent of the reaction would be troublesome due to the very broad peaks associated with solvent loss for this particular system. It would therefore not be possible to assign different peaks accurately to different solvents.  $^1\text{H}$  NMR would be a very quick and easy method to quantitatively determine the ratio of the different solvents present in the sample. This particular system is also rather ideal for NMR analysis since the peaks for the components of the framework are sharp and seldom undergo chemical shift due to the presence of a particular solvent because there are no strong interactions between the framework and the guest molecules. Using this method it would be possible to gather kinetic data on very nearly all of the solvents **1·THF** exchanges for which would make a valuable contribution towards fully understanding the properties of this unique framework. Should the exchange reaction take long enough, it could also be possible to determine the ratios of the two guests at a particular time using gas chromatography headspace analysis.

### 3.6. References

1. H. W. Langmi, J. Ren, B. North, M. Mathe and D. Bessarabov, *Electrochimica Acta*, 2014, **128**, 368-392.
2. D. Liu, J.-P. Lang and B. F. Abrahams, *J. Am. Chem. Soc.*, 2011, **133**, 11042-11045.
3. M. Meilikhov, K. Yusenkov and R. A. Fischer, *Dalton Trans.*, 2010, **39**, 10990-10999.
4. P. Li, Y. He, J. Guang, L. Weng, J. C.-G. Zhao, S. Xiang and B. Chen, *J. Am. Chem. Soc.*, 2014, **136**, 547-549.
5. A. Yamamoto, T. Hamada, I. Hisaki, M. Miyata and N. Tohnai, *Angew. Chem., Int. Ed.*, 2013, **52**, 1709-1712.
6. A. Yamamoto, T. Hirukawa, I. Hisaki, M. Miyata and N. Tohnai, *Tetrahedron Lett.*, 2013, **54**, 1268-1273.
7. J. R. Hunt, C. J. Doonan, J. D. LeVangie, A. P. Côté and O. M. Yaghi, *J. Am. Chem. Soc.*, 2008, **130**, 11872-11873.
8. S. Wan, J. Guo, J. Kim, H. Ihee and D. Jiang, *Angew. Chem., Int. Ed.*, 2008, **47**, 8826-8830.
9. N. J. Hinks, A. C. McKinlay, B. Xiao, P. S. Wheatley and R. E. Morris, *Micropor. Mesopor. Mat.*, 2010, **129**, 330-334.
10. F. Ke, Y.-P. Yuan, L.-G. Qiu, Y.-H. Shen, A.-J. Xie, J.-F. Zhu, X.-Y. Tian and L.-D. Zhang, *J. Mater. Chem.*, 2011, **21**, 3843 – 3848.
11. S. R. Miller, D. Heurtaux, T. Baati, P. Horcajada, J.-M. Greneche and C. Serre, *Chem. Commun.*, 2010, **46**, 4526 – 4528.
12. M. Vallet-Regi, A. Rámila, R. P. del Real and J. Pérez-Pariente, *Chem. Mater.*, 2001, **13**, 308-311.
13. H. Zhao, Z. Jin, H. Su, X. Jing, F. Sun and G. Zhu, *Chem. Commun.*, 2011, **47**, 6389 – 6391.
14. M. R. Caira, T. le Roex, L. R. Nassimbeni and E. Weber, *Cryst. Growth Des.*, 2006, **6**, 127 - 131.
15. O. T. Sorenson, *Journal of Thermal Analysis and Calorimetry*, 1999, **56**, 17 - 26.
16. M. E. Brown, *Thermochim Acta*, 1987, **110**, 153-158.
17. L. J. Barbour, M. R. Caira, T. le Roex and L. R. Nassimbeni, *J. Chem. Soc., Perkin Trans. 2*, 2002, 1973-1979.
18. L. J. Barbour, M. R. Caira and L. R. Nassimbeni, *J. Chem. Soc., Perkin Trans. 2*, 1993, 2321-2322.

19. A. Jacobs, N. Faleni, L. R. Nassimbeni and J. H. Taljaard, *Cryst. Growth Des.*, 2007, **7**, 1003-1006.
20. J. Nakazawa, Y. Sakae, M. Aida and Y. Naruta, *J. Org. Chem.*, 2007, **72**, 9448-9455.
21. L. R. Nassimbeni, *CrystEngComm*, 2003, **5**, 200-203.
22. A. V. Davis, D. Fiedler, G. Seeber, A. Zahl, R. van Eldik and K. N. Raymond, *J. Am. Chem. Soc.*, 2006, **128**, 1324-1333.
23. M. C. Letzel, C. Schäfer, F. R. Novara, M. Speranza, A. B. Rozhenko, W. W. Schoeller and J. Mattay, *J. Mass Spectrom.*, 2008, **43**, 1553-1564.
24. L. Nassimbeni, H. Su and L. Patel, *J. Chem. Crystallogr.*, 2014, **44**, 190-193.
25. T. Szabo, G. Hilmersson and J. Rebek, *J. Am. Chem. Soc.*, 1998, **120**, 6193-6194.
26. I. Vatsouro, E. Alt, M. Vysotsky and V. Bohmer, *Org. Biomol. Chem.*, *OBC*, 2008, **6**, 998-1003.
27. M. R. Caira, L. R. Nassimbeni, F. Toda and D. Vujovic, *J. Chem. Soc., Perkin Trans. 2*, 2001, 2119-2124.
28. M. E. Brown, *Introduction to thermal analysis: techniques and applications*, 2nd edn., Kluwer Academic Publishers, Dordrecht, 2001.
29. L. J. Barbour, K. Achleitner and J. R. Greene, *Thermochim Acta*, 1992, **205**, 171-177.
30. A. Khawam and D. R. Flanagan, *J. Phys. Chem. B*, 2006, **110**, 17315 - 17328.
31. T. Engel and P. Reid, *Thermodynamics, statistical thermodynamics, & kinetics*, 3rd edn., Pearson Education, Inc., Boston, 2010.
32. N. B. Báthori and L. R. Nassimbeni, in *Supramolecular chemistry: from molecules to nanomaterials*, eds. J. W. Steed and P. A. Gale, John Wiley & Sons Ltd, Chichester, 2012, vol. 6, pp. 3009 - 3016.
33. M. E. Brown and A. K. Galway, *Anal. Chem.*, 1989, **61**, 1136 - 1139.
34. L. R. Nassimbeni, H. Su and T.-L. Curtin, *Supramol. Chem.*, 2012, **24**, 344 - 349.
35. P. Atkins and J. de Paula, *Atkins' Physical Chemistry*, Oxford University Press, Oxford, 2010.
36. N. Branda, R. Wyler and J. Rebek, *Science*, 1994, **263**, 1267-1268.
37. B. C. Hamann, K. D. Shimizu and J. Rebek, *Angew. Chem., Int. Ed.*, 1996, **35**, 1326-1329.
38. T. Heinz, D. M. Rudkevich and J. Rebek, *Nature*, 1998, **394**, 764.
39. O. Mogck, M. Pons, V. Böhmer and W. Vogt, *J. Am. Chem. Soc.*, 1997, **119**, 5706-5712.

40. J. Nakazawa, M. Mizuki, Y. Shimazaki, F. Tani and Y. Naruta, *Org. Lett.*, 2006, **8**, 4275-4278.
41. R. Wyler, J. de Mendoza and J. Rebek, *Angew. Chem., Int. Ed.*, 1993, **32**, 1699-1701.
42. A. L. Spek, *J. Appl. Crystallogr.*, 2003, **36**, 7 - 13.
43. P. van der Sluis and A. L. Spek, *Acta Crystallogr., Sect. A: Found. Crystallogr.*, 1990, **46**, 194 - 201.
44. C. B. Aakeroy and D. S. Leinen, in *Crystal engineering: from molecules and crystals to materials*, eds. D. Braga, F. Grepioni and A. G. Orpen, Kluwer Academic Publishers, Netherlands, 1999, vol. 538, pp. 89 - 106.

# CHAPTER 4

## A HIGHLY SELECTIVE FRAMEWORK-TYPE STRUCTURE BASED ON THE PAMOATE ION

---

From previous work done in our group<sup>1-3</sup> with pamoic acid and the isomers of lutidine and picoline it was evident that even small changes in the crystallisation conditions could lead to the formation of a vast array of structures. This notion, as well as the shape and hydrogen bond forming abilities of pamoic acid, prompted us to investigate whether it is possible to form structures with other N-heterocycles in order to design frameworks. Pamoic acid was crystallised with pyridyl derivatives with a varying number of nitrogen atoms in the aromatic ring. Compounds such as 4,4'-bipyridyl, 1,2-bis(2-pyridyl)ethylene, 1,2-bis(4-pyridyl)ethylene, 1,2-bis(4-pyridyl)ethane and 1,10-phenanthroline were specifically chosen because they all have two possible sites for hydrogen bonding. This could potentially lead to the formation of cyclic units, as in the case of metallocycles, which could then stack together to form channels in the solid state. Two hydrogen-bonding sites may also allow for the formation of interesting new hydrogen bond motifs with pamoic acid which could lead to more insight regarding intermolecular interactions and the effect they have on solid state packing. This study was further expanded to include N-heterocycles that contain substituents such as methyl groups, halogens, acids, amides and bulkier groups such as phenyl rings. N-heterocycles that contain substituents with added hydrogen bond donor or acceptor sites introduce competition for the usual hydrogen bond formation between pamoic acid and the nitrogen atom. This could lead to the formation of new hydrogen bond motifs, which in turn could produce new structures with potentially new and interesting properties. Bulkier groups such as phenyl rings and halogenated substituents could cause inefficient packing in the solid state which could lead to the formation of voids in the crystal structures.

A list of all crystallisations with pamoic acid can be found in the electronic Appendix B. Since the formation of framework **1** (Chapter 2) relies heavily on the presence of water, almost all crystallisations were performed in 1:1 molar mixtures of THF:H<sub>2</sub>O in order to potentially incorporate water into the structure. Thirteen novel crystal structures with the pamoate ion were identified during this study, five of which are isostructural frameworks that



include solvent in cavities. It should be noted that these five isostructural compounds are not true framework materials as defined in Chapter 1. The definition proposed in Chapter 1 describes a framework as an extended and interconnected structure, usually through hydrogen bonds, that forms the basic support for the crystal structure. The five isostructural compounds do not contain an interconnected hydrogen bonded framework. Instead, discrete base-acid-base units of structure-type **B** stack together in the solid state and form cavities down the *c*-axis in which solvent resides. We will therefore refer to these structures as framework-type structures, since they contain a well-defined rigid framework that is interconnected *via* weaker noncovalent interactions such as C—H... $\pi$  interactions.

The framework-type structure with THF will be discussed first in Section 4.1, as well as the thermal studies and solvent exchange experiments conducted with this compound. In Section 4.2 the isostructural framework-type structures will be discussed. In Section 4.3 the results of competition studies with the framework-type structures will be discussed. Section 4.4 contains crystal structure descriptions of the eight remaining novel structures with the pamoate ion and in Section 4.5 the important requirements for framework formation will be discussed.

#### **4.1 Synthesis and description of the 4-phenylpyridine framework-type structure, 2·THF**

**2·THF** was grown from a solution of a 1:1 molar ratio of THF/H<sub>2</sub>O. Pamoic acid and 4-phenylpyridine were added in a 1:1 molar ratio and the resulting solution was heated and stirred until clear. The vial was capped and crystals grew within a day or two. The crystal structure is in the monoclinic space group *C2/c*. The asymmetric unit consists of half a pamoate molecule, one 4-phenylpyridinium molecule and a THF molecule on a special position with half occupancy (Figure 4.1). The stoichiometry of anion:cation:THF is therefore 1:2:1.

The pamoate ion forms hydrogen bonds to two 4-phenylpyridinium ions to form base-acid-base units, reminiscent of the structure type **B** identified during our previous work with the pamoate salts<sup>1</sup> and discussed in Chapter 2 (Figure 4.2a). These base-acid-base units stack next to each other to form a single layer (Figure 4.2b). The next layer is interdigitated with the first layer through C—H... $\pi$  interactions between the 4-phenylpyridinium and pamoate ions (Figure 4.2c). The THF molecules then fill the voids between these interdigitated layers to

form the channel-like structure seen in Figure 4.2d. The crystallographic data and hydrogen bond parameters of **2·THF** are listed in Table 4.2 and Table 4.3 in the section discussing the four isostructural frameworks (pages 157 and 158).

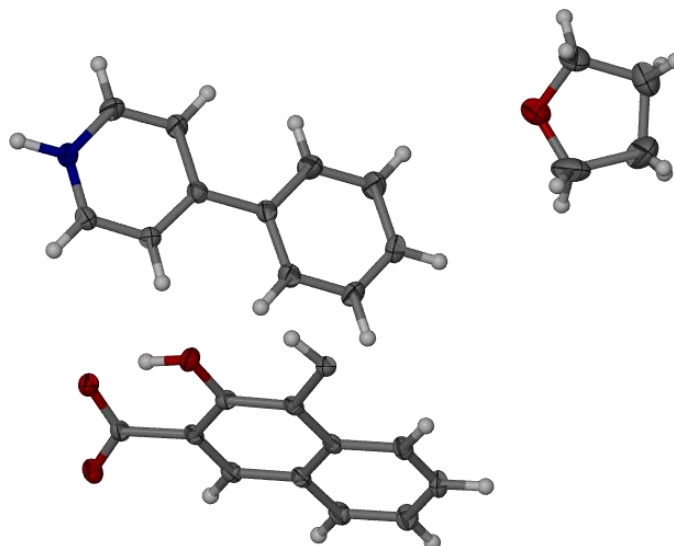


**Figure 4.1** The asymmetric unit of **2·THF**. It contains only half a pamoate molecule and the THF molecule has half occupancy since it is on a special position. A symmetry operator generates the symmetry related molecule with half occupancy.

Although it appears that there are continuous channels in this structure, this is however not the case. Each THF molecule occupies a small solvent accessible pocket and these pockets are not connected to each other. This was discovered by mapping the solvent accessible surface in Mercury<sup>4-7</sup> using the *VOIDS* function. A probe radius of 1.4 Å was used to map the contact and solvent accessible surfaces. In Figure 4.3 the void mapping of the contact surface and the solvent accessible surface is compared. In (a) the contact surface volume is calculated to be 583.5 Å<sup>3</sup>, 15.5% of the total cell volume. However, the solvent accessible volume is calculated to only be 125.4 Å<sup>3</sup>, 3.3% of the total cell volume. It is also apparent in Figure 4.3c that the solvent accessible surfaces of adjacent cavities are not connected. This indicates that the pores of adjacent cavities are restricted and therefore do not form a continuous channel. In this case only mapping the contact surface volume is somewhat misleading as this appears to link the voids to each other, creating the theoretical possibility of solvent movement through the structure.

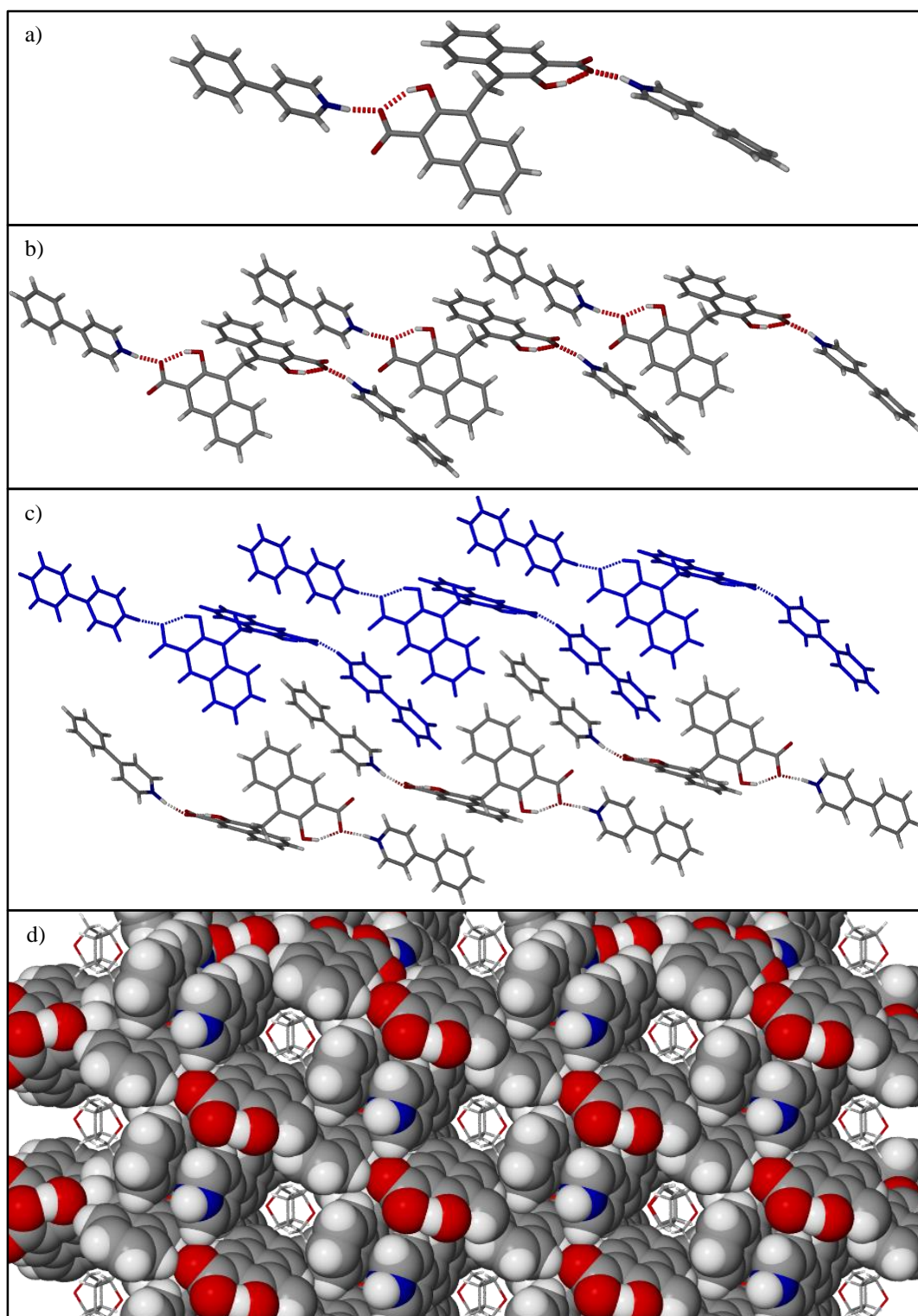


**Figure 4.2** The structure of 2·THF a) The hydrogen bonded base-acid-base unit. Hydrogen bonds are represented by dashed red lines. b) The base-acid-base units stack next to each other to form a layer. c) The next layer is interdigitated with the first layer by offset C—H... $\pi$  interactions of the 4-phenylpyridinium ions. d) The THF molecules fill the voids created between the interdigitated layers to form this channel-like structure, viewed down the *c*-axis.

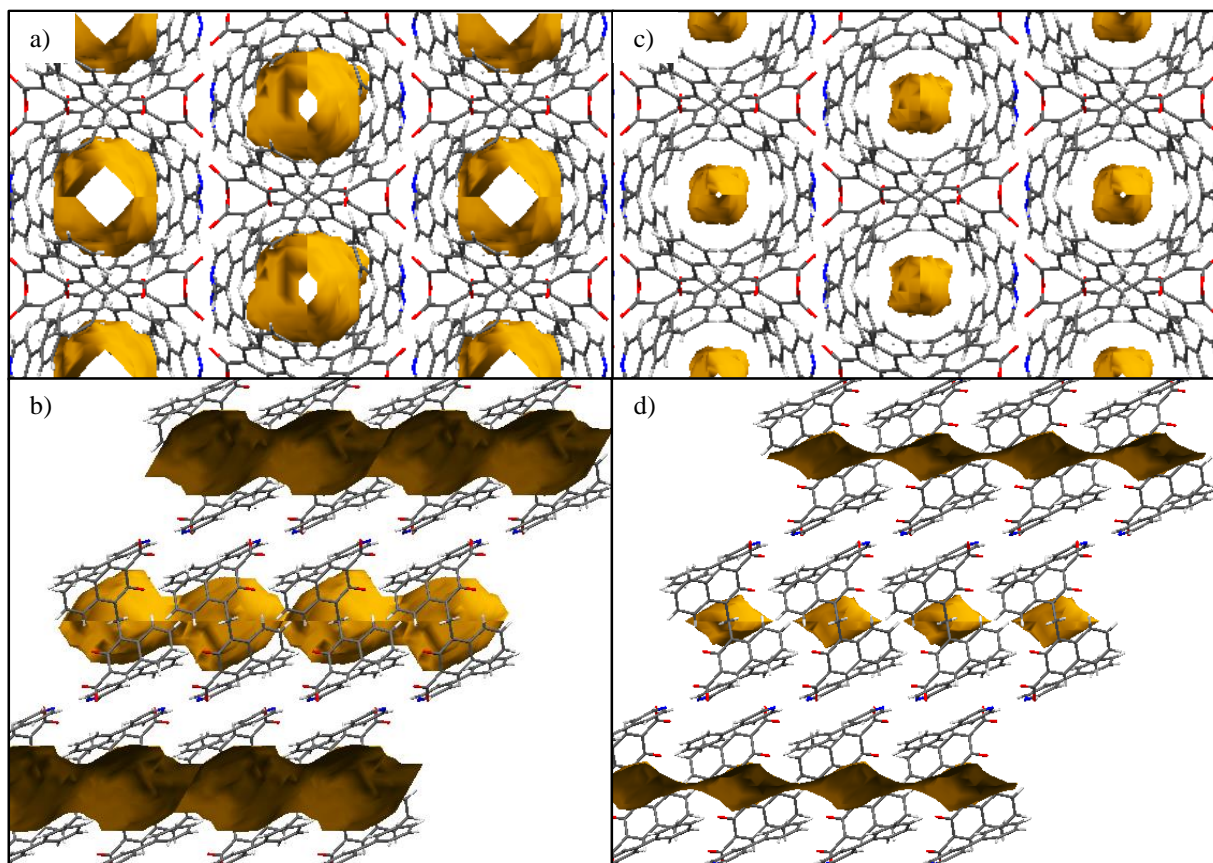


**Figure 4.3** a, b) The mapping of the contact surface of the void ( $583.5 \text{ \AA}^3$ ) of **2·THF** with a probe radius of  $1.4 \text{ \AA}$ . It appears to indicate that there is significant space for solvent to move through this “channel”. In (a) the structure is viewed down the *c* axis and in (b) down the *b* axis. c, d) The map of the solvent accessible surface, which is significantly smaller ( $125.4 \text{ \AA}^3$ ). In contrast to the map of the contact surface the solvent accessible spaces are shown to be discrete voids, and not a continuous channel as alluded to in a and b. In (c) the structure is viewed down the *c*-axis and in (d) down the *b* axis.

### 4.1.1 Solvent exchange studies with **2·THF**

Although void mapping analysis indicates that the solvent in **2·THF** lies in discrete pockets, it is still theoretically possible for the THF to be removed or replaced.<sup>8</sup> To test whether this is possible with **2·THF**, crystals were exposed to the vapour of various solvents.\* Crystals were dried on filter paper and placed in a glass vial. The glass vial was then placed in a bigger jar filled with approximately 1 ml of solvent. The jar was sealed with a lid and parafilm and left to stand for approximately one week. NMR analysis of the samples showed that no exchange had taken place. Should exchange have taken place, the THF peaks would have been significantly reduced or completely missing. This is however not the case, as can be seen from the  $^1\text{H}$  NMR of crystals of **2·THF** exposed to chloroform vapour in Figure 4.4. This is

\* Acetone, chloroform, diethyl ether, dichloromethane, benzene and acetonitrile.

shown as an example. NMR of the other vapour exchange experiments can be found in Appendix C.

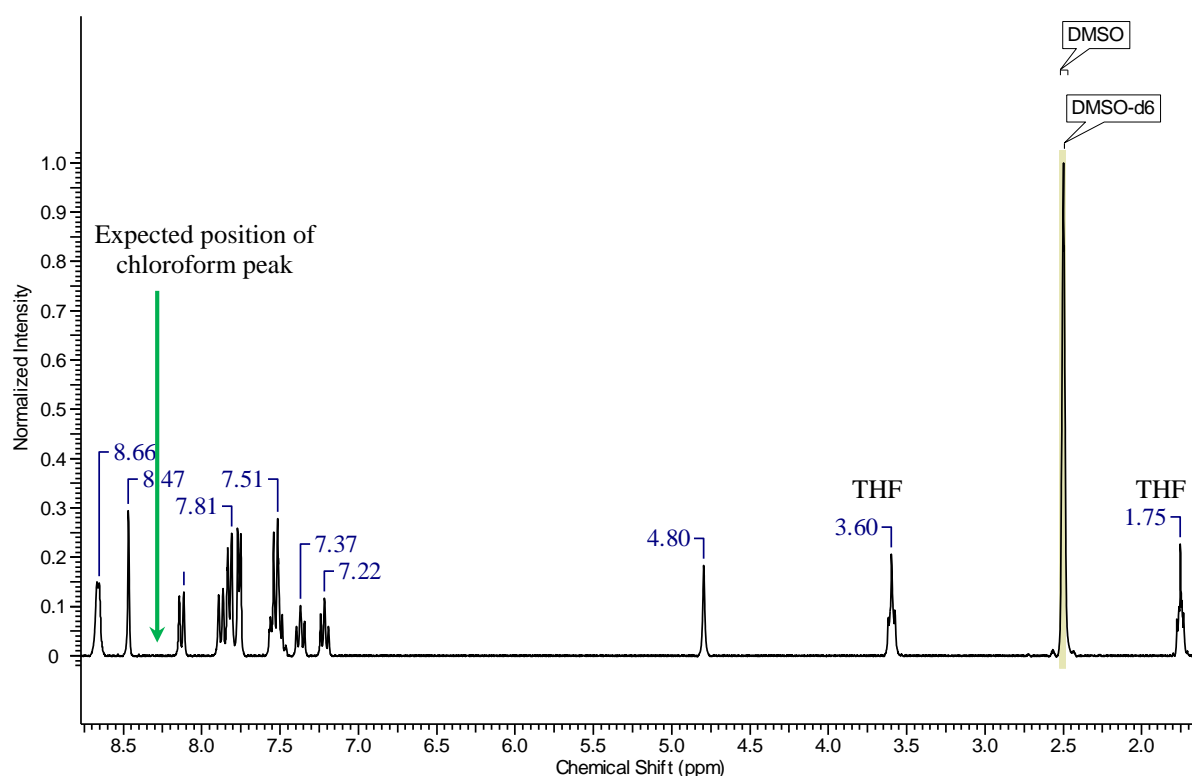


**Figure 4.4** <sup>1</sup>H NMR of **2·THF** crystals exposed to chloroform vapour for approximately one week. The THF peaks are still present and no peak for chloroform is seen. This peak would be found around 8.3 ppm and would integrate for one proton.

The possible exchange of the THF in the pockets was further investigated by immersing freshly dried crystals of **2** in each of the solvents for approximately one week. Just enough solvent was added to cover the crystals as too much solvent could possibly lead to the dissolution of the crystals. After one week crystals were analysed by NMR and PXRD. NMR analysis again showed no presence of any of the solvents in which the crystals were immersed. PXRD analysis also showed that all crystals retained the structure of the original **2·THF**, shown in Figure 4.5.



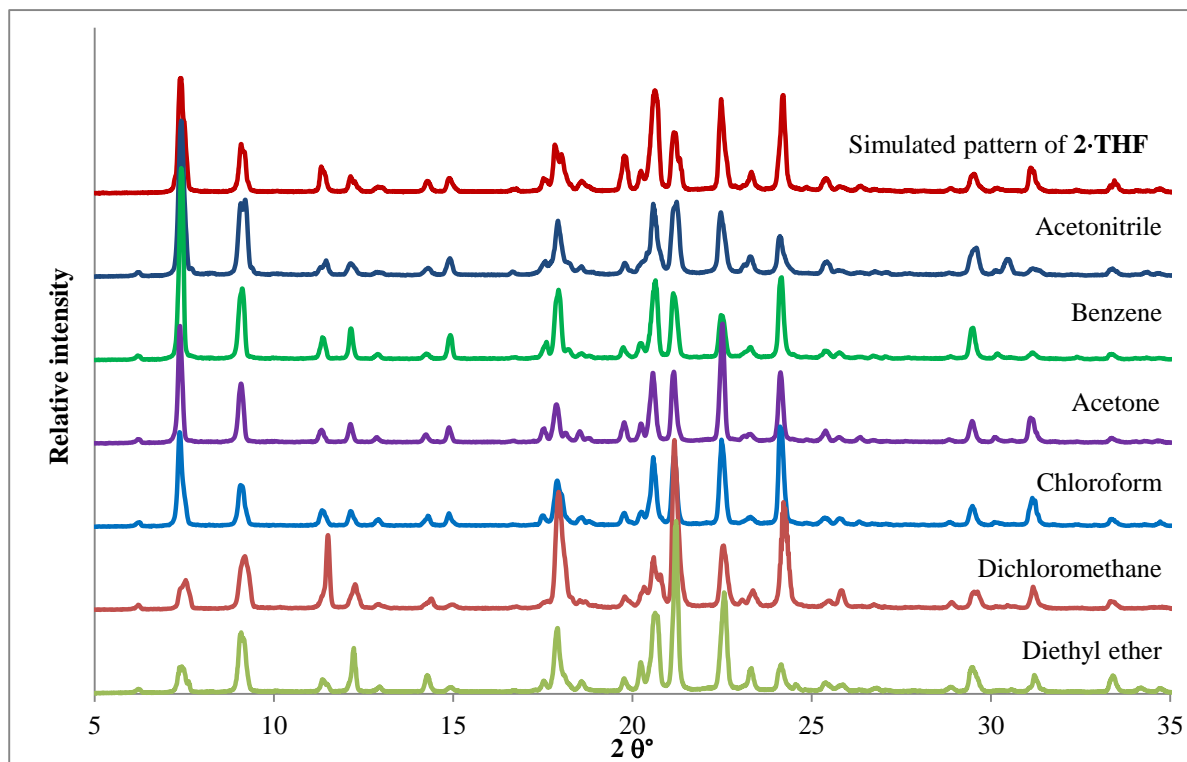


**Figure 4.5** PXRD patterns of the crystals of **2·THF** after being immersed in 6 different solvents for one week. The powder patterns all compare well to that of the original **2·THF** (simulated pattern). The discrepancies in the peak intensities can be explained by preferred orientation of the ground crystals.

Crystals of **2·THF** were also exposed to supercritical  $\text{CO}_2$  for thirty minutes. NMR analysis showed that there was still the same amount of THF present in the crystal structure and visual inspection of the crystals showed they remained intact. The unit cell parameters were found to be the same as those of the original structure. This indicates that this framework-type structure is quite robust since crystals of **2·THF** emerged virtually unscathed after immersion in supercritical  $\text{CO}_2$ .

#### 4.1.2 Thermal studies of **2·THF**

The thermal properties of **2·THF** were investigated to ascertain whether it is possible to remove the THF by heating, while leaving the framework intact. This would also give an indication of the robustness and stability of the framework. Thermogravimetric analysis and differential scanning calorimetry showed two well-defined mass-loss steps during a heating cycle from room temperature to 300 °C (Figure 4.6). The first mass loss step of 29.0% (calculated 29.5%) corresponds to the loss of half a THF molecule and half a 4-phenylpyridine molecule per asymmetric unit, which was confirmed by  $^1\text{H}$  NMR analysis of

crystals of **2·THF** after heating them to 160 °C (Appendix C). The second mass-loss step of 19.9% (calculated 22.2%) corresponds to the loss of the remaining 4-phenylpyridine.

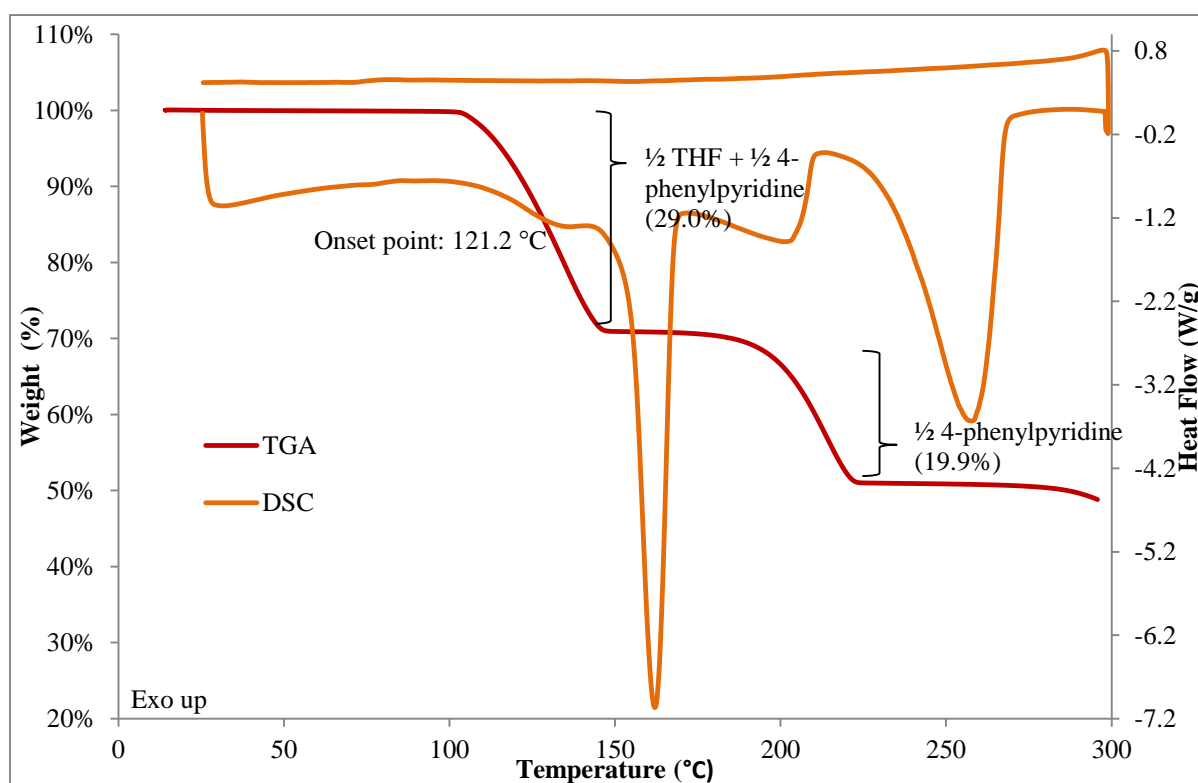


**Figure 4.6** The TG and DSC traces of the thermal response of **2·THF**. The first mass loss shown here by the TG trace corresponds to the loss of  $\frac{1}{2}$  a THF molecule and  $\frac{1}{2}$  a 4-phenylpyridine molecule per asymmetric unit (confirmed by NMR). The first mass loss step corresponds to the large exotherm seen in the DSC trace.

Variable temperature PXRD was also performed on this framework in order to investigate what happens to the structure during heating, since some of the 4-phenylpyridine is lost during the first mass loss step. The sample was ground to a fine powder to ensure an even distribution in particle size. The sample was then placed in a 0.5 mm capillary, sealed and spun to ensure minimal preferred orientation that would influence peak intensities. It is immediately apparent from the variable temperature PXRD shown in Figure 4.7 that the powder pattern remains the same up to 200 °C. This implies that the framework remains intact after the loss of solvent at approximately 120 °C. However, according to TGA and NMR results the first mass-loss step encompasses THF and 4-phenylpyridine which should significantly affect the framework structure. Between 200 and 210 °C the crystal structure changes and a different powder pattern is observed, which is the formation of a 1:1 4-phenylpyridinium salt **S2**. After reaching 220 °C the sample was cooled to room temperature and yet another powder pattern emerges. There are however marked similarities between the

powder pattern at 220 and 25 °C (after cooling). Interestingly, the extra peaks seen in the diffractogram at 25 °C after cooling are not due to the recrystallisation of 4-phenylpyridine. None of the peaks in the 4-phenylpyridine powder pattern correspond to any of the extra peaks seen in the powder pattern at 25 °C. In fact, the extra peaks appear to correspond better to the powder patterns of the framework up to 200 °C. This could imply that a very small amount of the original **2·THF** recrystallises upon cooling and that the final powder pattern contains a mixture of **2·THF** and the new 1:1 4-phenylpyridinium pamoate salt (**S2**). The final pattern does not contain any peaks that correlate to the powder pattern of pamoic acid.

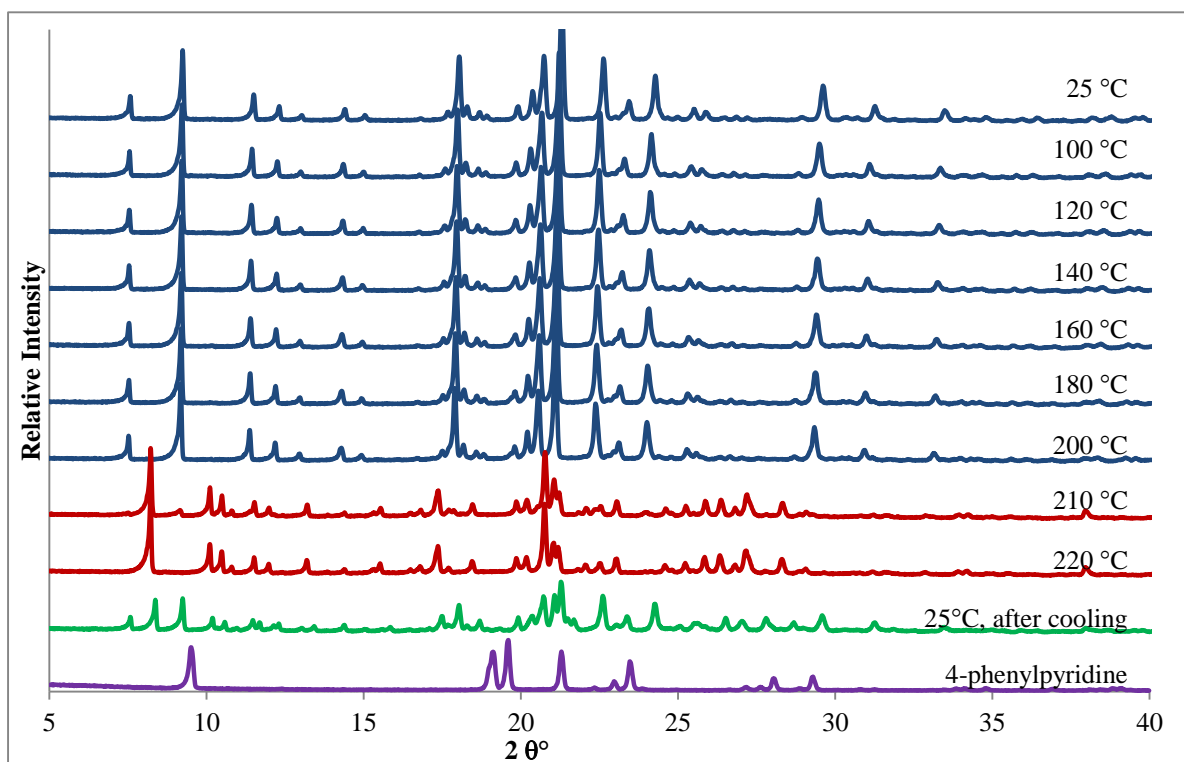


**Figure 4.7** The variable temperature powder pattern of the **2·THF**. The powder pattern of the framework appears to remain the same up to 200 °C. Between 200 and 210 °C the crystal structure changes and a different powder pattern emerges. This pattern has been identified as that of a 1:1 4-phenylpyridinium pamoate salt (**S2**). After 220 °C the sample was cooled back down to room temperature and yet another powder pattern is observed. This is a mixture of recrystallised **2·THF** and the salt **S2**.

**2·THF** therefore converts to a 1:1 4-phenylpyridinium pamoate salt at high temperatures. The simulated powder pattern for this salt is compared to that of **2·THF** at high temperatures in Figure 4.8.



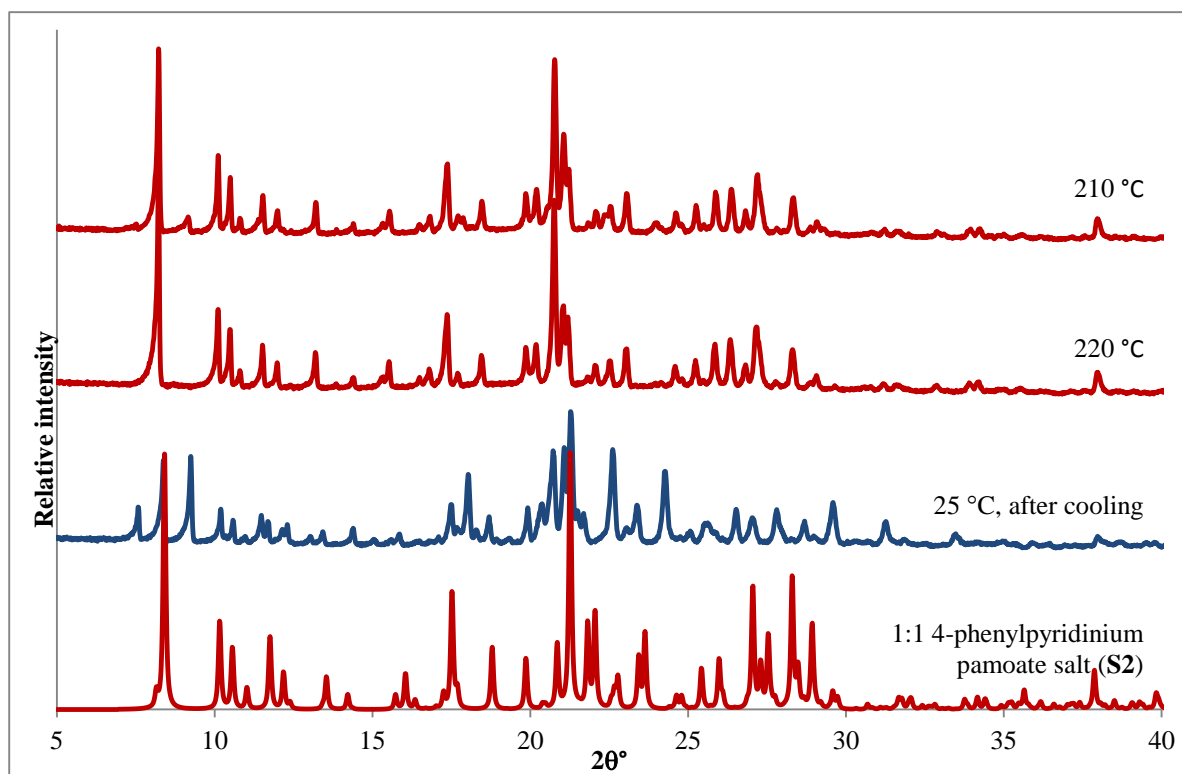


**Figure 4.8** The PXRD pattern of the 1:1 4-phenylpyridinium pamoate salt is compared to the patterns of **2·THF** at high temperatures. **2·THF** evidently converts to this 1:1 salt at high temperatures. At 25 °C after cooling there is a mixture of **2·THF** and the salt. The shifts observed in some of the peaks in the high temperature patterns from those of the simulated pattern of the 1:1 salt are due to the large difference in temperature at which the respective patterns were recorded.

Variable temperature PXRD suggests that the structure of **2·THF** remains stable during the loss of THF and 4-phenylpyridine between 100 and 150 °C but this is questionable since 4-phenylpyridine has an important structural role. This led us to investigate what causes the difference in onset temperatures in the TGA and PXRD results. A combination of TG, DSC and PXRD analysis was used to solve this interesting conundrum.

First, three samples of **2·THF** were each heated in the TGA to 130, 160 and 200 °C. In the case of sample 1 mass loss had just started as the TG reached 130 °C. In the case of sample 2 the first mass-loss step was approximately halfway (15.9% loss compared to 29% for complete mass loss) and in the case of sample 3 the first mass-loss step was complete. Powder diffraction analysis (shown in Figure 4.9) shows the difference in these patterns at the three stages. The pattern of sample 1 matches the experimental pattern of **2·THF**, but already extra peaks are observed (i). The patterns of samples 2 and 3 differ from that of the experimental pattern of **2·THF** (ii and iii). This is in contrast to the variable temperature PXRD results at these temperatures and shows that there are indeed structural changes occurring at this point, most probably due to the loss of 4-phenylpyridine.

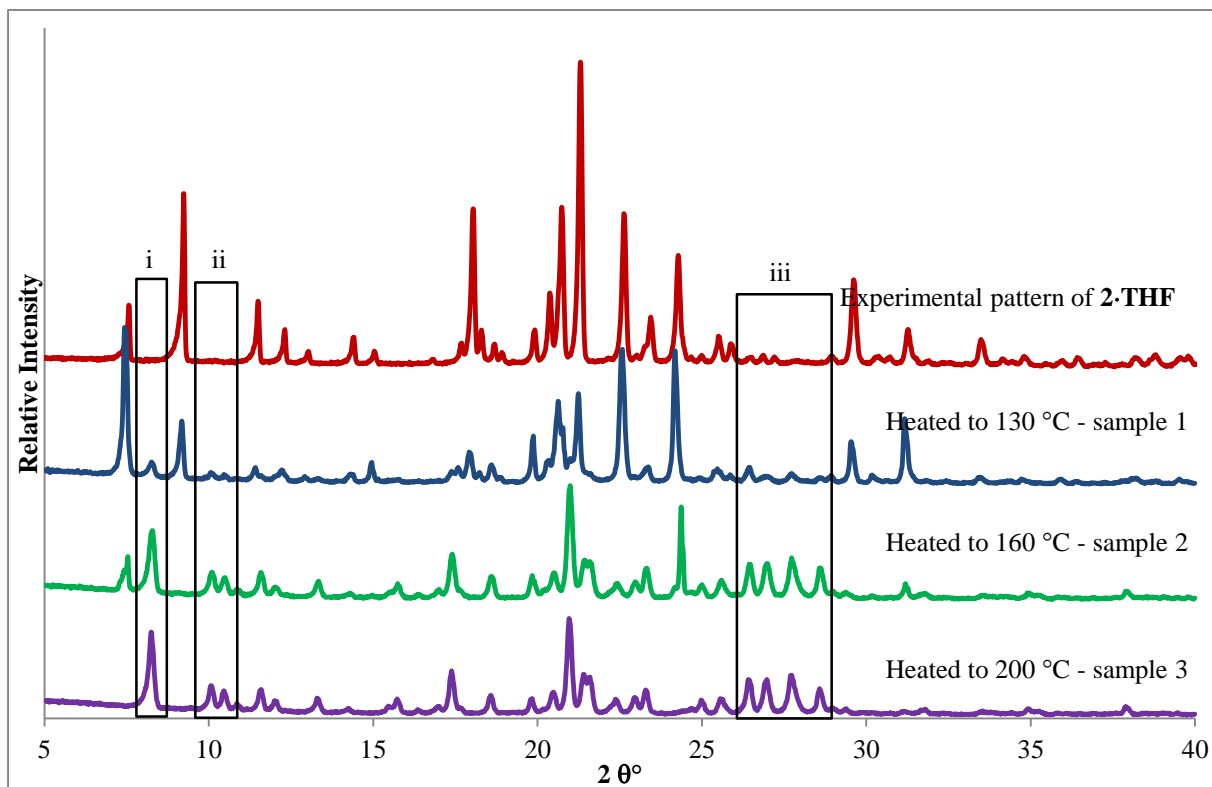


**Figure 4.9** The powder patterns of samples 1 to 3, which were heated using TGA. Sample 1 largely correlates to the experimental pattern of **2·THF**, although new peaks have appeared, indicated by (i). The patterns of samples 2 and 3 differ substantially from that of **2·THF** and various new peaks are observed and other peaks have disappeared (ii and iii). This clearly shows that the crystals are undergoing significant structural changes due to the loss of THF and 4-phenylpyridine, in contrast to the results of the variable temperature PXRD.

To simulate the environment in the sealed capillary, DSC analysis was performed on a sample of **2·THF** in a hermetically sealed sample pan. This was then compared to DSC analysis performed on a sample placed in a vented sample pan. The samples were heated to 200 °C in order to compare them to the TGA and VT PXRD results. The two DSC traces are compared in Figure 4.10 and it is clear that the profiles are quite similar despite one sample being hermetically sealed and the other being in a vented pan. The DSC results also further confirm that a structural event does in fact take place even though the variable temperature PXRD does not show this change. There is a small endothermic peak observed in both traces at about 120 °C which is due to the conversion of **2·THF** to the 1:1 salt **S2**. There is also an exothermic peak at 40 °C in the trace of the hermetically sealed sample (blue), which supports the idea that a very small amount of the original **2·THF** recrystallises, since PXRD shows no discernible peaks of 4-phenylpyridine in the final powder pattern at 25 °C. This peak is not seen in the trace of the vented sample since any component that was lost during heating would have been removed by the sample purge gas.

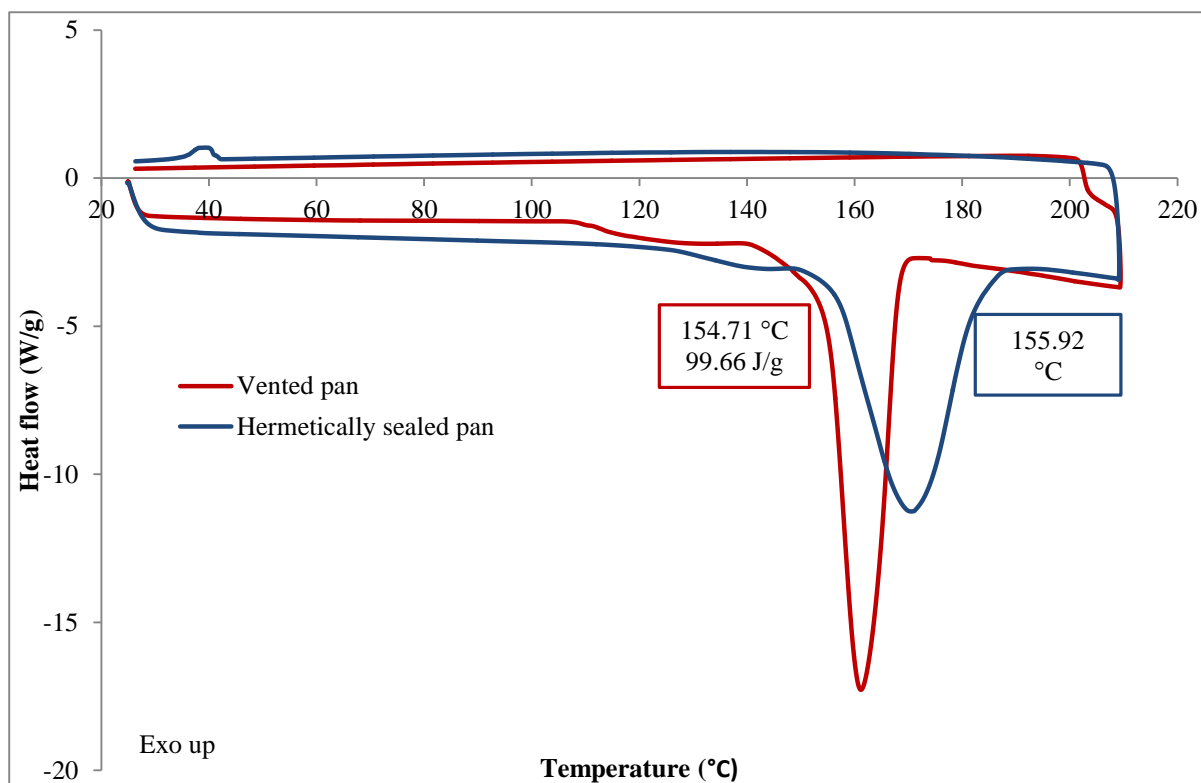


**Figure 4.10** The DSC traces of samples placed in a vented pan (red) and the other in a hermetically sealed pan (blue) and heated to 210 °C. The samples were only heated to 210 °C in order to compare them to that of the samples heated in the sealed capillary. The traces are similar although there is a delay in the onset point of the hermetically sealed sample compared to the vented sample. There also appears to be an exothermic recrystallisation event at 40 °C in the hermetically sealed sample which is due to the recrystallisation of a small portion of **2·THF**.

PXRD analysis shows that all powder patterns taken of samples heated to 210 °C match – whether the sample was placed in a vented pan for DSC analysis, hermetically sealed pan for DSC analysis or sealed in a capillary (Figure 4.11). In other words, regardless of the heating method and sample treatment, the end product after the first mass loss (THF and half of the 4-phenylpyridine) is the salt **S2** in all cases. If pressure genuinely had a large effect on the stability of **2·THF**, the DSC traces of the vented pan and the hermetically sealed pan would have shown quite a large difference. From Figure 4.10 it is clear that the traces are similar, although it should be noted that there appears to be a delay in the onset of the first event in the case of the hermetically sealed sample. This could be due to the fact that under pressure the sublimation of 4-phenylpyridine is slightly delayed, which leads to a slightly higher onset temperature and a much broader exotherm. With regard to the variable temperature PXRD, this could mean that the structural change during loss of THF and 4-phenylpyridine is occurring slower and misleadingly shows the powder pattern as remaining the same over the same temperature range.

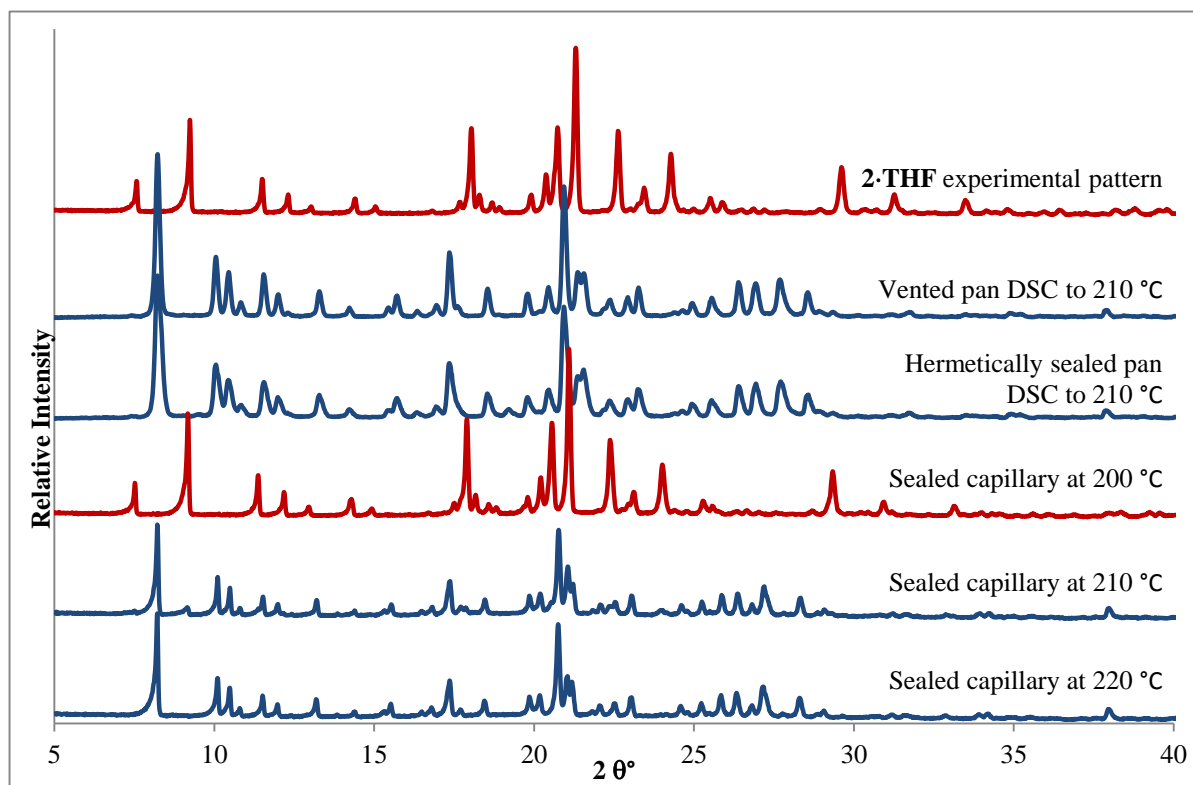


**Figure 4.11** The powder patterns of the DSCs performed on **2·THF** in a vented pan and a hermetically sealed pan are compared to the powder patterns of the samples sealed in the capillary for variable temperature PXRD. It is evident that the powder patterns all match at 210 °C, confirming that the same product is formed regardless of the method of heating.

From the analysis done it is evident that although the variable temperature PXRD suggested that the framework remained intact upon removal of the solvent and 4-phenylpyridine, this is simply not the case. The removal of half of the 4-phenylpyridine would put too much strain on the framework and therefore it would have to change or collapse. PXRD analysis of a sample heated to 160 °C also showed that the structure is already undergoing permanent changes (Figure 4.9) and a mixture of original **2·THF** and the new 1:1 4-phenylpyridinium pamoate salt **S2** is observed. This result supports the idea that under the pressure of the sealed capillary the whole process is slower and could cause the powder pattern to remain the same for longer. This also implies that while the framework is under pressure, proton transfer from 4-phenylpyridinium to the pamoate ion occurs in **2·THF** and 4-phenylpyridine is lost to form the 1:1 salt **S2**. On cooling and still under pressure, proton transfer occurs from pamoic acid back to 4-phenylpyridine and a small portion of **2·THF** is able to recrystallise.

## 4.2 Isostructural frameworks

Since it appeared to be impossible to replace the solvent in the guest pockets by simple exchange, attempts were made to grow crystals from different solvents. The original **2·THF**

crystals were grown from a 1:1 THF/H<sub>2</sub>O solvent mixture, yet no water was incorporated into the structure. To investigate whether water was necessary for the formation of the crystals pamoic acid and 4-phenylpyridine were dissolved in pure THF and also subsequently in pure NMP, DMF, 1,4-dioxane, pyrrole, dimethylacetamide, morpholine and DMSO. Solutions with NMP, DMF, pyrrole, dimethylacetamide, morpholine and DMSO yielded no crystals, but crystals were obtained from the solutions of THF and 1,4-dioxane although the crystals were of inferior quality. PXRD analysis indicated that the crystals were isostructural to **2·THF** (Figure 4.12). <sup>1</sup>H NMR analysis confirmed the presence of 1,4-dioxane and THF in the respective structures.

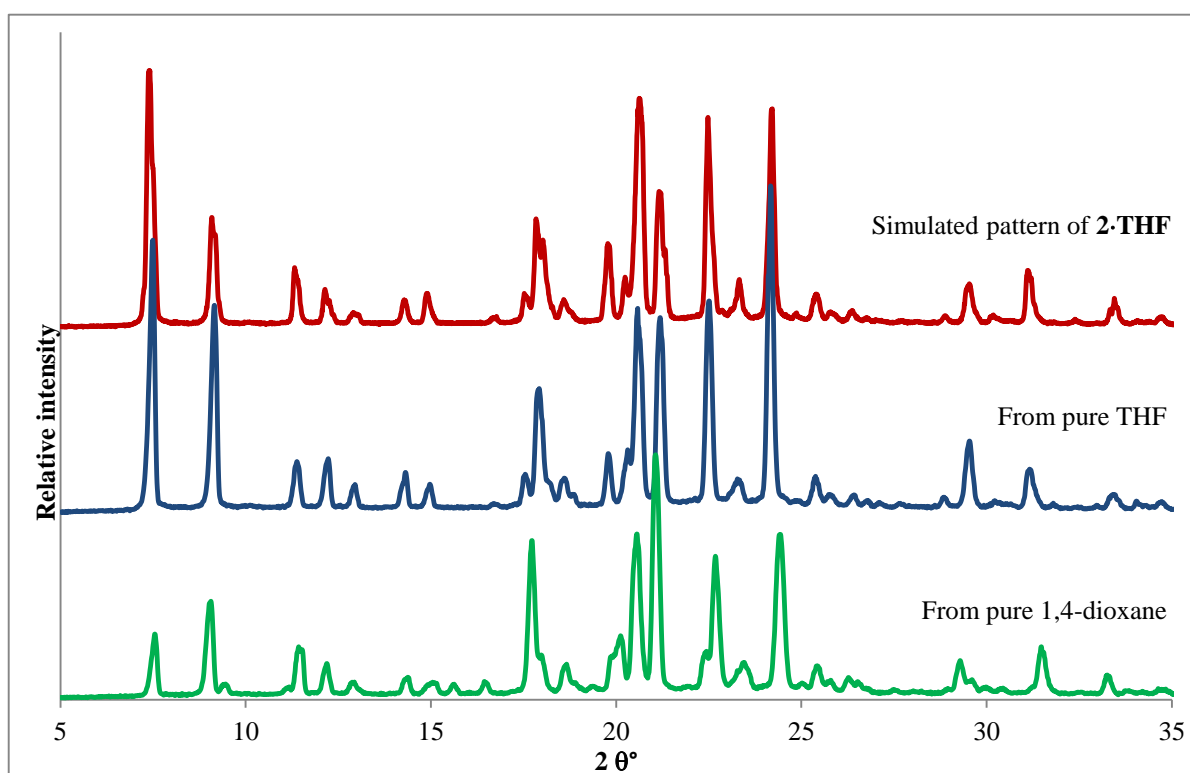


**Figure 4.12** PXRD patterns of crystals grown from pure THF and 1,4-dioxane. There is a very good correlation between the experimental patterns of crystals from pure THF and 1,4-dioxane to the simulated pattern of **2·THF**.

A rather interesting feature of the 1,4-dioxane framework-type crystals (**2·Dioxane**) is that pamoic acid does not dissolve in this solvent. A fine layer of crystals grows on top of the pamoic acid powder at the interface of the solvent (in which 4-phenylpyridine dissolves) and powder. It was therefore possible to investigate other solvents in which pamoic acid does not dissolve, especially since pamoic acid only dissolves in THF, DMF, DMSO and NMP. The following table lists the solvents and solvent mixtures used in this experiment.

**Table 4.1** Crystallisations of 4-phenylpyridine with pamoic acid from various solvents and solvent/water combinations. In cases where pamoic acid did not dissolve in the solvent or solvent mixture, the undissolved powder was left in the solution for a few days. In some cases crystals grew on the powder.

Solvent	Did pamoic acid dissolve?	Product
1:1 NMP/H <sub>2</sub> O	Yes	-
1:1 DMF/H <sub>2</sub> O	Yes	Framework 2 with DMF ( <b>2·DMF</b> )
1:1 dimethylacetamide/H <sub>2</sub> O	Yes	-
1:1 DMSO/H <sub>2</sub> O <sup>a</sup>	Yes	Framework 2 with DMSO ( <b>2·DMSO</b> )
1:1 DMSO/H <sub>2</sub> O <sup>a</sup>	Yes	1:1 4-phenylpyridinium pamoate salt ( <b>S1</b> )
1:1 1,4-dioxane/H <sub>2</sub> O	No	Framework 2 with 1,4-dioxane ( <b>2·Dioxane</b> )
1:1 acetone/H <sub>2</sub> O	No	Framework 2 with acetone ( <b>2·Acetone</b> )
1:1 acetonitrile/H <sub>2</sub> O	No	1:1 4-phenylpyridinium pamoate salt ( <b>S2</b> )
1:1 MeOH/H <sub>2</sub> O	No	Salt <b>S2</b>
1:1 EtOH/H <sub>2</sub> O	No	Salt <b>S2</b>
DCM	No	-
Chloroform	No	-
Diethyl ether	No	-

<sup>a</sup>Crystals of **2·DMSO** and **S1** were obtained from separate crystallisations. **S1** was only obtained once.

Table 4.1 shows that it was possible to grow frameworks isostructural to **2·THF** from four other 1:1 solvent/H<sub>2</sub>O mixtures, i.e. DMF, DMSO, 1,4-dioxane and acetone. These frameworks can also be described as homeotypic or isoskeletal, since the framework is superimposable in each case, but the guest molecules differ in each structure.

In four other cases a 4-phenylpyridinium pamoate salt was isolated: in three cases a salt **S2**, obtained from 1:1 solvent/water mixtures with acetonitrile, methanol and ethanol, and in the fourth case a salt **S1**, obtained from DMSO/H<sub>2</sub>O. The structures of these salts will be discussed in Section 4.4.1.

Powder patterns of each of the new frameworks were compared (shown in Figure 4.13) to the original **2·THF** grown from 1:1 THF/H<sub>2</sub>O. There is a good correlation between the patterns indicating that the materials are isostructural. There are subtle differences between the powder patterns of the structures, but this is expected since each structure contains a different solvent in the cavity.

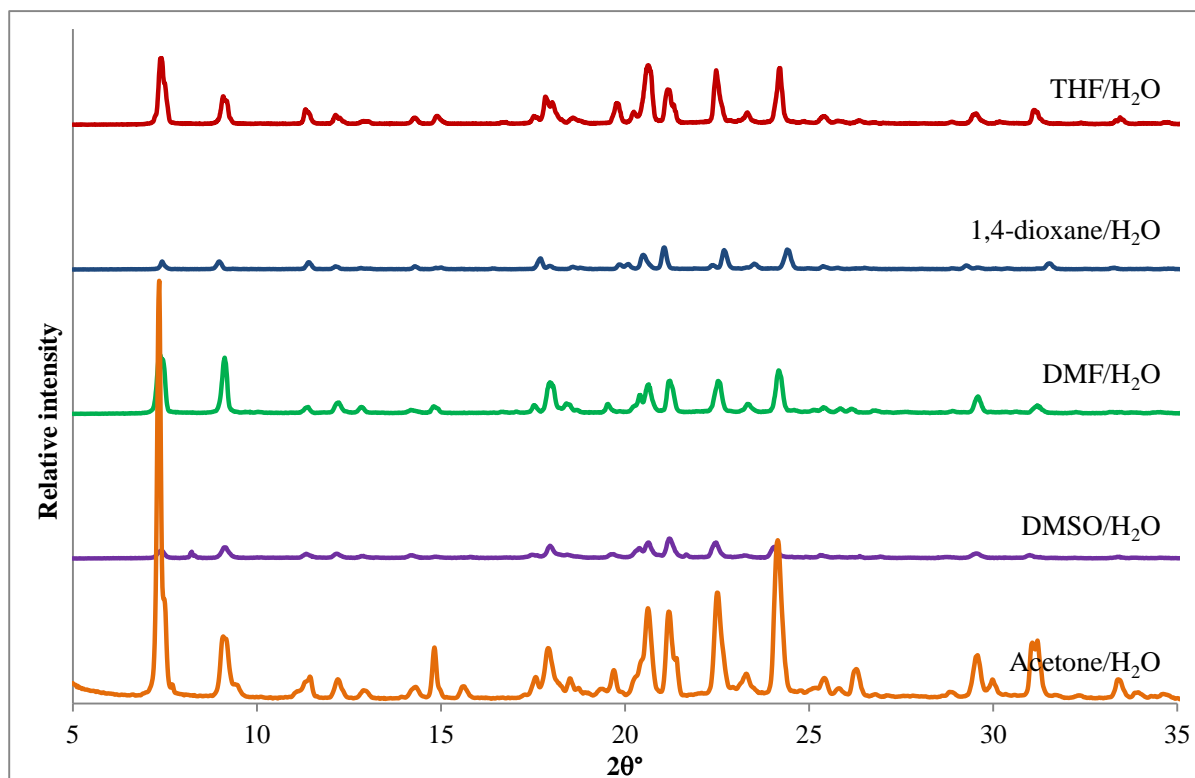


**Figure 4.13** The powder patterns of framework-type structures grown from different 1:1 solvent/water mixtures. There is good correlation between powder patterns, indicating that the compounds are all isostructural to **2·THF**.

The thermal mass loss profile for each framework is shown in Figure 4.14. In the first step half a solvent molecule and half a 4-phenylpyridinium molecule is lost per asymmetric unit.

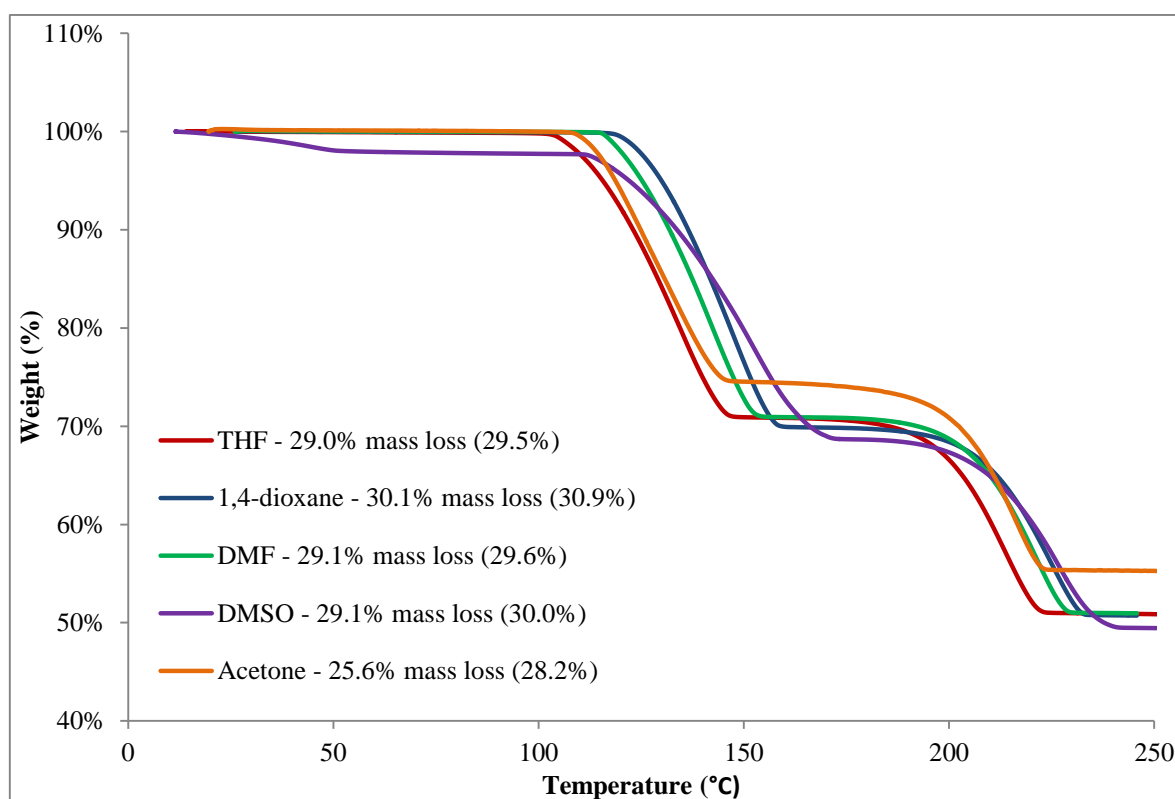


**Figure 4.14** The thermal mass loss profiles of the 5 framework-type structures. The experimental mass loss percentages are shown for each trace with the calculated values in brackets. In each case, the first mass loss step represents the loss of half a solvent molecule and half a 4-phenylpyridine molecule per asymmetric unit. The second mass loss step is the loss of the remaining 4-phenylpyridine until only pamoic acid is left.

Single-crystal diffraction data of each of the compounds were also collected and this further confirms that all the compounds are isostructural. Packing diagrams of each of the isostructural frameworks are shown in Figure 4.15. In all cases the walls of the framework are made of the base-acid-base units and only the solvent contained in the void is different. The unit cell parameters and other crystallographic data are listed in Table 4.2. In each case the solvent occupies a special position. In **2·DMF** it was not possible to model the methyl hydrogen atoms.



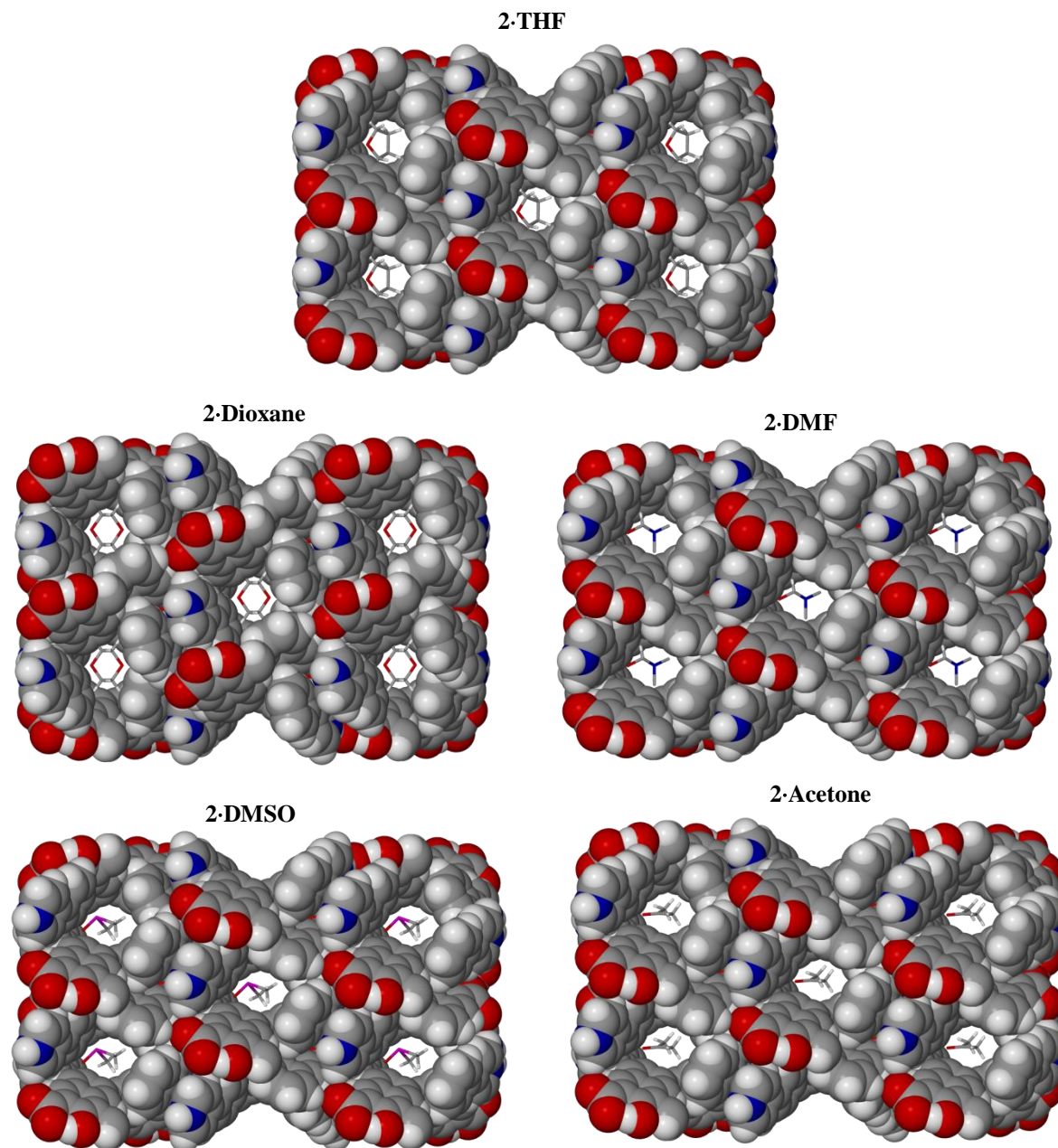


**Figure 4.15** The five isostructural framework-type materials with the framework shown in spacefill and the solvent in stick representation. In cases in which the solvent is disordered, only one orientation of the solvent is shown.

**Table 4.2** Selected crystallographic information for the five isostructural framework-type materials.

	<b>2·THF</b>	<b>2·Dioxane</b>	<b>2·DMF</b>	<b>2·DMSO</b>	<b>2·Acetone</b>
Stoichiometric ratio (anion: cation: solvent)	½:1:½	½:1:½	½:1:½	½:1:½	½:1:½
Chemical formula	C <sub>49</sub> H <sub>42</sub> N <sub>2</sub> O <sub>7</sub>	C <sub>49</sub> H <sub>42</sub> N <sub>2</sub> O <sub>8</sub>	C <sub>48</sub> H <sub>35</sub> N <sub>3</sub> O <sub>7</sub>	C <sub>36</sub> H <sub>29</sub> N <sub>1</sub> O <sub>7</sub> S <sub>1</sub>	C <sub>37</sub> H <sub>31</sub> N <sub>1</sub> O <sub>7</sub>
Formula weight/g.mol <sup>-1</sup>	770.84	786.84	765.79	776.87	756.82
Crystal system	Monoclinic	Monoclinic	Monoclinic	Monoclinic	Monoclinic
Space group	<i>C2/c</i>	<i>C2/c</i>	<i>C2/c</i>	<i>C2/c</i>	<i>C2/c</i>
Z	4	4	4	4	4
Z'	0	0	0	0	0
<i>a</i> /Å	26.859(5)	26.804(4)	27.355(7)	27.28(1)	27.121(6)
<i>b</i> /Å	10.558(2)	10.700(2)	10.464(3)	10.398(4)	10.418(2)
<i>c</i> /Å	15.311(3)	15.194(2)	15.401(4)	15.424(6)	15.424(3)
$\alpha$ /°	90	90	90	90	90
$\beta$ /°	119.508(2)	119.868(2)	119.512(3)	119.020(4)	118.915(3)
$\gamma$ /°	90	90	90	90	90
Calculated density/g.cm <sup>-3</sup>	1.355	1.383	1.326	1.349	1.318
Volume/Å <sup>3</sup>	3778.8(1)	3778.9(1)	3836.5(2)	3825(2)	3814.5(2)
Temperature/K	100(2)	100(2)	101(2)	100(2)	100(2)
$\mu$ /mm <sup>-1</sup>	0.091	0.094	0.095	0.143	0.088
Independent reflections	3853	4376	3921	3246	3884
<i>R</i> <sub>int</sub>	0.0415	0.0428	0.0385	0.0366	0.0734
<i>R</i> <sub>1</sub> [ <i>I</i> > 2( <i>I</i> )]	0.0497	0.0507	0.0961	0.0687	0.0571

It is interesting to note that the calculated densities of **2·Dioxane** and **2·THF** are higher than those of the other frameworks. This could be because 1,4-dioxane and THF are much larger molecules that fill the cavity more completely than the other solvent molecules do. The *a* and *c* axes of **2·Dioxane** are somewhat shorter compared to the unit cell dimensions of the other three frameworks. This could be due to the tilting of the 1,4-dioxane molecule which occupies less space in the direction of the *a* and *c* axes (Figure 4.16a). The *b* axes of **2·THF** and **2·Dioxane** are somewhat longer because THF and 1,4-dioxane occupy more space along the *b* axis due to the shape of the molecules (Figure 4.16b). Acetone, DMSO and DMF notably occupy less space in the direction of the *b* axis (Figure 4.16b).

Table 4.3 contains the hydrogen bond parameters for each of the five isostructural framework-type compounds. The contact O3—H3O...O2 represents the intramolecular hydrogen bond between the OH group and the carboxylate group of the pamoate ion. The contact N1—H1N...O2 represents the hydrogen bond formed between the 4-phenylpyridinium ion and the pamoate ion.

**Table 4.3** Hydrogen bond parameters of the five isostructural frameworks. D is the donor atom and A is the acceptor atom.

Complex	Contact	D-H (Å)	H...A (Å)	D...A (Å)	∠DHA (°)
<b>2·THF</b>	O3-H3O...O2	0.940 (3)	1.675(3)	2.56(2)	155(2)
	N1-H1N...O2	1.060 (3)	1.582(3)	2.625(2)	167(2)
<b>2·Dioxane</b>	O3-H3O...O2	0.96(3)	1.63(3)	2.55(2)	159(2)
	N1-H1N...O2	1.09(3)	1.58(3)	2.637(2)	164(2)
<b>2·DMSO</b>	O3-H3O...O2	0.92(5)	1.72(5)	2.560(3)	151(5)
	N1-H1N...O2	1.03(6)	1.60(6)	2.629(4)	173(5)
<b>2·Acetone</b>	O3-H3O...O2	0.92(3)	1.70(3)	2.557(2)	153(2)
	N1-H1N...O2	1.13(3)	1.51(3)	2.620(3)	160(3)
<b>2·DMF</b>	O3-H3O...O2	0.94(4)	1.70(4)	2.555(3)	150(4)
	N1-H1N...O2	1.07(4)	1.57(4)	2.629(3)	174(3)

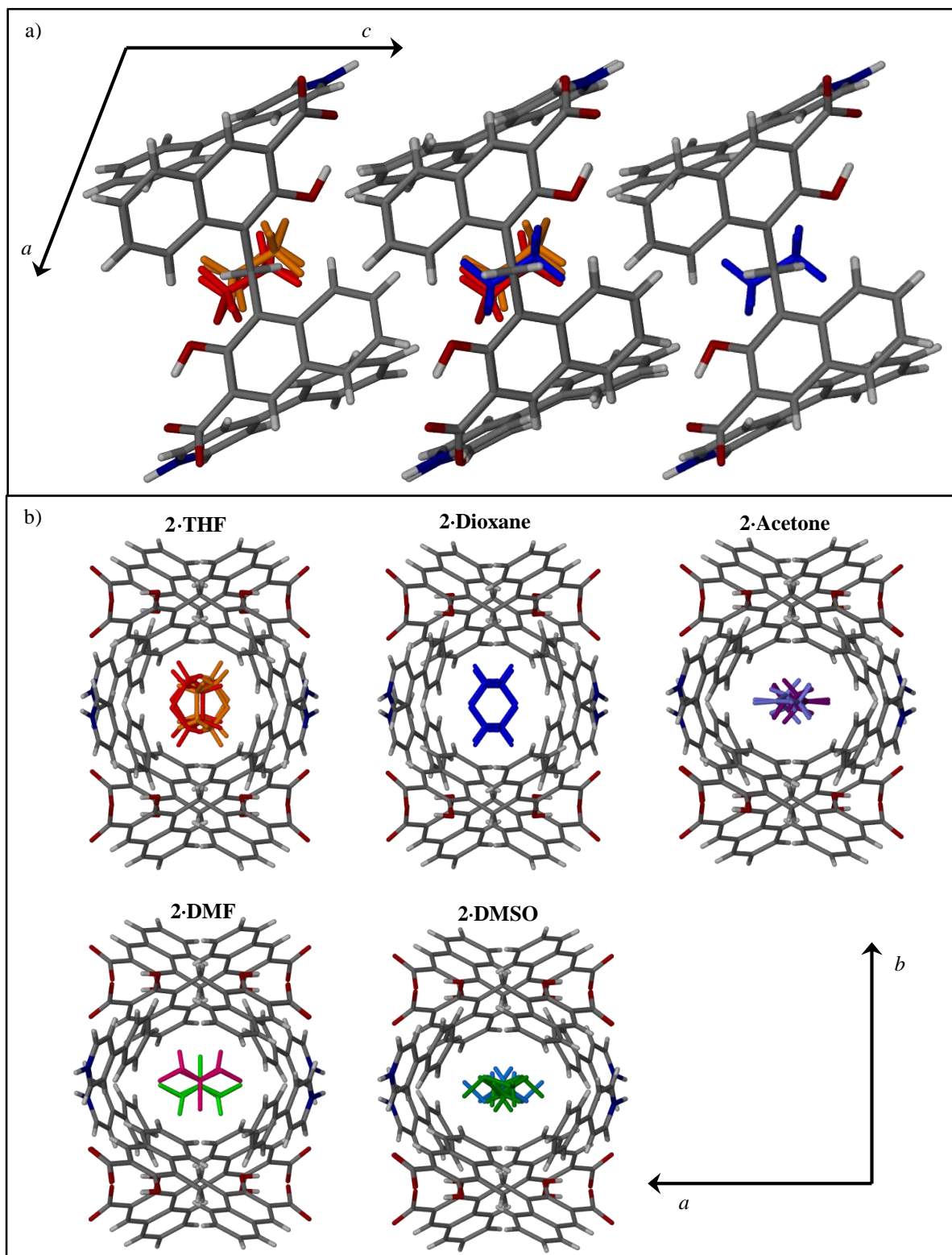


**Figure 4.16** a) The structures of **2·THF** and **2·Dioxane** are compared down the *b*-axis and are overlaid to show the orientation of the solvent molecules. The disordered THF is depicted in orange and red (left); 1,4-dioxane in blue (right); and in the centre the two molecules have been overlapped. The shortening along the *a* and *c* axes is possibly due to the slight tilting of the 1,4-dioxane molecule. b) The five isostructural frameworks viewed down the *c* axis. The different colours in each structure depicts the different orientations of the guest molecules. It is clear that acetone, DMF and DMSO occupy less space along the *b* axis than THF and 1,4-dioxane. This could explain why **2·THF** and **2·Dioxane** have longer *b* axes.

### 4.3 Competition experiments

Competition experiments were performed with the five isostructural frameworks in order to determine whether this framework can selectively include one solvent over another on crystallisation from a mixed solvent system. Molar ratios of two solvents were varied from 0 to 1 in increments of 0.1. Pamoic acid and 4-phenylpyridine (1:1) were then added to each of these solvent combinations and the solutions were left to stand in a glass vial sealed with parafilm to minimise solvent evaporation. In most cases crystals formed after a few days. Approximately 15 mg of crystals were collected, dried on filter paper and dissolved in approximately 0.5 ml DMSO- $d_6$  and then analysed by  $^1\text{H}$  NMR (Appendix C). Since the framework crystallises in a specific ratio it is possible to determine the number of protons of each solvent, which could then be related to a fraction of the total solvent content of the crystal. The fraction of a particular solvent in the crystal ( $Z_A$ ) was then plotted against the mole fraction of the particular solvent of the original solution ( $X_B$ ). The selectivity coefficient  $K_{A:B}$  can then be calculated as

$$K_{A:B} = \left( \frac{Z_A}{Z_B} \right) \times \left( \frac{X_B}{X_A} \right)$$

where  $X_A + X_B = 1$ .<sup>9</sup> There were 10 different possible solvent combinations and each combination had 11 crystallisations with solvent ratios ranging from 0 to 1. In total 110 crystallisations were analysed for the fraction of each solvent present in the crystals. Table 4.4 lists the different solvent combinations and whether crystals were obtained from these mixtures.

PXRD analysis (Appendix C) was also performed on each sample to ensure that all crystals that formed were that of framework **2**. This is important due to the tendency of pamoic acid to form the pamoic acid/DMF solvate (CSD-SIQCIF<sup>10</sup>) in many cases where DMF is the crystallisation solvent. In all cases only crystals of **2** formed. The crystals formed from 1,4-dioxane/acetone fractions were so small that some of the undissolved pamoic acid powder was inadvertently scooped up with the crystals and can be seen in the powder patterns of some of the fractions. This was however taken into account during integration of the protons in the  $^1\text{H}$  NMR spectrum and protons from the 4-phenylpyridine were used as integration reference.

**Table 4.4** The list of solvent combinations from which framework **2** was crystallised for selectivity studies. For each solvent combination it has been noted whether crystals were obtained from these combinations.

Solvent combination	Crystals obtained
THF/acetone	Crystals were obtained over the entire fraction range
THF/DMF	No crystals were obtained from any solvent mixture
THF/1,4-dioxane	Crystals were obtained over the entire fraction range
THF/DMSO	Crystals were obtained only from the 0.7 THF: 0.3 DMF crystallisation
DMSO/acetone	Crystals were obtained from the 0.3 DMSO: 0.7 acetone and 0.1 DMSO: 0.9 acetone combinations
DMSO/DMF	No crystals were obtained from any fraction combination
DMSO/1,4-dioxane	Crystals were obtained over the entire fraction range
1,4-dioxane/DMF	Crystals were obtained over the entire fraction range
1,4-dioxane/acetone	Crystals were obtained over the entire fraction range
DMF/acetone	No crystals were obtained from any fraction combination

The five solvent combinations that yielded crystals over the entire fraction range were used to plot selectivity curves, shown in Figure 4.17. These crystallisations were also repeated a second time to ensure that the trends observed are reproducible. In Figure 4.17 it is clear that framework **2** does show selectivity for certain solvents. When crystals are grown from a combination of THF and acetone, THF is selectively included over all fractions, even when only a fraction of 0.1 THF is present in the solvent mixture (Figure 4.17a). In the case of THF and 1,4-dioxane solvent mixtures, 1,4-dioxane is selectively included (Figure 4.17b), although compared to the other selectivity curves the preference is not quite as pronounced for 1,4-dioxane as with the other solvent combinations. This is possibly due to the similar shapes of THF and 1,4-dioxane and the fact that their crystal structures have similar densities. In the cases of 1,4-dioxane/DMSO, 1,4-dioxane/DMF and 1,4-dioxane/acetone it is clear that 1,4-dioxane certainly is the preferred solvent to be included in the crystal structure. This is probably due to 1,4-dioxane having a better fit in the cavity than acetone, DMF or DMSO.

What is interesting to note of the results of the competition experiments between 1,4-dioxane and DMF is that the crystals that formed were consistently that of framework **2**. Pamoic acid is known to readily form a solvate with DMF (SIQCIF<sup>10</sup>). It is especially interesting since the fractions in which all of the pamoic acid dissolved were those with a higher fraction of DMF,



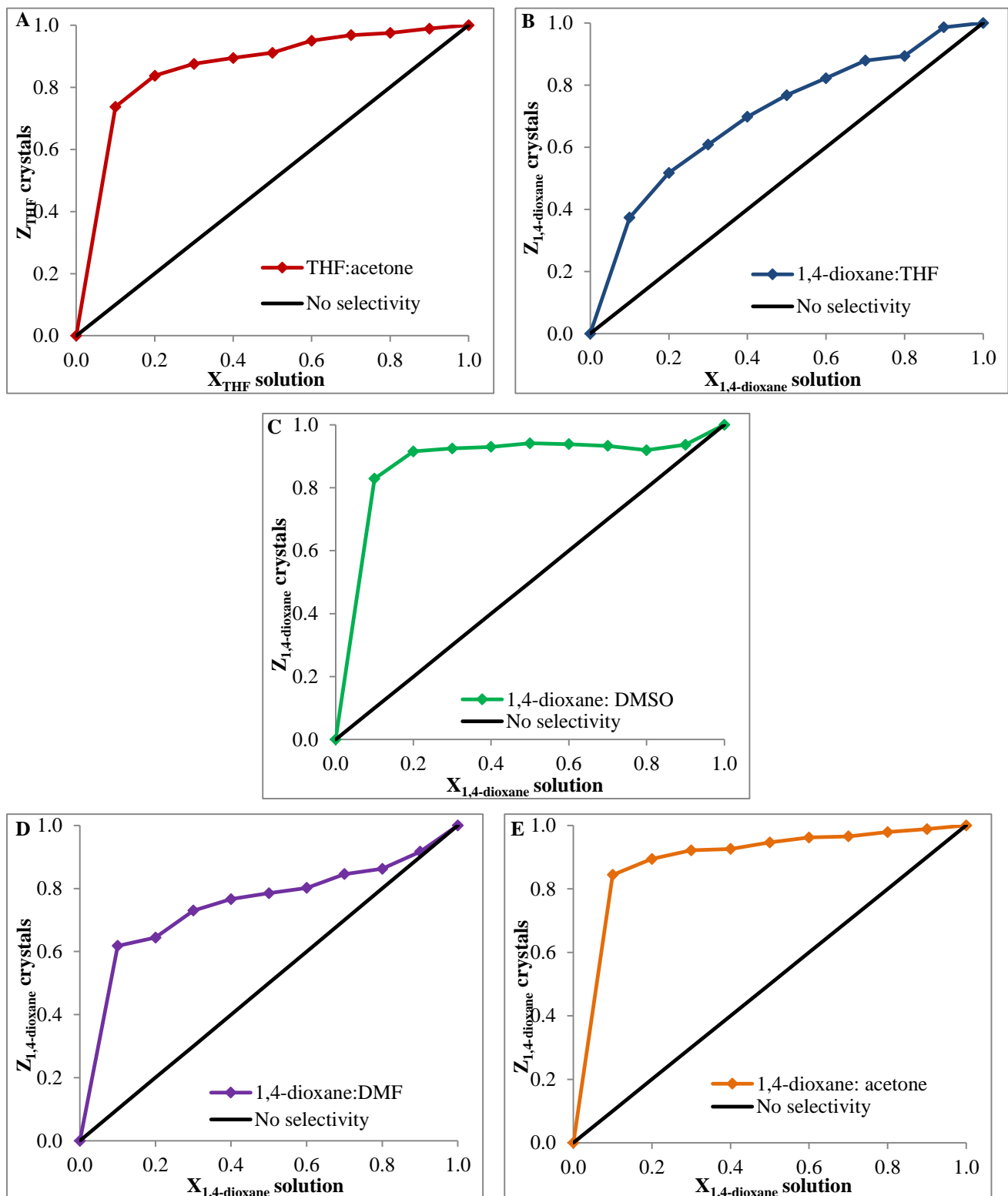


**Figure 4.17** The selectivity curves of the framework 2 when left to crystallise from mixed solvent systems. In each case the black line represents no selectivity. When crystals are grown from a mixture of THF and acetone, THF is preferentially included at every fraction (A). When any solvent is combined with 1,4-dioxane, 1,4-dioxane is selectively included in every case (B, C, D, E). This could be due to the shape of 1,4-dioxane that fills the voids better than any of the other solvents.

and yet 1,4-dioxane was still selectively included in the crystals. This could mean that framework **2** is a much more stable crystal structure than even the pamoic acid/DMF solvate that can form under almost any crystallisation conditions.

The clear preference for 1,4-dioxane over any other solvent could be explained by looking at the interactions at play between the solvent molecules and the framework. Each crystal structure was analysed by CrystalExplorer<sup>11</sup> and the Hirshfeld surface<sup>12</sup> of the solvent molecule was mapped in each case. The Hirshfeld surface of a molecule is generated by separating the space in a crystal into areas where the electron density for the molecule (or promolecule) dominates over the electron density of the crystal (procrystal). The weight function for the molecule in the crystal can be defined as<sup>12</sup>

$$\begin{aligned}w_A(\mathbf{r}) &= \frac{\sum_{i \in \text{molecule } A} \rho_i^{at}(\mathbf{r})}{\sum_{i \in \text{crystal}} \rho_i^{at}(\mathbf{r})} \\ &= \rho_{\text{promolecule}}(\mathbf{r}) / \rho_{\text{procrystal}}(\mathbf{r})\end{aligned}$$

where  $\rho_i^{at}(\mathbf{r})$  is the spherically averaged electron densities of the various atoms (*at*).<sup>12</sup> This leads to an isosurface where  $w_A(\mathbf{r}) = 0.5$ . This particular isosurface is termed the Hirshfeld surface which defines the space where the electron density of the promolecule is greater than that of the other surrounding molecules.<sup>12</sup> This ensures the closest possible proximity of molecular volumes to each other without overlapping,<sup>12</sup> which in turn can give us valuable information regarding the close contacts between these molecules. The Hirshfeld surface mapped by CrystalExplorer gives a good visual representation through colour coded areas relating to the proximity of molecules to each other and where possible close contacts may occur. It is however also necessary for these computer-generated close contacts to make chemical sense within the crystal structure and it is therefore vital that a keen crystallographer's eye evaluates all the contacts indicated by the Hirshfeld surface. Different properties can be encoded on the Hirshfeld surface.<sup>13</sup> One of the most important functions and graphical displays that can be mapped onto the surface is that of  $d_e$ . The term is defined as the distance between the Hirshfeld surface and the nearest nucleus in a neighbouring molecule outside the surface.<sup>13</sup> This paints a clear picture of any close contacts formed between the two molecules being investigated and also about the crystal packing environment around the molecule.<sup>13</sup> In the images shown in Figure 4.18 and Figure 4.19 all surfaces mapped are that of  $d_e$ .



The Hirshfeld surfaces of each solvent molecule in the five frameworks were compared and the environment and possible close contacts were also evaluated to determine whether there were certain interactions present in one crystal structure and not another which could lend added stability to a structure. The first set of images compares the five framework materials down the *a*-axis (Figure 4.18). The colours encoded on the Hirshfeld surface are directly related to the contact distance between atoms. White is where the distance *d* is equal to the van der Waals distance, blue is where *d* is greater than the van der Waals distance and red is where *d* is less than the van der Waals distance.<sup>14</sup> Therefore, the shorter the distance between two atoms, the closer the colour on the Hirshfeld surface will be to red. The range of *d<sub>e</sub>* in Figure 4.18 is 0.850 to 2.850 Å. For structures that contain disordered solvent, both parts of the disorder were selected when generating the Hirshfeld surface of the solvent molecule. This then represents an average position of the solvent molecule and interactions for both parts of the disorder can be seen this way. In most of the cases shown below the same type of interactions appear to be at play, where the hydrogen atoms of the phenyl groups of the pamoate and 4-phenylpyridine ions appear to interact with the solvent molecules. In the case of THF and 1,4-dioxane this interaction appears to be more prevalent than in the case of the other three solvents since there are more short contacts indicated by the orange areas. The Hirshfeld surfaces of DMSO and acetone appear to be quite similar with slightly fewer short contacts than THF and 1,4-dioxane as indicated by the orange areas and more blue areas, whereas the surface of DMF differs quite a lot from all the other solvents.

In Figure 4.19 the Hirshfeld surfaces of each of the solvent molecules are viewed down the *b*-axis. Here it is also possible to see that there are different intermolecular interactions present in the different crystal structures. The most notable interaction is that of the inward facing methylene protons of the pamoate ions with the protons of THF and 1,4-dioxane, indicated by the red circles in Figure 4.19. This particular interaction appears to be completely absent in the case of DMSO and acetone (circled in orange), and present to a lesser extent in the case of DMF.

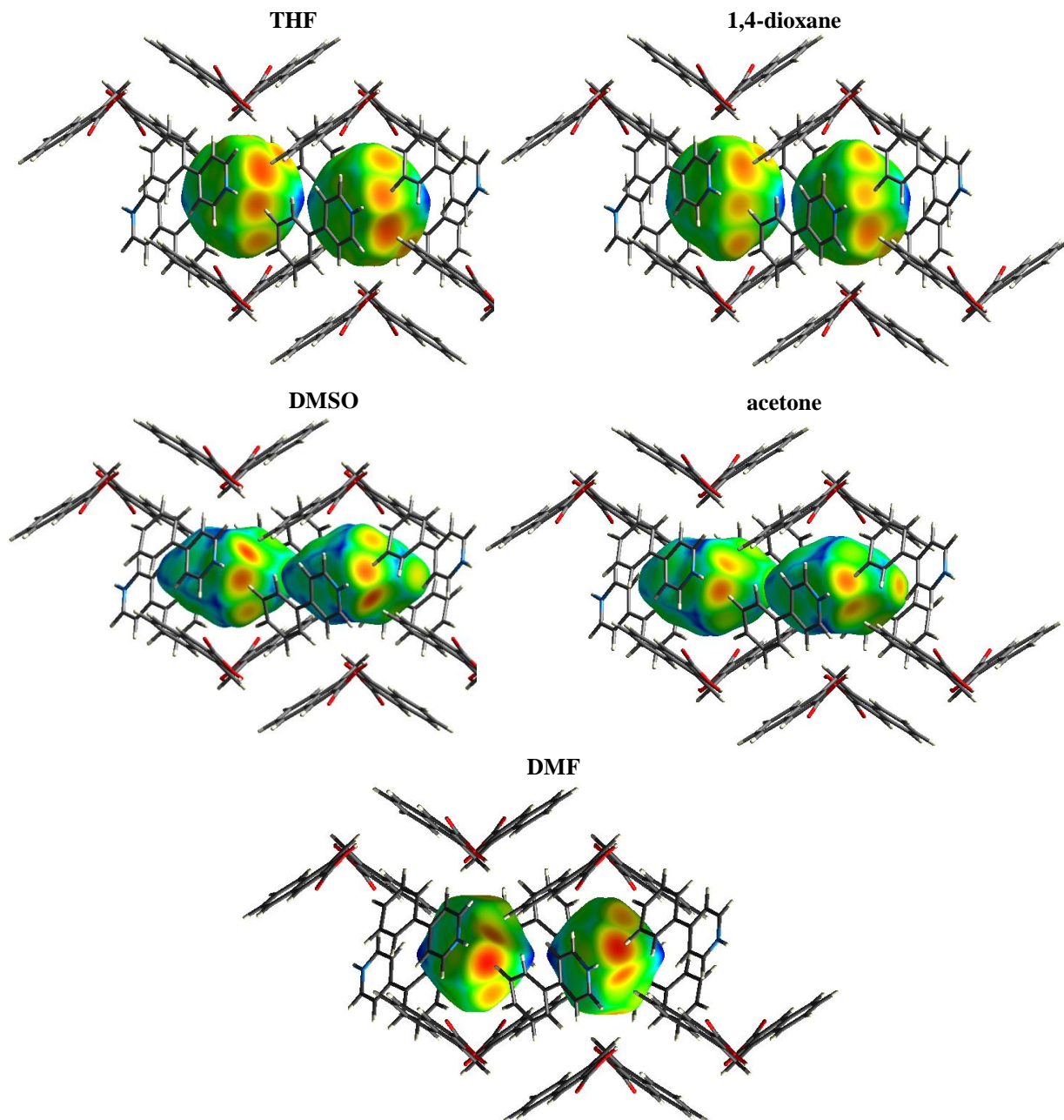


**Figure 4.18** The Hirshfeld surfaces of the solvent molecules of each of the five framework materials viewed down the  $a$  axis. It is clear that the surfaces of THF and 1,4-dioxane are quite similar and therefore similar interactions are at play in their respective crystal structures. The surfaces of DMSO and acetone appear to correlate, though differing quite significantly from the first two. The shape of the DMF surface corresponds to that of THF and 1,4-dioxane, but there appear to be somewhat different interactions at play in this particular structure.

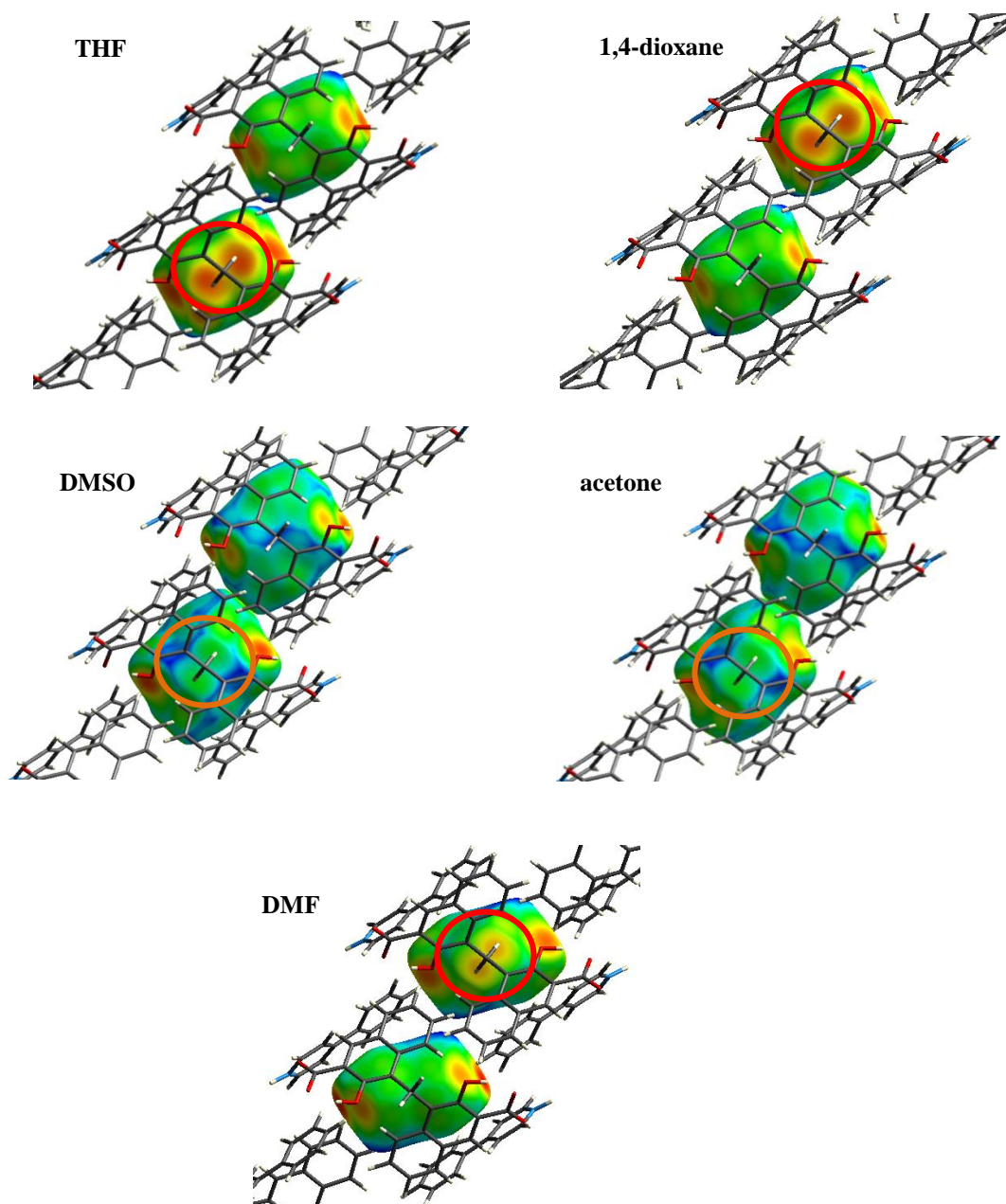


**Figure 4.19** The Hirshfeld surfaces of the solvent molecules, viewed down the  $b$  axis of the crystal structures. THF, 1,4-dioxane and to a lesser extent DMF all experience an additional interaction *via* the methylene protons of the pamoate ion that point toward the solvent molecule, circled in red. This interaction is however not seen (or is present to a much lesser extent) in the case of DMSO and acetone, circled in orange.

Fingerprint plots generated from the Hirshfeld surface can be used to visualise the different contacts present for the specific molecule for which the Hirshfeld surface is mapped. Previously  $d_e$  was defined as the distance between the Hirshfeld surface and the nearest nucleus in a neighbouring molecule outside the surface.<sup>13</sup> Another property that can be plotted on the Hirshfeld surface is  $d_i$ , defined as the distance from the surface to the nearest nucleus within the molecule itself.<sup>13</sup> Since  $d_e$  and  $d_i$  relate to what is occurring both outside and inside the Hirshfeld surface, respectively, these two terms are used to visually express which atom-to-atom contacts exist for a specific molecule.<sup>15</sup> A  $d_e;d_i$  pair is plotted for each possible contact.<sup>16</sup> These points on the graph are also colour coded in order of the magnitude of their contribution on the surface, i.e. the distance of the contact. Longer contact distances are coloured blue, green contact distances are neither close nor distant and closer contacts range from yellow to orange to red.<sup>16</sup> In single-component crystals this would then reflect all possible atom-atom contacts within the crystal structure, but in the case of multi-component systems this depends on the molecule for which the Hirshfeld surface was generated. For the five frameworks, the Hirshfeld surface for the solvent molecule was generated (as shown in figures 4.18 and 4.19). The fingerprint plots of these five frameworks therefore display the interactions surrounding the solvent molecules in the crystal structure. Generally fingerprint plots for single component crystal structures are symmetrical, but in this case the fingerprint plots are not symmetrical. This is because only the Hirshfeld surface of the solvent molecule was generated and not any of the other components in the crystal structure and therefore there are some interactions that dominate, causing the fingerprint plot to be asymmetrical. Only the interactions around the solvent molecule are seen and not the contribution of the interactions of pamoic acid and 4-phenylpyridine. If a Hirshfeld surface is generated for all three components in the framework the fingerprint plot is symmetrical.

In Figure 4.20 the fingerprint plots of the five frameworks are shown with all relevant close contacts in the graph indicated by arrows. It is clear from the fingerprint plots that the different solvent molecules experience very different environments in the crystal structure. It is also evident that different contacts are more predominant in different structures, which could explain why some solvents are more selectively encapsulated over others in competition experiments.

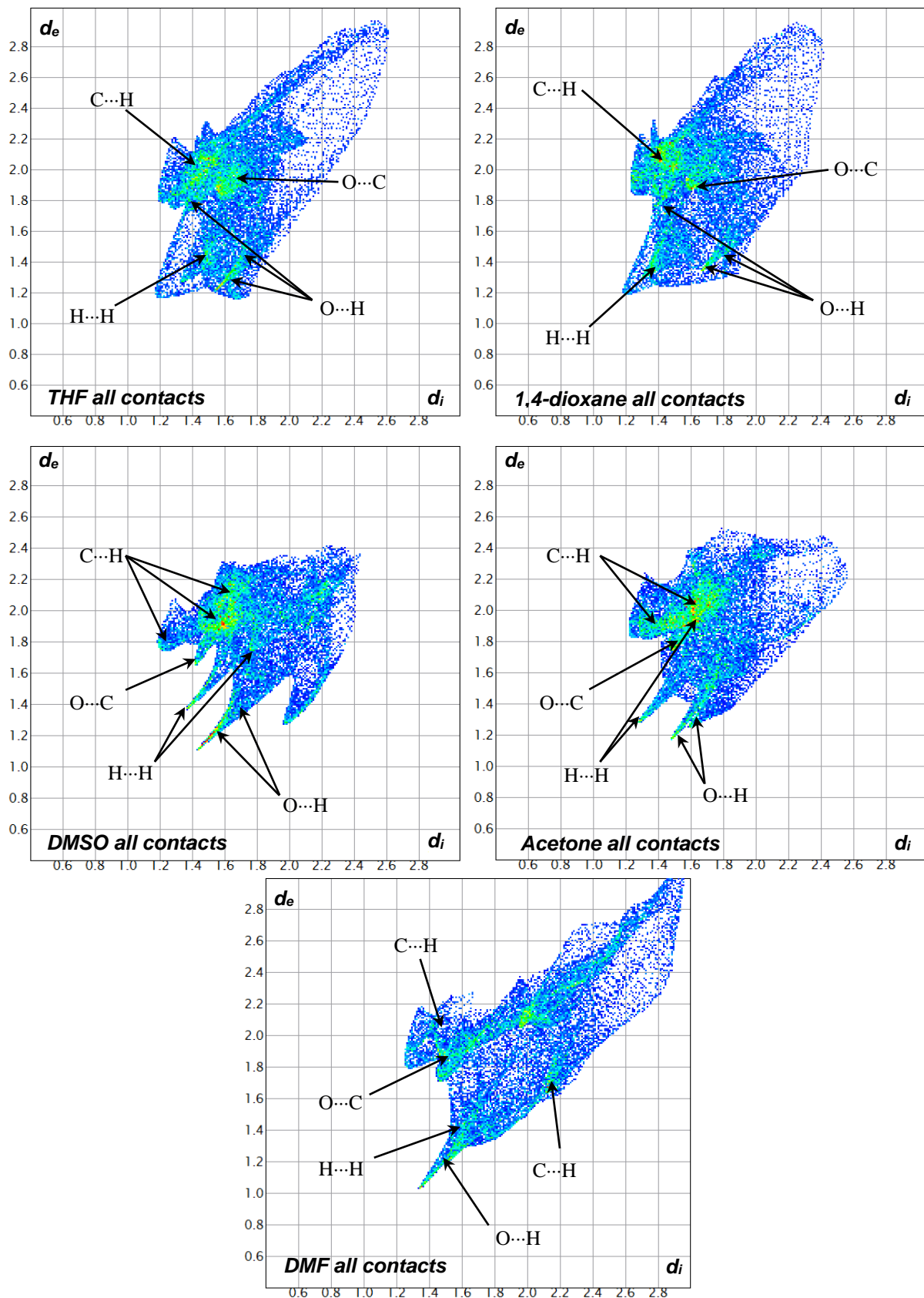


**Figure 4.20** The fingerprint plots of the solvent molecules of each of the five frameworks. The different types of contacts and their relative distances are indicated by arrows. The solvent molecules clearly experience very different environments in each crystal structure. Some interactions are also more prevalent in some structures, which could explain why some solvents, specifically 1,4-dioxane, are selectively encapsulated in competition experiments.



Specifically comparing the Hirshfeld surfaces and fingerprint plots of THF and 1,4-dioxane, one might be able to rationalise why 1,4-dioxane is the preferred solvent for inclusion. THF and 1,4-dioxane for the most part encounter the same environment in the crystal structure and therefore appear to largely have the same close contacts (Figure 4.21).

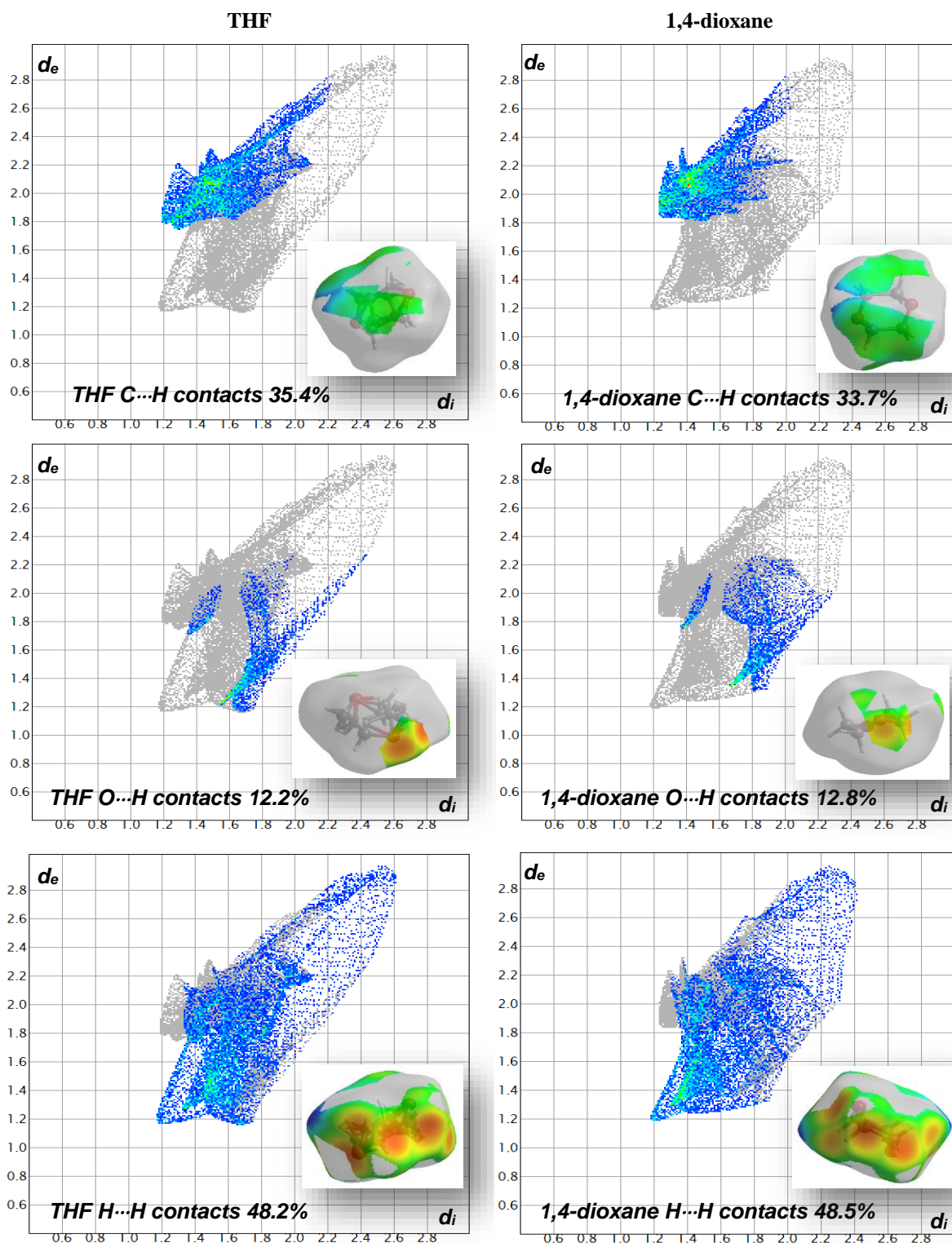


**Figure 4.21** The deconstructed fingerprint plots of THF and 1,4-dioxane. The transparent Hirshfeld surface is shown where the areas that correspond to the contacts in the fingerprint plots of the solvent of **2·THF** and **2·Dioxane** have been highlighted.

In the fingerprint plot of the C...H contacts for 1,4-dioxane there appears to be a higher collection of close contacts with shorter atom-atom distances than in the corresponding fingerprint plot for THF. THF does seem to have more C...H contacts (35.4% compared to 33.7% for 1,4-dioxane), but 1,4-dioxane appears to have a higher number of close C...H contacts, indicated by the larger number of green points on the fingerprint plot compared to that of THF. This could imply that a more stable structure is formed with 1,4-dioxane due to more short contacts with shorter distances between atoms. The fingerprint plots for the O...H contacts for both solvents are fairly similar regarding the intensities of the points on the graph. There are however slightly more of these O...H contacts present in the structure with 1,4-dioxane, as seen by the larger number of blue points on the 1,4-dioxane fingerprint plot. As stated earlier, the blue points generally indicate longer distances, but in this case it could mean that there is a long-range stabilisation effect in the structure with 1,4-dioxane, more so than in the structure with THF. H...H contacts seem to be the dominating interaction in both crystal structures. This includes the interaction of the methylene protons of the pamoate ion with the protons of THF and 1,4-dioxane discussed previously. This interaction seems to largely stabilise these two solvents within the cavities, more so than for DMSO and acetone.

It is also entirely possible that merely the shape of 1,4-dioxane allows it to be more easily included in the crystal structure. It is slightly larger than THF which means it would fill the void better and lead to more efficient packing. Its shape may also allow for better interactions with the framework, as is illustrated by the Hirshfeld surfaces shown in Figure 4.18 and Figure 4.19, which again adds stability to the framework as a whole. The density rule,<sup>17</sup> which is based on Kitaigorodskii's principle of close packing,<sup>18</sup> states that the most stable polymorph will have the highest density. Polymorphs arise when the same components pack in different ways in the solid state. This implies that **2·Dioxane** is the more stable framework of the five isostructural frameworks, indicated by the high density of the crystal structure. In **2·Dioxane** the molecules pack more efficiently, minimising void space, and consequently forming a more stable structure. This further explains why **2·Dioxane** selectively crystallises from different solvent combinations.

## 4.4 Novel crystal structures obtained with pamoic acid

During the course of this investigation, a number of novel pamoate salts were obtained with various bases. These were isolated from experiments where the aim was to produce framework materials. Two salts, **S1** and **S2**, have been mentioned in the preceding sections. These salts will be described first in Section 4.4.1 and thereafter each new crystal structure will be discussed in a separate section. The crystallographic data for the structures discussed in this section can be found in Table 4.12 at the end of this section.

### 4.4.1 Salt formation with pamoic acid and 4-phenylpyridine

In the section discussing the isostructural frameworks obtained during the course of this study, the formation of two novel 4-phenylpyridinium pamoate salts was mentioned (Section 4.1.2 and 4.2). These structures are polymorphs of one another. Polymorphism is the ability of molecules to pack in different ways in the solid state.<sup>19, 20</sup> One was grown from a 1:1 molar ratio of DMSO/H<sub>2</sub>O and the other was grown from 1:1 molar ratio solutions of acetonitrile/H<sub>2</sub>O, MeOH/H<sub>2</sub>O and EtOH/H<sub>2</sub>O. The first salt isolated from DMSO/H<sub>2</sub>O shall be referred to as **S1** and the second salt shall be referred to as **S2**. **S2** was also mentioned during the thermal studies of framework **2** where **2·THF** converts to **S2** at high temperatures.

**S1** conforms to the space group  $P2_1/n$ . The asymmetric unit contains one singly deprotonated pamoate ion and one 4-phenylpyridinium ion (Figure 4.22).

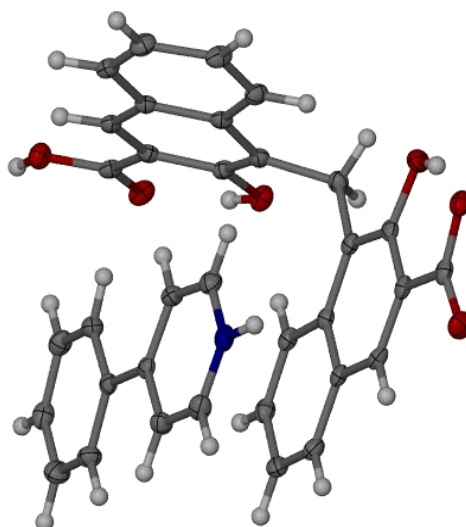


**Figure 4.22** The asymmetric unit of **S1** with one singly deprotonated pamoate ion and one 4-phenylpyridinium ion.



The singly deprotonated pamoate ion forms an infinite chain of pamoate ions through  $\text{COOH}\cdots\text{OOC}$  hydrogen bonding between the carboxyl and carboxylate groups (Figure 4.23a). In this particular structure a slightly more condensed pamoate chain is observed in comparison to other known structures with pamoic acid, such as in the 2,5-lutidinium pamoate THF solvate CSD-TAPCIY<sup>1</sup> (Figure 4.23a). The 4-phenylpyridinium ions hydrogen bond to the remaining oxygen atom of the pamoate ion. Adjacent chains stack alongside one another *via*  $\pi - \pi$  stacking interactions of the 4-phenylpyridinium ions and the pamoate ions.

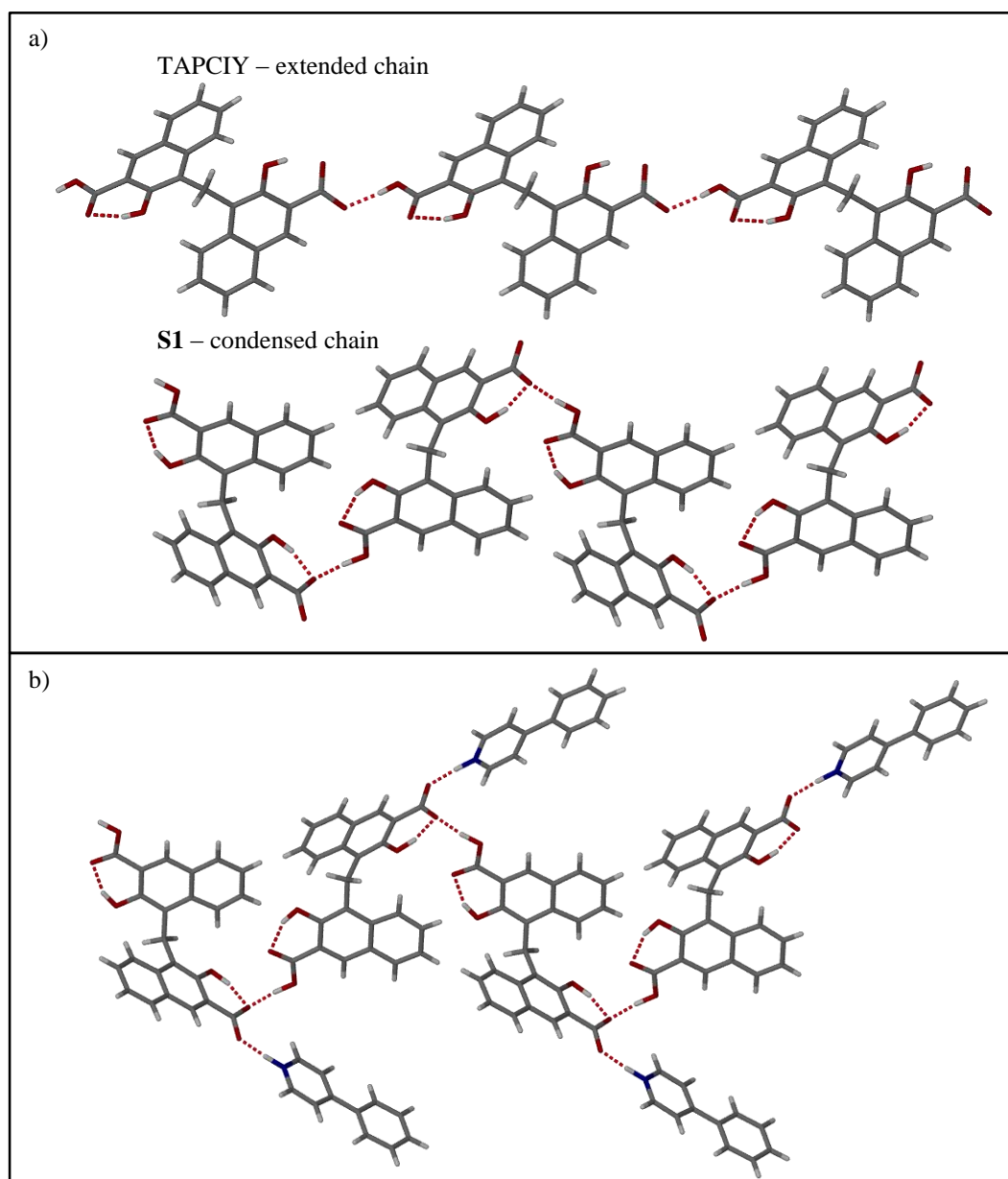


**Figure 4.23** Hydrogen bonding motifs in S1. a) The singly deprotonated pamoate ions in S2 form infinite hydrogen-bonded chains. In this structure the chain appears to be somewhat more condensed compared to the chain motif usually found in the pamoate structures. The example shown here is TAPCIY, a 2,5-lutidinium pamoate THF solvate. b) The 4-phenylpyridinium ions hydrogen bond to the remaining oxygen atom of the pamoate ion.

**S2** conforms to the centrosymmetric space group  $P2_1/c$  and also contains one singly deprotonated pamoate ion and one 4-phenylpyridinium ion (Figure 4.24).

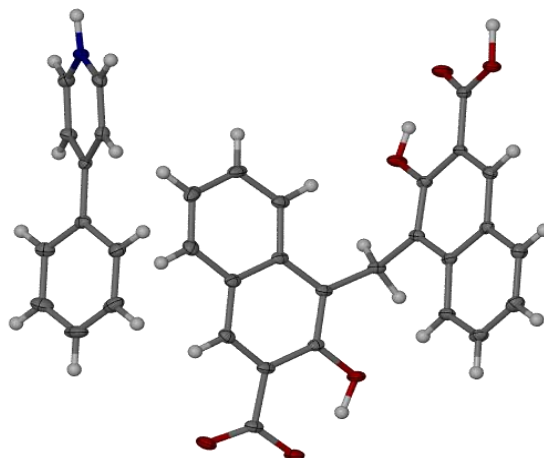


**Figure 4.24** The asymmetric unit of **S2**.

The singly deprotonated pamoate ions form infinite chains through hydrogen bonding of the carboxyl and carboxylate moieties and form a more elongated chain than **S1** (Figure 4.25a). The 4-phenylpyridinium ions form hydrogen bonds to the remaining oxygen atom of the carboxylate group on the pamoate ion (Figure 4.25b). Adjacent chains then stack together *via*  $\pi-\pi$  interactions to form the extended structure.

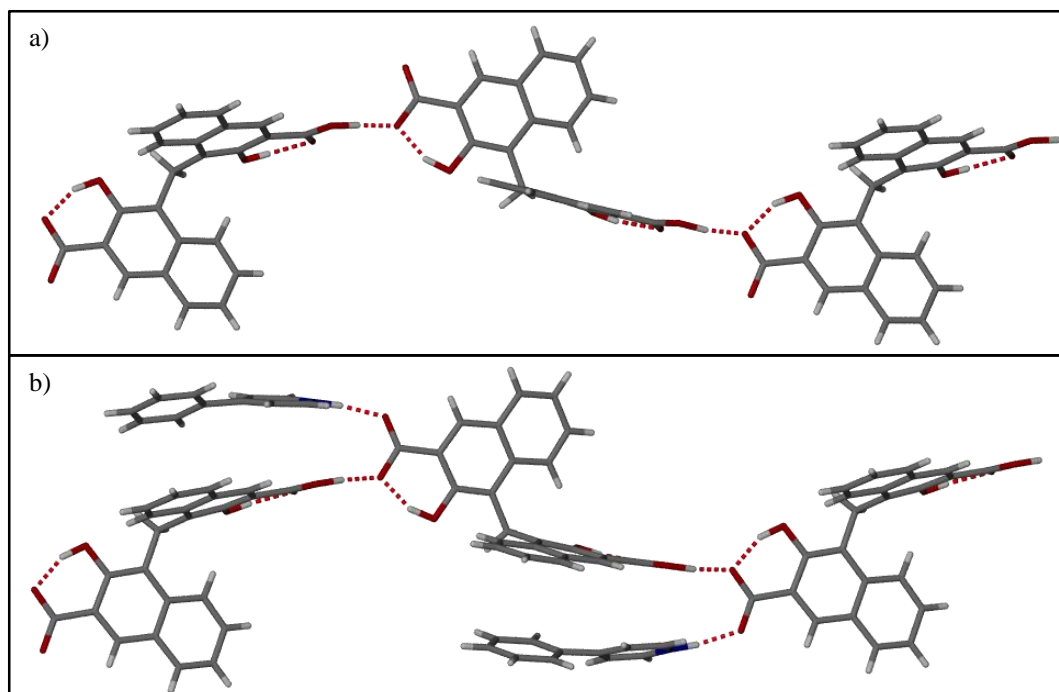


**Figure 4.25** Hydrogen bonding motifs in **S2**. a) Hydrogen bonding of the pamoate ions form infinite chains that are slightly more elongated than those of **S1**. b) The 4-phenylpyridinium ions hydrogen bond to the remaining oxygen atom of the carboxylate group.

The main difference between the two crystal structures appears to be the angles of the hydrogen bonds between the different ions. In both structures the pamoate ions are singly deprotonated. In **S1** the proton of one carboxylate group hydrogen bonds to the deprotonated carboxylate of a neighbouring pamoate ion. This hydrogen bond is however at an angle. If one naphthyl group of the pamoate ion is taken as the horizontal plane, then the hydrogen bond is formed at an angle of  $116.31^\circ$  below the plane (Figure 4.26). This allows the pamoate ions to be closer to each other, effectively shortening the pamoate chain in **S1**.

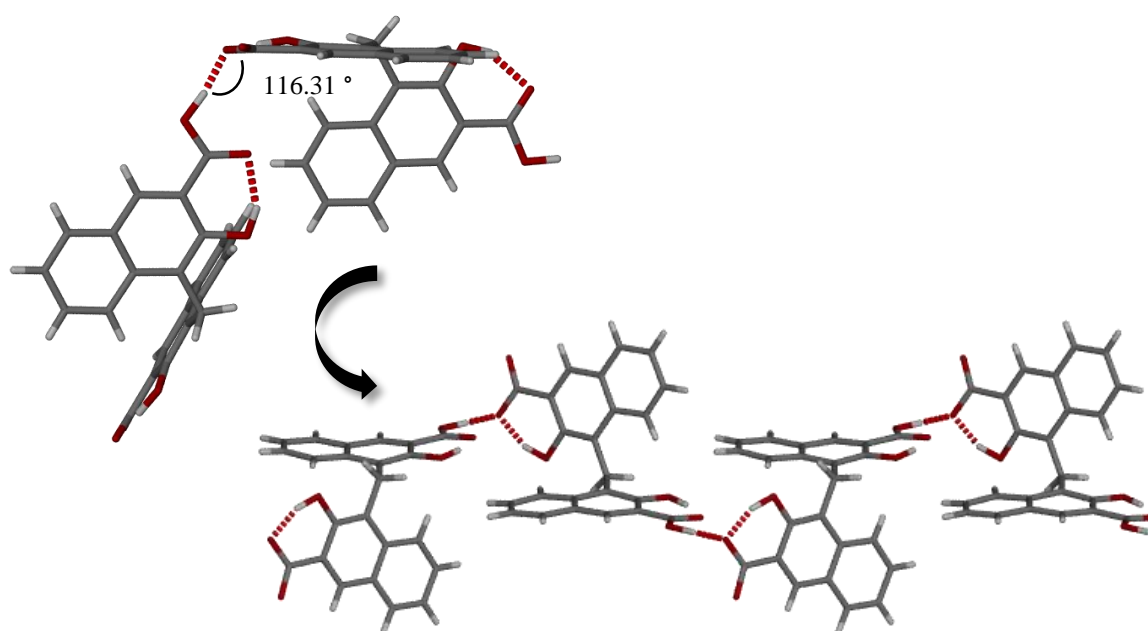


**Figure 4.26** The hydrogen bonding motif observed in **S1**. The hydrogen bonding angle in this structure is below the plane of the one naphthyl group of the pamoate ion ( $116.31^\circ$ ), causing the pamoate ions to be closer together and subsequently shortening the pamoate chain.

In **S2** the proton of the carboxylate group also hydrogen bonds to the deprotonated carboxylate group of a neighbouring pamoate ion, but in this case the hydrogen bond is head-on and in the same plane as that of the naphthyl moiety of the pamoate ion (Figure 4.27). This leads to a hydrogen bonding motif with the pamoate chain more open and extended.

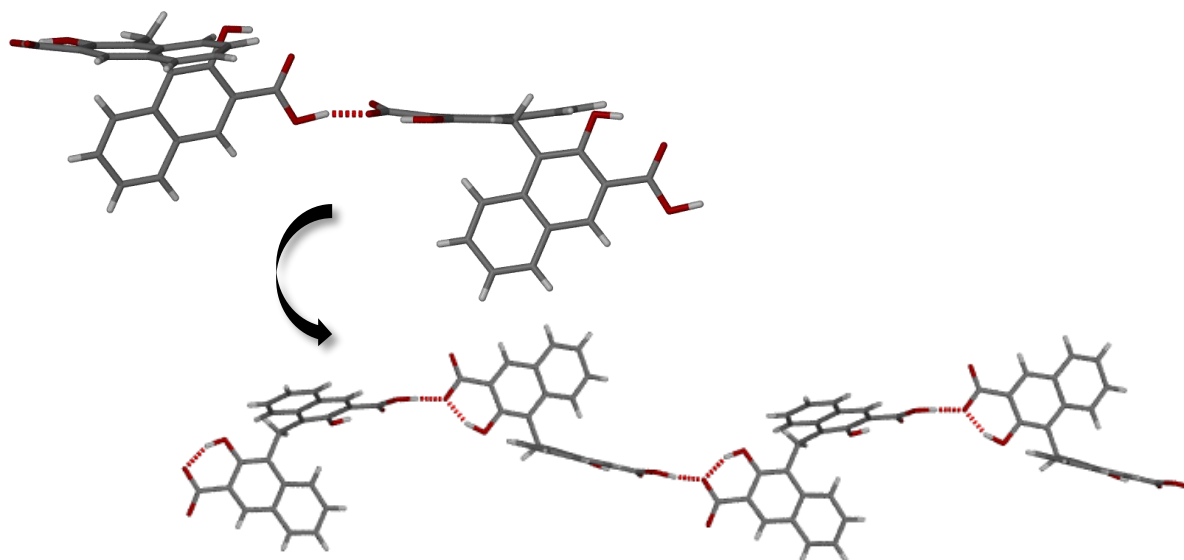


**Figure 4.27** The hydrogen bonding motif observed in **S2**. The hydrogen bond formed between the two pamoate ions is head-on and in the same plane as the naphthyl moiety of the pamoate ion. The pamoate ions are therefore further apart from one another, forming a somewhat more open and extended chain.

There is also a difference in the way the 4-phenylpyridinium ion hydrogen bonds to the pamoate ion in **S1** and **S2**. In **S1** the 4-phenylpyridinium ion lies in the same plane as the naphthyl moiety with which it forms a hydrogen bond. In **S2** the 4-phenylpyridinium ion is perpendicular to the naphthyl moiety it hydrogen bonds to (Figure 4.28).

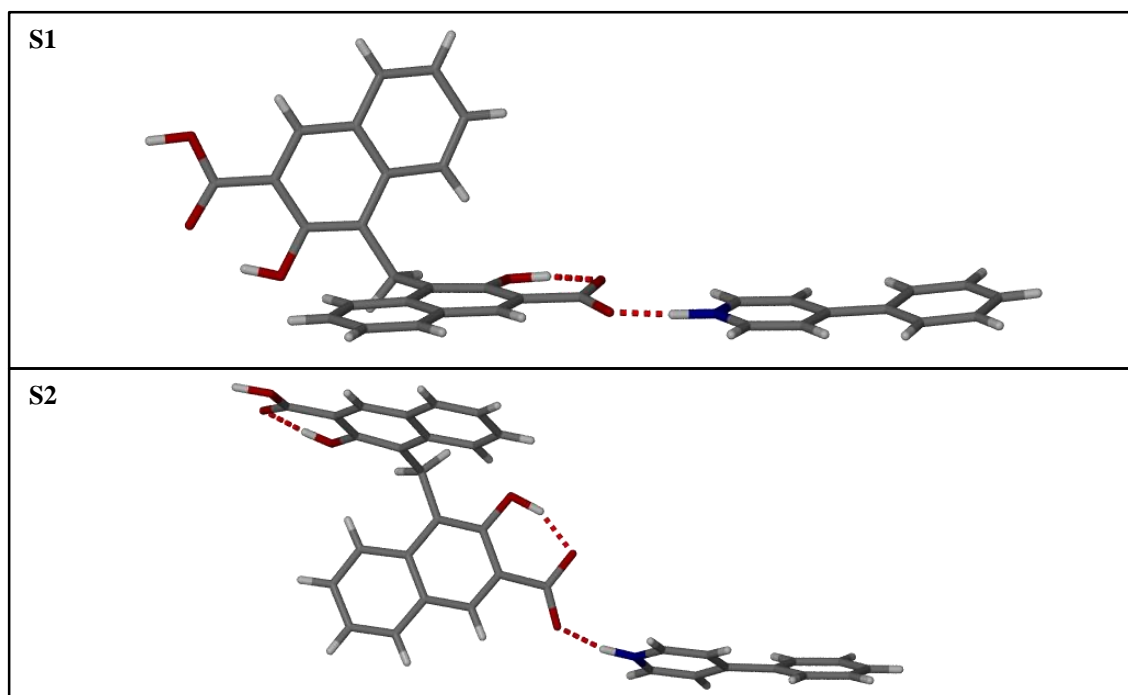


**Figure 4.28** A comparison of the hydrogen bond angles between 4-phenylpyridinium and the pamoate ion of **S1** and **S2**. In **S1** the 4-phenylpyridinium ion lies in the same plane as the naphthyl moiety of the pamoate ion it hydrogen bonds to. The 4-phenylpyridinium ion of **S2** however is perpendicular to the naphthyl moiety pamoate ion it hydrogen bonds to.

They hydrogen bond parameters for **S1** and **S2** are listed in Table 4.5 and the labeling scheme is shown in Figure 4.29.

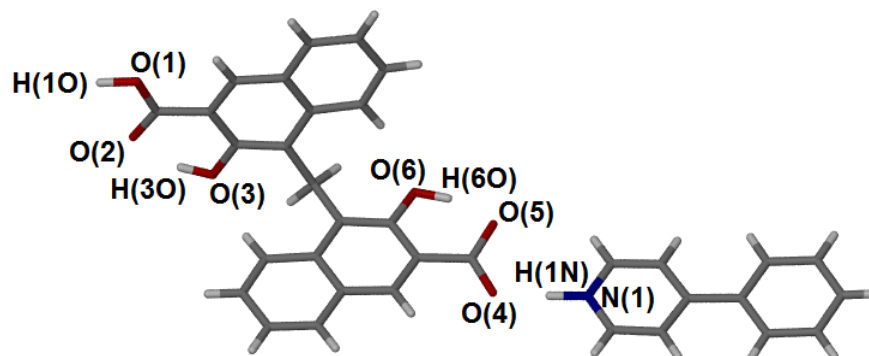


**Figure 4.29** The labeling scheme for the hydrogen bond parameters of **S1** and **S2**.

**Table 4.5** Hydrogen bond parameters for **S1** and **S2**. The labeling scheme is shown in the above figure.

	Contact	D-H (Å)	H...A (Å)	D...A (Å)	∠DHA (°)
<b>S1</b>	O3 – H3O...O2	0.91(2)	1.76(2)	2.6066(15)	152.7(17)
	O6 – H6O...O5	0.98(2)	1.61(2)	2.5473(15)	159.1(18)
	O1 – H1O...O5 <sup>a</sup>	1.03(2)	1.54(2)	2.5632(14)	171(2)
	N1 – H1N...O4 <sup>b</sup>	1.06(2)	1.59(2)	2.6528(16)	176.9(18)
<b>S2</b>	O3 – H3O...O2	0.89(2)	1.79(2)	2.6003(15)	150.5(19)
	O6 – H6O...O5	0.98(2)	1.61(2)	2.5264(14)	155.0(18)
	O1 – H1O...O5 <sup>c</sup>	1.07(2)	1.48(2)	2.5342(14)	165.4(19)
	N1 – H1N...O4 <sup>d</sup>	0.990(19)	1.712(19)	2.6638(16)	159.8(17)

<sup>a</sup> -x+1/2, y+1/2, -z+1/2; <sup>b</sup> -x+1, -y, -z; <sup>c</sup> x-1, -y+3/2, z-1/2; <sup>d</sup> x-1, -y+1/2, z-1/2

It is also interesting to note that the aromatic rings of the 4-phenylpyridinium ion of **S2** are not exactly coplanar (Figure 4. 30) as they are in **S1**. There is a slight twist between the two phenyl rings in **S2**, with a torsion angle of  $152.6^\circ$ .

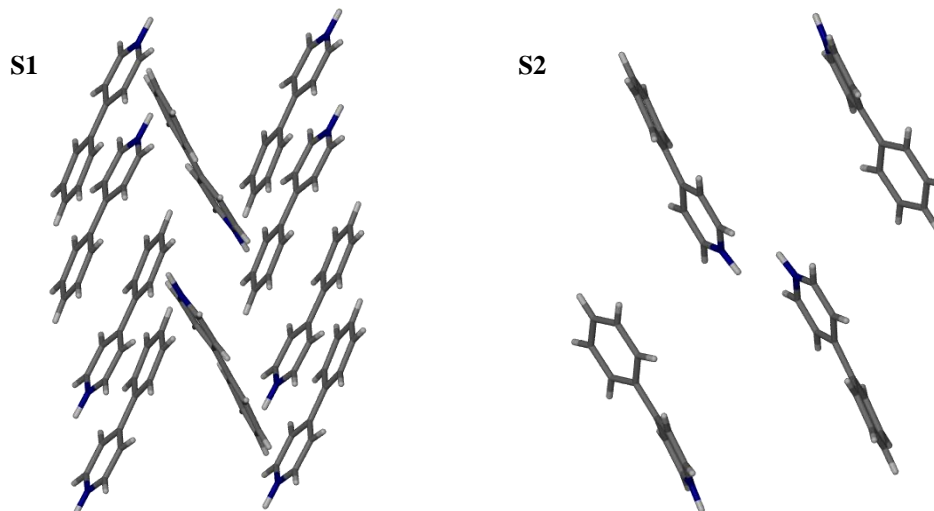


**Figure 4. 30** The planar rings of **S1** and the twisted phenyl rings of **S2**, with a torsion angle of  $152.6^\circ$ .

The twist in the 4-phenylpyridinium ions in **S2** possibly disturbs the  $\pi$  -  $\pi$  stacking observed in **S1**, therefore leading to a different packing motif. As can be seen in Figure 4.31, the centroid-to-centroid distances are slightly longer in **S2** which is possibly due to the twisting of the phenyl rings of the 4-phenylpyridinium ion. The molecules are then further from each other which could lead to the type of head-on hydrogen bonding we observe in **S2**.

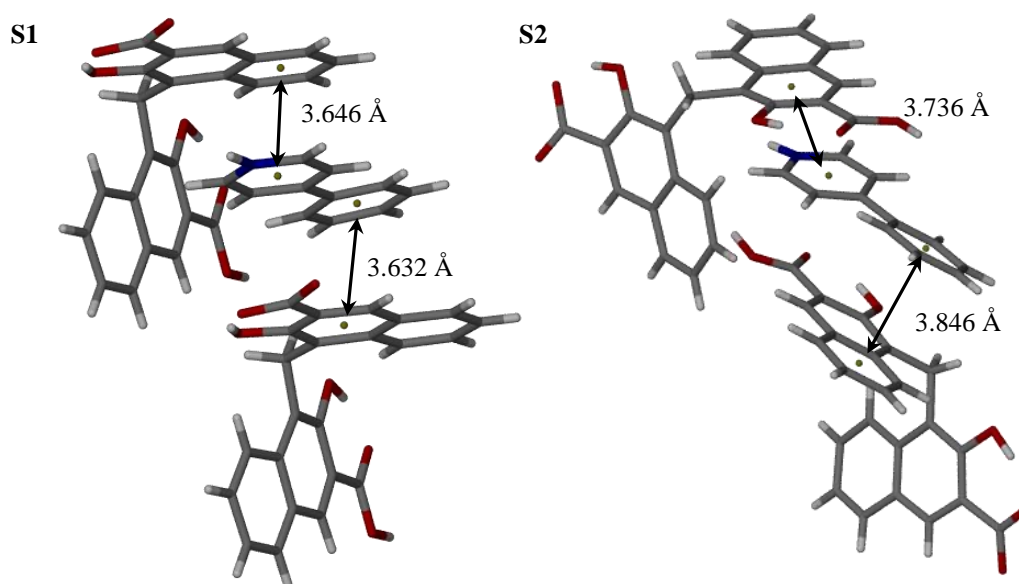


**Figure 4.31** A comparison of the centroid-to-centroid distances between the 4-phenylpyridine rings and the aromatic region of the pamoate ions. The centroid-to-centroid distance in **S2** appear to be somewhat longer, which is possibly due to the twisting of the phenyl rings of 4-phenylpyridine.

A CSD search<sup>21-23</sup> showed that there are 25 reported organic structures that contain a free 4-phenylpyridine molecule. In the majority of these structures (20 out of 25) the phenyl rings are twisted to varying degrees with respect to each other. This appears to be the general and possibly more favourable conformation for the 4-phenylpyridine molecule. This also correlates with the fact that **S2** was isolated from three different crystallisations (EtOH/H<sub>2</sub>O, MeOH/H<sub>2</sub>O and MeCN/H<sub>2</sub>O) whereas **S1** was only ever isolated from one crystallisation. The 25 structures in the CSD do not indicate any discernible relationship between crystallisation solvent and conformation of the 4-phenylpyridine rings.

The crystallisation of salt **S1** was set up at the same time as the crystallisation of **2·DMSO**. Both crystallisations used approximately 100 mg pamoic acid and 40 mg 4-phenylpyridine. Both were dissolved in a 1:1 DMSO/H<sub>2</sub>O mixture and filtered, however, the solution that yielded crystals of the salt **S1** used 0.8 ml less of the DMSO/H<sub>2</sub>O mixture. This could mean that the slight excess of DMSO/H<sub>2</sub>O in one solution led to the formation of **2·DMSO**. This is strange since crystals of **2·DMSO** would repeatedly form during the competition experiments between 1,4-dioxane and DMSO at all ranges of 1,4-dioxane/DMSO fractions. It may however be the case that the presence of 1,4-dioxane at any fraction was driving the formation of the framework-type crystals and therefore served as a template for the formation of the few **2·DMSO** crystals. It has also been seen from the Hirshfeld surfaces of the solvent molecules discussed in the previous section that DMSO might not have the most favourable interactions with the framework, and therefore a slight change in crystallisation conditions could lead to the formation of the **S1** solvent-free salt instead. Pamoic acid is after all a well-known salt former in the pharmaceutical industry<sup>24, 25</sup> and would rather form a more stable salt with 4-phenylpyridine than the seemingly less favourable host-guest structure with DMSO.

**S1** was isolated only once, whereas **S2** was repeatedly obtained from four different crystallisations. This could indicate that **S1** is a more unstable salt that is possibly the kinetic product of the crystallisation from DMSO/H<sub>2</sub>O.



#### 4.4.2 1,2-(2-(4-pyridyl)ethyl)pyridinium pamoate salt, PA1

Crystals of **PA1** were grown by dissolving equimolar amounts of 1,2-bis(4-pyridyl)ethane and pamoic acid separately in a 1:1 molar ratio of NMP/DMF. The two solutions were then carefully layered in order to avoid precipitation of the product. The resultant salt is in the orthorhombic crystal system in the polar space group  $Pna2_1$ , with one singly deprotonated pamoate ion and one singly protonated 1,2-(2-(4-pyridyl)ethyl)pyridinium ion in the asymmetric unit (Figure 4.32).

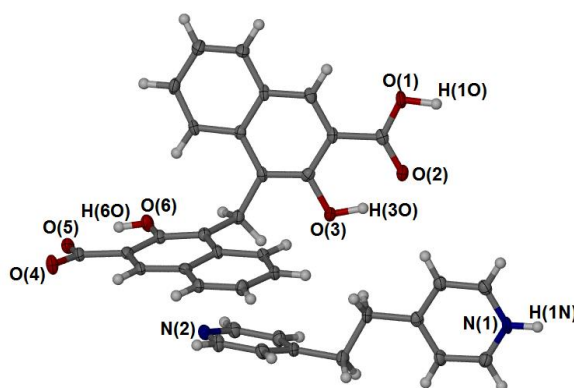


Figure 4.32 The asymmetric unit of **PA1**.

The pamoate ion and 1,2-(2-(4-pyridyl)ethyl)pyridinium ion form a chain of alternating base-acid-base units through alternating  $\text{COOH}\cdots\text{N}/\text{COO}^-\cdots\text{H}^+\text{N}$  hydrogen bonds (Figure 4.33a). In the case of the charge-assisted hydrogen bond the proton is shared between the pamoate ion and the pyridinium ion. Adjacent chains stack next to each other through offset  $\pi-\pi$  interactions between the pyridyl and naphthyl moieties (Figure 4.33b). The hydrogen bond parameters are listed in Table 4.6.

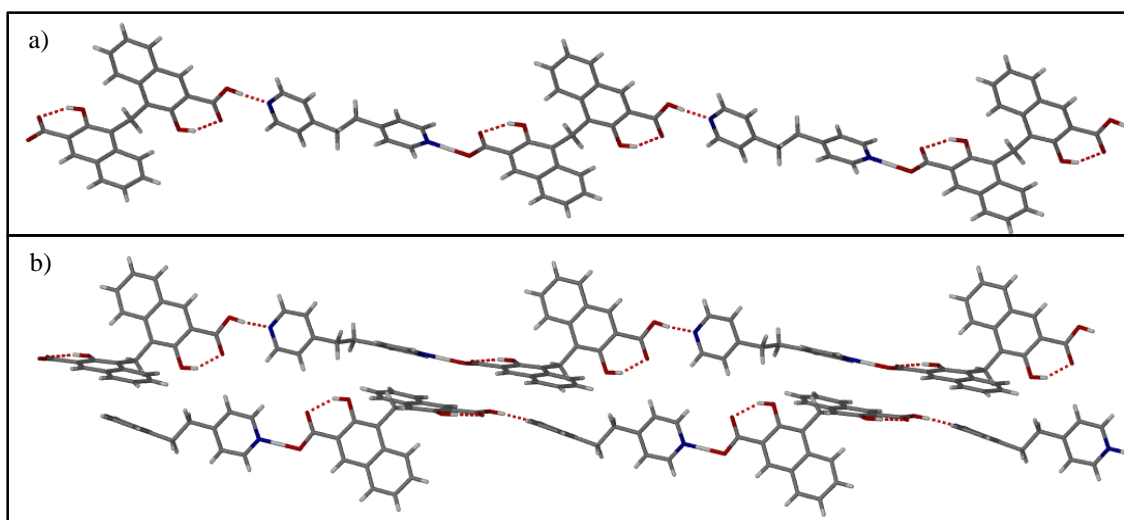
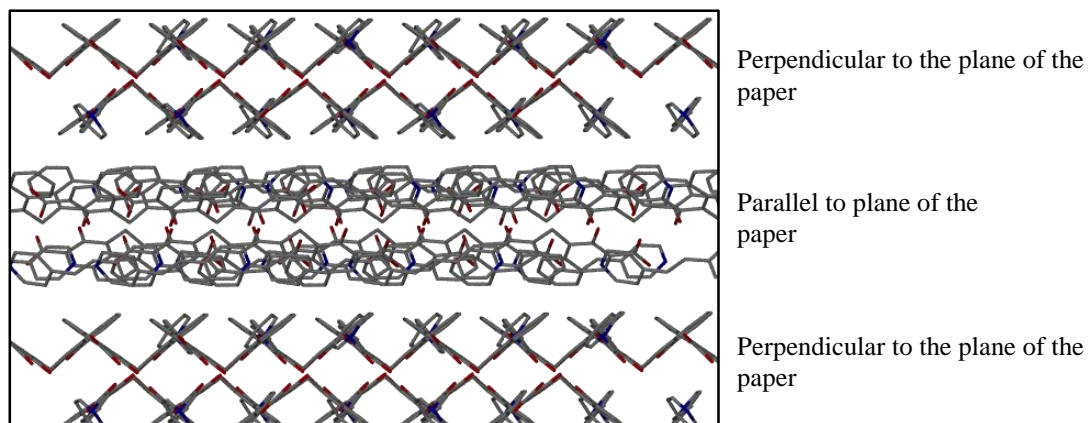


Figure 4.33 a) The chain of alternating base-acid-base units connected *via* neutral and charge-assisted hydrogen bonds. b) Offset  $\pi-\pi$  stacking interactions between the pyridyl and naphthyl moieties allow adjacent chains to stack together.

The base-acid-base chains stack in such a way that two layers of chains run parallel to each other while the next two layers are perpendicular to the previous layer. The result is a structure with alternating layers of base-acid-base chains (Figure 4.34).



**Figure 4.34** The alternating layers of chains where the chains in one layer are perpendicular to the chains in the next layer. Hydrogens have been omitted for clarity.

**Table 4.6** Hydrogen bond parameters for **PA1**. The labeling scheme is shown in **Figure 4.32**.

Contact	D-H (Å)	H...A (Å)	D...A (Å)	∠DHA (°)
O3 – H3O...O2	1.01(5)	1.62(5)	2.540(3)	149(4)
O1 – H1O...N2 <sup>a</sup>	1.07(5)	1.46(5)	2.530(3)	171(4)
N1 – H1N...O4 <sup>b</sup>	0.94(2)	1.59(2)	2.530(4)	176(5)
O6 – H6O...O5	0.86(6)	1.75(6)	2.558(3)	157(5)

<sup>a</sup>  $-x+1/2, y-1/2, z+1/2$ ; <sup>b</sup>  $-x+1/2, y-3/2, z+1/2$

### 4.4.3 1,10-phenanthrolineium pamoate THF solvate, PA2

Crystals of this THF solvate were obtained by dissolving equimolar amounts of 1,10-phenanthroline and pamoic acid in a molar ratio of 1:1 THF:H<sub>2</sub>O. It is in the triclinic crystal system in the space group  $P\bar{1}$ . It is isostructural to the known 1,10-phenanthrolineium pamoate DMF solvate (CSD-QEXJEJ<sup>26</sup>) and contains one 1,10-phenanthrolineium ion, one pamoate ion and one THF molecule in the asymmetric unit (Figure 4.35).

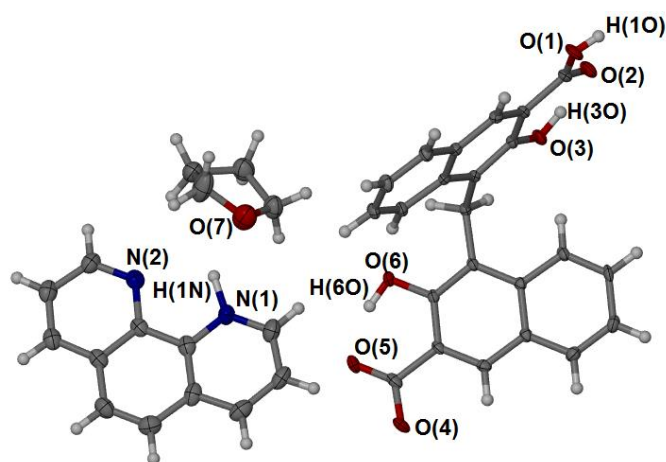


**Figure 4.35** The asymmetric unit of the 1,10-phenanthrolineium pamoate THF solvate PA2.

The pamoate ions form chains through COOH...OOC hydrogen bonds, but no hydrogen bonds are formed between the 1,10-phenanthrolineium ion and the pamoate ion. Instead, the 1,10-phenanthrolineium ion forms an intramolecular hydrogen bond to the nitrogen atom of the phenanthroline moiety and another hydrogen bond to the oxygen atom of the THF molecule (Figure 4.36a). The hydrogen bond parameters are listed in Table 4.7. The pamoate chains and solvent-base units stack together through C—H... $\pi$  and  $\pi$ — $\pi$  interactions (Figure 4.36b). Due to the positioning of the THF molecules and the 1,10-phenanthrolineium ions the THF molecules are restricted to discrete solvent pockets (Figure 4.36c).

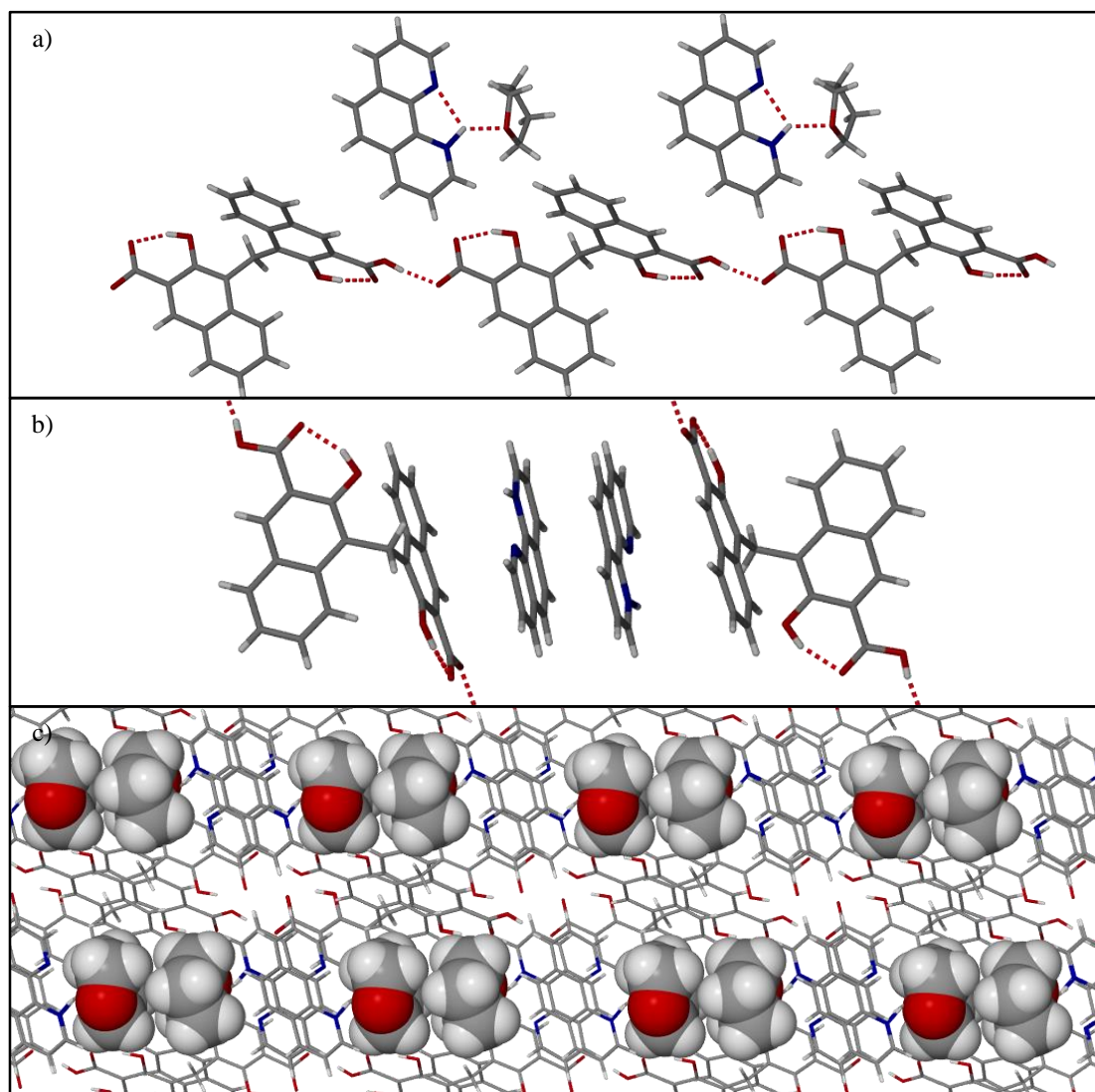


**Figure 4.36** Hydrogen bonding motifs of **PA2**. a) Pamoate ions form hydrogen bonded chains that do not hydrogen bond to the 1,10-phenanthroline ions. Instead the 1,10-phenanthroline ions hydrogen bond to THF molecules. b) There are  $\pi-\pi$  stacking interactions between the pamoate chains and 1,10-phenanthroline ions. c) The THF molecules reside in discrete pockets.

**Table 4.7** Hydrogen bond parameters for **PA2**. The labeling scheme is shown in **Figure 4.35**.

Contact	D-H (Å)	H...A (Å)	D...A (Å)	$\angle$ DHA (°)
O3 – H3O...O2	0.91(4)	1.69(4)	2.549(2)	156(3)
O6 – H6O...O5	0.90(3)	1.66(3)	2.524(2)	159(3)
O1 – H1O...O4 <sup>a</sup>	0.79(5)	1.67(5)	2.458(2)	171(6)
N1 – H1N...O7	1.15(2)	1.81(2)	2.732(4)	134(2)

<sup>a</sup> x, y, z+1

#### 4.4.4 2-aminopyrimidinium pamoate THF solvate, PA3

Equimolar amounts of 2-aminopyrimidine and pamoic acid were dissolved in a 1:1 molar ratio of THF:H<sub>2</sub>O and resulted in crystals of 2-aminopyrimidinium pamoate THF solvate, **PA3**. It is in the monoclinic crystal system in the space group *C2/c* and the asymmetric unit consists of one 2-aminopyrimidinium ion, half a pamoate ion and half of a THF molecule. The symmetry related parts of the pamoate ion and THF molecule are shown in green in Figure 4.37. The hydrogen atom is shared between the pamoate and 2-aminopyrimidinium, but the N–H distance is slightly shorter than the O–H distance (1.248 Å and 1.312 Å, respectively).

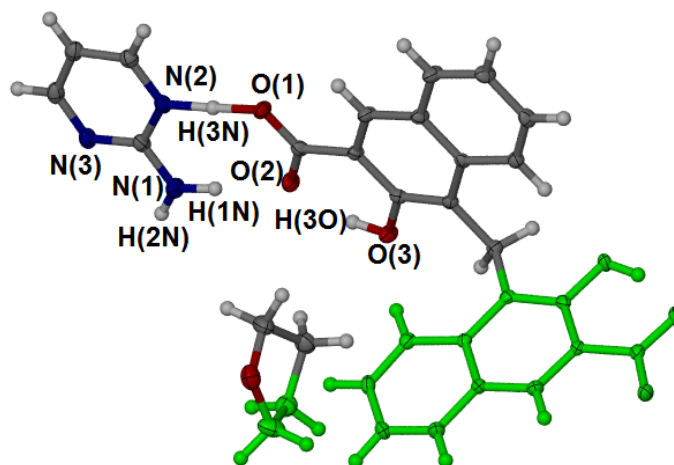


**Figure 4.37** The asymmetric unit of **PA3**. The symmetry-related parts of the pamoate ion and THF molecule are shown in green.

The pamoate ion hydrogen bonds to two 2-aminopyrimidinium ions through  $\text{COO}^- \cdots \text{H}^+\text{N}$  hydrogen bonds to the nitrogen atom on the pyrimidine ring. Each 2-aminopyrimidinium ion forms complementary  $\text{N}-\text{H} \cdots \text{N}$  hydrogen bonds between the amino group and the nitrogen atom on the ring of another 2-aminopyrimidinium ion. This hydrogen bonding motif forms infinite chains throughout the structure (Figure 4.38a). The hydrogen bond parameters are listed in Table 4.8. The neighbouring chains close pack through offset  $\pi-\pi$  stacking interactions (Figure 4.38b). THF molecules fill the spaces between adjacent chains (Figure 4.38c).

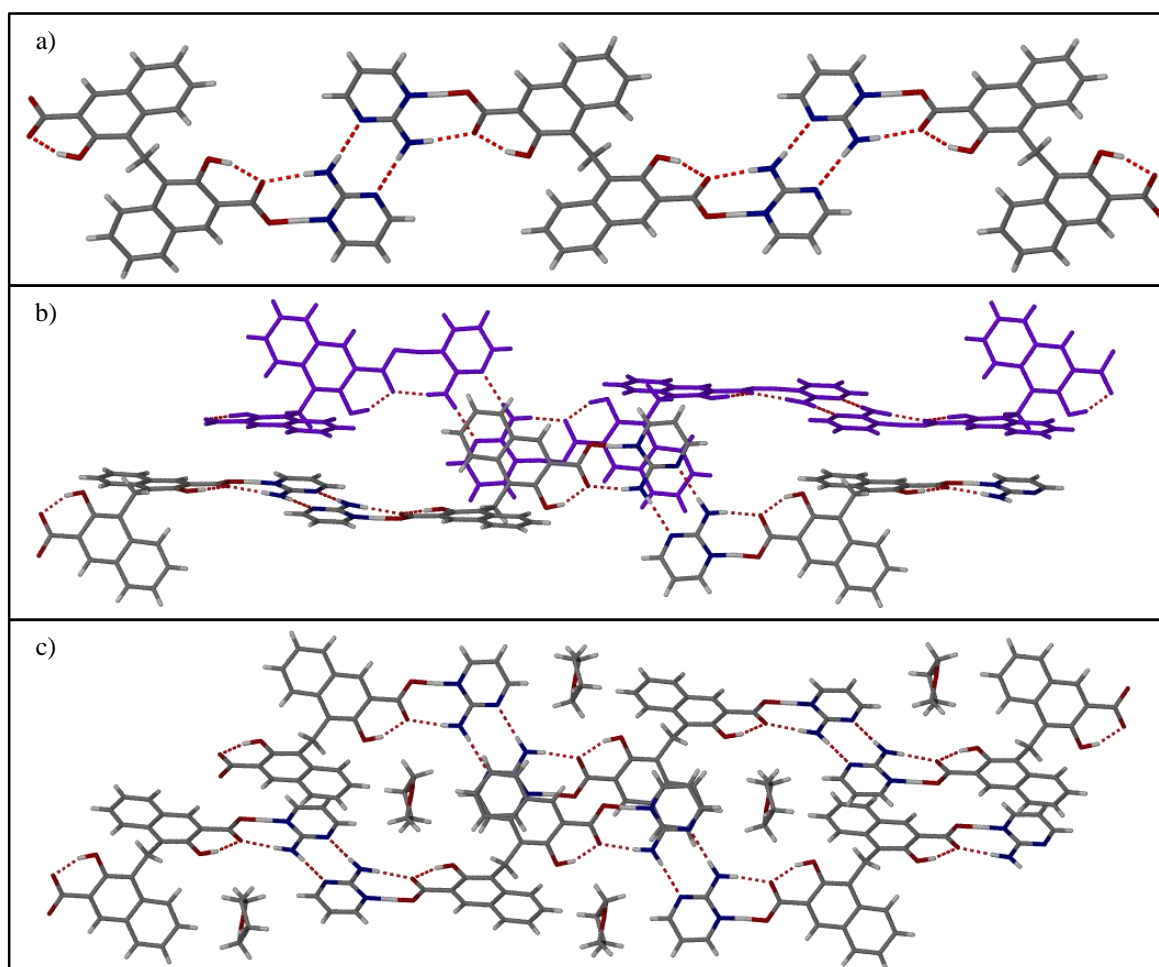


**Figure 4.38** Hydrogen bond motifs of PA3. a) The hydrogen-bonded chains of the 2-pyrimidinium and pamoate ions. b) The chains close-pack through offset  $\pi-\pi$  stacking interactions. c) Spaces between adjacent chains are filled by THF molecules.

**Table 4.8** The hydrogen bond parameters for PA3. The labeling scheme is shown in Figure 4.37.

Contact	D-H (Å)	H...A (Å)	D...A (Å)	$\angle$ DHA (°)
O3 – H3O...O2	0.92(2)	1.69(2)	2.554(1)	155(2)
N2 – H3N...O1 <sup>a</sup>	1.25(2)	1.31(2)	2.555(1)	172(2)
N1 – H1N...O2	0.95(2)	1.90(2)	2.841(2)	171(2)
N1 – H2N...N3 <sup>b</sup>	0.91(2)	2.13(2)	3.045(2)	178(2)

<sup>a</sup> x, y, z; <sup>b</sup> -x-1/2, -y+3/2, -z

#### 4.4.5 2,4-lutidinium pamoate dihydrate, PA4

A 2,4-lutidinium pamoate dihydrate was previously isolated by our group<sup>3</sup> (CSD-BEVXUX<sup>3</sup>) and yet another dihydrate has been discovered during the course of this study. **PA4** was grown by slow evaporation from a 1:1 THF:H<sub>2</sub>O solution by combining equimolar amounts of 2,4-lutidine, pamoic acid and pentafluorobenzonitrile. The dihydrate was also obtained from crystallisations of 2,4-lutidine and pamoic acid with benzonitrile, cinnamonnitrile, *m*-tolunitrile, *p*-tolunitrile and methyl terephthalonitrile (Appendix A) and in each case the nitrile was not included in the structure. **PA4** is in the space group  $P\bar{1}$  and contains one singly deprotonated pamoate ion, one 2,4-lutidinium ion and two water molecules in the asymmetric unit (Figure 4.39).

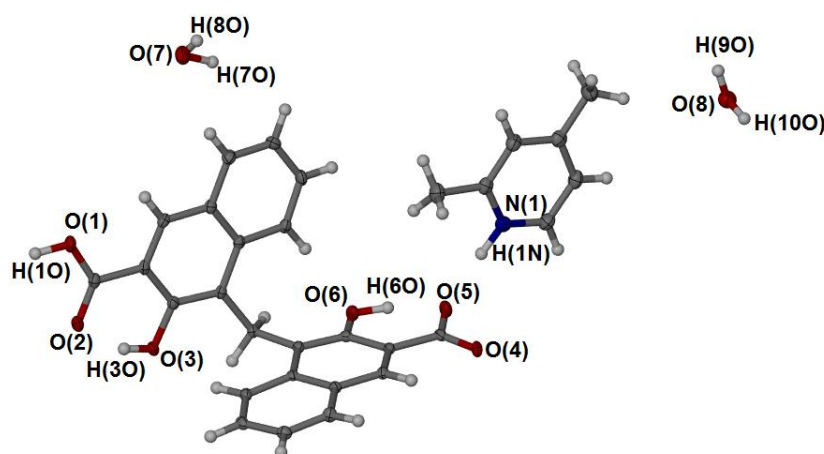
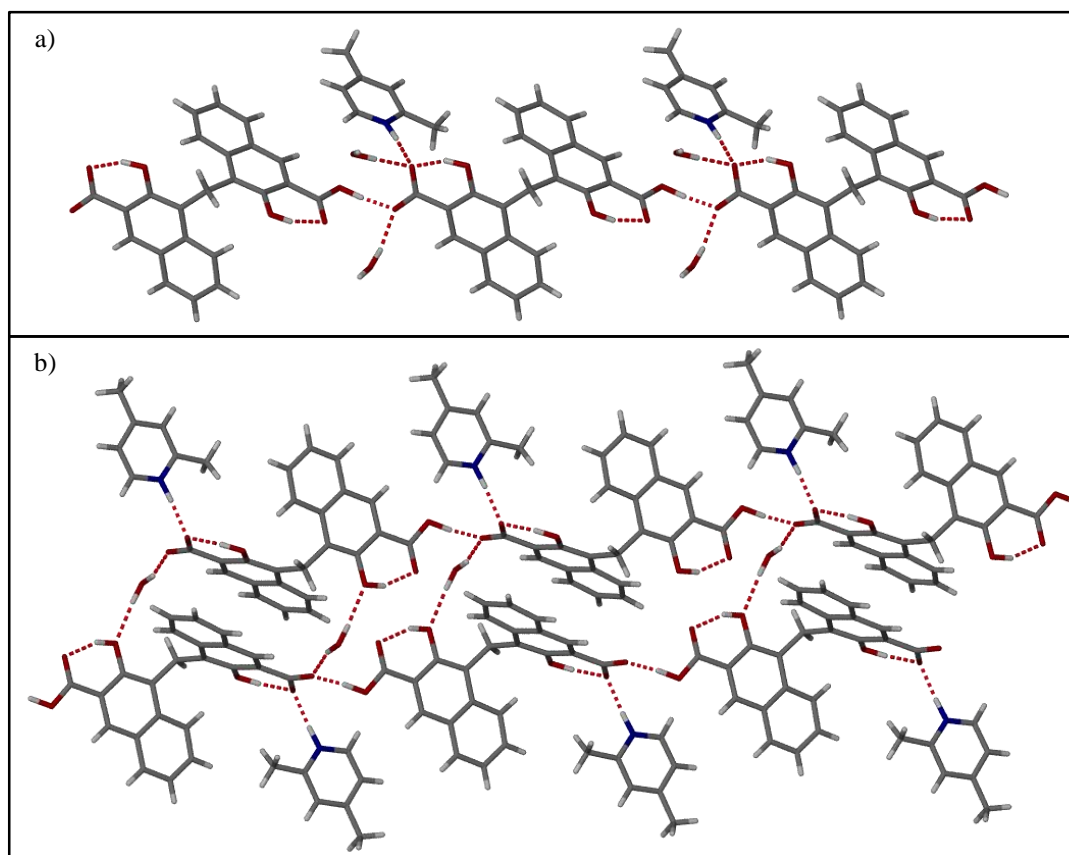


Figure 4.39 The asymmetric unit of **PA4**.

The pamoate ions form hydrogen bonded chains and the 2,4-lutidinium ions hydrogen bond to the pamoate ions only on one side of the pamoate chain, while water molecules hydrogen bond to both sides of the chain (Figure 4.40a). Adjacent chains are connected to each other *via* one of the water molecules to form a sheet (Figure 4.40b).





**Figure 4.40** The hydrogen bond motifs of PA4. a) The hydrogen-bonded chains of pamoate ions with pendant 2,4-lutidinium ions on one side of the chain. The water molecules form hydrogen bonds to either side of the chain. b) Adjacent chains are connected through one of the water molecules and form hydrogen-bonded sheets.

The sheets are joined to each other through hydrogen bond formation between two water molecules and form an extended hydrogen-bonded 3-D network (Figure 4.41). The hydrogen bond parameters are listed in Table 4.9.

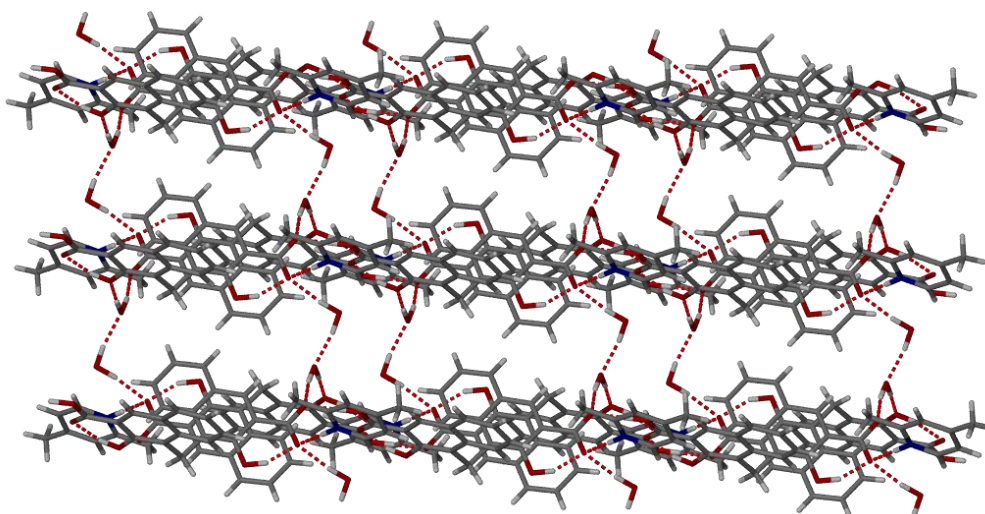


**Figure 4.41** In PA4 the sheets are joined to each other through hydrogen bonds between water molecules and form an extended 3-D network.

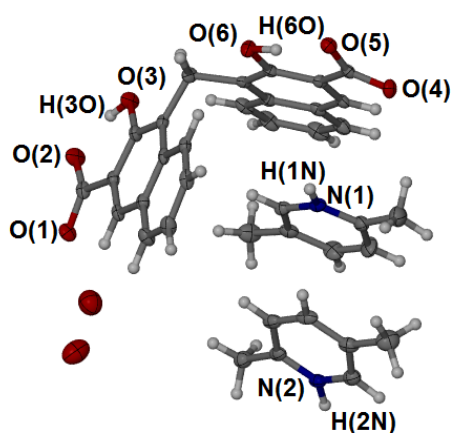
**Table 4.9** Hydrogen bond parameters for **PA4**. The labeling scheme is shown in **Figure 4.39**.

Contact	D-H (Å)	H...A (Å)	D...A (Å)	∠DHA (°)
O3 – H3O...O2	0.90(3)	1.72(3)	2.565(2)	155(2)
O6 – H6O...O5	0.96(3)	1.67(3)	2.558(2)	153(2)
O7 – H8O...O8 <sup>a</sup>	0.96(3)	1.84(3)	2.787(2)	171(3)
O7 – H7O...O5	1.01(3)	1.91(3)	2.918(2)	172(3)
O8 – H10O...O4 <sup>b</sup>	0.92(3)	1.89(3)	2.784(2)	166(2)
O8 – H9O...O3 <sup>c</sup>	0.93(3)	2.02(3)	2.944(2)	174(2)
O1 – H1O...O4 <sup>d</sup>	1.01(3)	1.51(3)	2.520(2)	174(3)
N1 – H1N...O5	0.99(2)	1.78(2)	2.766(2)	176(2)

<sup>a</sup> -x, -y+1, -z+1; <sup>b</sup> -x+1, -y+1, -z+1; <sup>c</sup> x, y+1, z-1 <sup>d</sup> x, y, z+1

#### 4.4.6 2,5-lutidinium pamoate dihydrate, PA5

Crystals of 2,5-lutidinium pamoate dihydrate were grown from a 1:1 THF:H<sub>2</sub>O molar ratio solution in which equimolar amounts of 2,5-lutidine, pamoic acid and *m*-tolunitrile were dissolved. No *m*-tolunitrile was included in the structure. The components crystallise in the orthorhombic crystal system in the Sohncke space group *P*2<sub>1</sub>2<sub>1</sub>2<sub>1</sub>. The asymmetric unit of **PA5** contains two 2,5-lutidinium ions, one doubly deprotonated pamoate ion and two uncoordinated water molecules (Figure 4.42).

**Figure 4.42** The asymmetric unit of **PA5**.

The doubly deprotonated pamoate ion hydrogen bonds to two 2,5-lutidinium pamoate ions to form the structure type **B** base-acid-base units (Figure 4.43a). The units then stack together through  $\pi-\pi$  interactions to form columns that run parallel to the *a* axis (Figure 4.43b). The uncoordinated water molecules fill spaces between the columns. The hydrogen bond parameters are listed in Table 4.10.

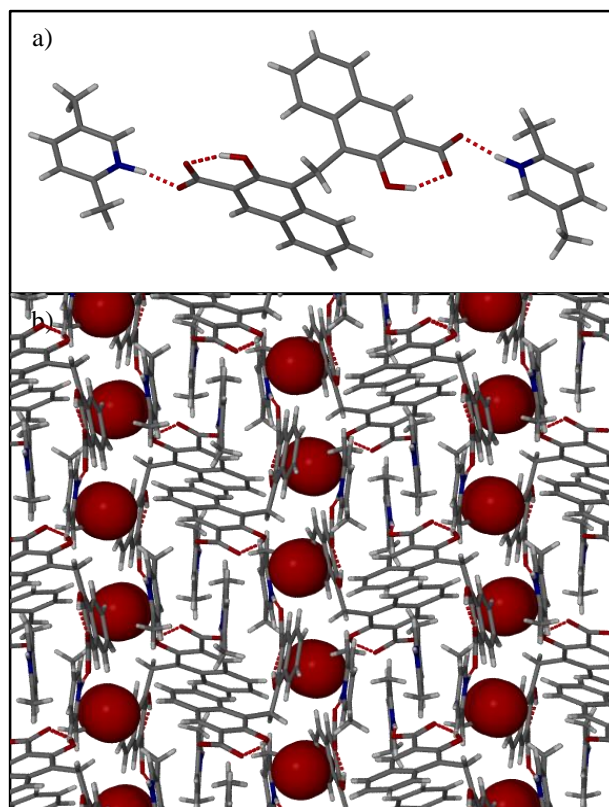


**Figure 4.43** The hydrogen bond motif and packing diagram of **PA5**. a) The doubly deprotonated pamoate ion hydrogen bonds to two 2,5-lutidinium ions to form the base-acid-base unit. b) The base-acid-base units stack together to form columns, viewed down the *b* axis, and water molecules fill the spaces between the columns (shown in spacefill representation).

**Table 4.10** Hydrogen bond parameters for **PA5**. The labeling scheme is shown in **Figure 4.42**.

Contact	D-H (Å)	H...A (Å)	D...A (Å)	$\angle$ DHA (°)
O3 – H3O...O2	0.93(6)	1.62(6)	2.502(3)	155(6)
O6 – H6O...O5	1.05(5)	1.55(6)	2.539(3)	153(5)
N1 – H1N...O1 <sup>a</sup>	1.02(5)	1.54(5)	2.551(3)	169(5)
N2 – H2N...O4 <sup>b</sup>	1.00(4)	1.67(4)	2.655(4)	172(4)

<sup>a</sup>  $-x+1, y+1/2, -z+1/2$ ; <sup>b</sup>  $-x+2, y-1/2, -z+1/2$

#### 4.4.7 4-picolinium pamoate hydrate DMF solvate, PA6

Crystals of **PA6** grew as long rods among crystals of the DMF/pamoic acid solvate (CSD-SIQCIF<sup>10</sup>) from a solution of a 1:1 molar ratio of THF:DMF. These crystals were obtained only once. **PA6** is in the space group  $P\bar{1}$  and the asymmetric unit consists of one singly deprotonated pamoate ion, one 4-picolinium ion, one DMF molecule and one water molecule (Figure 4.44).

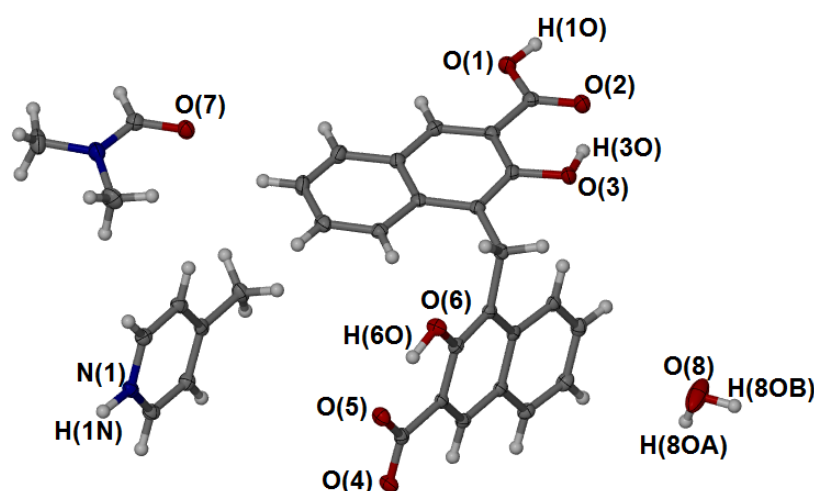
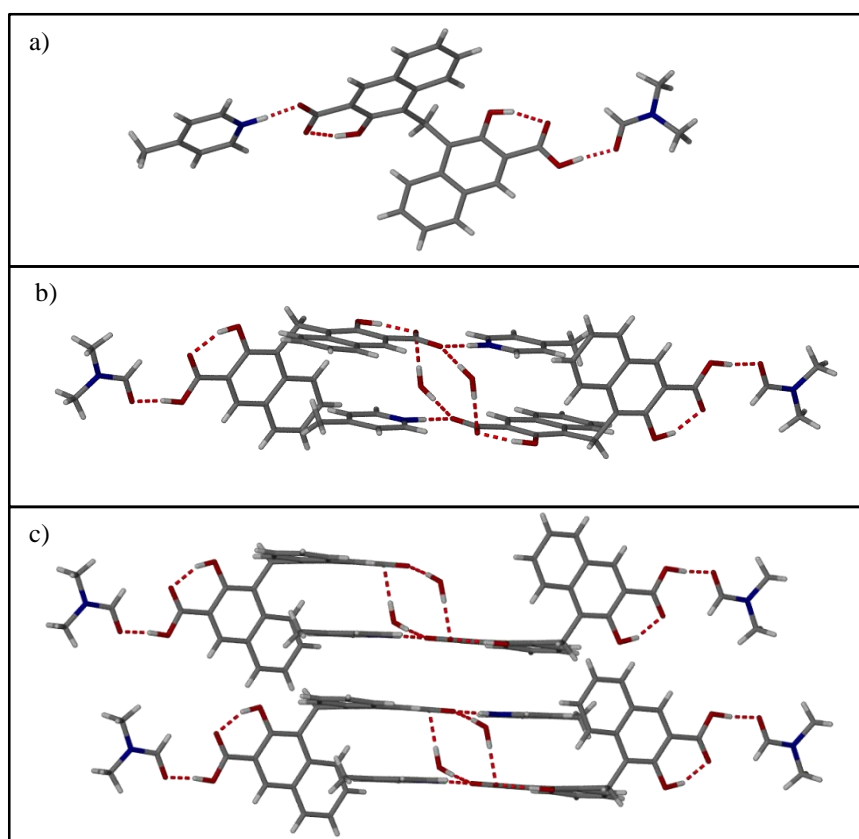


Figure 4.44 The asymmetric unit of **PA6**.

The singly deprotonated pamoate ion hydrogen bonds to 4-picolinium through a  $\text{COO}^- \cdots \text{H}^+\text{N}$  interaction and to a DMF molecule through a  $\text{COOH} \cdots \text{O}$  interaction (Figure 4.45a). The base-acid-solvent unit is connected to other units through hydrogen bond formation between pamoate ions *via* two water molecules (Figure 4.45b). The hydrogen-bonded dimers stack together through offset  $\pi - \pi$  interactions (Figure 4.45c). The hydrogen bond parameters are listed in Table 4.11.



**Figure 4.45** The hydrogen bond motifs observed for **PA6**. a) The base-acid-solvent unit of **PA6**. b) Two units are linked through hydrogen bond formation between the pamoate ions and water molecules. c) The hydrogen-bonded dimers stack together through offset  $\pi-\pi$  interactions.

**Table 4.11** Hydrogen bond parameters for **PA6**. The labeling scheme is shown in **Figure 4.44**.

Contact	D-H (Å)	H...A (Å)	D...A (Å)	$\angle$ DHA (°)
O3 – H3O...O2	0.91(2)	1.70(2)	2.563(1)	157(2)
O6 – H6O...O5	0.96(2)	1.61(2)	2.527(1)	157(2)
O8 – H8OA...O4	0.94(2)	1.94(2)	2.858(2)	166(2)
O8 – H8OB...O5 <sup>a</sup>	0.95(2)	1.91(2)	2.856(2)	176(2)
O1 – H1O...O7 <sup>b</sup>	0.97(2)	1.55(2)	2.519(1)	174(2)
N1 – H1N...O4 <sup>c</sup>	1.04(2)	1.57(2)	2.615(1)	176(2)

<sup>a</sup> -x, -y+1, -z; <sup>b</sup> -x+1, -y+2, -z+1; <sup>c</sup> -x+1, -y+1, -z

**Table 4.12** Selected crystallographic information for the crystal structures discussed in Section 4.4.

	<b>S1</b>	<b>S2</b>	<b>PA1</b>	<b>PA2</b>	<b>PA3</b>	<b>PA4</b>	<b>PA5</b>	<b>PA6</b>
Stoichiometric ratio (anion: cation: solvent:other)	1:1	1:1	1:1	1:1:1	1:2:1	1:1:2	1:1:2	1:1:1:1
Chemical formula	C <sub>34</sub> H <sub>25</sub> NO <sub>6</sub>	C <sub>34</sub> H <sub>25</sub> NO <sub>6</sub>	C <sub>35</sub> H <sub>28</sub> N <sub>2</sub> O <sub>6</sub>	C <sub>39</sub> H <sub>32</sub> N <sub>2</sub> O <sub>7</sub>	C <sub>35</sub> H <sub>34</sub> N <sub>6</sub> O <sub>7</sub>	C <sub>30</sub> H <sub>29</sub> NO <sub>8</sub>	C <sub>37</sub> H <sub>34</sub> N <sub>2</sub> O <sub>8</sub>	C <sub>32</sub> H <sub>32</sub> N <sub>2</sub> O <sub>8</sub>
Formula weight/g.mol <sup>-1</sup>	543.55	543.55	572.59	640.66	650.68	531.54	634.66	572.59
Crystal system	Monoclinic	Monoclinic	Orthorhombic	Triclinic	Monoclinic	Triclinic	Orthorhombic	Triclinic
Space group	<i>P2<sub>1</sub>/n</i>	<i>P2<sub>1</sub>/c</i>	<i>Pna2<sub>1</sub></i>	<i>P<math>\bar{1}</math></i>	<i>C2/c</i>	<i>P<math>\bar{1}</math></i>	<i>P2<sub>1</sub>2<sub>1</sub>2<sub>1</sub></i>	<i>P<math>\bar{1}</math></i>
Z	4	4	4	2	4	2	4	2
<i>a</i> /Å	7.7618(7)	11.0358(19)	17.145(3)	10.653(3)	12.3106(11)	7.6996(14)	10.5605(12)	7.3534(16)
<i>b</i> /Å	17.3278(16)	13.172(2)	8.4603(15)	11.153(3)	11.4800(10)	11.975(2)	15.1593(17)	9.866(2)
<i>c</i> /Å	18.8269(17)	17.721(3)	18.465(3)	13.566(4)	21.981(2)	13.665(3)	19.758(2)	19.879(4)
$\alpha$ /°	90	90	90	85.062(4)	90	85.111(2)	90	97.748(3)
$\beta$ /°	99.8670(10)	101.056(2)	90	74.512(3)	102.6820(10)	89.933(2)	90	90.645(3)
$\gamma$ /°	90	90	90	72.396(3)	90	84.171(2)	90	101.441(2)
Calculated density/g.cm <sup>-3</sup>	1.447	1.428	1.420	1.437	1.426	1.414	1.333	1.359
Volume/Å <sup>3</sup>	2494.7(4)	2528.2(8)	2678.4(8)	1480.6(7)	3030.8(5)	1248.8(4)	3163.1(6)	1399.5(5)
Temperature/K	100(2)	100(2)	105(2)	108(2)	100(2)	100(2)	100(2)	105(2)
$\mu$ /mm <sup>-1</sup>	0.100	0.098	0.098	0.099	0.101	0.103	0.094	0.098
Independent reflections	5752	5802	4033	7068	3518	5658	6526	6700
<i>R</i> <sub>int</sub>	0.0329	0.0289	0.0474	0.0289	0.0230	0.0244	0.0391	0.0186
<i>R</i> <sub>1</sub> [I > 2(I)]	0.0652	0.0584	0.0536	0.0966	0.0549	0.0644	0.0616	0.0504

## 4.5 Important structural requirements for framework formation

One of the important questions regarding the work discussed in this chapter – other than the age-old question, “*What can it do?*” – is how/why does it form? Is there an obvious structural design feature that allows five seemingly robust isostructural host-guest systems to be isolated?

The five isostructural framework-type materials (**2** for ease of reference) and the salts **S1** and **S2** discussed in Section 4.4.1 contain similar components, i.e. pamoic acid and 4-phenylpyridine. The first obvious difference between these structures is the degree of ionisation of the pamoate ion. In **2** the pamoate ion is doubly deprotonated, allowing for the formation of base-acid-base units. From a previous study conducted in our group<sup>1</sup> it was found that the base-acid-base unit is the less observed structure type for pamoate solvates but it is observed in the solvent-free salts of three of the lutidinium pamoate series. In the salts **S1** and **S2** the pamoate ion is singly deprotonated, allowing for the formation of the hydrogen-bonded pamoate chains which is more often observed in the pamoate solvates.<sup>1</sup> The previously-mentioned study suggested that the ionisation of the pamoate ion, and consequently the structure type observed, is possibly due to a  $pK_a$  effect of solvent and co-crystallisation agent. Table 4.13 contains a summary of hydrogen bonding motifs observed in structures described so far in this chapter, namely the framework-type series **2** and the structures discussed in Section 4.4. Figure 4.46 illustrates the different pamoate hydrogen bonding motifs mentioned in Table 4.13. From the table it is evident that if the pamoate ion is singly deprotonated it is highly likely to form a hydrogen-bonded pamoate chain, unless there are water molecules present in the structure in which case the water molecules then interrupt the chain formation by rather forming an array of hydrogen bonded acid and water molecules (**PA4**) or a hydrogen-bonded dimer consisting of solvent-acid-base units (**PA6**).



**Table 4.13** The co-crystallisations with pamoic acid and the resulting pamoate bonding motif. All crystallisations were done in a 1:1 pamoic acid: co-former ratio. In bold in brackets is the code for the structure for ease of reference.

Cofomer	Solvent system	Product	
		Ionisation of pamoic acid	Structural unit
4-phenylpyridine ( <b>2·THF</b> )	1:1 THF/H <sub>2</sub> O	Doubly deprotonated	b-a-b unit
4-phenylpyridine ( <b>2·Dioxane</b> )	1:1 1,4-dioxane/H <sub>2</sub> O	Doubly deprotonated	b-a-b unit
4-phenylpyridine ( <b>2·DMSO</b> )	1:1 DMSO/H <sub>2</sub> O	Doubly deprotonated	b-a-b unit
4-phenylpyridine ( <b>2·Acetone</b> )	1:1 acetone/H <sub>2</sub> O	Doubly deprotonated	b-a-b unit
4-phenylpyridine ( <b>2·DMF</b> )	1:1 DMF/H <sub>2</sub> O	Doubly deprotonated	b-a-b unit
4-phenylpyridine ( <b>S1</b> )	1:1 DMSO/H <sub>2</sub> O	Singly deprotonated	Pamoate chain
4-phenylpyridine ( <b>S2</b> )	1:1 MeCN/H <sub>2</sub> O, MeOH/H <sub>2</sub> O, EtOH/H <sub>2</sub> O	Singly deprotonated	Pamoate chain
1,2-bis(4-pyridyl)ethane ( <b>PA1</b> )	1:1 NMP/DMF (layered)	Singly deprotonated (shared proton)	Infinite b-a-b-a chain
1,10-phenanthroline ( <b>PA2</b> )	THF	Singly deprotonated	Pamoate chain
2-aminopyrimidine ( <b>PA3</b> )	1:1 THF/H <sub>2</sub> O	2 shared protons	Infinite b-a-b-a chain
2,4-lutidine ( <b>PA4</b> )	1:1 THF/H <sub>2</sub> O	Singly deprotonated	Infinite hydrogen bond array of acid-water
2,5-lutidine ( <b>PA5</b> )	1:1 THF/H <sub>2</sub> O	Doubly deprotonated	b-a-b unit
4-picoline ( <b>PA6</b> )	1:1 THF/H <sub>2</sub> O	Singly deprotonated	Base-acid-solvent h-bonded dimer <i>via</i> H <sub>2</sub> O molecules

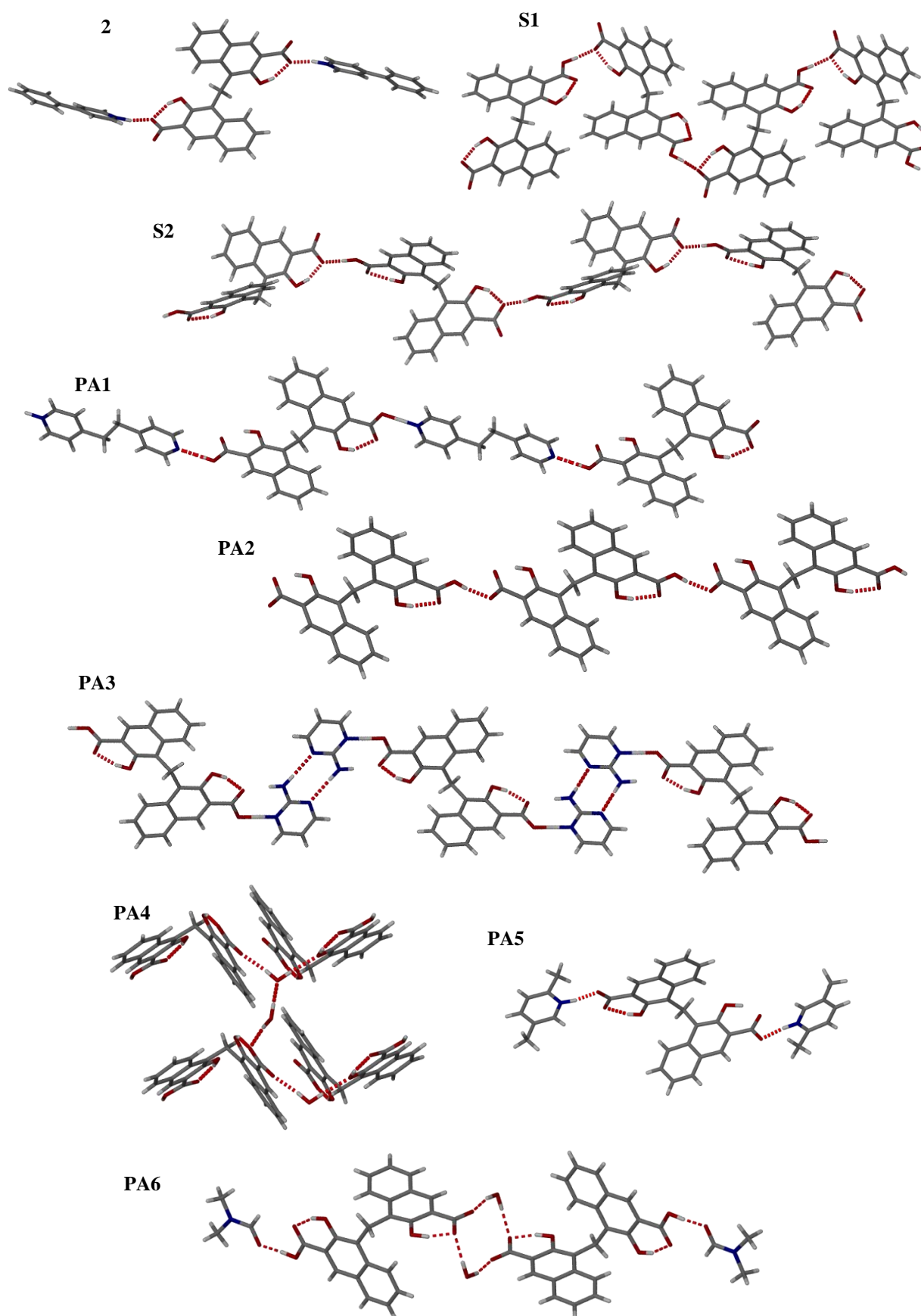


**Figure 4.46** The different hydrogen bonding motifs observed in structures obtained with pamoic acid discussed in this chapter.

If the pamoate ion is doubly deprotonated it appears to be extremely likely that a base-acid-base unit will be formed. From the results of the previously published study<sup>1</sup> and the evidence from the current study, it seems that if a pamoate chain is the basic structural feature of the crystal structure, it is highly unlikely that the molecules will pack in such a way as to form a framework. Although the chances of actually isolating a framework structure is quite low, it does appear to be more likely should the pamoate ion form the base-acid-base units or if the pamoate chain is interrupted by the presence of water molecules in the structure. It is however clear that even if the characteristic base-acid-base units are formed, it is in no way a guarantee that a framework will be formed. This is probably due to the unique size and shape of 4-phenylpyridine as well as the number of nitrogen atoms in this molecule. If one studies a related compound, 4,4'-bipyridine, with pamoic acid (CSD-MOXRUN<sup>27</sup>) the structure is completely different to any formed with 4-phenylpyridine simply due to the presence of an extra nitrogen atom. The extra hydrogen bond acceptor site allows for the disruption of the base-acid-base unit, which leads to the formation of an infinite acid-base chain, similar to the one seen in **PA1** in Figure 4.46. However, base-acid-base units are known to form with some of the isomers of lutidine<sup>1</sup> and yet these did not lead to the formation of frameworks. This is possibly due to the shape of 4-phenylpyridine and the presence of an extra phenyl ring. The walls of the framework are formed by the C—H... $\pi$  interactions of the phenyl ring of 4-phenylpyridine with the aromatic region of pamoic acid. This allows the pamoate ion and the 4-phenylpyridinium ion to form a slightly curved structure, consequently creating a pocket for the solvent molecule to reside in (Figure 4.47).

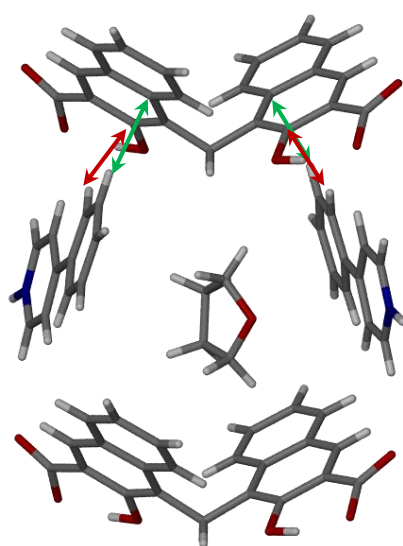


**Figure 4.47** The C—H... $\pi$  interaction of the 4-phenylpyridinium ion with the pamoate ion creates a pocket for the solvent to reside in.

In the salts **S1** and **S2** the C–H... $\pi$  interactions are not observed, but rather  $\pi$ - $\pi$  stacking between aromatic rings of 4-phenylpyridinium and the pamoate ions. This does not lead to the construction of the curved structure therefore it does not form a channel-like structure in the solid state.

There is a very delicate balance between the cocrystallisation agent chosen and the solvent system used for a crystallisation in order to purposely engineer a specific structure type in the case of pamoate salts. It is possible that the  $pK_a$  (Table 4.14) of the cocrystallisation agent in the chosen solvent system has an effect on the ionisation of pamoic acid which, in turn, determines the hydrogen bond motif of the crystal structure. The information in Table 4.13 suggests that the particular combination of 4-phenylpyridine with any of 1:1 THF/H<sub>2</sub>O, 1,4-dioxane/H<sub>2</sub>O, DMSO/H<sub>2</sub>O, acetone/H<sub>2</sub>O and DMF/H<sub>2</sub>O reliably produces a framework structure. However, the combination of 4-phenylpyridine with EtOH/H<sub>2</sub>O, MeOH/H<sub>2</sub>O and acetonitrile/H<sub>2</sub>O does not create the correct environment for the double deprotonation of pamoic acid, therefore only forming the pamoate chains. This could be due to a combination of the  $pK_a$  of 4-phenylpyridine and the solvent not allowing charge transfer to occur from pamoic acid to 4-phenylpyridine.

**Table 4.14** The  $pK_a$  values of the isomers of lutidine and picoline, 1,10-phenanthroline<sup>28</sup> and 4-phenylpyridine<sup>29</sup> at 25 °C.

Base	$pK_a$
2,3-lutidine	6.57
2,4-lutidine	6.99
2,5-lutidine	6.40
2,6-lutidine	6.65
3,4-lutidine	6.46
3,5-lutidine	6.15
2-picoline	6.00
3-picoline	5.70
4-picoline	5.99
4-phenylpyridine	5.50
1,10-phenanthroline	4.84

In summary, from the results presented in this chapter, it seems that in order to obtain a framework material a dianion should be combined with a monocation. This combination seems to produce the structure types most likely to form framework materials. However, the shape of the acid and base also seems to play an important role in the formation of a framework material.

## 4.6 Summary and conclusion

This chapter discussed the synthesis of a second host-guest system with a framework-like structure and the subsequent investigation into the thermal behaviour and stability of the framework. The 4-phenylpyridinium pamoate framework does not possess actual channels, but rather discrete voids in which the solvent resides. Exchange studies were performed even though the framework did not possess channels since it is well known that some structures may be intrinsically porous<sup>30</sup> even though they do not have continuous channels. This was unfortunately not the case for this particular framework, although it is possible to crystallise the framework from 1:1 solvent/H<sub>2</sub>O combinations such as THF/H<sub>2</sub>O, 1,4-dioxane/H<sub>2</sub>O, DMSO/H<sub>2</sub>O, acetone/H<sub>2</sub>O and DMF/H<sub>2</sub>O with the particular solvent present in the voids. This framework also has the remarkable ability to selectively include 1,4-dioxane from mixtures of 1,4-dioxane with THF, DMSO, acetone and DMF. Only when 1,4-dioxane is not present will it selectively include THF in the case of mixtures of THF/acetone. Mapping the Hirshfeld surface of each solvent molecule helped to identify whether there were certain intermolecular interactions present that would favour one solvent molecule over another. There is an interaction in the structures containing THF and 1,4-dioxane that is not present in the other structures and it is surmised that this interaction may have an added stabilisation effect. The methylene protons of the pamoate ion that point in towards the cavity have a favourable interaction with the solvent molecules, possibly creating a complementary shape that particularly suits the shapes of THF and 1,4-dioxane. This is also reflected in the densities of the crystal structures of **2·THF** and especially **2·Dioxane**. The density of **2·Dioxane** is significantly higher than those of the other frameworks, which indicates, according to the density rule, that this is the most stable structure. Since 1,4-dioxane has a better fit in the cavity of the framework, the molecules are able to pack more efficiently, which leads to less void space in the structure and an overall more stable structure. This further explains why 1,4-dioxane is the preferred solvent for encapsulation in the competition experiments. The selectivity between THF and 1,4-dioxane was also not as pronounced as for the other solvent

combinations with acetone. This could be due to the similar shape of THF and 1,4-dioxane, and indeed smaller difference in crystal density between the two ( $1.35 \text{ g cm}^{-3}$  for THF and  $1.38 \text{ g cm}^{-3}$  for 1,4-dioxane), which indicates that **2·THF** is also a more stable structure, yet not as stable as **2·Dioxane**.

The basic structural feature of **2** was compared to that of the two isolated salts **S1** and **S2** and various other structures obtained with pamoic acid during the course of this study. This was done in order to identify any structural features that appeared to be more likely to form framework-like structures. Initially the aim was to use N-heterocycles with more than one nitrogen atom. These could potentially be used as linkers between two pamoic acid molecules to form cyclic structures that could stack together to form channels in the solid state. The particular shape of pamoic acid with the bend between the two naphthyl moieties would also play an important role in the design of this cyclic structure. Unfortunately the extra hydrogen bond acceptor site only allowed for the formation of infinite chains of acid-base units in cases such as 1,2-bis(4-pyridyl)ethane and 2-aminopyrimidine. These structures also tended to not include any solvent. It was therefore decided to also include N-heterocycles with only one nitrogen atom in the study to see what effect this has on the crystal structure. This led to the discovery of a number of crystal structures that contained either pamoate chains or base-acid-base units as their main structural feature. It was exactly the formation of this particular base-acid-base unit that led to the solid-state packing motif of the five isostructural frameworks with 4-phenylpyridine. Base-acid-base units have however been previously identified as a motif in structures with pamoic acid, yet none of these have ever formed frameworks. This is possibly due to the extra phenyl ring of 4-phenylpyridine which allows for very specific CH -  $\pi$  interactions between the 4-phenylpyridinium and pamoate ions. This allows the two ions to form a cyclic structure – ironically *not* through hydrogen bonding between the carboxylate group and nitrogen atom – consisting of two pamoate ions and two 4-phenylpyridinium ions that form a discrete pocket for the solvent.

This of course begs the question of how we can modify the components that we know to form a framework-type system in order to design a system that is in fact permeable or porous? This could be investigated by the “simple” addition of a methyl group to various positions on 4-phenylpyridine (Figure 4.48). The *meta* and *ortho* isomers shown in the first two diagrams could be of great interest. If the methyl groups are only added on one side of the phenyl group it could create extra space on the side of 4-phenylpyridine that does not form the C – H... $\pi$

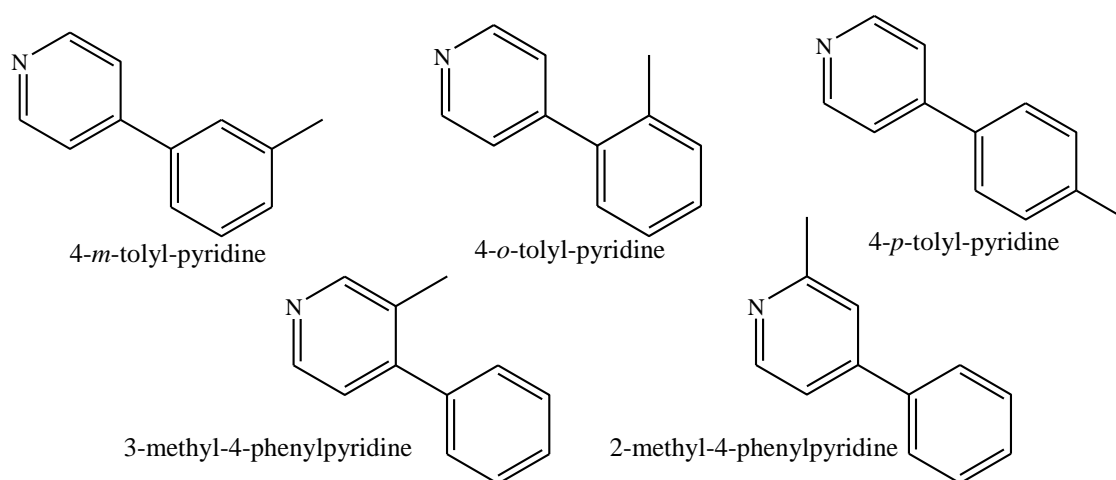


**Figure 4.48** The various possible positions for methyl substitution on 4-phenylpyridine.

stacking interactions with the pamoate ion, effectively lengthening the void and making it large enough to connect to a neighbouring void, forming a continuous channel. Addition of methyl groups on the pyridine ring might influence the  $pK_a$  of 4-phenylpyridine to such an extent that it changes the interaction with the solvent system potentially leading to a different degree of ionisation of pamoic acid. It has been shown that the ionisation of the pamoate ion determines the hydrogen bond motif. The addition of a methyl group on the pyridine ring could either increase or decrease the ability of the nitrogen atom to be a hydrogen bond acceptor, depending on the position of the methyl group. However, 3,4-lutidine appears to be a very good compound for framework formation and the positions of the methyl groups seem to be essential, therefore it would be interesting to investigate the effect on the crystal structure of including a methyl group in the 3 position on the pyridyl ring of 4-phenylpyridine.

From this study it is however clear that chain formation of only pamoate ions should be avoided, unless water molecules form part of the chain, since this hydrogen bonding motif does not seem to be able to form framework structures. This can be achieved by finely tuning the solvent system and the choice of cocrystallisation agent to ensure the correct ionisation of pamoic acid.



## 4.7 References

1. H. Wahl, D. A. Haynes and T. le Roex, *CrystEngComm*, 2011, **13**, 2227-2236.
2. H. Wahl, D. A. Haynes and T. le Roex, *Chem. Commun.*, 2012, **48**, 1775 - 1777.
3. H. Wahl, D. A. Haynes and T. le Roex, *CrystEngComm*, 2013, **15**, 2450-2455.
4. I. J. Bruno, J. C. Cole, P. R. Edgington, M. Kessler, C. F. Macrae, P. McCabe, J. Pearson and R. Taylor, *Acta Crystallogr. B*, 2002, **B58**, 389 - 397.
5. C. F. Macrae, I. J. Bruno, J. A. Chisholm, P. R. Edgington, P. McCabe, E. Pidcock, L. Rodriguez-Monge, R. Taylor, J. van de Streek and P. A. Wood, *J. Appl. Crystallogr.*, 2008, **41**, 466 - 470.
6. C. F. Macrae, P. R. Edgington, P. McCabe, E. Pidcock, G. P. Shields, R. Taylor, M. Towler and J. van de Streek, *J. Appl. Crystallogr.*, 2006, **39**, 453 - 457.
7. R. Taylor and C. F. Macrae, *Acta Crystallogr. B*, 2001, **B57**, 815 - 827.
8. L. J. Barbour, *Chem. Commun.*, 2006, 1163-1168.
9. A. M. Pivovar, K. T. Holman and M. D. Ward, *Chem. Mater.*, 2001, **13**, 3018-3031.
10. M. Du, C.-P. Li, X.-J. Zhao and Q. Yu, *CrystEngComm*, 2007, **9**, 1011-1028.
11. S. K. Wolff, D. J. Grimwood, J. J. McKinnon, M. J. Turner, D. Jayatilaka and M. A. Spackman, *CrystalExplorer (Version 3.1)*, (2012), University of Western Australia.
12. M. A. Spackman and D. Jayatilaka, *CrystEngComm*, 2009, **11**, 19 - 32.
13. J. J. McKinnon, M. A. Spackman and A. S. Mitchell, *Acta Crystallogr. B*, 2004, **60**, 627-668.
14. A. S. Tayi, A. K. Shveyd, A. C.-H. Sue, J. M. Szarko, B. S. Rolczynski, D. Cao, T. J. Kennedy, A. A. Sarjeant, C. L. Stern, W. F. Paxton, W. Wu, S. K. Dey, A. C. Fahrenbach, J. R. Guest, H. Mohseni, L. X. Chen, K. L. Wang, J. F. Stoddart and S. I. Stupp, *Nature*, 2012, **488**, 485 - 489.
15. J. J. McKinnon, D. Jayatilaka and M. A. Spackman, *Chem. Commun.*, 2007, 3814 - 3816.
16. M. A. Spackman and J. J. McKinnon, *CrystEngComm*, 2002, **4**, 378 - 392.
17. S. Lohani and J. D. W. Grant, in *Polymorphism in the pharmaceutical industry*, ed. R. Hilfiker, Wiley-VCH Verlag GmbH & Co., Weinheim, Germany, 2006, pp. 21 - 42.
18. A. Kitaigorodskii, *Molecular crystals and molecules*, Academic Press, Inc., New York, 1973.
19. M. R. Caira, in *Encyclopedia of supramolecular chemistry*, eds. J. L. Atwood and J. W. Steed, M. Dekker, 2004, vol. 2, p. 1129.

20. W. C. McCrone, in *Physics and chemistry of the organic solid state*, eds. D. Fox, M. M. Labes and A. Weissberger, Interscience, 1965, vol. 2, pp. 726 - 766.
21. *Cambridge Structural Database version 5.35 (2013) with 3 updates.*
22. F. H. Allen, *Acta Crystallogr. B*, 2002, **B58**, 380 - 388.
23. F. H. Allen and O. Kennard, *Chem. Des. Autom. News*, 1993, **8**, 31 - 37.
24. D. A. Haynes, W. Jones and W. D. S. Motherwell, *CrystEngComm*, 2005, **7**, 538-543.
25. D. A. Haynes, Z. F. Weng, W. Jones and W. D. S. Motherwell, *CrystEngComm*, 2009, **11**, 254-260.
26. T.-M. Shang, Q.-F. Zhou and J.-H. Sun, *Acta Crystallogr. E*, 2007, **63**, o506-o508.
27. M. Du, Z.-H. Zhang, W. Guo and X.-J. Fu, *Cryst. Growth Des.*, 2009, **9**, 1655-1657.
28. R. C. Weast, ed., *CRC handbook of chemistry and physics*, 66th edn., CRC Press, Boca Raton, FL, 1985.
29. R. K. Bansal, *Heterocyclic chemistry*, 3rd edn., New Age International, New Delhi, 1999.
30. L. Dobrzańska, G. O. Lloyd, H. G. Raubenheimer and L. J. Barbour, *J. Am. Chem. Soc.*, 2005, **128**, 698-699.

# CHAPTER 5

## A HOST FRAMEWORK BASED ON N,N'-BIS(GLYCINYL) PYROMELLITIC DIIMIDE

---

During the investigation into identifying compounds that could potentially form framework materials numerous acids were combined with various bases. In general, acids that had two carboxylic acid groups were selected, since this appeared to be a helpful feature in the previously discussed framework materials. An extended hydrogen-bonded network with channels in the solid state was formed in framework **1** (Chapter 2) due to the combination of singly protonated pamoate ions and water molecules. In the framework-type structures discussed in chapter four the ionisation of pamoic acid again determined the solid state packing. In this particular case, due to the doubly deprotonated pamoate ion, it was possible to form base-acid-base units that stacked together in such a way that constricted solvent pockets were formed in the solid state. The particular shape of pamoic acid also plays a vital role in the formation of these structures. The bend in the pamoic acid molecule combined with the water molecules in framework **1** dictate the shape of the hydrogen bonded pamoate-water units, which in turn determines the size and shape of the channels formed upon close packing. In the framework-type structures discussed in chapter 4 the bulky shape and bend in the pamoate ion causes solvent molecules to be trapped between two pamoate ions, consequently forming a series of constricted pockets upon close packing. Therefore dicarboxylic acids that either had a bend or twist in their structure, such as diphenic acid, were selected for further studies. The basis on which N,N'-bis(glyciny)pyromellitic diimide (pyromellitic diimide from here on) was selected was the two carboxylic acid groups that could freely rotate around their methylene linkage. This could allow the carboxylic acid groups to either adopt a *cis* or *trans* configuration (Figure 5.1). This is illustrated using structures taken from the Cambridge Structural Database.<sup>1-3</sup> The structures are titled CSD-GENNAP<sup>4</sup>, CSD-OWIFEG<sup>5</sup> and OWIFIK<sup>5</sup> from left to right. The *trans* conformation allows the aromatic region of the molecule to lie completely flat, while the *cis* conformation causes a slight flexing of the aromatic region of the molecule.

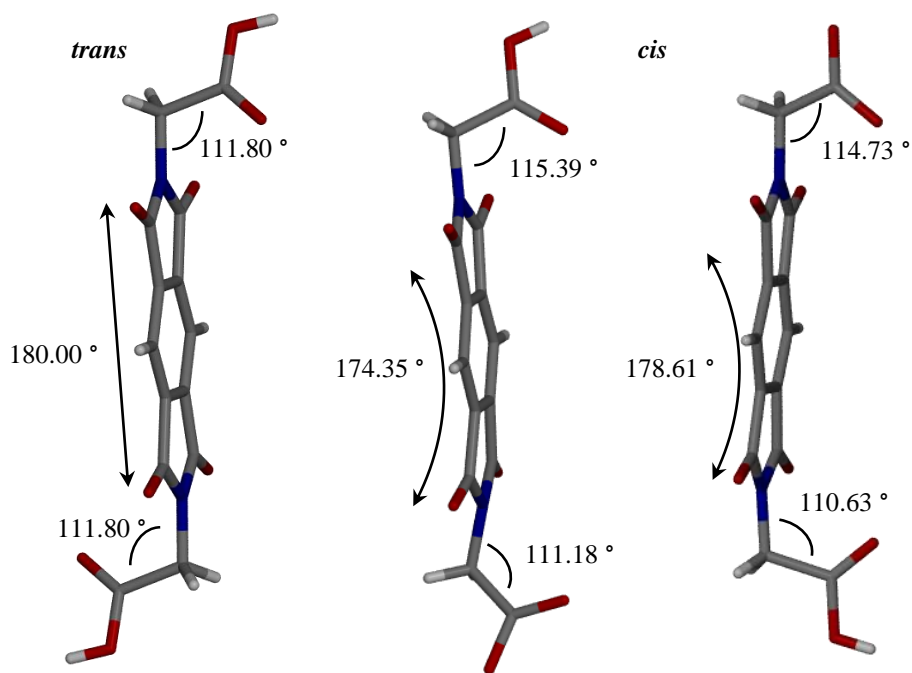


**Figure 5.1** The two conformations of the pyromellitic diimide in CSD-GENNAP<sup>4</sup>, CSD-OWIFEG<sup>5</sup> and OWIFIK<sup>6</sup> from left to right. The *trans* configuration allows the aromatic part of the molecule to lie perfectly flat. This *cis* conformation however causes a slight bend in the aromatic part. It is not clear whether the conformation of the molecule is solvent dependent.

The *cis* conformation would be ideal for the aims of this project. If it were possible to crystallise the pyromellitic diimide in the *cis* conformation in such a way that it would hydrogen bond to a neighbouring pyromellitic diimide molecule to form a square-shaped unit, we could potentially include solvent in the space created (Figure 5.2).

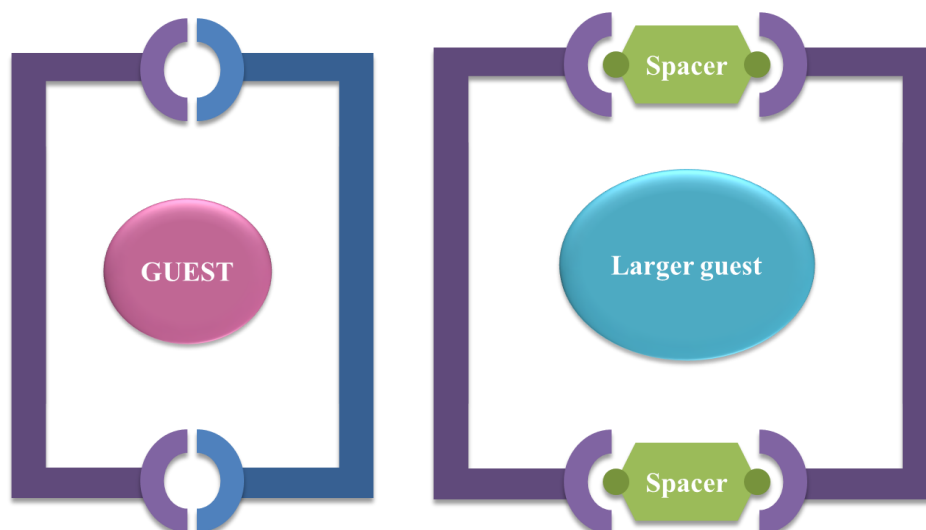


**Figure 5.2** A diagram representing the design aim with the pyromellitic diimide. If the pyromellitic diimide adopts the *cis* conformation in the crystal structure, it could possibly form complementary hydrogen bonds to another pyromellitic diimide molecule to form the square unit seen on the left that could include a guest molecule in the space created. Alternatively, in the diagram on the right a spacer molecule can be used to hydrogen bond to two pyromellitic diimide molecules. This could possibly enlarge the space created, allowing a larger guest to occupy the space.

It is theoretically possible to include a spacer molecule that could hydrogen bond to the pyromellitic diimide molecule on either side, thus creating a larger space in between to possibly accommodate a larger guest molecule (shown in Figure 5.2).

There are 17 organic crystal structures in the CSD containing pyromellitic diimide.<sup>6</sup> Of these, only 5 have the carboxylic acid groups of pyromellitic diimide in the *cis* position. It is presumably not a favoured conformation for the molecule. Two of these crystal structures (CSD-OWIFEG<sup>5</sup> and CSD-OWIFIK<sup>5</sup>) will be briefly discussed due to their interesting hydrogen bonding patterns. OWIFIK forms the square hydrogen-bonded units between pyromellitic diimide molecules as described in Figure 5.2. The structure of OWIFEG however demonstrates that although the pyromellitic diimide is in the *cis* conformation, the packing motif of OWIFIK is not always observed. Therefore even if the pyromellitic diimide is in the “correct” conformation it is not a guarantee that the dimers will be formed.

The asymmetric unit of OWIFIK contains two pyromellitic diimide molecules and one protonated 1,10-phenanthroline molecule. The two pyromellitic diimide molecules face each other to resemble the square unit discussed above, but each pyromellitic diimide hydrogen bonds to the molecule adjacent, which in turn hydrogen bonds to the other pyromellitic diimide molecule found in the asymmetric unit (Figure 5.3a). This forms an infinite double-stranded chain of pyromellitic diimide molecules. The 1,10-phenanthroline fills the space in between the hydrogen bonded strands while forming a hydrogen bond to one of the pyromellitic diimide molecules in the chain (Figure 5.3b). The next double-stranded chain with the hydrogen-bonded 1,10-phenanthroline interdigitates with the first chain, shown as the blue spacefill molecules in Figure 5.3c.

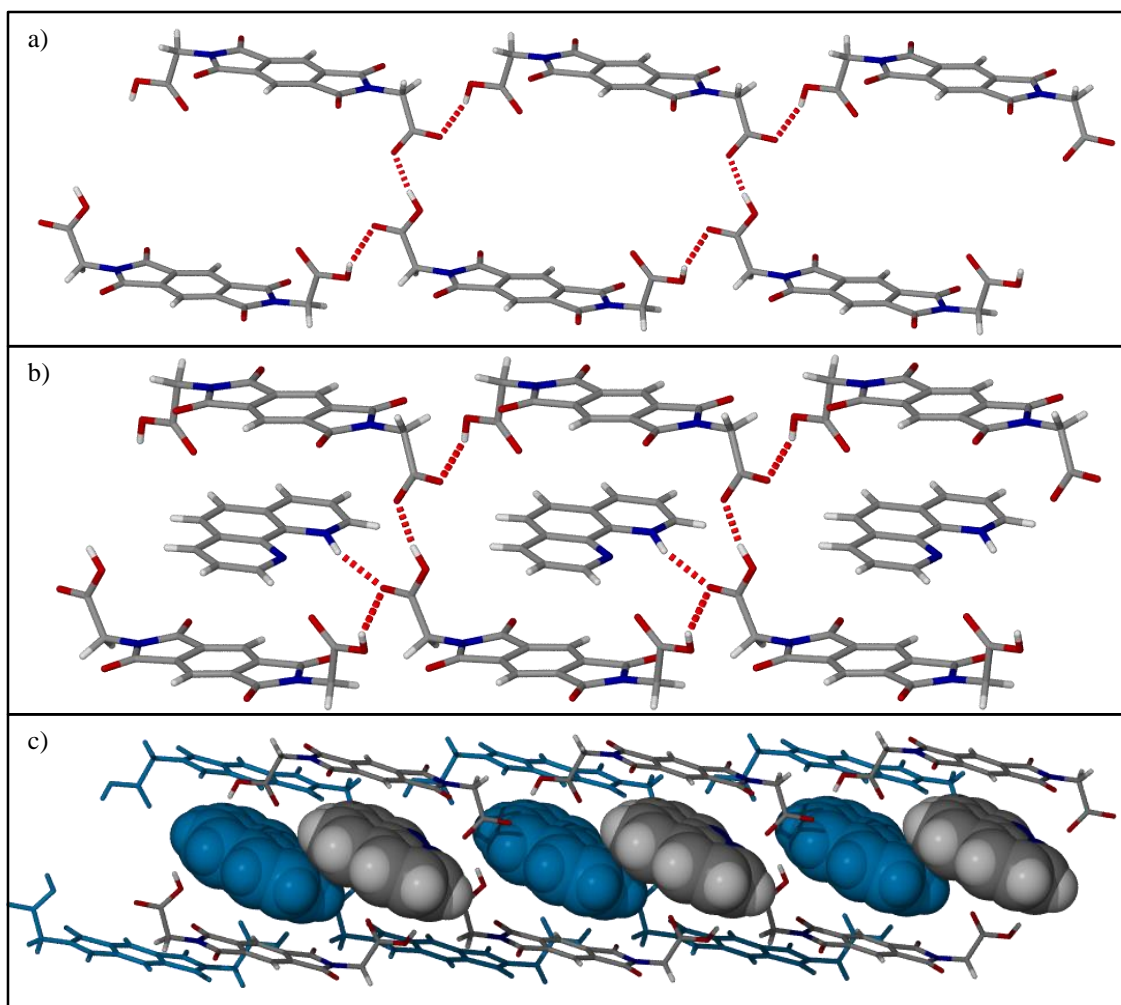


**Figure 5.3** The hydrogen bond motifs in OWIFIK a) The hydrogen-bonded pyromellitic diimide molecules form a double-stranded chain. b) The 1,10-phenanthroline hydrogen bonds to one of the pyromellitic diimide molecules in the chain, filling the space in between the molecules. c) The 1,10-phenanthroline ions of the second chain (shown here in blue) insert halfway into the first chain.

The pyromellitic diimide molecules of OWIFEG do not form the double-stranded chains seen in OWIFIK. On the contrary, they form a single hydrogen-bonded chain (Figure 5. 4a) with pendant hexamethylenetetrammonium ions (Figure 5. 4b). The chains of pyromellitic diimide ions and the pendant hexamethylenetetrammonium ions stack together as shown in Figure 5. 4c.

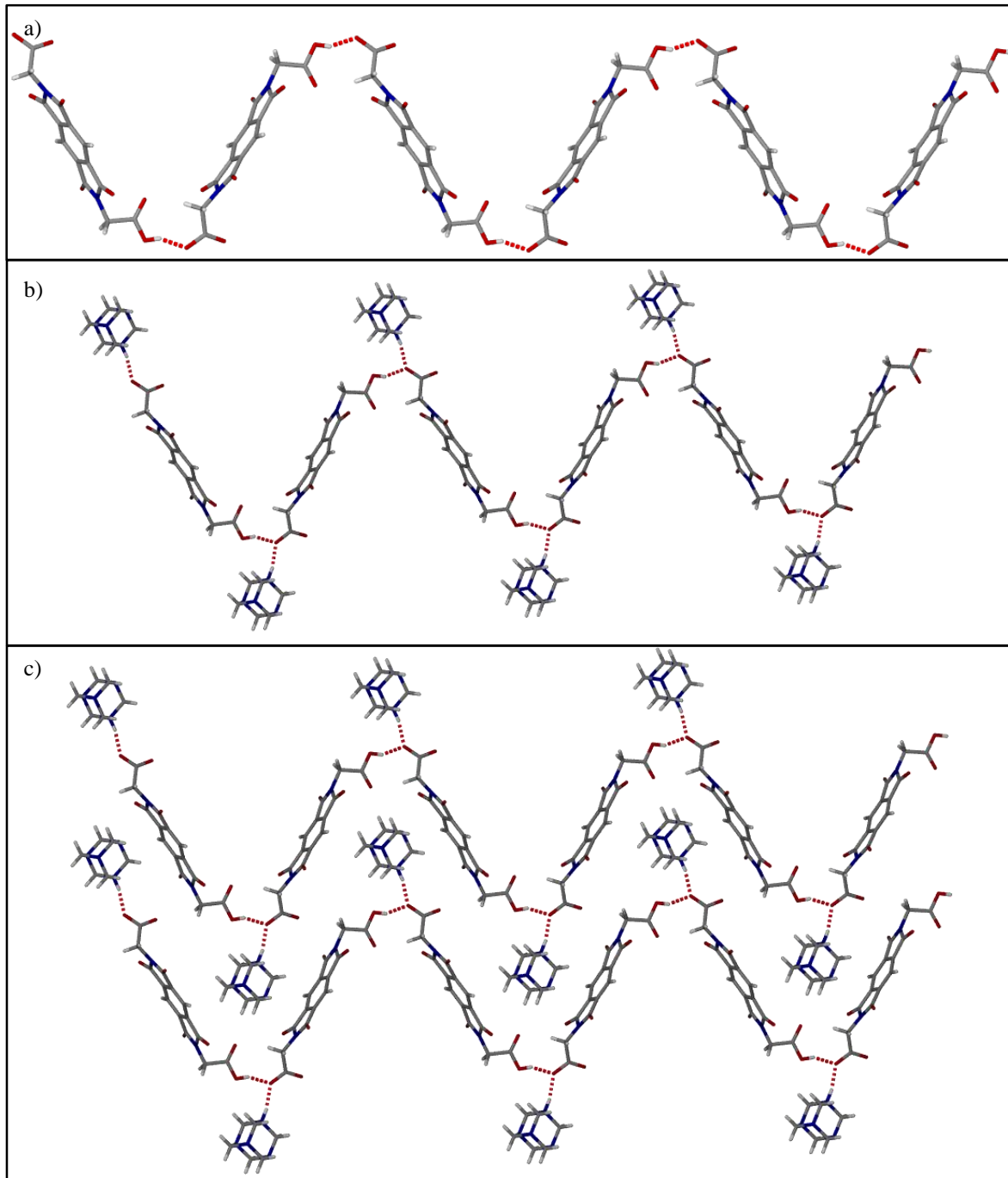


**Figure 5.4** a) The pyromellitic diimide ions form a single hydrogen-bonded chain. b) The hexamethylenetetrammonium ions hydrogen bond to the pyromellitic diimide ions like pendants on a chain. c) The chains then stack together and form a zig-zag pattern throughout the structure.

The reason for analysing previous structures of pyromellitic diimide is to investigate whether it would be theoretically possible to obtain a framework material with this compound. It seems unlikely that the *cis* conformation of the molecule will be obtained since only five of the 17 structures in the CSD that contain pyromellitic diimide crystallise in this conformation. It is also possible that the cation could coordinate to the pyromellitic diimide in such a way



that it fills the space between the two pyromellitic diimide molecules as seen in OWIFIK. This obstacle could be overcome by crystallising the pyromellitic diimide and cocrystallisation agent from solvents with possible hydrogen bond acceptor or donor sites. If the solvent contains hydrogen bond donor sites it could potentially directly coordinate to the carboxylic acid group of pyromellitic diimide in such a way that it could fill the space between two pyromellitic diimide molecules in the *cis* conformation. If the solvent has hydrogen bond acceptor sites, not only could it potentially coordinate to the pyromellitic acid, but it could also potentially coordinate to the cation and prohibit the coordination of the cation within the space between two pyromellitic diimide molecules.

Inclusion studies with N,N'-bis(glyciny)pyromellitic diimide have shown that the hydrogen bond formation between the carboxylic acids is a reliable and robust supramolecular synthon that produces hydrogen-bonded networks with well-defined spaces for guest molecules in the solid state.<sup>4, 7</sup> It would therefore be interesting to investigate what effect the inclusion of various N-heterocycles with hydrogen bond donor or acceptor sites would have on the hydrogen bond formation between pyromellitic diimide molecules, and whether it is possible to identify structural motifs from these cocrystallisations that could aid in the formation of framework materials.

The synthesis of the pyromellitic diimide molecule will first be discussed in Section 5.1 after which the cocrystallisations with pyromellitic diimide that yielded crystals will be discussed in Section 5.2. Section 5.3 contains a description and discussion of a third framework material isolated in this study, as well as subsequent analysis of the framework. In Section 5.4 the results discussed in this chapter will be analysed and discussed in order to draw conclusions about the requirements for framework formation in this system.

## 5.1. Synthesis of N,N'-bis(glyciny)pyromellitic diimide

Pyromellitic diimide is a relatively easy molecule to synthesise. The synthetic procedure published by Baroah *et al.*<sup>4</sup> was followed, although a few changes were made to the procedure. Pyromellitic dianhydride (1.114 g, 5.1 mmol) was dissolved in acetic acid (50 ml) by warming the mixture to 100 °C as opposed to 40 °C, as reported in the literature. Glycine (0.790 g, 10.5 mmol) was ground to a fine powder and added to the acetic acid solution, and the mixture refluxed overnight at 130 °C. After addition of glycine the mixture remained clear for a minute after which a white precipitate formed, contrary to the literature which reports the formation of a clear yellow solution. Once the solution cooled the white precipitate was filtered and washed with ethanol. <sup>1</sup>H and <sup>13</sup>C NMR confirmed that it was the desired product (Figure 5.5 and Figure 5.6) with a percentage yield of 87%. The pyromellitic diimide does not melt but decomposes at 220 °C.

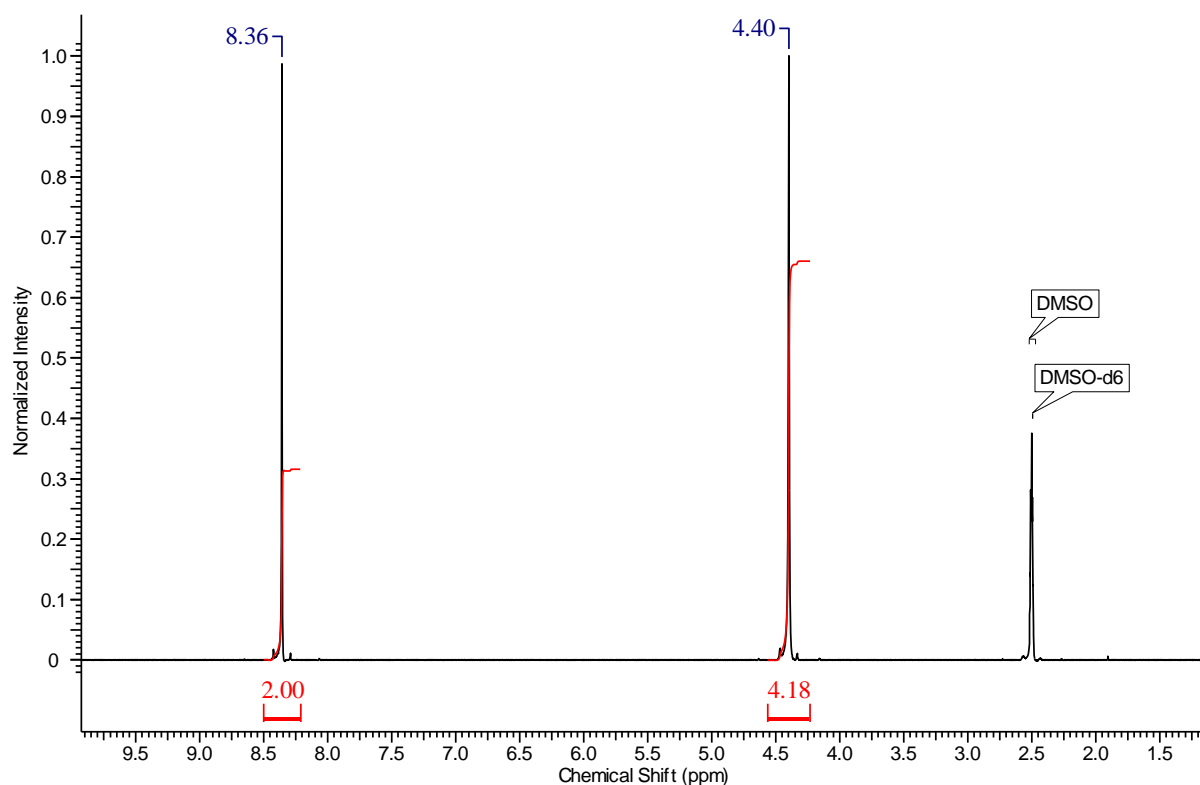


**Figure 5.5** <sup>1</sup>H NMR analysis of the pyromellitic diimide. The peak at 8.36 ppm corresponds to the two aromatic protons and the peak at 4.40 corresponds to the methylene protons that roughly integrate for four protons. There are no other peaks observed in the spectrum which indicates that the product is pure.

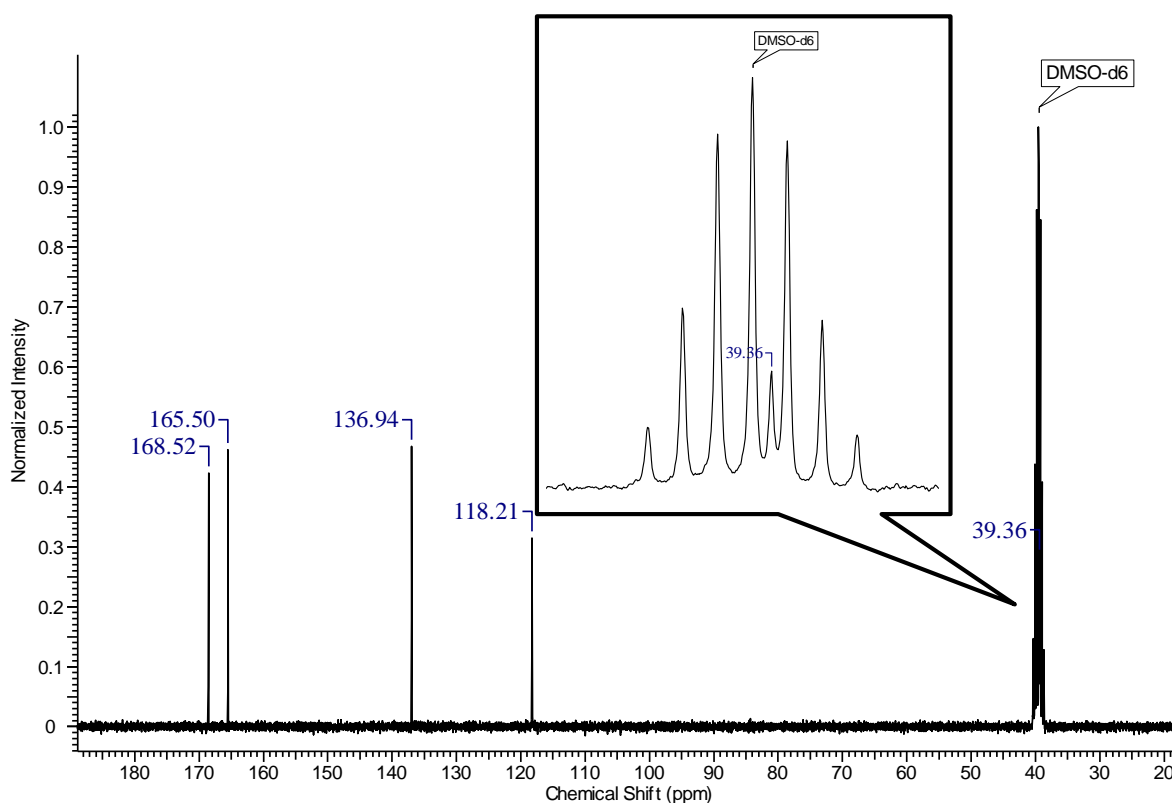


**Figure 5.6** The  $^{13}\text{C}$  NMR analysis of the pyromellitic diimide. There are 5 carbon signals present in the spectrum due to the symmetry of the molecule. The methylene carbon peak is however hidden under the DMSO- $\text{d}_6$  peaks, as is evident by the extra peak shown in the enlarged section. The peak at 168.52 ppm is that of the carbonyl carbons of the carboxylic acid groups. The peak at 165.50 ppm correlates to the 4 carbonyl carbons of the 5 membered ring. The peak at 136.94 ppm corresponds to the  $\text{sp}^2$  carbons shared by the five and six membered rings. The peak at 118.21 corresponds to the two remaining aromatic carbons of the six-membered ring.

Fourier transform solid state infrared analysis was also used to confirm the presence of the carboxylic acid groups, shown in Figure 5.7. The broad stretch ranging from 3300 to 2600  $\text{cm}^{-1}$  is characteristic of the O–H stretch.<sup>8</sup> This peak is broadened due to the hydrogen bonding of the dimers<sup>8</sup> of the carboxylic acid groups in the solid state. The C=O stretch is observed around 1700  $\text{cm}^{-1}$  and the C–O stretch around 1215  $\text{cm}^{-1}$ .

Pyromellitic diimide appears to only dissolve in THF, DMF or DMSO and a structure of the molecule was obtained from a cocrystallisation attempt with benzimidazole from a layered solution of THF and DMF. The structure is the same as the one found in the literature (CSD-GENNAP<sup>4</sup>). The simulated powder pattern of the crystal structure of pyromellitic diimide was also compared to the bulk of the as-synthesised material in order to further confirm the purity of the synthesised pyromellitic diimide (Figure 5.8). There are no extra peaks observed in the as-synthesised powder pattern of pyromellitic diimide compared to the simulated pattern, indicating that the synthesised material is very pure.

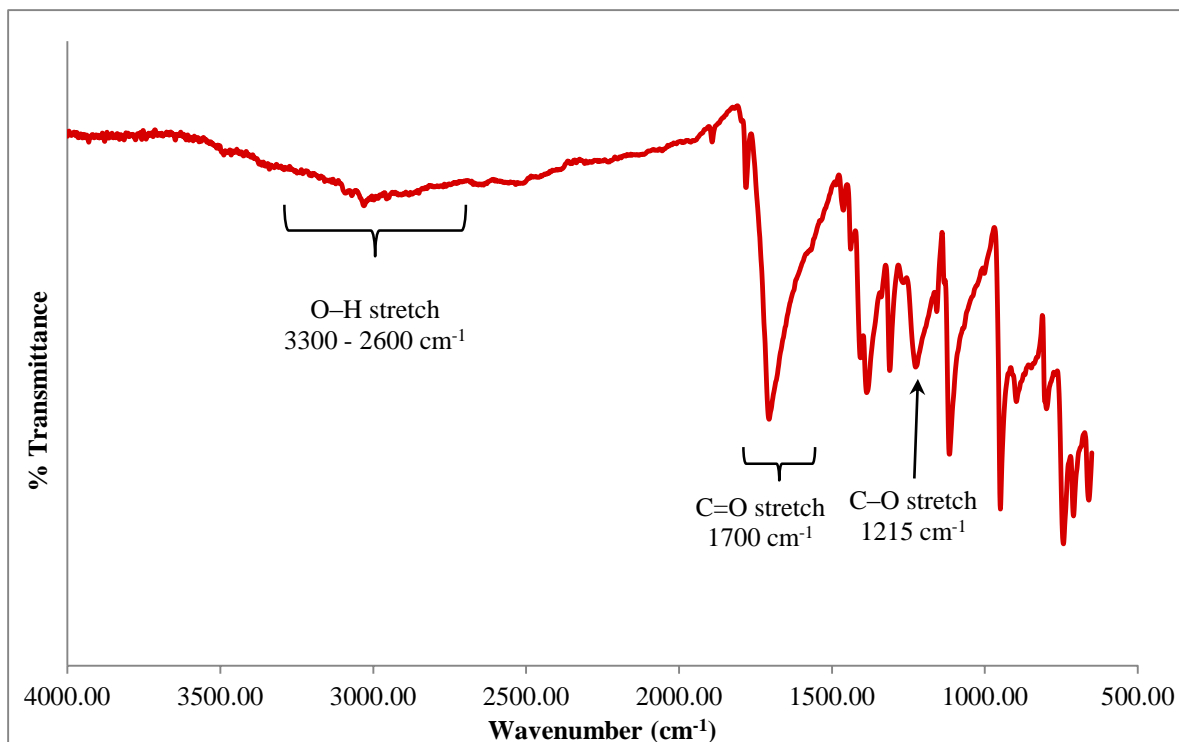


**Figure 5.7** The infrared spectrum of pyromellitic diimide. The O-H stretch of the carboxylic acid group can be found between 3300 and 2600 cm<sup>-1</sup>. This peak is usually broad due to hydrogen bonding. The C=O stretch is found at 1700 cm<sup>-1</sup> and the C-O stretch is found at 1215 cm<sup>-1</sup>.

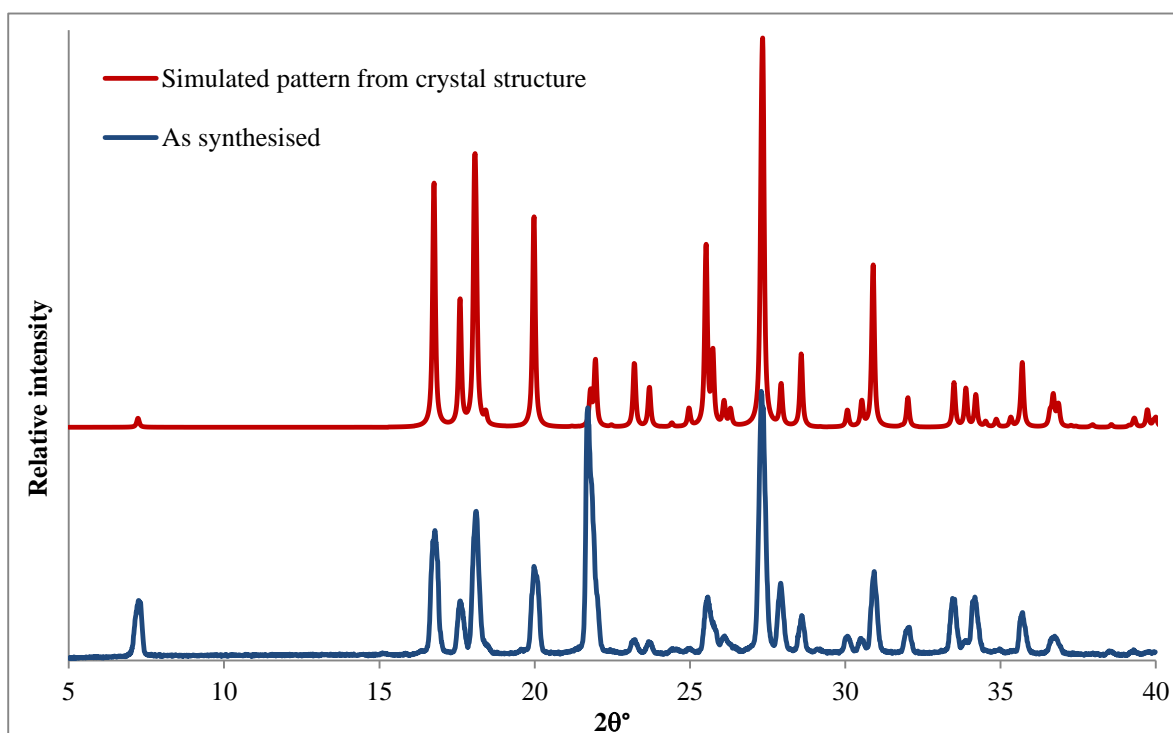


**Figure 5.8** A comparison of the simulated powder pattern from the crystal structure of pyromellitic diimide and the as-synthesised product. There are no extra peaks observed which confirms that the synthesised product is pure. Some peaks are somewhat broader in the experimental pattern than in the simulated pattern, but this is due to the synthesised product being less crystalline.

## 5.2. Cocrystallisations with N,N'-bis(glyciny)pyromellitic diimide

Pyromellitic diimide was cocrystallised with a range of N-heterocycles and amines. Tables of these crystallisations can be found in Appendix A (Tables A33 – A37). In quite a few cases, the pyromellitic diimide crystallised on its own or as the known pyromellitic/DMF solvate (CSD-CUCYIJ<sup>9</sup>). Pyromellitic diimide was initially crystallised with N-heterocycles containing two nitrogen atoms, with the aim of forming the square unit with the N-heterocycle acting as a linker between two pyromellitic diimide molecules, in order to potentially create larger cavities which could be occupied by guest molecules. Stacking of these units could then potentially lead to the formation of channels. Nitrogen-containing heterocycles were specifically chosen due to the directional hydrogen bonds formed between carboxylic acids and pyridine derivatives. Proton transfer from the carboxylic acid to the nitrogen atom of the N-heterocycles can also occur under the right crystallisation conditions, potentially allowing for the formation of stronger charge-assisted hydrogen bonds which could lend extra stability to the hydrogen-bonded network.

Pyromellitic diimide was also crystallised with various other N-heterocycles and amines since, even with N-heterocycles containing two nitrogen atoms, it is not guaranteed that the square units will be obtained. By including other functional groups such as the amine group it creates more potential sites for hydrogen bond formation which in turn creates more opportunities for the formation of potentially interesting structures.

We have obtained seven novel crystal structures with pyromellitic diimide of which one is a potential framework material. The cocrystallisation agents, crystallisation conditions and the product obtained in each case are listed in Table 5.1. The first six structures listed in the table (**PD001** – **PD006**) will be discussed in this section and the crystallographic data can be found in Table 5.7 at the end of Section 5.2 on page 226. The synthesis and structure of the framework (framework **3**) will be discussed in the next section (5.3) along with the thermal studies conducted with framework **3**.

**Table 5.1** The crystallisations performed with pyromellitic diimide that produced novel crystal structures. A complete list of cocrystallisations performed with pyromellitic diimide can be found in Appendix A, Tables A33 – A37. In all cases a 1:1 molar ratio of acid:base was used.

Base	Crystallisation conditions	Product	Code
2,6-lutidine	1:1 THF/H <sub>2</sub> O, slow evaporation	1:1:2 2,6-lutidinium N,N'-bis(glyciny)-pyromellitic diimide dihydrate	<b>PD001</b>
DABCO	DMF 0.5 ml DMF THF	1:2:2 N,N'-bis(glyciny)pyromellitic diimide 1,4-diazabicyclo[2.2.2]octane dihydrate	<b>PD002</b>
3,5-lutidine	1:1 THF/H <sub>2</sub> O, slow evaporation	1:1 3,5-lutidinium N,N'-bis(glyciny)-pyromellitic diimide	<b>PD003</b>
Isonicotinamide	1:1 THF/H <sub>2</sub> O, slow evaporation	1:1 N,N'-bis(glyciny)pyromellitic diimide isonicotinamide	<b>PD004</b>
1,10-phenanthroline	DMF layered with THF	1:2 N,N'-bis(glyciny)pyromellitic diimide 1,10-phenanthroline	<b>PD005</b>
2,9-dimethyl-1,10-phenanthroline	DMF layered with THF	1:2 N,N'-bis(glyciny)pyromellitic diimide 2,9-dimethyl-1,10-phenanthroline	<b>PD006</b>
3-picolyamine	DMF 1 ml DMF THF	1:1:1 3-picolylammonium N,N'-bis(glyciny)pyromellitic diimide DMF solvate	<b>3</b>

### 5.2.1. Hydrate formation in PD001 and PD002

First the structures of the two hydrates, **PD001** and **PD002**, will be discussed. **PD001** is a 2,6-lutidinium diimide dihydrate salt in the space group  $P\bar{1}$ . The asymmetric unit consists of one singly deprotonated pyromellitate diimide ion in the *cis* conformation, one 2,6-lutidinium ion and two water molecules (Figure 5.9).

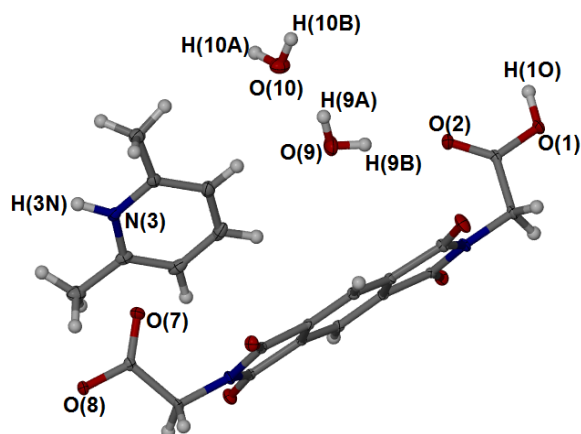


Figure 5.9 The asymmetric unit of PD001.

Adjacent pyromellitic diimide ions hydrogen bond to each other through  $\text{COOH}\cdots\text{OOC}^-$  interactions and form an infinite chain. Two chains are connected to each other through four water molecules to form a double-stranded chain, viewed down the  $a$  axis in Figure 5.10a. Due to the *cis* conformation of the carboxylate groups the square unit discussed earlier in the chapter is formed. The double-stranded chains are connected to adjacent strands *via* the hydrogen bonding of the water molecules to the water molecules of the adjacent strands, viewed down the  $b$  axis in Figure 5.10b.

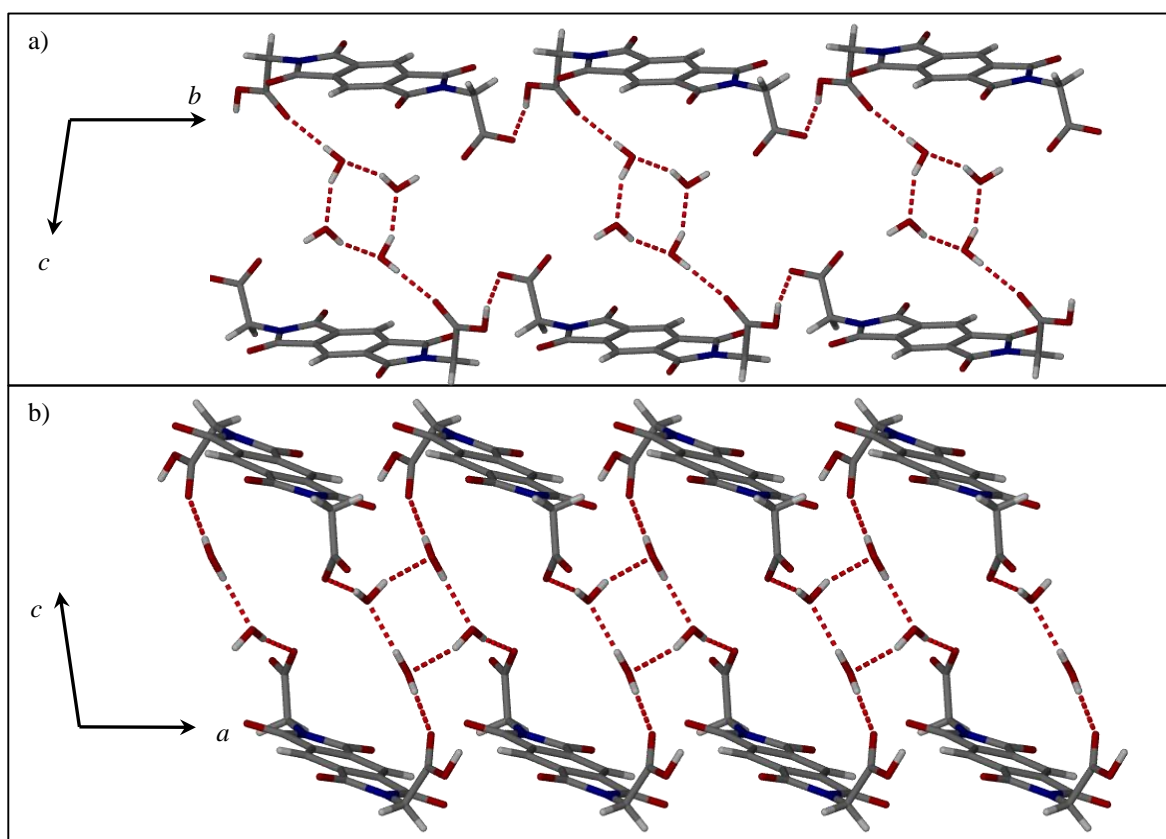
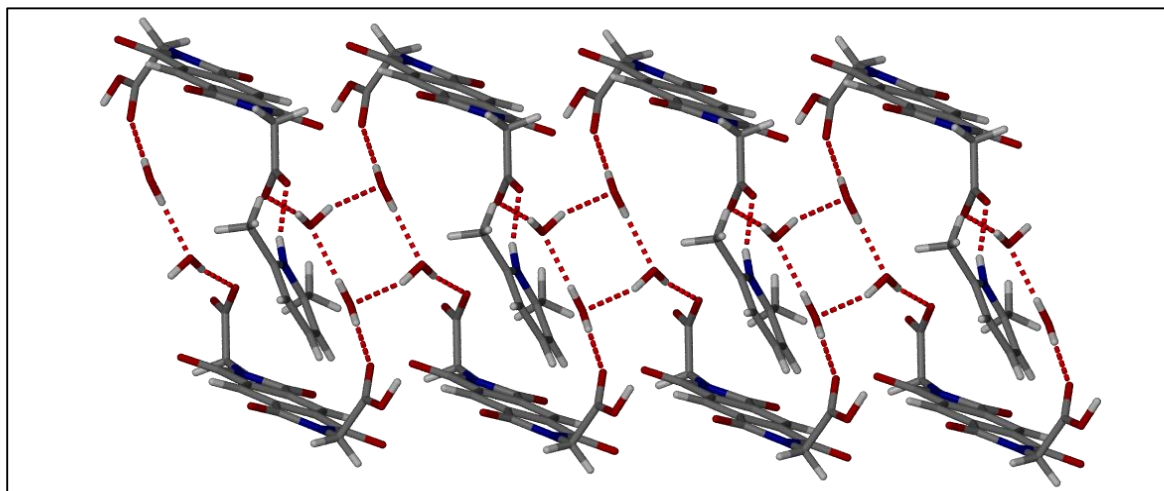


Figure 5.10 a) Double-stranded chains are formed in PD001 by two pyromellitic diimide ions that are connected by four water molecules. b) Adjacent chains are connected by hydrogen bond formation between two of the four water molecules.

The 2,6-lutidinium ion hydrogen bonds to the remaining carboxylate oxygen of the pyromellitic diimide as shown in Figure 5.11. The hydrogen bond parameters of **PD001** are listed in Table 5.2.



**Figure 5.11** In **PD001** the 2,6-lutidinium ion hydrogen bonds to the remaining carboxylate oxygen of the pyromellitic diimide.

**Table 5.2** Hydrogen bond parameters for **PD001**. The labeling scheme is shown in **Figure 5.9**.

Contact	D–H (Å)	H···A (Å)	D···A (Å)	∠DHA
N3 – H3N···O8 <sup>a</sup>	0.93(2)	1.83(2)	2.723(1)	160(2)
O1 – H1O···O8 <sup>b</sup>	0.94(2)	1.61(2)	2.540(1)	163(2)
O9 – H9A···O10	0.87(2)	1.96(2)	2.794(2)	158(2)
O9 – H9B···O2	0.83(2)	2.05(2)	2.880(1)	179(2)
O10 – H10B···O7 <sup>c</sup>	0.86(2)	2.06(2)	2.907(1)	171(2)
O10 – H10A···O9 <sup>d</sup>	0.87(3)	2.01(3)	2.837(2)	160(2)

<sup>a</sup> -x, -y+2, -z+1; <sup>b</sup> x+1, y-1, z; <sup>c</sup> -x, -y+1, -z+1; <sup>d</sup> -x+1, -y+1, -z+1

**PD002** is in the polar space group *Pc*, with one doubly deprotonated pyromellitic diimide ion, two singly protonated DABCO ions and two water molecules in the asymmetric unit (Figure



5.12). In this structure the carboxylate groups are in the *trans* conformation and it is not possible to form the double-stranded chain.

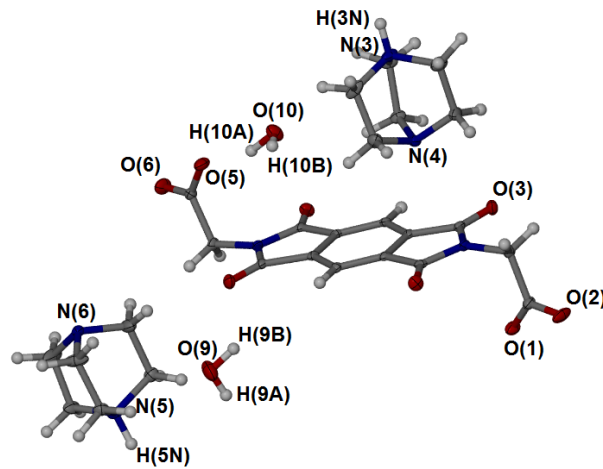


Figure 5.12 The asymmetric unit of PD002.

A single-stranded chain of pyromellitate diimide ions connected by two water molecules is formed (Figure 5.13a). The DABCO ions form a hydrogen bond to the remaining carboxylate oxygen as shown in Figure 5.13b.

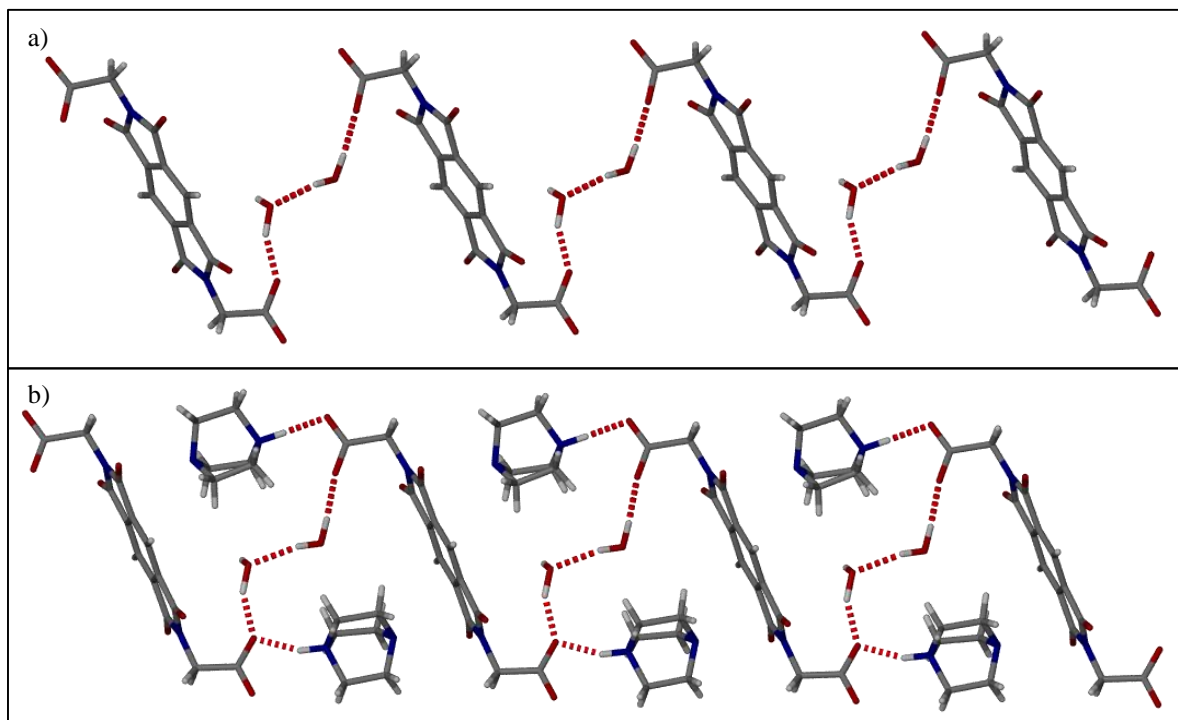
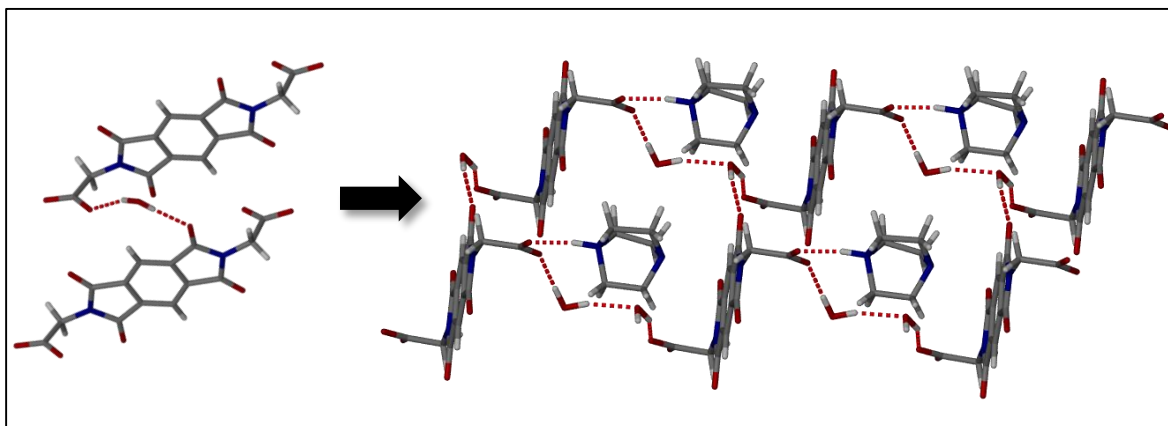


Figure 5.13 The hydrogen bond motifs in PD002. a) The doubly deprotonated pyromellitic diimide ion forms a single-stranded chain of diimide ions that are connected *via* two water molecules. b) The DABCO ions hydrogen bond to the remaining carboxylate oxygen.

The chains are connected to each other through a hydrogen bond between a water molecule and a carbonyl oxygen on the aromatic backbone of the pyromellitic diimide ion (Figure

5.14). The adjacent chains then stack slightly offset with respect to one another. The hydrogen bond between the carbonyl oxygen and the water molecule is observed in only four of the 17 structures in the CSD containing pyromellitic diimide (CSD-KEKFIQ<sup>7</sup>, CSD-KEKGIR<sup>7</sup>, CSD-OWIFOQ<sup>5</sup> and CSD-OWIFUW<sup>7</sup>), two of which are hydrates. The hydrogen bond parameters for **PD002** are listed in Table 5.3.



**Figure 5.14** In **PD002** a hydrogen bond between a water molecule and a carbonyl oxygen on the aromatic backbone of the pyromellitic diimide links adjacent chains to each other.

**Table 5.3** Hydrogen bond parameters for **PD002**. The labeling scheme is shown in **Figure 5.12**.

Contact	D–H (Å)	H···A (Å)	D···A (Å)	∠DHA
N5 – H5N···O5 <sup>a</sup>	0.97(4)	1.74(4)	2.677(3)	161(3)
N3 – H3N···O2 <sup>b</sup>	0.93(4)	1.79(4)	2.708(3)	169(3)
O10 – H10A···O5	1.03(5)	1.72(5)	2.720(3)	162(4)
O9 – H9B···O1 <sup>c</sup>	0.92(5)	1.84(5)	2.765(3)	176(4)
O10 – H10B···O3 <sup>c</sup>	0.78(4)	2.11(4)	2.894(3)	174(4)
O9 – H9A···O10 <sup>a</sup>	0.87(5)	2.01(5)	2.854(4)	164(5)

<sup>a</sup> x, y, z-1; <sup>b</sup> x+1, y, z+1; <sup>c</sup> x+1, y, z

An interesting feature of **PD002** is the fact that the protonated nitrogen atoms of the DABCO ions are aligned in the same direction. There are two rows of DABCO ions aligned in one direction, as shown in Figure 5.15 where the molecules in **A** have their protonated nitrogen atoms aligned to the right. The following two rows of DABCO (**B**) molecules have their

protonated nitrogen atoms aligned in the opposite direction (to the left in Figure 5.15). In Figure 5.15 the DABCO ions are viewed down the  $a$  axis.

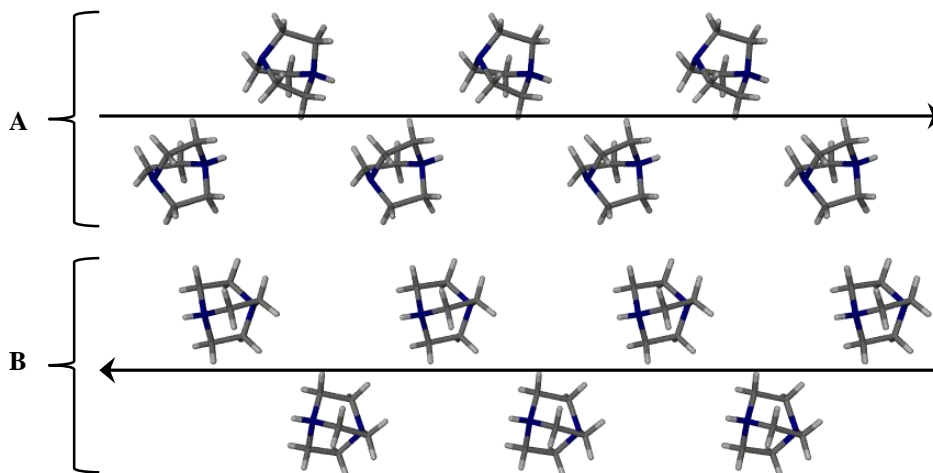


**Figure 5.15** The alignment of the DABCO ions in **PD002**, viewed down the  $a$  axis. Two rows of DABCO ions (**A**) are aligned in the same direction. The following two rows (**B**) are aligned in the opposite direction.

It would be interesting to investigate in the future whether **PD002** has any interesting properties such as second harmonic generation or non-linear optical properties due to the alignment of the DABCO ions. This does however seem unlikely since the two rows of DABCO ions align in opposite directions, possibly cancelling the dipole.

It is evident in these two structures that the degree of ionisation of the pyromellitic diimide molecule determines what type of hydrogen-bonded chain is formed. In the case of a singly deprotonated ion (**PD001**) it is possible for the diimide ions to hydrogen bond to each other and to a water molecule therefore forming the double-stranded chain. However, in **PD002** this is not the case since the diimide ion is doubly deprotonated and can only form hydrogen bonds to water molecules, consequently forming a single-stranded chain of ions linked *via* water molecules. The degree of ionisation of the diimide ion is possibly due to the crystallisation conditions. **PD001** was grown from a 1:1 THF/H<sub>2</sub>O solution while **PD002** was grown from a layered solution of THF and DMF.

### 5.2.2. Salt *versus* cocrystal formation in **PD003** and **PD004**

The next set of structures to be discussed is that of **PD003**, a 1:1 3,5-lutidinium pyromellitic diimide salt, and **PD004**, a 1:1 isonicotinamide pyromellitic diimide cocrystal. Single-crystal X-ray diffraction data of **PD003** were collected at room temperature because the crystals deteriorated under the flow of nitrogen at 100 K. This could be due to sudden uneven

contraction along a face of the crystal which causes it to crack. There is therefore some disorder in the structure due to the movement of the molecules at room temperature. The crystal is in the triclinic crystal system in the space group  $P\bar{1}$ . The asymmetric unit contains one 3,5-lutidinium ion and one pyromellitic diimide ion in the *trans* conformation (Figure 5.16). One of the carboxylic acid groups is disordered over two positions with 64% occupancy for the major component of the disorder. The disorder involves only a slight rotation of the carboxylate group.

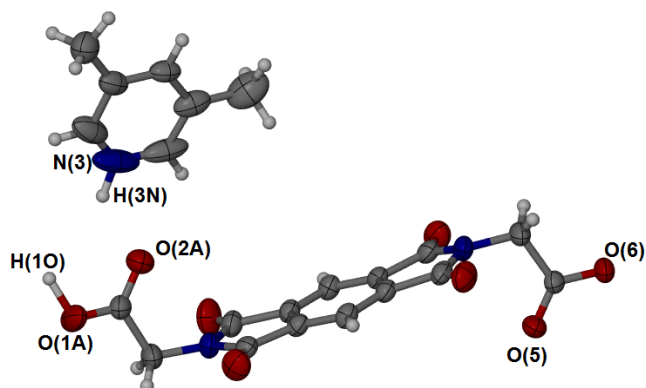


**Figure 5.16** The asymmetric unit of **PD003**. Only one component of the carboxylic acid disorder is shown (O1A and O2A). The thermal ellipsoids of the molecules are quite large due to the movement of the molecules in the crystal structure since the SCD data were obtained at room temperature.

The pyromellitic diimide ions form a hydrogen-bonded chain through a shared proton with the lesser component of disorder shown in pink in Figure 5.17a. Pendant 3,5-lutidinium ions hydrogen bond to one side of the pyromellitic diimide chain to oxygen atoms of neighbouring pyromellitic diimide ions, as shown in Figure 5.17b.

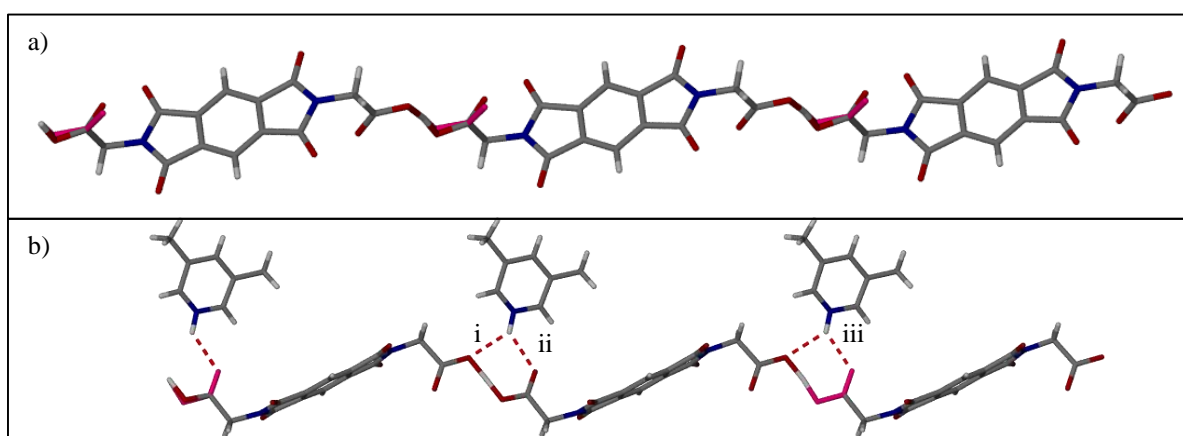


**Figure 5.17** The hydrogen bond motif in **PD003**. a) The pyromellitic diimide ions form a hydrogen-bonded chain through a shared proton. The lesser component of the carboxylate disorder is shown in pink. b) The 3,5-lutidinium ions hydrogen bond to the carboxylate oxygen atoms of two pyromellitic diimide ions. The other orientation of the carboxylate group is shown in pink. The different hydrogen bonds are indicated by i, ii and iii.

Three hydrogen bonds are formed between the 3,5-lutidinium ion and the pyromellitic diimide ion, indicated by (i), (ii) and (iii) in Figure 5.17b. The first two hydrogen bonds, (i) and (ii), are formed between the 3,5-lutidinium ion and the major component of the carboxylate disorder (O2A). The third hydrogen bond indicated by (iii) is the hydrogen bond formed between the 3,5-lutidinium ion and the lesser component of the disordered carboxylate group (O1B). The lengths of the different hydrogen bonds are given in Table 5.4.

**Table 5.4** The hydrogen bond parameters for **PD003**. The labeling scheme is shown in **Figure 5.16**.

Contact	D–H (Å)	H···A (Å)	D···A (Å)	∠DHA
N3 – H3N···O6 <sup>a</sup>	0.96(5)	2.26(4)	3.014(3)	134(3)
N3 – H3N···O2A	0.96(5)	2.23(5)	2.97(2)	133(3)
N3 – H3N···O1B	0.96(5)	2.17(5)	2.92(2)	134(3)
O1A – H1O···O6 <sup>b</sup>	1.18(4)	1.29(4)	2.47(1)	169(3)
O2B – H1O···O6 <sup>b</sup>	1.23(5)	1.29(4)	2.52(2)	173(3)

<sup>a</sup> x, y+1, z+1; <sup>b</sup> x, y+1, z+1

**PD004** is a 1:1 isonicotinamide pyromellitic diimide cocrystal in the space group  $P\bar{1}$ . The asymmetric unit consists of one pyromellitic diimide molecule in the *trans* conformation and two isonicotinamide molecules with half occupancy, which are situated on a centre of inversion. The carboxylic acid groups of the pyromellitic diimide molecule are also disordered over two positions with half occupancy for each component. One component of disorder is shown in pink for the carboxylate acid groups (Figure 5.18).

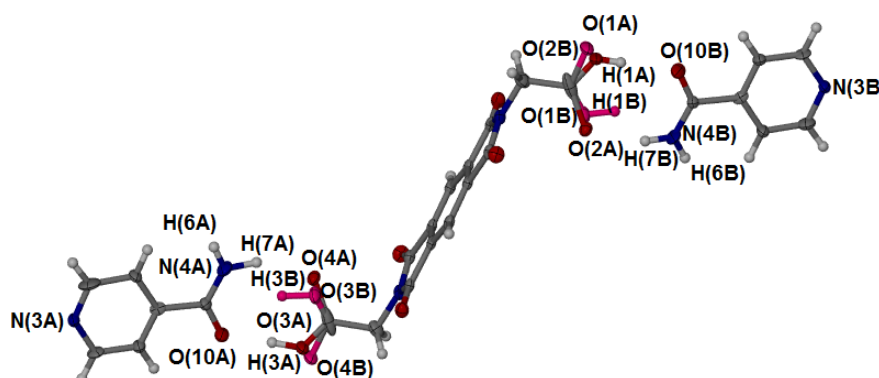


**Figure 5.18** The asymmetric unit of **PD004**. One component of disorder of the carboxylic acid groups is shown in pink. The isonicotinamide molecules are related by an inversion centre, with half occupancy for each.

Pyromellitic diimide and isonicotinamide hydrogen bond to each other to form infinite chains. In Figure 5.19a each chain is shown with one component of disorder for both molecules. This leads to anti-parallel chains of pyromellitic diimide/isonicotinamide. The chains form hydrogen bonds to each other through N-H...O interactions. These hydrogen-bonded chains form sheets that are stacked offset with respect to one another. Figure 5.19b illustrates how the sheets stack on top of each other. In Figure 5.20 the packing diagram is viewed down the *a* axis which shows the offset stacking of one sheet above/below another. The hydrogen bond parameters for **PD004** are listed in Table 5.5.

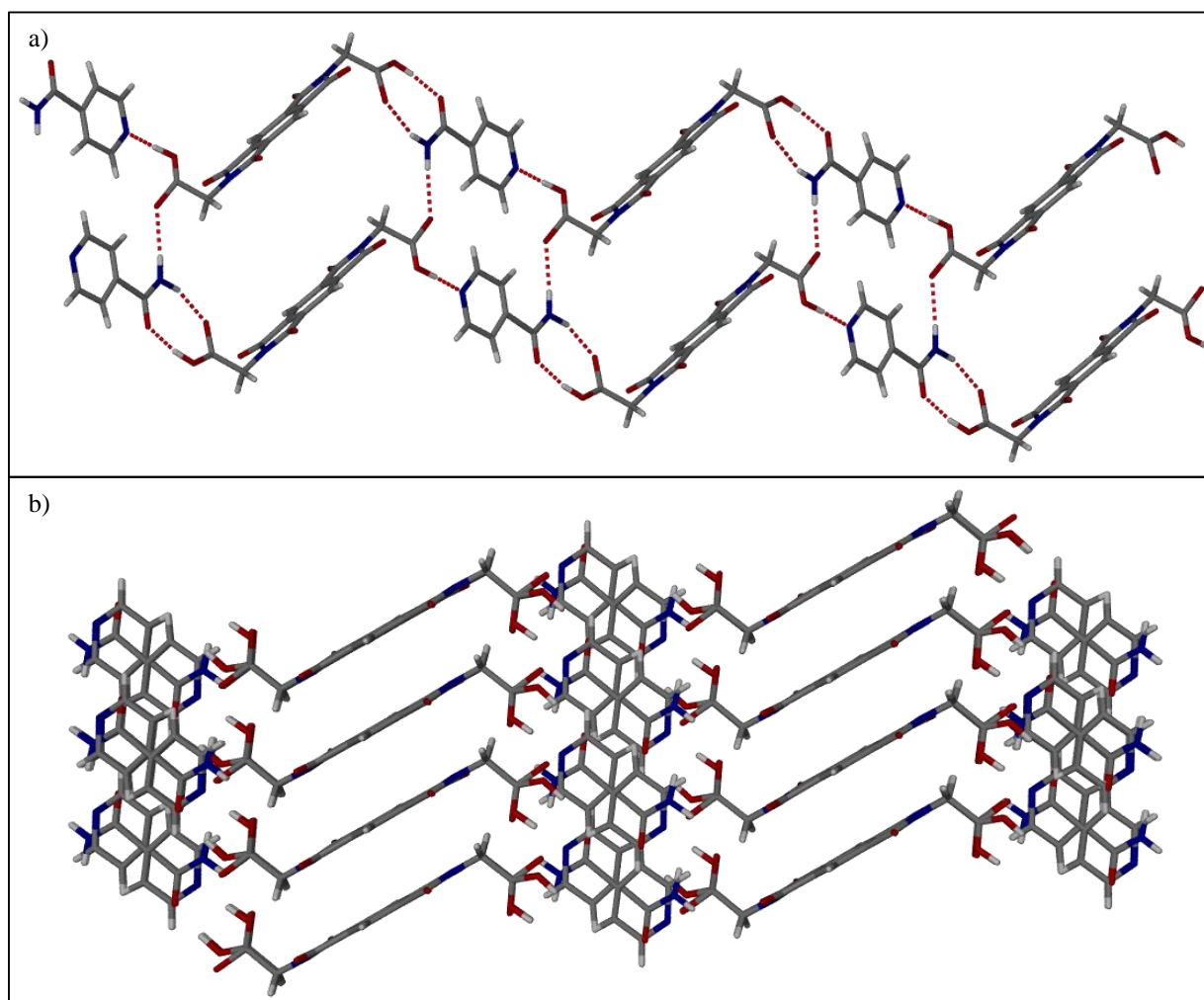


**Figure 5.19** The hydrogen bonding motif observed in **PD004**. a) One component of disorder is shown for each molecule. In one chain isonicotinamide is shown facing one direction and in the next chain in the opposite direction. b) The packing diagram viewed down the *b* axis to show how the sheets stack on top of one another.

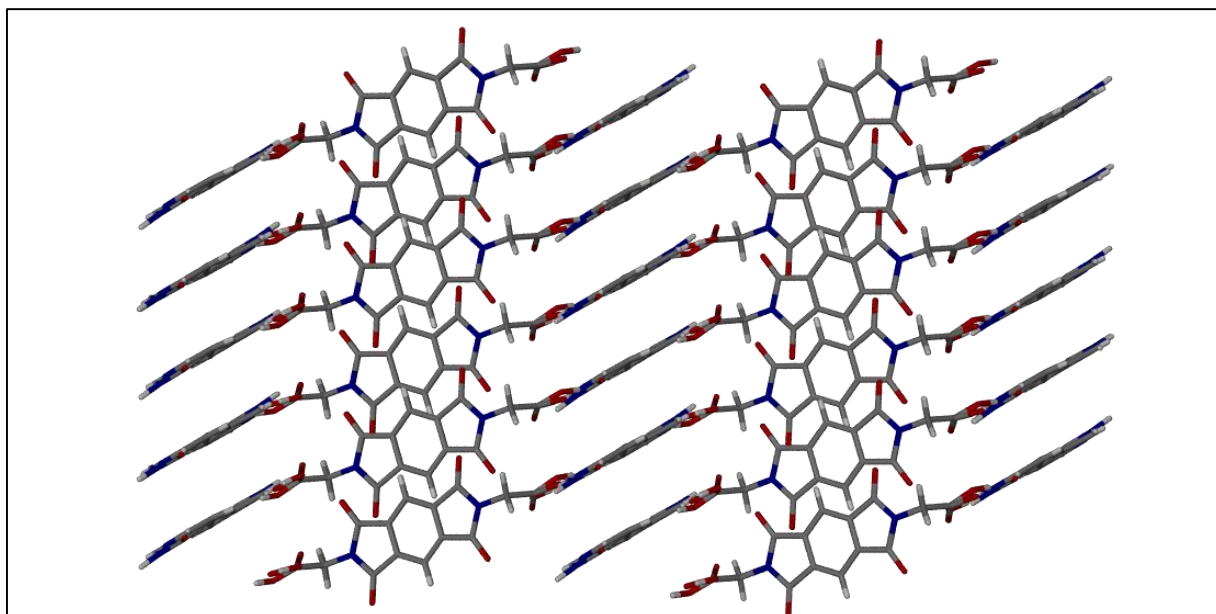


**Figure 5.20** The packing diagram of **PD004** viewed down the *a* axis in order to show the offset nature in which the sheets stack on top of each other.

**Table 5.5** The hydrogen bond parameters for **PD004**. The labeling scheme is shown in **Figure 5.18**.

Contact	D–H (Å)	H...A (Å)	D...A (Å)	∠DHA
O3A – H3A...O10A	0.96(5)	1.65(6)	2.596(13)	169(4)
O1A – H1A...N3A <sup>a</sup>	0.78(5)	2.08(5)	2.738(4)	142(5)
O3B – H3B...N3B <sup>b</sup>	1.03(4)	1.55(4)	2.570(5)	170(4)
O1B – H1B...N4B	0.97(4)	2.15(4)	3.018(7)	148(3)
O1B – H1B...O10B	0.97(4)	2.36(4)	3.254(1)	153(3)
O1A – H1A...O10B	0.78(5)	1.86(5)	2.64(1)	176(5)
N4B – H7B...O2A	0.94(5)	2.07(5)	2.977(7)	161(4)
O1B – H1B...N3A <sup>a</sup>	0.97(4)	1.62(4)	2.584(6)	174(4)
N4B – H6B...O2B <sup>c</sup>	0.92(4)	2.17(4)	3.080(7)	170(4)
N4A – H6A...O4B <sup>d</sup>	0.89(4)	2.18(4)	3.072(7)	177(3)
N4A – H7A...O4A	1.07(5)	1.95(5)	2.957(6)	155(4)

<sup>a</sup> x+1, y+1, z+1; <sup>b</sup> x-1, y-1, z-1; <sup>c</sup> x+1, y, z; <sup>d</sup> x-1, y, z



**PD003** and **PD004** were both grown from 1:1 THF/H<sub>2</sub>O solutions, but the degree of ionisation of pyromellitic diimide is different. In **PD003** it is singly deprotonated forming infinite chains of diimide ions, and in **PD004** no deprotonation occurred which led to cocrystal formation and infinite a-b chains. In these two instances it is possible that the cocrystallisation agents in combination with the solvent system influenced the degree of ionisation of the pyromellitic diimide molecule.

### 5.2.3. Cocrystals with aromatic molecules and pyromellitic diimide

The next two structures that will be discussed are **PD005**, a 2:1 1,10-phenanthroline pyromellitic diimide cocrystal, and **PD006**, a 2:1 2,9-dimethyl-1,10-phenanthroline pyromellitic diimide cocrystal. **PD005** is in the space group  $P2_1/c$  with half a pyromellitic diimide molecule and one molecule of 1,10-phenanthroline in the asymmetric unit. The asymmetric unit of **PD005** is shown in Figure 5.21 with the symmetry-generated half of the pyromellitic diimide shown in purple. The hydrogen atoms associated with the carboxylic acid moieties of pyromellitic diimide could both be located in the electron density map, indicating that no proton transfer occurred between pyromellitic diimide and 1,10-phenanthroline.

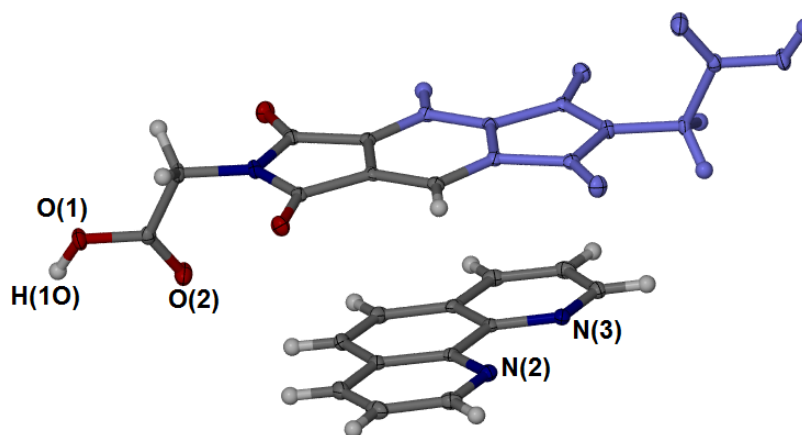


**Figure 5.21** The asymmetric unit of **PD005**. The symmetry-related half of the pyromellitic diimide molecule is shown in purple.

The pyromellitic diimide molecule forms a hydrogen bond to two 1,10-phenanthroline molecules to form a base-acid-base unit (Figure 5.22a). The carboxylic acid groups are in the same plane as the 1,10-phenanthroline molecule. The base-acid-base units stack together through  $\pi-\pi$  interactions between the aromatic region of pyromellitic diimide and 1,10-



phenanthroline, as well as  $\pi-\pi$  stacking interactions between 1,10-phenanthroline molecules (Figure 5.22b).

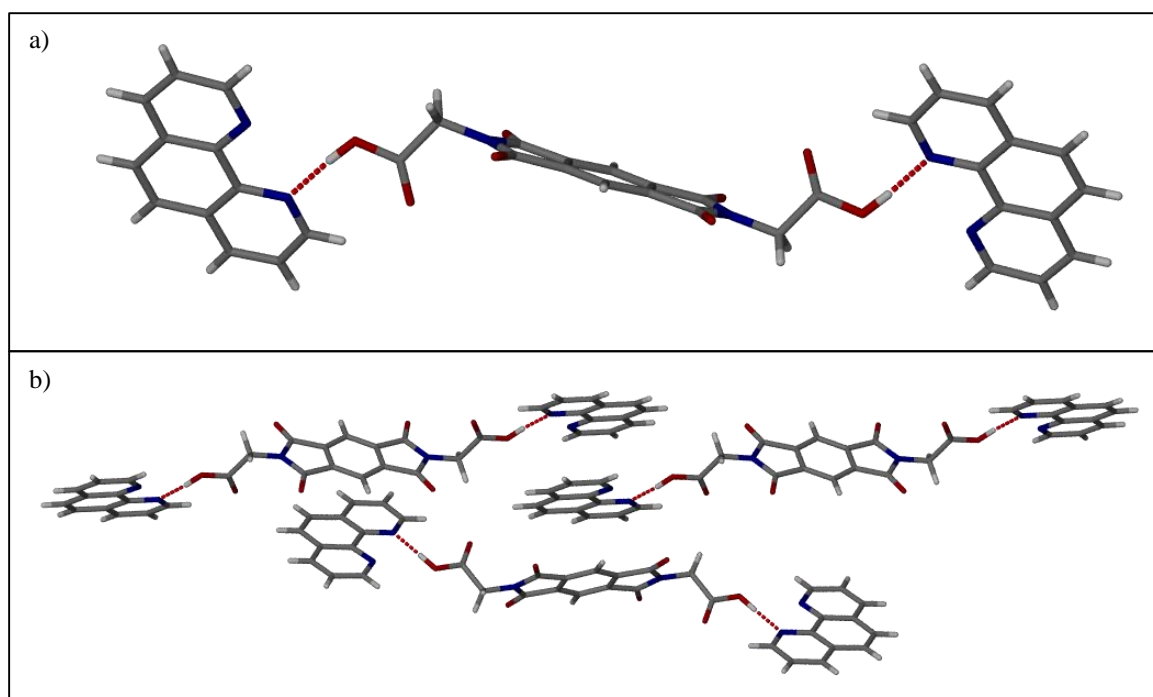


**Figure 5.22** The hydrogen bond motif and packing of **PD005**. a) The hydrogen bonded base-acid-base unit of **PD005**. b) The base-acid-base units stack together through  $\pi-\pi$  stacking interactions between pyromellitic diimide and 1,10-phenanthroline, as well as 1,10-phenanthroline molecules with each other.

**PD006** is a 2:1 2,9-dimethyl-1,10-phenanthroline pyromellitic diimide cocrystal in the space group  $P2_1/c$ . The asymmetric unit consists of one 2,9-dimethyl-1,10-phenanthroline molecule and half a pyromellitic diimide molecule. Again no proton transfer occurred from the carboxylic acid to the nitrogen and the proton on the carboxylic acid group could be located in the electron density map. In Figure 5.23 the asymmetric unit of **PD006** is shown with the symmetry-related half of the pyromellitic diimide molecule shown in teal.

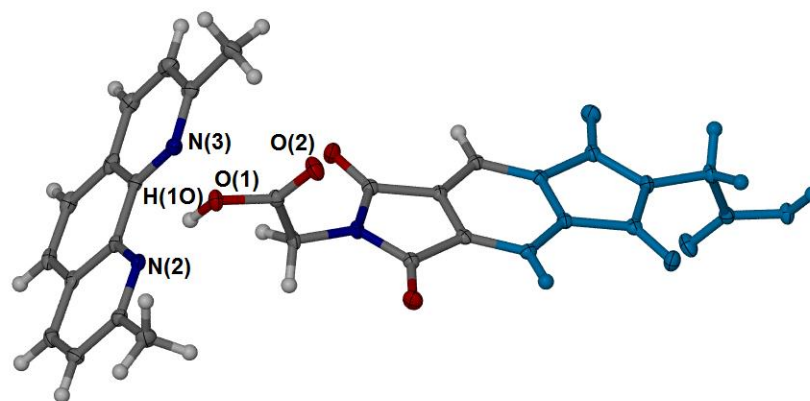


**Figure 5.23** The asymmetric unit of **PD006** with the symmetry-related half of the pyromellitic diimide molecule shown in teal.

The base-acid-base units that were observed in **PD005** are again seen in **PD006** but the orientation of the constituents in the base-acid-base unit in **PD006** differs significantly from that of **PD005**.

The presence of the two methyl groups on the phenanthroline moiety has a large effect on the packing of the molecules. The pyromellitic diimide molecule can no longer form a head-on hydrogen bond with the nitrogen atom since there is no proton available next to the nitrogen atom to stabilise the COOH...N interaction, as was possible in **PD005**. The carboxylic acid groups of pyromellitic diimide now lie perpendicular to the plane of the phenanthroline ring in order to form a hydrogen bond. The hydrogen atom has rotated outwards in order to form the hydrogen bond. The carboxylic acid is therefore in the *anti* conformation relative to the carbonyl oxygen (Figure 5.24). The pyromellitic diimide molecule of one unit and two 2,9-dimethyl-1,10-phenanthroline molecules from neighbouring units close-pack through  $\pi-\pi$  stacking interactions (Figure 5.25).

In **PD005** the phenanthroline moieties were able to form  $\pi-\pi$  stacking interactions with each other as well as pyromellitic diimide due to the orientation of the hydrogen between the carboxylic acid and the nitrogen atom. However, in **PD006** the orientation of the hydrogen bond has changed since the stabilising hydrogen atom next to the nitrogen atom has been replaced by a methyl group. This disrupts the ability of the phenanthroline moieties to form  $\pi-\pi$  stacking interactions with each other, forcing the molecules to adapt a different packing arrangement than that of **PD005**. The hydrogen bond parameters for **PD005** and **PD006** are listed in Table 5.6.

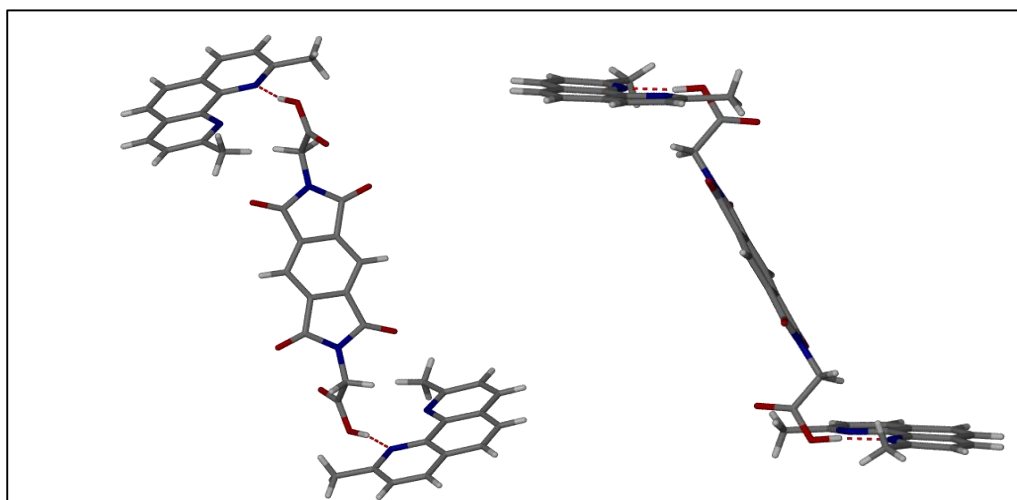


**Figure 5.24** The hydrogen-bonded unit observed in **PD006**. The carboxylic acid groups of pyromellitic diimide are perpendicular to the plane of the phenanthrene ring. The carboxylic acid is in the *anti* conformation in order to form the hydrogen bond to the nitrogen atom due to the presence of the methyl groups.

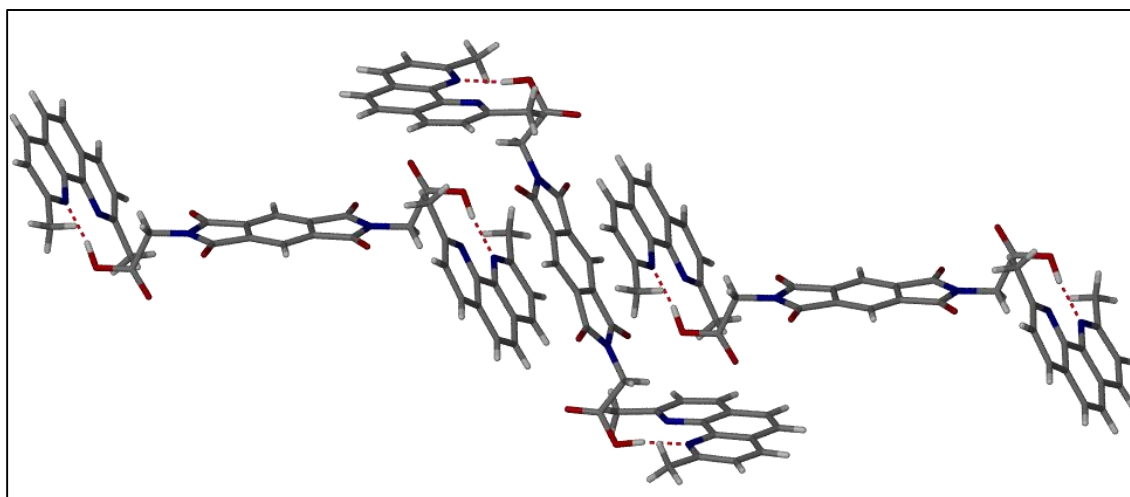


**Figure 5.25** The packing motif observed in **PD006**. Neighbouring b-a-b units close packing *via*  $\pi-\pi$  stacking interactions between pyromellitic diimide and the phenanthroline moiety.

**Table 5.6** Hydrogen bond parameters for **PD005** and **PD006** with labeling schemes for the atoms of each structure shown in **Figure 5.21** and **Figure 5.23**, respectively.

	Contact	D-H (Å)	H...A (Å)	D...A (Å)	$\angle$ DHA
<b>PD005</b>	O1-H1O...N3 <sup>a</sup>	0.91(2)	1.78(2)	2.689(1)	170(2)
<b>PD006</b>	O1-H1O...N2	0.97(3)	1.72(3)	2.680(2)	169(2)

<sup>a</sup>  $x-1, -y+1/2, z-1/2$

**Table 5.7** Crystallographic data for structures discussed in Section 5.2.

	<b>PD001</b>	<b>PD002</b>	<b>PD003</b>	<b>PD004</b>	<b>PD005</b>	<b>PD006</b>
Stoichiometric ratio (acid:base:other)	1:1:2	1:2:2	1:1	1:1	1:2	1:2
Chemical formula	C <sub>21</sub> H <sub>21</sub> N <sub>3</sub> O <sub>10</sub>	C <sub>26</sub> H <sub>36</sub> N <sub>6</sub> O <sub>10</sub>	C <sub>21</sub> H <sub>17</sub> N <sub>3</sub> O <sub>8</sub>	C <sub>20</sub> H <sub>14</sub> N <sub>4</sub> O <sub>9</sub>	C <sub>38</sub> H <sub>24</sub> N <sub>6</sub> O <sub>8</sub>	C <sub>42</sub> H <sub>32</sub> N <sub>6</sub> O <sub>8</sub>
Formula weight/g.mol <sup>-1</sup>	475.41	592.61	439.38	454.35	692.63	748.73
Crystal system	Triclinic	Monoclinic	Triclinic	Triclinic	Monoclinic	Monoclinic
Space group	<i>P</i> $\bar{1}$	<i>Pc</i>	<i>P</i> $\bar{1}$	<i>P</i> $\bar{1}$	<i>P</i> 2 <sub>1</sub> / <i>c</i>	<i>P</i> 2 <sub>1</sub> / <i>c</i>
Z	2	2	2	2	2	2
<i>a</i> /Å	7.322(1)	6.829(1)	7.7420(8)	7.243(2)	9.729(1)	9.270(2)
<i>b</i> /Å	11.032(2)	21.354(4)	10.547(1)	7.309(2)	11.031(1)	19.646(4)
<i>c</i> /Å	13.533(2)	9.362(2)	13.468(1)	18.047(5)	14.990(2)	10.364(2)
$\alpha^\circ$	99.524(2)	90	105.753(1)	91.397(3)	90	90
$\beta^\circ$	94.622(2)	94.948(3)	103.848(1)	97.013(3)	107.177(1)	115.405(2)
$\gamma^\circ$	101.859(2)	90	100.970(1)	92.049(3)	90	90
Calculated density/g.cm <sup>-3</sup>	1.507	1.447	1.476	1.593	1.497	1.458
Volume/Å <sup>3</sup>	1047.6(3)	1360.1(5)	988.5(2)	947.2(4)	1537.0(3)	1705.0(5)
Temperature/K	100(2)	100(2)	296(2)	100(2)	100(2)	100(2)
$\mu$ /mm <sup>-1</sup>	0.122	0.112	0.116	0.129	0.108	0.103
Independent reflections	4795	4214	4483	4335	3559	3789
<i>R</i> <sub>int</sub>	0.0161	0.0250	0.0216	0.0167	0.0217	0.0251
<i>R</i> <sub>1</sub> [I > 2(I)]	0.0389	0.0407	0.0727	0.0581	0.0415	0.0553

### 5.3. The pyromellitic diimide framework

The pyromellitic diimide framework (framework **3**) was grown from a carefully layered solution. Pyromellitic diimide was dissolved in 2 ml DMF which was carefully layered with a 1 ml layer of pure DMF. A third layer of 3-picolylamine in 1 ml THF was then added. On contact of the THF layer with the DMF layer very fine feathery crystals formed. The crystals are long, extremely thin plates that appear multi-coloured under plane-polarised light. The crystals are weakly diffracting and therefore the structure quality is rather poor, even after repeated SCD data collection. The crystals are in the orthorhombic crystal system, in the polar space group *Fdd2*. The asymmetric unit consists of one DMF molecule, one *trans* pyromellitic diimide ion and one 3-picolylammonium ion (Figure 5.26). The hydrogen bond parameters for **3** are listed in Table 5.8 and selected crystallographic data can be found in Table 5.9.

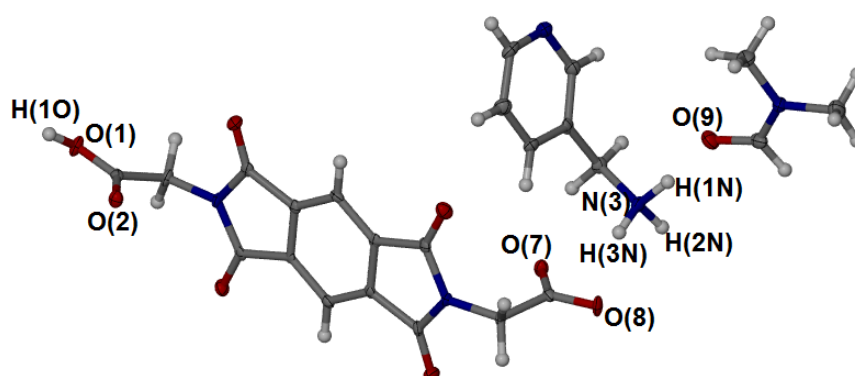


**Figure 5.26** The asymmetric unit of the pyromellitic diimide framework, **3**. One of the carboxylic acid groups has donated a proton to the amine group of 3-picolylamine.

**Table 5.8** The hydrogen bond parameters for framework **3**. The labeling scheme is shown in **Figure 5.26**.

Contact	D—H (Å)	H...A (Å)	D...A (Å)	∠DHA
O1—H10...O8 <sup>a</sup>	1.02(9)	1.43(8)	2.431(5)	168(8)
N3—H2N...O2 <sup>b</sup>	0.99(6)	1.99(6)	2.940(5)	161(5)
N3—H1N...O9	1.08(7)	1.69(7)	2.766(6)	174(5)
N3—H3N...O7 <sup>c</sup>	0.96(6)	1.97(6)	2.907(6)	164(5)

<sup>a</sup>  $-x+1/4, y-1/4, z+3/4$ ; <sup>b</sup>  $-x+1/4, y+1/4, z-3/4$ ; <sup>c</sup>  $x, y, z-1$

**Table 5.9** Selected crystallographic data for framework 3.

<b>Framework 3</b>	
Stoichiometric ratio (acid:base:solvent)	1:1:1
Chemical formula	C <sub>23</sub> H <sub>23</sub> N <sub>5</sub> O <sub>9</sub>
Formula weight/g.mol <sup>-1</sup>	513.46
Crystal system	Orthorhombic
Space group	<i>Fdd2</i>
Z	16
<i>a</i> /Å	33.706(4)
<i>b</i> /Å	57.081(9)
<i>c</i> /Å	4.7976(6)
$\alpha$ /°	90
$\beta$ /°	90
$\gamma$ /°	90
Calculated density/g.cm <sup>-3</sup>	1.478
Volume/Å <sup>3</sup>	9230(2)
Temperature/K	100(2)
$\mu$ /mm <sup>-1</sup>	0.116
Independent reflections	3280
$R_{\text{int}}$	0.0538
$R_1$ [ $I > 2(I)$ ]	0.0556

The pyromellitic diimide ions form hydrogen bonds to each other *via* a shared proton to form infinite strands (Figure 5.27a). Two 3-picolylammonium ions form hydrogen bonds to each pyromellitic ion *via* an oxygen atom of the carboxylate group (Figure 5.27b). They hydrogen bond to the pyromellitic diimide ions in an alternating fashion where one 3-picolylammonium ion is in front of the chain (shown in green in Figure 5.27b) and the following one behind the chain (shown in blue). The remaining proton of the 3-picolylammonium ion hydrogen bonds to the carbonyl oxygen of the DMF molecule (Figure 5.27a), also in an alternating fashion where the DMF molecules shown in pink are in front of the chain and the molecules shown in purple are behind the chain.

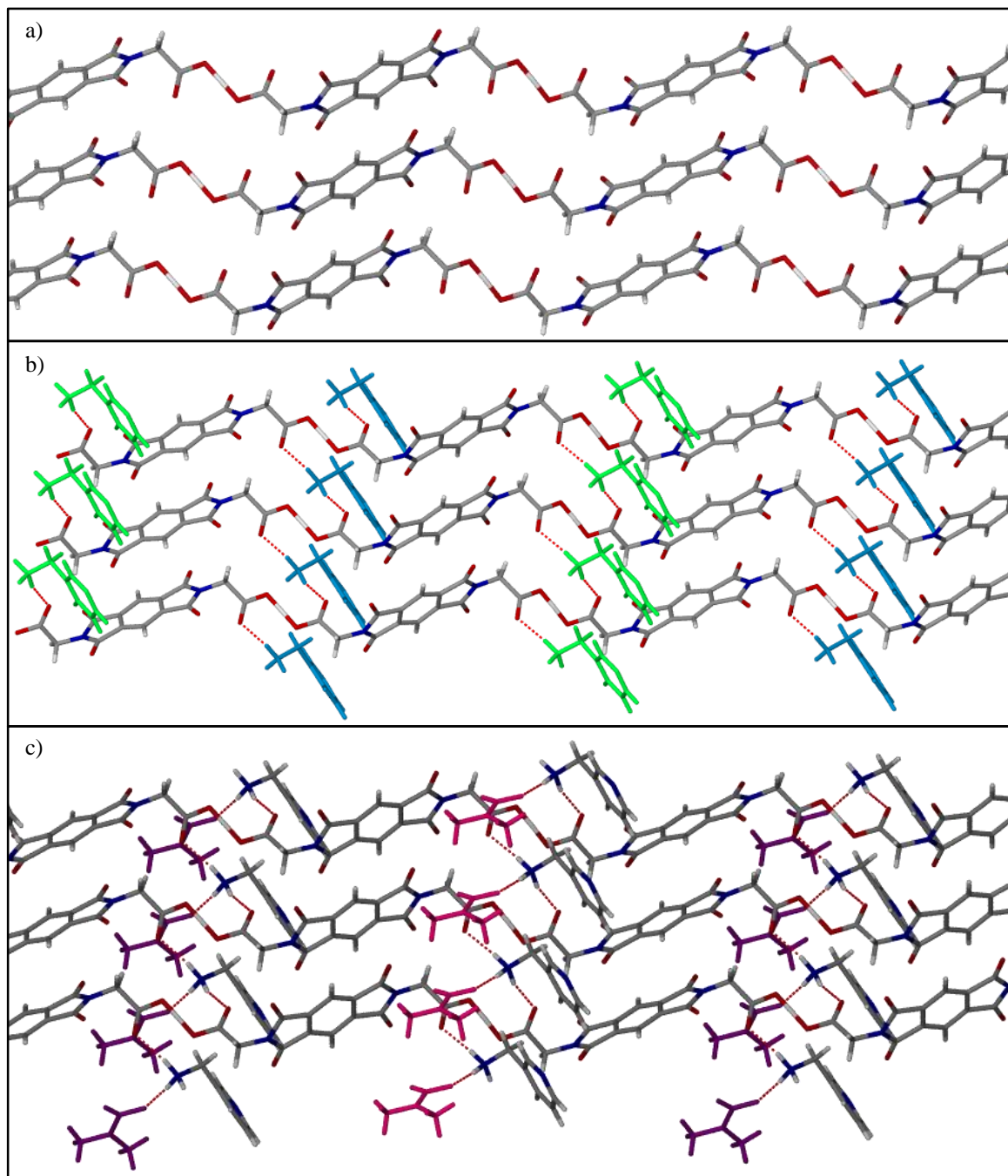


**Figure 5.27** The hydrogen bond motifs observed in framework **3**. a) The pyromellitic diimide ions hydrogen bond to each other through a shared proton to form parallel chains. b) Two 3-picolylammonium ions hydrogen bond to each pyromellitic diimide ion through the carbonyl oxygen in an alternating fashion – one in front of the chain (shown in green) and the next behind the chain (shown in blue). c) The 3-picolylammonium ions also hydrogen bond to the carbonyl oxygen of the DMF molecules. The DMF molecules also alternate between being behind the chain (purple) and in front of the chain (pink).



The hydrogen bonded-strands then pack together to form undulating ribbons throughout the crystal structure in which the DMF molecules perfectly align, as shown in Figure 5.28.

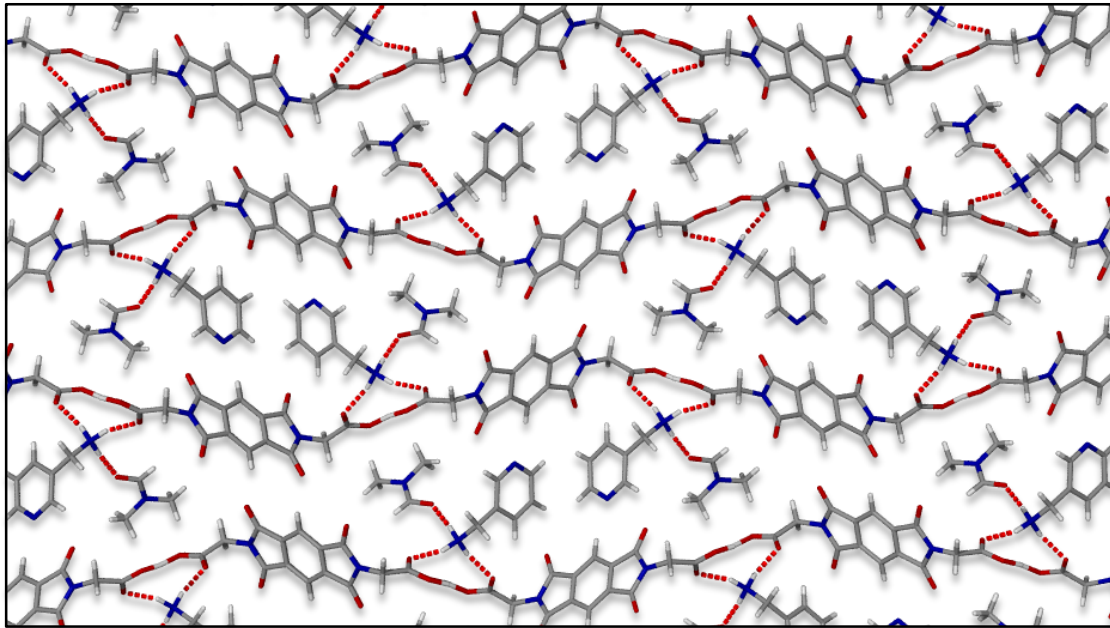


**Figure 5.28** The packing diagram of framework **3**. Shown here are the undulating ribbons formed by the hydrogen-bonded chains, viewed down the *c* axis.

Upon closer examination of the structure it becomes apparent that the ammonium groups of 3-picolylammonium are aligned in one direction. The alignment of the 3-picolylammonium ions is clearly seen when viewed down the *a* axis where the ions are arranged in columns down *c* (Figure 5.29a).

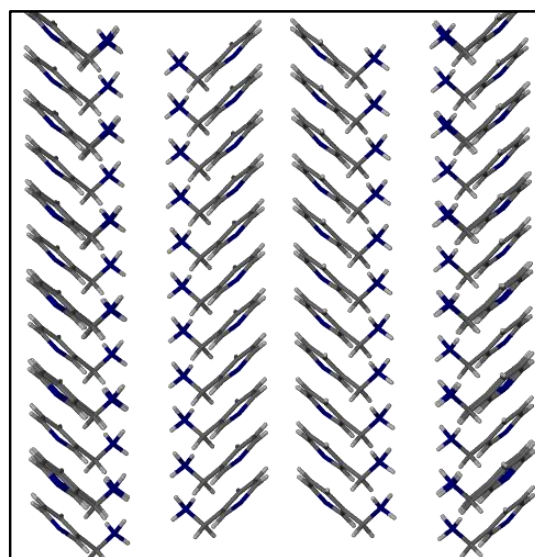


**Figure 5.29** The 3-picolylammonium ions in framework **3** are arranged in columns down the *c* axis with the ammonium moieties aligned in the same direction.



This indicates that framework **3** could have potential interesting properties such as second harmonic generation. Further investigations into these properties did not form part of the current study, but will be included in future studies with this framework.

In Figure 5.30a and b the contact and solvent accessible surfaces are shown, generated by the *Voids* function in Mercury<sup>10-13</sup> with a probe radius of 1.4 Å. The DMF molecules in the structure perfectly align in channels and therefore, if it were possible to remove the DMF, an empty framework could be generated. In Figure 5.30c the solvent accessible surface is viewed down the *b* axis, clearly showing that the guest pockets are connected, which further suggests that solvent permeation is theoretically possible. However, the DMF molecules hydrogen bond to the walls of the framework, which could make it difficult to remove the DMF and could lead to the collapse of the structure. Therefore the thermal stability of framework **3** was investigated and will be discussed in the next section.

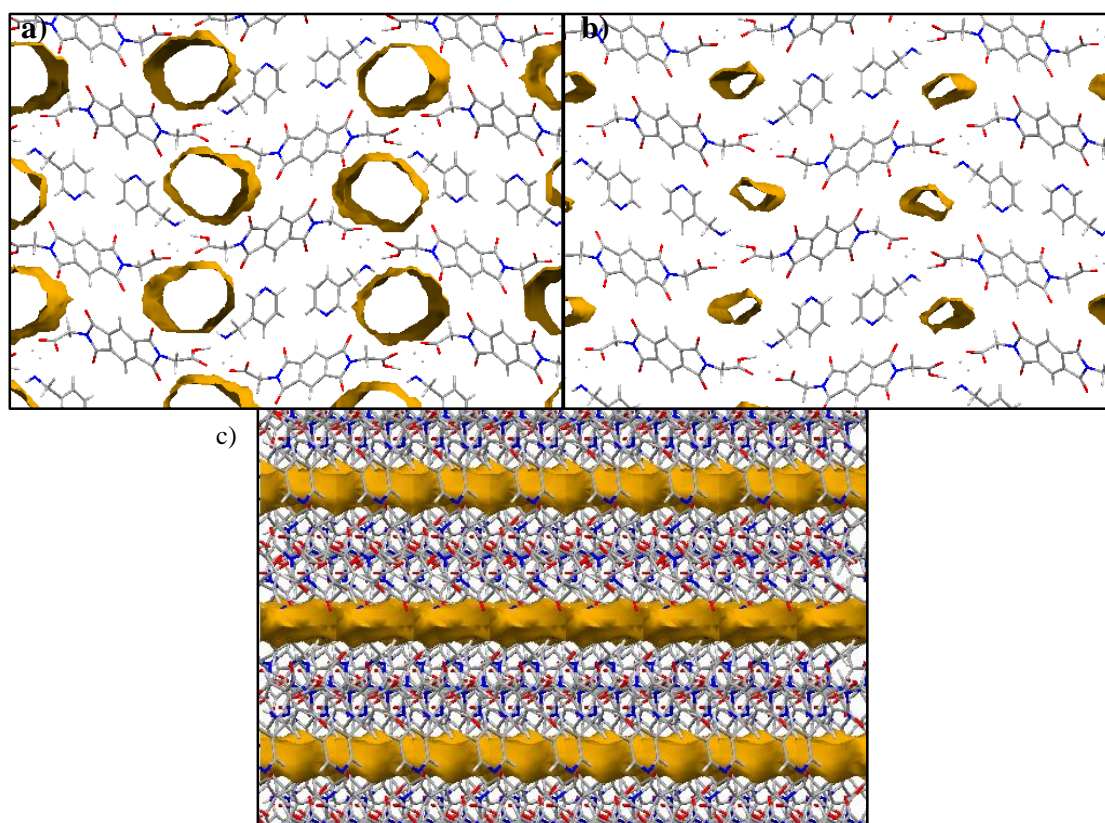


**Figure 5.30** The results of the *Void* analysis of framework **3**. a) The contact surface of the channels in framework **3** generated by Mercury with a void volume of 1720.02 Å<sup>3</sup>. b) The solvent accessible surface generated by Mercury with a void volume of only 348.21 Å<sup>3</sup>. For both surfaces a probe radius of 1.4 Å was used. c) The solvent accessible surface is viewed down the *b* axis, indicating that the guest pockets are connected, which indicates that guest movement through the channels could be possible.

### 5.3.1. Thermal behaviour of the framework

The thermal stability of framework **3** was investigated using TGA, DSC and variable temperature powder diffraction. Thermogravimetric analysis showed a large mass loss from room temperature of 18.9% and a second mass loss step of 14.0% (shown as the red line in Figure 5.31). It was not possible to calculate what the first mass loss step of the TGA represented by the red line equated to, and therefore it was thought that it was the loss of DMF from the surface of the crystals. The crystals are very fine and resemble a fine white powder that is very difficult to dry. To test whether the first step was the loss of only surface DMF the crystals were washed with acetone and dried on filter paper and another TGA was performed (the blue line in Figure 5.31). In this case the first mass loss of 18.9% is no longer present and only the mass loss step of 14.0% is observed, which represents the loss of one DMF molecule per asymmetric unit (calculated to be 14.23%). The second and third mass loss steps of 11.0% in the blue trace equate to the loss of half a 3-picolyamine molecule per asymmetric unit.

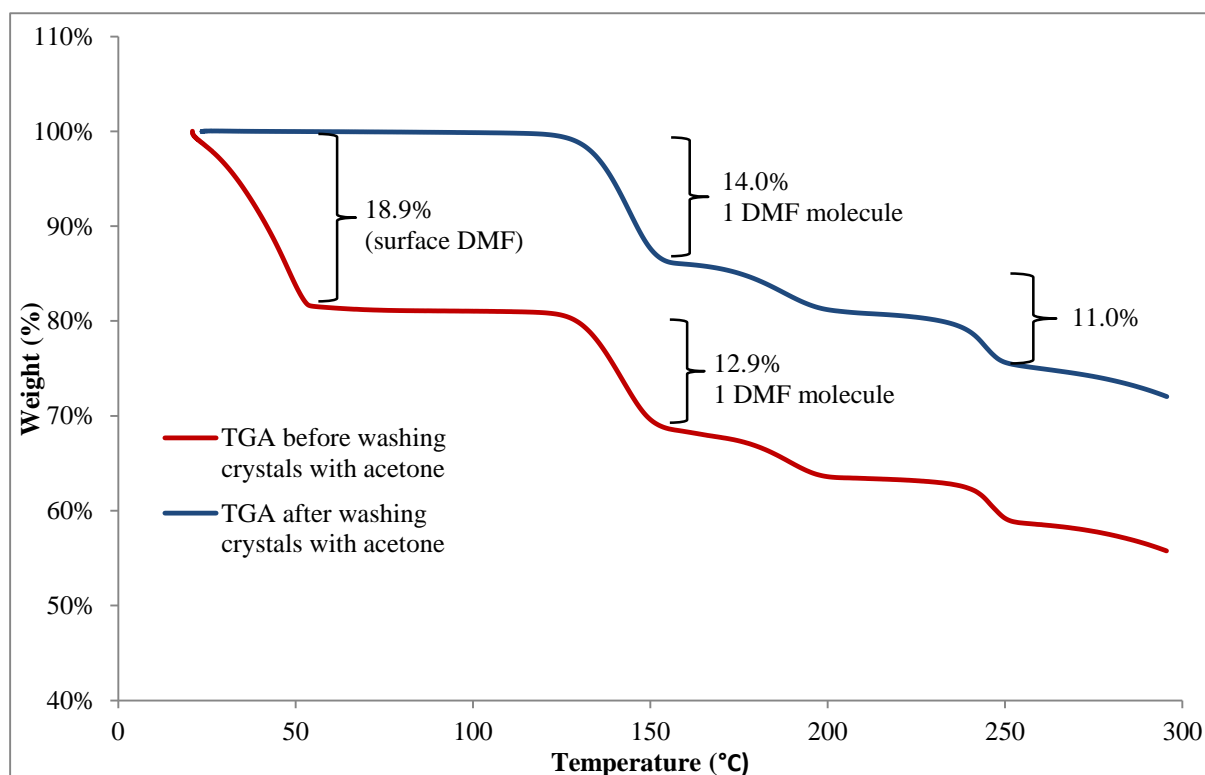


**Figure 5.31** Thermogravimetric analysis of framework **3** of the crystals before and after washing with acetone. The mass loss of 18.9% is not observed after washing the crystals with acetone, which confirms that the loss from room temperature was surface DMF. The mass loss step of 14.0% is the loss of one DMF molecule per asymmetric unit (calculated 14.23%) and the second and third mass loss steps of 11.0% in the blue trace equates to the loss of half a 3-picolyamine per asymmetric unit (calculated 12.28%).

DSC analysis (Figure 5.32) of the washed crystals also shows an endotherm with an onset temperature of 140 °C which corresponds to the loss of DMF. The second endotherm consists of a sharp peak that overlaps with a much broader peak and corresponds to the loss of half a 3-picolylamine molecule per asymmetric unit, represented by the second and third mass loss steps observed in the TG trace. The second endotherm in the DSC trace does however not overlap perfectly with the second and third mass loss steps in the TGA. It could be that the second and third mass loss steps are so close together that they have merged into one broad endotherm in the DSC trace. Although both the TG and DSC experiments were performed at a heating rate of 10 °C/minute there could have been slight differences in the heating rate, causing the second endotherm to occur at a slightly later stage.

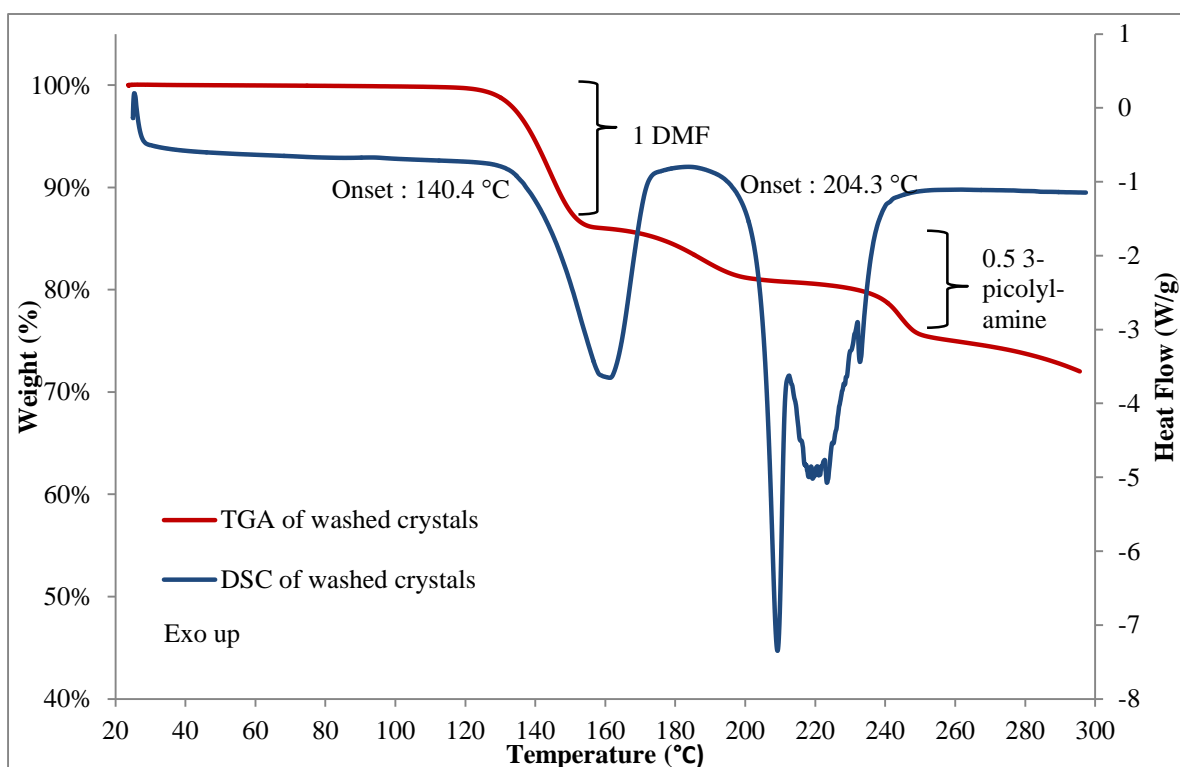


**Figure 5.32** The DSC and TG analysis of washed crystals of framework **3**. The DSC trace shows an endotherm at 140.4 °C that corresponds to the loss of DMF. The second endotherm consists of overlapping peaks which represent the loss of 3-picolylamine.

PXRD analysis of the crystals washed with acetone also confirmed that the structure remained intact (Figure 5.33) and  $^1\text{H}$  NMR of the washed crystals indicated that the DMF had not been removed from the structure and no acetone was present (Figure 5.34).

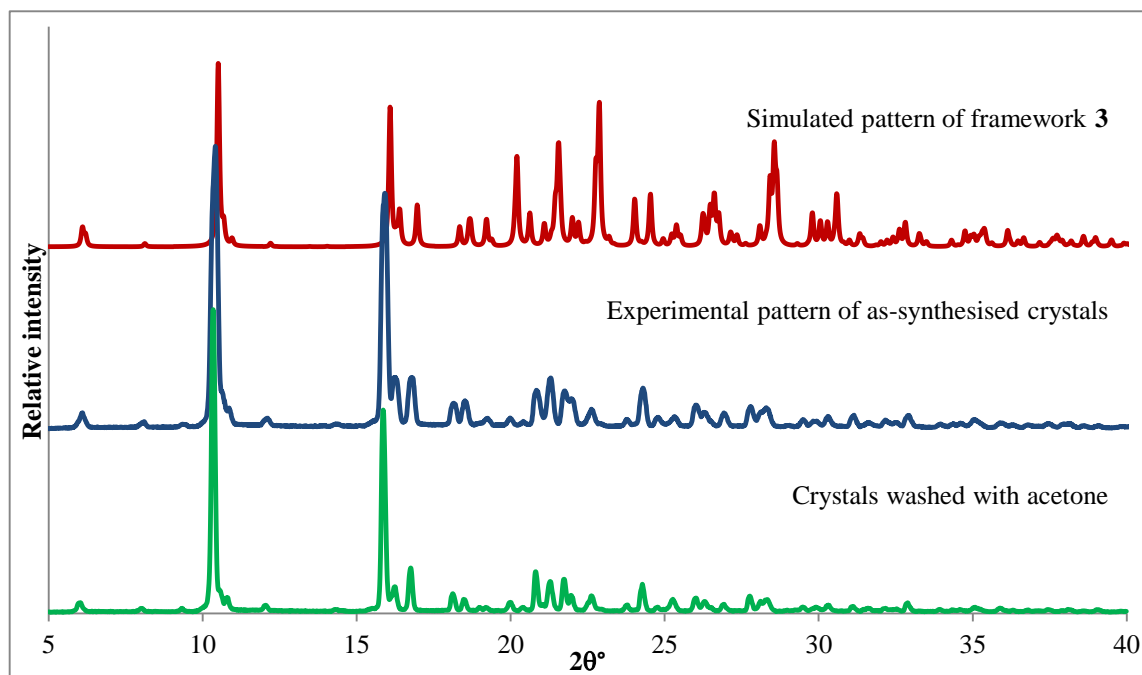


**Figure 5.33** PXR D analysis of crystals of **3** after washing with acetone. The powder patterns are similar, indicating that the framework has remained intact.

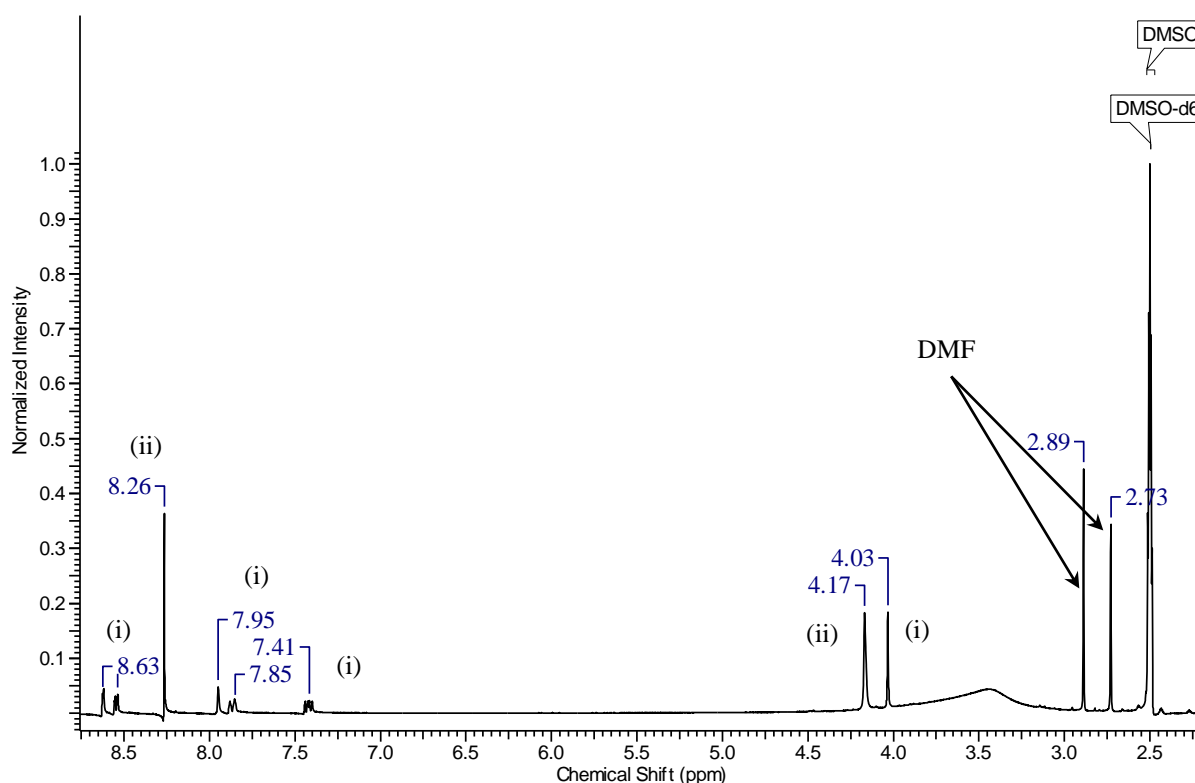


**Figure 5.34** The  $^1\text{H}$  NMR analysis of framework **3** after washing the crystals with acetone. DMF is still present in the correct stoichiometric amount. Both peaks integrate for approximately three protons (3.6). The number (i) refers to peaks associated with 3-picolylamine and the number (ii) refers to peaks associated with pyromellitic diimide. The broad peak seen at 3.5 ppm is due to water present in the DMSO- $d_6$ .

TGA results suggest that it could be possible to remove DMF without complete collapse of the structure although the following mass loss steps are rather close to the loss of DMF. This could be due to the fact that the DMF is hydrogen bonded to the framework, which makes the structure dependent on the presence of DMF. Variable temperature PXRD was performed in order to investigate whether the structure would survive the loss of DMF (shown in Figure 5.35). The powder pattern remains unchanged up to 170 °C, at which point there is significant loss in crystallinity of the sample as is indicated by the loss of intensity in the powder pattern. It is encouraging that the powder pattern remains the same in the region of 130 to 150 °C when loss of DMF occurs according to thermal analysis. The powder pattern only starts to change once loss of 3-picolyamine starts after 170 °C. These results suggest that it is possible to remove DMF without collapse of the structure. However, due to the small and fragile nature of the crystals, we were unable to investigate the thermal stability of a single crystal by single crystal X-ray diffraction.

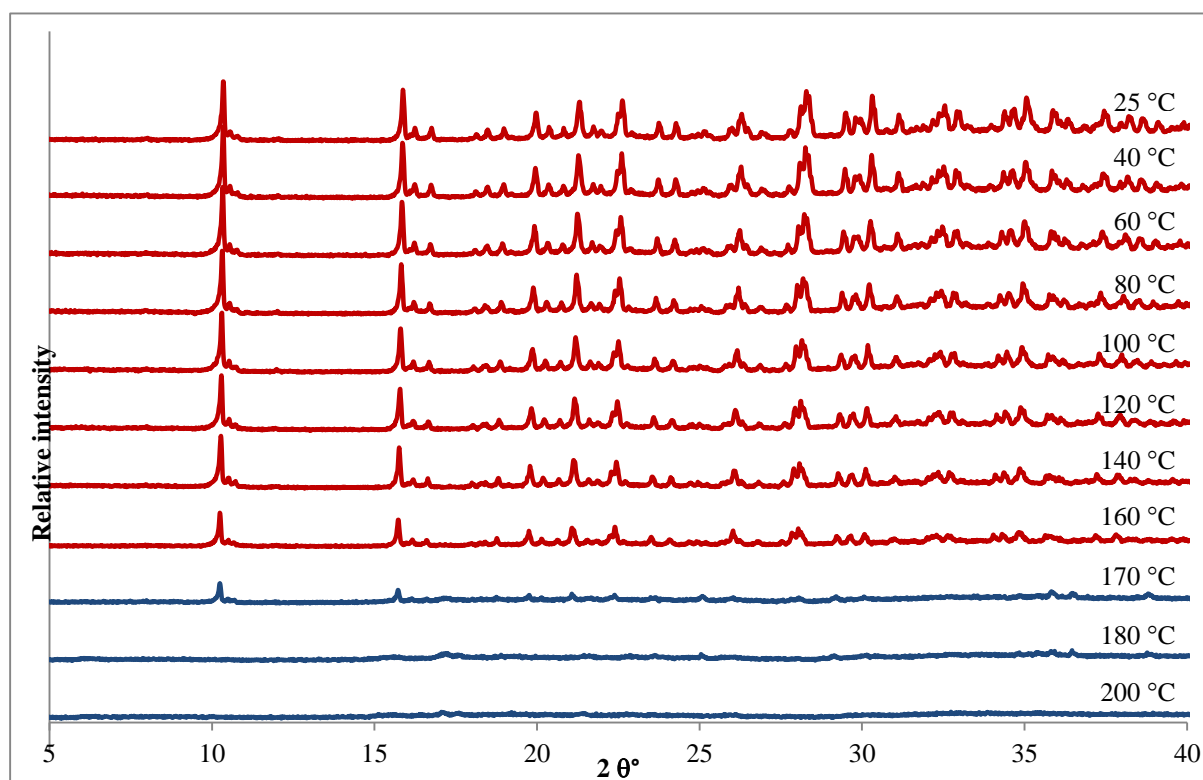


**Figure 5.35** The variable temperature PXRD of framework 3. The powder pattern remains unchanged after solvent loss between 130 and 150 °C. Loss of crystallinity has started to occur at 160 and 170 °C, but only after that does the powder pattern change significantly. This is due to the loss of 3-picolyamine after 170 °C.

### 5.3.2. Mechanochemical synthesis of framework **3**

Attempts have been made to crystallise framework **3** from other solvents such as THF, DMSO and dimethylacetamide but without success. Dimethylacetamide was the most promising solvent since it has the same general shape as DMF, but instead of a hydrogen it has a methyl group. The effects on the structure would have been interesting to investigate but no single crystals could be obtained. Pyromellitic diimide does not dissolve in many solvents therefore the number of solvents for attempted crystallisation was rather limited.

It is however possible to synthesise framework **3** by mechanochemical synthesis. Pyromellitic diimide (51 mg, 0.15 mmol) and 3-picolylamine (17 mg, 0.16 mmol) were ground together with a mortar and pestle while drops of DMF were gradually added to the powdered mixture. In total five drops of DMF was used and the sample was ground for approximately 10 minutes until it was dry and powdery again. In Figure 5.36 the simulated pattern from the crystal structure of framework **3**, the powder pattern of the synthesised crystals and the powder pattern of the product of mechanochemical synthesis are compared. Although the peaks in the pattern of the product obtained from grinding are quite broad, this could be due to the very small crystallite size generated when the sample is ground for 10 minutes. It is however possible to see that the peaks correlate well with that of the simulated and experimental patterns of framework **3**. The slight shift in the peaks of the simulated pattern is due to the large temperature difference at which the two patterns were generated. There are no peaks observed corresponding to pyromellitic diimide, indicating that the conversion to framework **3** was complete.

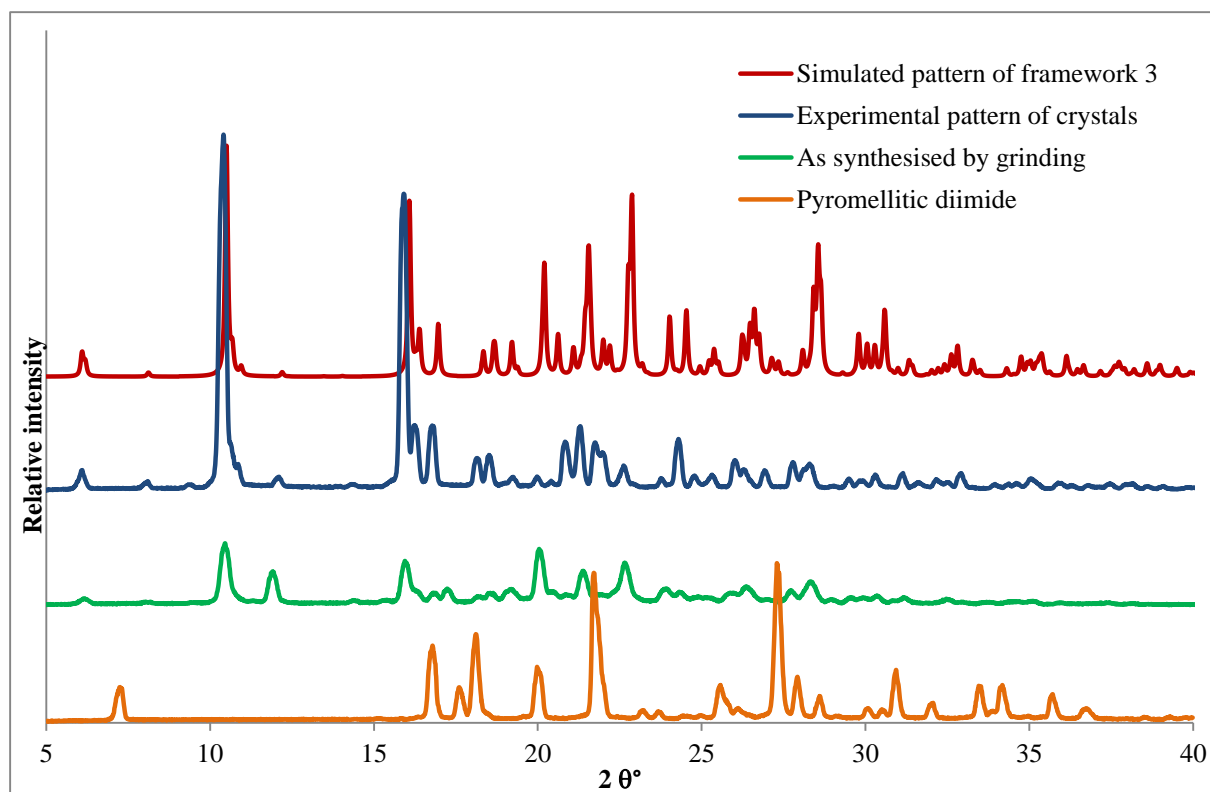


**Figure 5.36** The powder pattern of the product of mechanochemical synthesis correlates well with the simulated and experimental patterns of framework **3**. No peaks corresponding to pyromellitic diimide are observed, indicating that 100% conversion occurred.

We were not able to conduct single crystal exchange experiments with framework **3** due to the difficulty in obtaining crystals of diffraction quality and also isolating sufficient quantities of the crystals for meaningful and accurate analysis. The investigation into the permeability of framework **3** will therefore form part of future work with this material. The future work will include investigating other methods of crystallisation that have not yet been attempted during this study in order to isolate better crystals of framework **3**. If this is not possible exchange experiments will be performed with powdered samples of **3** made by mechanochemical synthesis in order to draw preliminary conclusions regarding the porosity of framework **3** and whether the hydrogen bonding of DMF to the framework impedes the exchange of guests.

We have further turned our attention to analysis of the structures obtained with pyromellitic diimide in order to determine whether there are defining features of the specific building blocks used in this study that have led to the discovery of a third framework material. This will be discussed in the next section.



## 5.4. Structural features needed for framework formation

It is necessary to study other crystal structures with pyromellitic diimide to determine why framework **3** was unique in forming a framework-type structure. Table 5.10 contains a summary of the basic structure type of the crystal structures discussed in this section. There appears to be a subtle interplay between the type of cocrystallisation agent and the solvent system that determines the degree of ionisation of the pyromellitic diimide molecule. Framework **3** will be compared to the structures discussed in the previous section to determine which structural features are responsible for the formation of a framework-type material and whether this agrees with results discussed in Chapter 4.

**Table 5.10** A summary of the crystallisation conditions, cocrystallisation agents and the resulting structure type of crystals formed with pyromellitic diimide during the course of this study.

Cofomer	Solvent system	Ionisation of pyromellitic diimide	Structure type
2,6-lutidine ( <b>PD001</b> )	1:1 THF/H <sub>2</sub> O	Singly deprotonated	Double-stranded chains with water molecules
DABCO ( <b>PD002</b> )	DMF 0.5 ml DMF THF	Doubly deprotonated	Single-stranded chains with water molecules
3,5-lutidine ( <b>PD003</b> )	1:1 THF/H <sub>2</sub> O	Singly deprotonated (shared proton)	Infinite chain of pyromellitic diimide ions
Isonicotinamide ( <b>PD004</b> )	1:1 THF/H <sub>2</sub> O	Fully protonated	Infinite base-acid chains
1,10-phenanthroline ( <b>PD005</b> )	DMF layered with THF	Fully protonated	Base-acid-base units
2,9-dimethyl-1,10-phenanthroline ( <b>PD006</b> )	DMF layered with THF	Fully protonated	Base-acid-base units
3-picolylamine (framework <b>3</b> )	DMF 1 ml DMF THF	Singly deprotonated	Infinite pyromellitic diimide chains

Results from Chapter 4 led to the conclusion that the ionisation of pamoic acid is the determining factor in whether a framework material could be obtained. The results also indicate that for an increased chance of framework formation, infinite chains of pamoate ions should be avoided, unless water molecules disrupt these chains. However, in the case of framework **3** it appears as if the situation is reversed. With chain formation there is a better chance of forming a framework-type structure, but this is also not a guarantee that a framework will form, as seen from **PD001**, **PD002** and **PD003**. In these structures the pyromellitic diimide molecules all lie perfectly flat with respect to each other. In framework **3**



however, only every second molecule is parallel causing a slight twist in the chain (Figure 5.37).

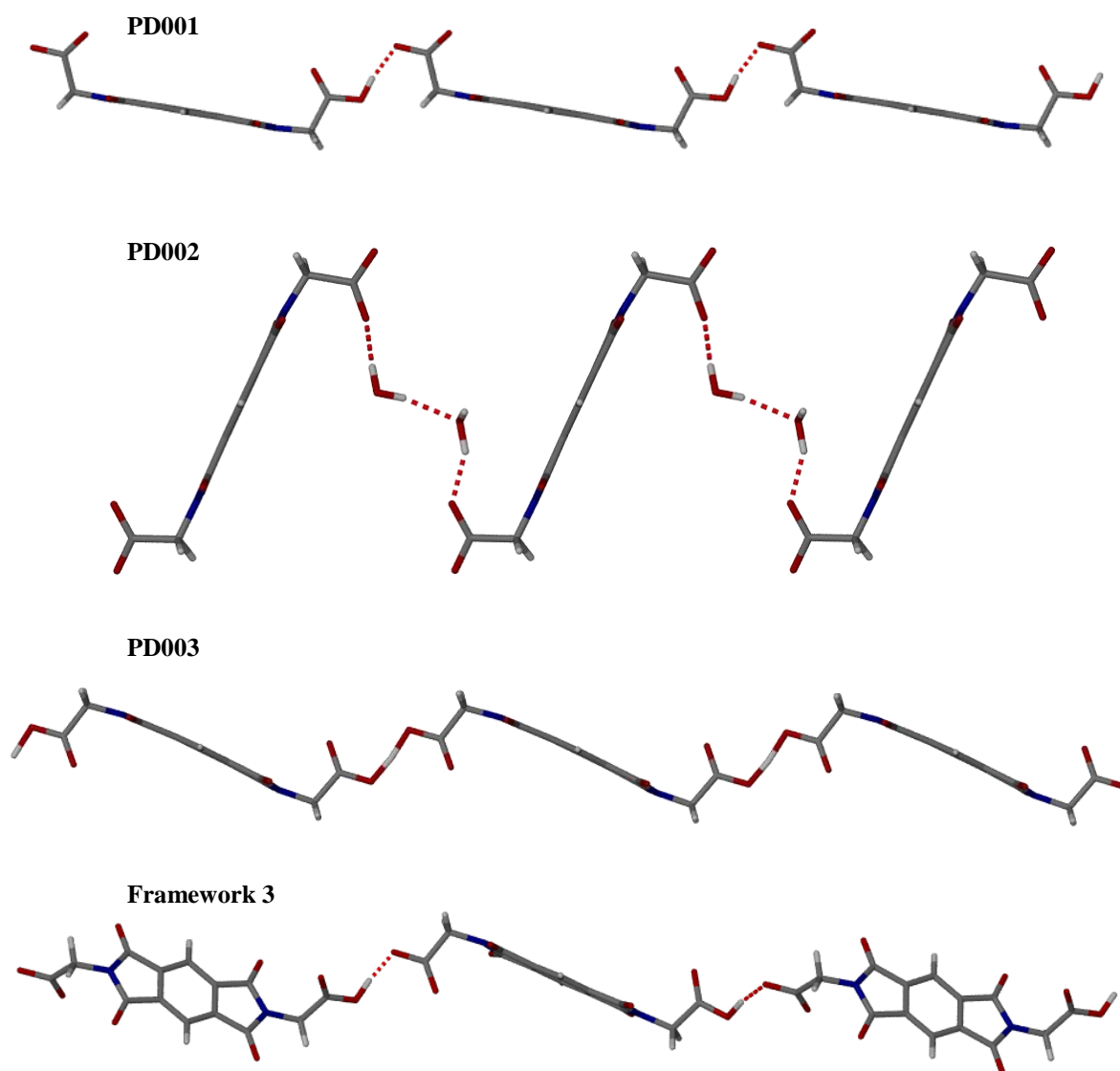


**Figure 5.37** The hydrogen-bonded chains from a series of pyromellitic diimide salts and co-crystals. In the first four structures the pyromellitic diimide molecules all lie perfectly flat with respect to each other. In framework **3** there is a twist in the chain of pyromellitic diimide ions causing every second molecule to be parallel.

In Figure 5.38a the hydrogen bonding of the amine group in one orientation of the pyromellitic diimide chain, and then the hydrogen bonding of the amine group in the rotated chain, are shown. Due to the twist in the pyromellitic diimide chain the 3-picolylammonium ions extend on either side of the chain (Figure 5.38b). This feature is not seen in any of the structures discussed in the previous section. **PD002** is shown as an example in (c) where the

3,5-lutidinium ions only extend on one side of the chain because there is no twist in the chain to position the 3,5-lutidinium ions on either side.

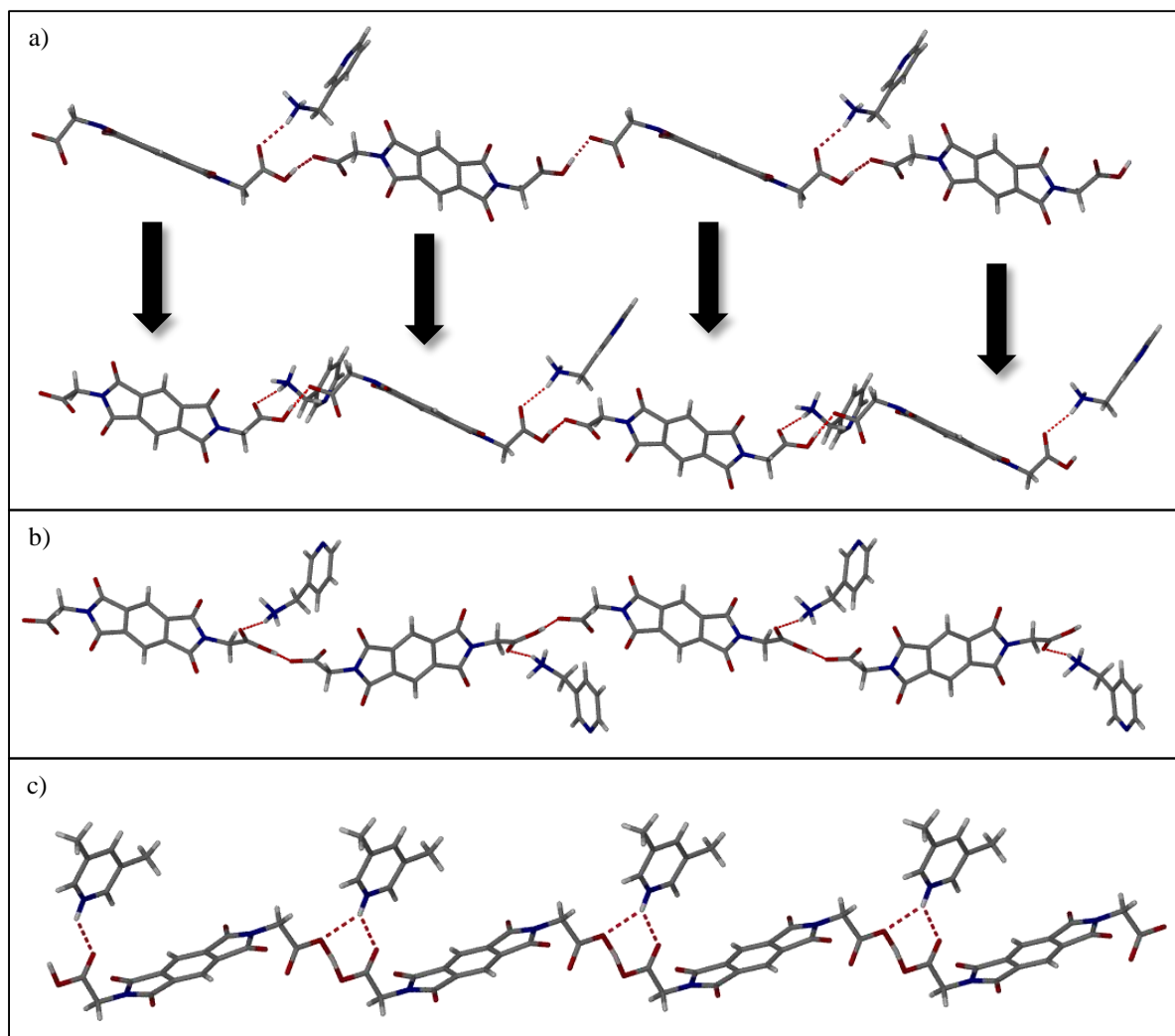


**Figure 5.38** A comparison of the hydrogen-bonded chains of framework **3** and **PD003**. a) The hydrogen bonding of the 3-picolylammonium ion to the pyromellitic diimide is shown here for different orientations of the chain. b) Due to the twist in the chain the 3-picolylammonium ions extend on either side of the chain. c) In **PD002** the 3,5-lutidinium ions only hydrogen bond on one side of the chain since there is no twist in the chain positioning the ions on either side.

The twist in the pyromellitic diimide chain could be induced by the shape of the cation. 3-picolylammonium has a bent “tail” with an amine group through which it forms hydrogen bonds with adjacent pyromellitic diimide chains. Therefore the angle of the hydrogen bond formed between the 3-picolylammonium ion and two pyromellitic diimide molecules induces a twist in the chain. The DMF molecules then form hydrogen bonds to the 3-picolylammonium ions, extending the side chain (Figure 5.39a). Due to the directional hydrogen bond formed and the twist in the pyromellitic diimide chain, the DMF molecules

are in a position to fill space between the undulating ribbons. The chains stack together and align in a continuous channel down the *c*-axis, as shown in Figure 5.39b. None of the previously discussed structures included any solvent, other than water, which was able to form more than one hydrogen bond in the structure. Since DMF can only form one hydrogen bond and 3-picolylamine can form three hydrogen bonds, this could lead to the unique packing seen in framework **3**.

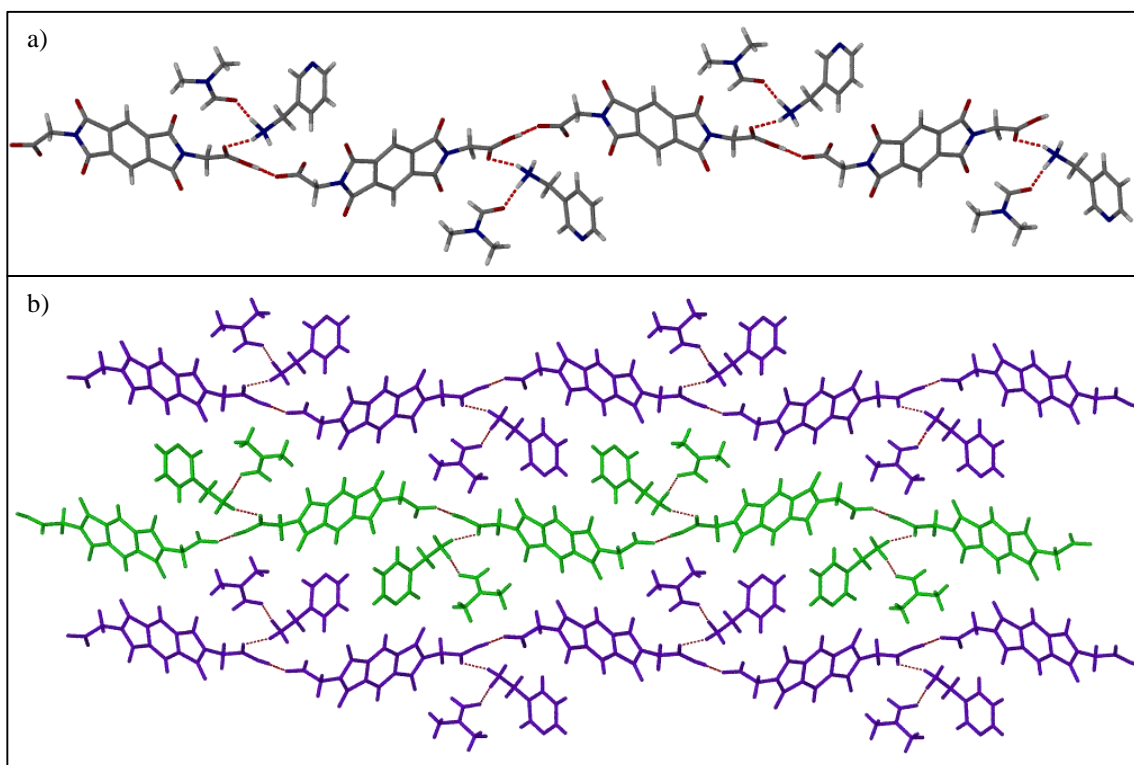


**Figure 5.39** The hydrogen-bonded network of framework **3**. a) The DMF molecules hydrogen bond to the 3-picolylammonium ions. b) The DMF molecules are in a position to fill the spaces between the chains. The chains align perfectly down the *c*-axis, causing the DMF molecules to occupy a continuous channel.

In the case of framework **3** it also seems that the *trans* conformation of pyromellitic diimide is more beneficial than the *cis* conformation that was the original design aim. However, what appear to be the crucial structure-determining factors are the presence of 3-picolylamine, and more specifically, the presence of the amine group and the highly directional hydrogen bonds that it forms with pyromellitic diimide and DMF, and the twist it induces in the chain.

## 5.5. Conclusions and future work

In this chapter the synthesis and crystal structure of a third framework-type material, N,N'-bis(glyciny)pyromellitic diimide 3-picolylammonium DMF solvate, was discussed. Variable temperature powder diffraction indicates that it remains stable upon removal of the DMF, and collapse of the structure only occurs once the loss of 3-picolylamine begins. The *Void* function in Mercury was used to map the solvent accessible surface and it shows that the DMF molecules reside in cavities that are connected to each other when the surface is mapped with a probe radius of 1.4 Å. Down the *a* axis, as shown on the left in Figure 5.40, and the *b* axis as shown on the right, it is clear that the solvent accessible surface forms a continuous channel throughout the structure. The combination of the results of variable temperature powder diffraction and *Void* analysis suggest that framework **3** has the potential to be porous. No single crystal exchange experiments were however performed with this framework due to the difficulty in obtaining SCD quality crystals and obtaining crystals in sufficient quantities for accurate analysis. Therefore exchange studies did not form part of this work, but will definitely be included in future work with framework **3**.

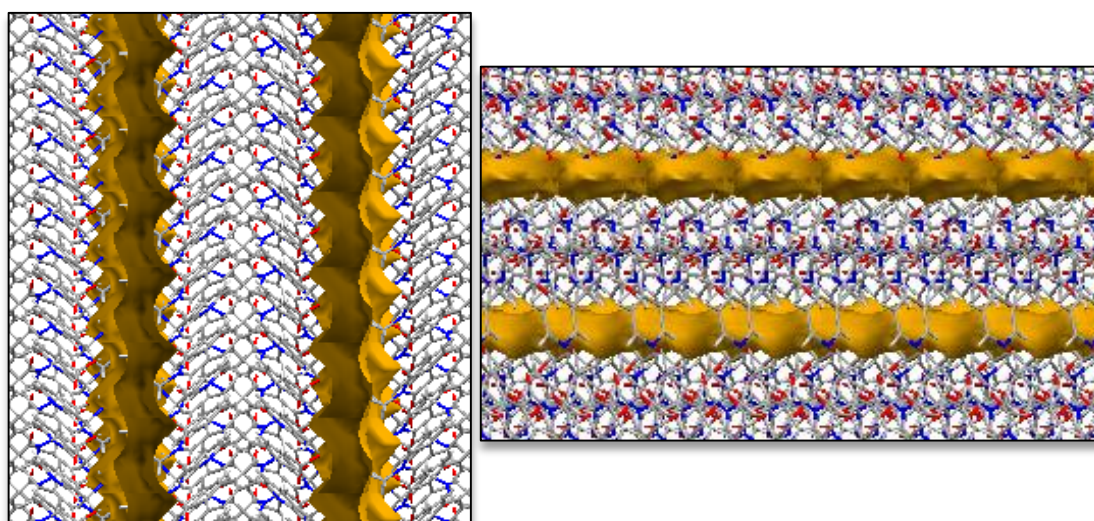


**Figure 5.40** The continuous solvent accessible volume shown down the *a* axis on the left and down the *b* axis on the right.

Attempts to crystallise framework **3** from other solvents were not successful. Pyromellitic diimide has limited solubility in most solvents, therefore we were restricted to crystallisations from DMSO, THF and dimethylacetamide. However, chapter four described how it was possible to grow crystals of the isostructural frameworks of **2** from solvents in which pamoic acid did not dissolve by leaving the powder in solution and allowing crystals to form on the pamoic acid powder. This will certainly be attempted with pyromellitic diimide and 3-

picolylamine in future. Since crystals of framework **3** formed at the interface of a layered solution of DMF and THF, it might be possible that crystals could form at the interface between the powder (pyromellitic diimide) and the solvent in which 3-picolylamine is dissolved. It is however possible to obtain framework **3** in powdered form by grinding stoichiometric amounts of the components together in a mortar and pestle. PXRD analysis showed that complete conversion had taken place. If it is therefore not possible to obtain higher quality single crystals of **3** from different crystallisation methods, exchange experiments can initially be performed with powdered samples of **3** and can then be analysed by PXRD and  $^1\text{H}$  NMR. It would also be interesting to determine whether exchange can take place by exposing the powder to the vapour of the solvent or by immersing the powder in the relevant solvent, since both methods of exchange were successful with framework **1** (Chapter 2).

Six other novel crystal structures were also obtained with pyromellitic diimide and the crystal structures were discussed and compared. The main structural features of these crystal structures were then analysed and compared to framework **3** in order to identify the unique structural features necessary for framework formation.

Firstly, it appears as if chain formation is essential in this case. Framework **3** also has a unique feature in the chain of pyromellitic diimide molecules. Each pyromellitic diimide molecule is twisted with respect to the other, forming a chain of molecules where every second molecule is parallel, whereas in the other structures every single pyromellitic diimide molecule is parallel to the others. The twist in the chain is possibly induced by the 3-picolylammonium ion hydrogen bonding to pyromellitic diimide ions in neighbouring chains. The twist in the pyromellitic diimide chain positions the 3-picolylammonium ions on either side of the chain, also not seen in any of the other structures, where the cation usually only hydrogen bonds to one side of the pyromellitic diimide chain. It is also important to note here that the 3-picolylammonium ion hydrogen bonds through the amine group, not the pyridyl moiety. This allows the ammonium moieties to form three hydrogen bonds (two to pyromellitic diimide molecules and one to DMF), and consequently place the DMF molecules between the chains. Due to the  $\pi-\pi$  stacking interactions of the pyromellitic diimide molecules, the chains stack directly above and below one another, allowing the DMF molecules to perfectly align. Attempts were also made to grow crystals of pyromellitic diimide with 2- and 4-picolylamine but unfortunately no single crystals could be obtained.

Theoretically these two amines should form the same structure with pyromellitic diimide since no hydrogen bonding occurs with the pyridyl nitrogen in framework **3**, indicating that the position of the nitrogen is not important. Continuing with this particular assumption, it should theoretically be possible to form the same type of structure with benzylamine and aniline.

Results from this study appear to indicate that it is rather important that proton transfer take place from the acid to the base. In all of the framework structures this has been the case. This influences the electronics of the system, allowing for the formation of charge-assisted hydrogen bonds that are highly directional, placing molecules in favourable positions for framework formation. We endeavoured to use charge-assisted hydrogen bonds in this study to lend extra strength and stability to framework materials in order to be able to remove the guest molecules without collapse of the structure. This has been achieved in two framework materials where the variable temperature powder patterns of both framework **1** and **3** indicate that the framework survives the loss of solvent. To a lesser extent this is true for framework **2**, since the solvent cannot be removed without collapse of the structure. Framework **2** is however able to withstand supercritical CO<sub>2</sub> conditions without much damage to the crystals, indicating that there are very strong interactions that keep the framework intact.

Two structures with pyromellitic diimide with possible polar properties have been identified during this study. One is a hydrate formed with DABCO and the other is framework **3**. The possible polar properties of these structures will be investigated in future. Framework **3** crystallises in the polar space group *Fdd2* and closer examination of the structure showed that the 3-picolylammonium ions are stacked in columns down the *c* axis with the ammonium groups aligned in the same direction. If there is a large enough net dipole in the structure it could have possible non-linear optical properties.



## 5.6. References

1. *Cambridge Structural Database version 5.35 (2013) with 3 updates.*
2. F. H. Allen, *Acta Crystallogr. B*, 2002, **B58**, 380 - 388.
3. F. H. Allen and O. Kennard, *Chem. Des. Autom. News*, 1993, **8**, 31 - 37.
4. N. Barooah, R. J. Sarma and J. B. Baruah, *CrystEngComm*, 2006, **8**, 608-615.
5. C.-H. Ge, X.-D. Zhang, H.-D. Zhang, Y. Zhao, X.-Q. Li and R. Zhang, *Mol. Cryst. Liq. Cryst.*, 2011, **534**, 114.
6. *Cambridge Structural Database version 5.35 (2013) with 3 updates. Searching for only organic structures with 3D coordinates determined.*
7. N. Barooah, R. J. Sarma, A. S. Batsanov and J. B. Baruah, *J. Mol. Struct.*, 2006, **791**, 122-130.
8. L. Pavia, G. M. Lampman, G. S. Kriz and J. R. Vyvyan, *Introduction to spectroscopy*, 4th edn., Brooks/Cole, California, 2001.
9. C. Ge, X. Li, X. Zhang, Y. Zhao and R. Zhang, *Acta Crystallogr. E*, 2009, **65**, o2400.
10. I. J. Bruno, J. C. Cole, P. R. Edgington, M. Kessler, C. F. Macrae, P. McCabe, J. Pearson and R. Taylor, *Acta Crystallogr. B*, 2002, **B58**, 389 - 397.
11. C. F. Macrae, I. J. Bruno, J. A. Chisholm, P. R. Edgington, P. McCabe, E. Pidcock, L. Rodriguez-Monge, R. Taylor, J. van de Streek and P. A. Wood, *J. Appl. Crystallogr.*, 2008, **41**, 466 - 470.
12. C. F. Macrae, P. R. Edgington, P. McCabe, E. Pidcock, G. P. Shields, R. Taylor, M. Towler and J. van de Streek, *J. Appl. Crystallogr.*, 2006, **39**, 453 - 457.
13. R. Taylor and C. F. Macrae, *Acta Crystallogr. B*, 2001, **B57**, 815 - 827.

## CHAPTER 6

### SUMMARY AND CONCLUDING REMARKS

---

In crystal engineering aspects of various fields of chemistry are employed in order to design novel supramolecular assemblies with interesting properties. However, for many years researchers have largely relied on the serendipitous discovery of interesting materials since it has remained a difficult task to predict the way in which small molecules pack in the solid state. It therefore remains essential to go through the cycle of forming a design strategy, testing this strategy experimentally and drawing conclusions regarding the success of the design strategy and whether it is a feasible way of predicting or directing the aggregation of molecules in the solid state. The results from these studies make a valuable contribution to our understanding of interactions between molecules, which enables us to make informed decisions about choosing building blocks when the aim is to purposely design a material with specific properties. This is especially valid for studies with framework materials since they can have a wide range of useful properties, as was discussed in Chapter 1, such as fluorescence for sensing, separation due to selectivity of the framework and guest uptake or exchange due to porosity. In order to engineer specific properties into a material it is important to understand how the components will interact and pack together in the solid state. To some extent we have attempted to address this complex problem in this study. We aimed to design ionic organic framework materials by using charge-assisted hydrogen bonds formed between carboxylic acids and N-heterocycles to direct the assembly of organic molecules, with the intention of engineering interesting properties such as porosity into these materials. This study was inspired by the chance discovery of an ionic organic framework, 3,4-lutidinium pamoate hemihydrate with THF-filled channels, and during the course of the study a further two framework materials were isolated. In this chapter a brief summary will be given of each chapter and the most important aspects of each will be discussed.

**Chapter 1** introduced the background of supramolecular chemistry and crystal engineering as well as important key concepts from these fields. Concepts such as intermolecular interactions were described, along with the most important intermolecular interactions pertaining to this project. The hydrogen bond was discussed at length since it is an integral part of this project. It is a highly directional interaction formed between a donor (D) and acceptor atom (A) through a partially polarised hydrogen atom. The hydrogen atom is partially polarised due to



the difference in electronegativity between the donor atom and the hydrogen atom. The strength of this interaction can be further increased by allowing proton transfer to occur, in the case of this study, from the carboxylic acid to the nitrogen atom of the N-heterocycle. The interaction is then between charged species, which leads to a much stronger interaction. We exploited this type of interaction in our framework materials in order to afford some control over the crystallisation process and, most importantly, to lend greater strength and stability to the framework. We therefore intended that the ionic interaction would allow the framework to remain intact upon guest removal or exchange. The hydrogen-bonded organic framework materials (HOFs) such as the diamondoid porous organic salts reported by Yamamoto and co-workers<sup>1-4</sup> also make extensive use of the stability that charge-assisted hydrogen bonds provide for a framework material. Chapter 1 contained further discussion on the design strategy employed for this study. The first strategy involved using molecules that have a C-shape. The carboxylic acid groups on these molecules could then enable the molecules to either form self-complementary hydrogen-bonded units, or hydrogen bond to N-heterocycles that act as linkers between two C-shaped molecules. These “doughnut-shaped” units could then potentially stack together to form continuous channels in the solid state. The second strategy involved controlling the number of functional groups that are able to form hydrogen bonds. This leads to stricter control over interactions formed between molecules. Combining this with bulky molecules such as pamoic acid could lead to the formation of voids in the solid state.

In **Chapter 2** the first framework material, 3,4-lutidinium pamoate hemihydrate (**1·THF**), and the results of experiments conducted with this framework were discussed. This material consists of a 3-D hydrogen-bonded network of pamoate ions, 3,4-lutidinium ions and water molecules with 1-D channels that are filled with THF molecules. Previous work in our group<sup>5</sup> determined that the THF in the channels could be exchanged for guests such as acetone, diethyl ether and dichloromethane in a single-crystal to single-crystal fashion. These results led to the detailed study of **1·THF** regarding its thermal stability, porosity and selectivity. TG and variable temperature PXRD analyses indicated that the framework remained stable on removal of THF, since the powder pattern of **1·THF** only changed once the loss of 3,4-lutidine occurred. Investigations into the removal of the THF from the channels by a combination of heat and vacuum also indicated that the framework remains intact even though a significant portion of the solvent had been removed. This was also possible with **1·Ether**, the exchange product of crystals of **1·THF** exposed to diethyl ether. The porosity of

**1·THF** was further investigated by exposing crystals of **1·THF** to the vapour of 28 different compounds. Of these compounds, 21 undergo exchange with the THF in the channels of **1·THF**. It was possible to prove that in 14 instances the exchange occurred in a single-crystal to single-crystal fashion, two of which involved the inclusion of the volatile solids pyrazine and iodine. To the best of our knowledge this is the first reported case of an ionic organic framework including volatile solids such as pyrazine and iodine. **1·THF** was further investigated to determine whether it exhibits any selectivity towards certain compounds when exposed to a mixture of these compounds. When crystals of **1·THF** were exposed to the vapour of varying fractions of benzene:toluene, clear selectivity was shown for toluene even at very low fractions of toluene present in the vapour phase. The same trend was observed when crystals of **1·THF** were immersed in varying fractions of benzene:toluene. Studies of the crystal structures of **1·Benzene** and **1·Toluene** showed that this may be due to favourable C–H $\cdots$  $\pi$  interactions between the toluene molecules, which are not observed for the benzene molecules. This could lead to the *cooperative* guest inclusion of toluene, causing the framework to be selective for toluene. Further selectivity experiments also indicated that **1·THF** selectively excludes solvents such as chloroform, dichloromethane and acetonitrile. This could be due to less favourable interactions between these guest molecules and the framework. It was suggested that future work should include an investigation of whether there is any change in selectivity if competition experiments are performed with the empty framework. This could indicate whether the guest already residing in the channel has any influence on the selectivity of the framework.

In **Chapter 3** the investigation into the kinetics of exchange of **1·THF** was discussed. It was not possible to study the desolvation kinetics of **1·THF** due to the overlap of the loss of THF and 3,4-lutidine. The loss of THF could therefore not be isolated for kinetic study. The exchange kinetics of iodomethane for the THF in **1·THF** was successfully studied by measuring the increase in weight of a sample of **1·THF** upon exposure to the vapour of iodomethane at different constant temperatures. The deceleratory kinetic model of contracting volume best described the exchange process. This implies that the rate of exchange is dependent on the volume of the particle/crystal exposed to the vapour of iodomethane. From the  $\alpha$ -time plots at different constant temperatures the rate constant ( $k$ ) of the reaction at each temperature was calculated. This showed that the exchange rate increases as the temperature increases in the order  $k_{25} < k_{30} < k_{35}$ . A plot of  $\ln(k)$  versus  $1/T$  formed a straight line from

which the Arrhenius parameters  $E_a$  and  $A$  could be calculated. The activation energy  $E_a$  was determined to be 21.41 kJ/mol and the pre-exponential factor  $A$  was determined to be 33.10 min<sup>-1</sup>. The activation energy indicates that an energy barrier of 21.41 kJ/mol has to be overcome for exchange to take place. This is not a very high energy barrier, which explains why **1·THF** readily undergoes exchange with a wide variety of solvents, possibly due to the fact that there are no hydrogen bonds between the framework and the guest molecules. The exchange process was further investigated by exposing single crystals of **1·THF** to iodomethane for specific time intervals at 25 °C, after which SCD data collections were performed on the crystals. Data collections after one and two hours could be solved, but for the longer exposure times of four and six hours it was not possible to solve the data since the crystals had undergone significant deterioration. SQUEEZE<sup>6</sup> analysis of the structures after one and two hours of exposure to iodomethane showed an increase in the electron count in the channels. These results were supplemented by thermogravimetric analysis of crystals of **1·THF** that were exposed to iodomethane vapour for specific time intervals. These results also showed a steady increase in the percentage mass loss as the exposure time to iodomethane increased. The mass loss percentages could be related to the amount of iodine and THF present in the structure fairly accurately. These results indicated that the exchange of THF for iodomethane in **1·THF** does not occur *via* the formation of the apohost, but rather through the simultaneous inflow of iodomethane and outflow of THF from the channels. It was suggested that future work include the kinetic exchange study of all the compounds that the THF in **1·THF** exchanges for by using <sup>1</sup>H NMR analysis and a sensitive balance. If the starting weight of the crystals of **1·THF** is known it could be possible to calculate the relative ratio of THF to the new guest by integration of the relevant peaks in the <sup>1</sup>H NMR spectrum, and then relating that to a physical mass of each component. In this way it may be possible to determine the kinetics of exchange for nearly all compounds with which the THF in **1·THF** undergoes exchange.

**Chapter 4** focused on the discovery of a framework-type material, 4-phenylpyridinium pamoate THF solvate (**2·THF**) as well as the subsequent isolation of four other isostructural framework-type materials, namely **2·Dioxane**, **2·Acetone**, **2·DMSO** and **2·DMF**. These frameworks are not true frameworks as described in chapter 1, where the term “framework” was defined as an extended and interconnected structure, usually through hydrogen bonds, that forms the basic support for the crystal structure. **2** consists of discrete base-acid-base units which

stack together in the solid state to form constricted cavities down the *c*-axis. These materials were therefore defined as framework-*type* materials, since they are made of rigid yet discrete units that form an interconnected framework *via* weaker intermolecular interactions such as C–H... $\pi$  interactions. Exchange studies with **2·THF** proved unsuccessful, whether crystals of **2·THF** were exposed to the vapour of solvents or directly immersed in the solvent. Thermal analysis of **2·THF** indicated that the loss of half a THF molecule and half a 4-phenylpyridine molecule per asymmetric unit occur simultaneously from 120 °C and the framework structure is consequently not retained. The loss of THF and half the 4-phenylpyridine leads to the formation of a 1:1 4-phenylpyridinium pamoate salt **S2**. **2·THF** does however appear to be a robust framework-*type* material since even immersion in supercritical CO<sub>2</sub> did not destroy the crystals or remove the THF from the pockets. A study of the crystallographic data of the five isostructural frameworks showed that **2·Dioxane** has the highest density of the five frameworks. This implies that **2·Dioxane** is the more stable of the five structures since the packing efficiency is better due to the shape of the 1,4-dioxane molecule that fills the cavity better. This was further confirmed by competition experiments conducted with the five isostructural frameworks. Crystals were grown from varying fractions of THF/acetone, THF/1,4-dioxane, DMSO/1,4-dioxane, DMF/1,4-dioxane and acetone/1,4-dioxane. In each case crystals of **2·Dioxane** were selectively obtained over all fractions and all solvent combinations. Selectivity between THF and 1,4-dioxane was somewhat less pronounced than in the case of the other solvent combinations, possibly due to the shape similarity between THF and 1,4-dioxane.

During the investigation into framework formation with the pamoate ion, eight novel crystal structures were obtained by combining the pamoate ion with various bases. The packing motif of each structure was analysed in order to draw conclusions regarding the structural features required for framework formation with the pamoate ion. This study, along with results from a previous study conducted by our group,<sup>7</sup> indicated that hydrogen bond formation between pamoate ions to form infinite chains in the solid state does not create a motif suitable for framework formation. In structures where pamoate chains are formed the chains close-pack and either include no solvent, or only include solvent in discrete pockets. If water molecules interrupt the chain formation of the pamoate ions it is possible to generate a framework structure such as **1·THF**, discussed in chapter 2, but it is also not a guarantee that a framework will form. To some extent this appears to be dependent on the choice of cation. When the pamoate ion is combined with a dication, infinite cation-anion chains form, as was seen in combinations with 1,2-bis(4-pyridyl)ethane, 2-aminopyrimidine and 4,4'-bipyridine (CSD-MOXRUN<sup>8</sup>). From these results it seems as though a combination of a dianion, such as the pamoate ion, with a monocation such as 3,4-lutidinium or 4-

phenylpyridinium has a higher chance of forming a framework material. In the case of framework **2** it also seems that the shape of the pamoate ion plays an important role. Due to the bend in the pamoate ion it is possible for guest molecules to be nestled between the naphthyl moieties, forming constricted cavities along the *c* axis in the crystal structure when the base-acid-base units close-pack.

**Chapter 5** focused on cocrystallisations with N,N'-bis(glyciny)pyromellitic diimide (pyromellitic diimide). Seven novel crystal structures were obtained with pyromellitic diimide, of which one is a framework material (framework **3**). This is a framework in the true sense since it forms an extended hydrogen-bonded network between the components. In **3** the guest molecule, DMF, also hydrogen bonds to the cation, 3-picolylamine, and subsequently all the DMF molecules align perfectly in channels along the *c*-axis. Although it was not possible to conduct exchange experiments with framework **3**, largely due to quality of the crystals and the difficulty in obtaining crystals, the results of variable temperature PXRD suggested that the framework may be porous. The powder pattern of **3** only changed after 170 °C, which is well after the loss of DMF from the framework has occurred. Future work with this material will therefore certainly focus on determining whether it is possible to exchange the DMF in the channel for different guests. An interesting feature of **3** that was discussed in chapter 5 is the fact that the 3-picolylammonium ions stack in columns down the *c*-axis with the ammonium groups aligned in the same direction. This could imply that framework **3** may have polar properties such as second harmonic generation and non-linear optical properties. Although studies into the polar properties of this framework did not form part of the current study, it was suggested that future work should include further investigation into this interesting feature of framework **3**.

The structural motifs of the remaining six structures with pyromellitic diimide were studied and discussed in Chapter 5 in order to determine what the structural requirements are for framework formation with pyromellitic diimide. Originally the aim was to form a dimeric unit, either through self-complementary hydrogen bond formation between pyromellitic diimide molecules in the *cis* conformation, or by linking two pyromellitic diimide molecules in the *cis* conformation to each other through hydrogen bond formation with N-heterocycles. However, the *cis* conformation was only observed in one structure, **PD001**, in a cocrystallisation with 2,6-lutidine. In this structure the pyromellitic diimide ions are connected to each other through hydrogen bonds to water molecules. Although a dimeric unit was formed in this case, no channel was formed in which guest molecules could reside. In most cases, as well as in the case of framework **3**, the main structural motif was the formation of hydrogen-bonded pyromellitic diimide chains. However, the pyromellitic diimide chain in **3** is twisted, causing only every second pyromellitic diimide molecule to be parallel as

opposed to every molecule being parallel in the other chain-containing structures. It was suggested that the shape of the 3-picolylammonium ion and its ability to form hydrogen bonds to adjacent chains through the ammonium group, induced the twist in the pyromellitic diimide chain. Consequently, due to the twist in the chain and the position of the 3-picolylammonium ion, the DMF molecules hydrogen bond to the 3-picolylammonium ion and align in a channel along the *c*-axis. From these results it was clear that the choice of N-heterocycle is vitally important for framework formation. It was therefore suggested to attempt cocrystallisations of pyromellitic diimide with benzylamine as well as continue efforts to obtain crystals of pyromellitic diimide with 2- and 4-picolylamine in the hopes that similar framework structures could be obtained.

The results from this study indicate that while it is difficult to obtain robust ionic organic framework materials, it is in fact possible with the right combination of cocrystallisation agents under the right crystallisation conditions. This does however involve an intense screening process, but the results from this process allows insight into the subtle balance of interactions between organic molecules and may help to form better design strategies in future for the engineering of ionic organic framework materials.

## References

1. A. Yamamoto, T. Hamada, I. Hisaki, M. Miyata and N. Tohnai, *Angew. Chem., Int. Ed.*, 2013, **52**, 1709-1712.
2. A. Yamamoto, T. Hasegawa, T. Hamada, T. Hirukawa, I. Hisaki, M. Miyata and N. Tohnai, *Chem-Eur J*, 2013, **19**, 3006 – 3016.
3. A. Yamamoto, T. Hirukawa, I. Hisaki, M. Miyata and N. Tohnai, *Tetrahedron Lett.*, 2013, **54**, 1268-1273.
4. A. Yamamoto, S. Uehara, T. Hamada, M. Miyata, I. Hisaki and N. Tohnai, *Cryst. Growth Des.*, 2012, **12**, 4600-4606.
5. H. Wahl, D. A. Haynes and T. le Roex, *Chem. Commun.*, 2012, **48**, 1775 - 1777.
6. A. L. Spek, *J. Appl. Crystallogr.*, 2003, **36**, 7-13.
7. H. Wahl, D. A. Haynes and T. le Roex, *CrystEngComm*, 2011, **13**, 2227-2236.
8. M. Du, Z.-H. Zhang, W. Guo and X.-J. Fu, *Cryst. Growth Des.*, 2009, **9**, 1655-1657.



# APPENDIX A

## INSTRUMENTS AND EXPERIMENTAL PROCEDURES

---

This appendix contains details of all instrumentation and software packages used, experimental procedures and details of data solution and refinement used during the course of this study.

### 1. Thermogravimetric analysis (TGA)

Thermogravimetric analysis was performed using a TA Instruments Q500 system under a N<sub>2</sub> gas purge, with a sample flow rate of 60 ml/min. A typical ramp rate of 10 °C/min was used. Samples of crystals (ranging from 5 - 15 mg) were removed from the mother liquor, dried on filter paper and placed in open aluminium pans. Samples were generally heated to 250 or 300 °C.

### 2. Differential scanning calorimetry (DSC)

Differential scanning calorimetry was carried out using a TA Instruments Q20 and Q100 system under a N<sub>2</sub> gas purge, with a flow rate of 50.0 ml/min. A typical ramp rate of 10 °C/min and cooling rate of 5 °C/min were used and samples were generally heated to 220 °C. Samples (ranging from 3 – 5 mg) were placed in aluminium pans that were non-hermetically sealed with vented aluminium lids. The reference pans were prepared using the same method. The investigation into the thermal behaviour of **2·THF** described in chapter 4 involved experiments in which crystals of **2·THF** were placed in hermetically sealed aluminium pans and heated to 220 °C. The reference pans were prepared using the same method.

### 3. Powder X-ray diffraction (PXRD)

Diffraction patterns of intensity versus  $2\theta$  with a step-size of 0.016° were collected on a PANalytical X'Pert PRO diffractometer in Bragg-Brentano geometry using an X'Celerator detector and Cu-K<sub>α</sub> radiation source ( $\lambda = 1.5418 \text{ \AA}$ ) with a Ni filter. Crushed samples were run on a zero-background holder and spun during data collection. Scans ranged from 5° to 45°  $2\theta$ .

Some diffractograms were also recorded with a Bruker D2 PHASER with Lynxeye 1-D detector and Ni-filtered Cu-K $\alpha$  radiation (30 kV, 10 mA generator parameters; restricted by a 1.0 mm divergence slit and a 2.5° Soller collimator) with a 0.016° step width. Samples were run on a zero-background holder and spun during data collection. Scans generally ranged from 5° to 45° 2 $\theta$ .

Variable temperature PXRD analysis was performed on the PANalytical X'Pert PRO diffractometer using the capillary spinner configuration equipped with an Oxford Cryostream cooling system. Powdered samples and finely ground samples of crystals were placed in 0.5 mm Lindemann glass capillaries and flame-sealed. The capillary was spun during collection over a range of 2° - 50° 2 $\theta$ .

Simulated powder patterns from the crystal structures were generated using Mercury.<sup>1-4</sup>

#### **4. <sup>1</sup>H and <sup>13</sup>C nuclear magnetic resonance spectroscopy (NMR)**

NMR was carried out on either a Varian Unity Innova 400 MHz instrument or a Varian VNMRS 300 MHz instrument. All samples were dissolved in deuterated DMSO.

#### **5. Fourier transform infrared spectroscopy (FT-IR)**

IR spectra were recorded on a Thermo Nicolet Avatar 330 FT-IR spectrometer with a Smart Performer (Zn/Se) ATR attachment in the 4000 – 600 cm<sup>-1</sup> region. All samples were dry powdered samples and for each sample a background scan was collected before the IR spectrum of the sample was collected.

#### **6. Single-crystal X-ray diffraction (SCD)**

Suitable crystals for SCD analysis were chosen according to their morphology, clarity and ability to uniformly extinguish plane polarised light. The crystals were then placed on a commercially available MiTeGen MicroMount<sup>5</sup> in paratone oil. In the SCD experiments monitoring the exchange process of THF with iodomethane in **1·THF** in chapter 3, suitable crystals were glued to glass fibres while taking care not to cover the entire crystal in glue. Intensity data were collected either on a Bruker SMART<sup>6</sup> APEXII diffractometer equipped with a Mo fine-focus sealed tube and a 0.5 mm MonoCap collimator, or a Bruker APEX DUO diffractometer equipped with Incoatec I $\mu$ S Mo and Cu microfocus X-ray sources and an APEXII

detector. In both instruments crystals were cooled to 100 K (unless otherwise specified in the crystallographic data) under N<sub>2</sub> flow from an Oxford Cryosystems Cryostat (700 Series Cryostream Plus). Data reduction was performed by a standard procedure using SAINT<sup>7</sup> and empirical corrections were performed, where necessary, using SADABS.<sup>8, 9</sup> Both programs were executed from within the APEX 2 software suite. Crystal structures were solved using SHELXS-2013<sup>10</sup> by direct methods and all ordered non-hydrogen atoms were refined anisotropically by means of full-matrix least-squares calculations on  $F^2$  by SHELXL-2013.<sup>10</sup> X-Seed<sup>11, 12</sup> was used as the graphical interface for SHELX. Most hydrogen atoms were placed in calculated positions using riding models. Hydrogen atoms on nitrogen or oxygen atoms were located in the electron density difference map. Images of crystal structures in this thesis were generated using POV-Ray.<sup>13</sup>

## 7. PLATON SQUEEZE

For structures in Chapter 2 where it was not possible to adequately model the disordered guest in the channel, the presence of the guest was inferred through PLATON<sup>14, 15</sup> SQUEEZE<sup>16</sup> analysis. SQUEEZE calculates the number of electrons present in the solvent accessible volume of the *P1* unit cell. Disordered guest molecules were deleted from the .ins or .res file and the structure was refined after correcting the structural formula. SQUEEZE analysis then returns, among others, values for the void volume and the electron count which is then written to a PLATON.sqf file. Details of the SQUEEZE results can then be appended to the cif file. It is therefore possible to infer the presence of a guest molecule and its occupancy due to a comparison of its electron count to that of the SQUEEZE results.

## 8. Void mapping

For compounds that contained channels or voids in the crystal structure the *Void* function in Mercury<sup>1-4</sup> was used in order to determine the solvent accessible volume, the contact volume and the void volume. The guest molecules residing in cavities or channels were deleted from the .res file and in Mercury the function *Display Voids* was used to map the subsequent void. A probe radius of 1.4 Å was used and the presence of connected solvent accessible surface pockets was used as an indication of whether a material was theoretically porous.

## 9. Synthesis of N,N'-bis(glycinyl)pyromellitic diimide

Pyromellitic dianhydride (1.114 g, 5.1 mmol) was dissolved in acetic acid (50 ml) by warming the mixture up to 100 °C. Glycine (0.790 g, 10.5 mmol) was ground to a fine powder and added to the acetic acid solution, and the mixture refluxed overnight at 130 °C. After addition of glycine the mixture remained clear for a minute after which a white precipitate formed. Once the solution cooled the white precipitate was filtered and washed with ethanol.<sup>17</sup> Percentage yield: 87%. Melting point: >300 °C.

<sup>1</sup>H NMR (300 MHz, DMSO-d<sub>6</sub>) δ ppm 8.36 (2H, s), 4.40 (4H, s). <sup>13</sup>C NMR (300 MHz, DMSO-d<sub>6</sub>) δ ppm 168.52, 165.50, 136.94, 118.21, 39.36. IR (solid state, cm<sup>-1</sup>) 3300 – 2600, 1700 (s), 1215 (s).

## 10. References

1. I. J. Bruno, J. C. Cole, P. R. Edgington, M. Kessler, C. F. Macrae, P. McCabe, J. Pearson and R. Taylor, *Acta Crystallogr. B*, 2002, **B58**, 389 - 397.
2. C. F. Macrae, I. J. Bruno, J. A. Chisholm, P. R. Edgington, P. McCabe, E. Pidcock, L. Rodriguez-Monge, R. Taylor, J. van de Streek and P. A. Wood, *J. Appl. Crystallogr.*, 2008, **41**, 466 - 470.
3. C. F. Macrae, P. R. Edgington, P. McCabe, E. Pidcock, G. P. Shields, R. Taylor, M. Towler and J. van de Streek, *J. Appl. Crystallogr.*, 2006, **39**, 453 - 457.
4. R. Taylor and C. F. Macrae, *Acta Crystallogr. B*, 2001, **B57**, 815 - 827.
5. Mitegen, 95 Brown Rd - Suite 183, NY 14850, 2004.
6. *SMART Data Collection Software, version 2012.10-0*, Bruker AXS Inc., 2003, Madison, WI.
7. *SAINT Data Collection Software, version V7.99A*, Bruker AXS Inc., 2012, Madison, WI.
8. *SADABS, version 2012/1*, Bruker AXS Inc., 2012, Madison, WI.
9. R. H. Blessing, *Acta Crystallogr., Sect. A: Found. Crystallogr.*, 1995, **51**, 33.
10. G. M. Sheldrick, *Acta Crystallogr., Sect. A Found. Crystallogr.*, 2008, **64**, 112.
11. L. J. Barbour, *Journal of Supramolecular Chemistry*, 2001, **1**, 189.
12. J. L. Atwood and L. J. Barbour, *Cryst. Growth Des.*, 2003, **3**, 3.
13. *POV-Ray<sup>TM</sup> for Windows, version 3.6*, Persistence of Vision Raytracer Pty. Ltd., 2004, Williamstown, Australia.
14. A. L. Spek, *PLATON, a multipurpose crystallographic tool*, Utrecht University, Utrecht, The Netherlands, 2005.
15. A. L. Spek, *J. Appl. Crystallogr.*, 2003, **36**, 7-13.
16. P. van der Sluis and A. L. Spek, *Acta Crystallogr., Sect. A: Found. Crystallogr.*, 1990, **46**, 194 - 201.
17. N. Barooah, R. J. Sarma and J. B. Baruah, *CrystEngComm*, 2006, **8**, 608-615.